



UNIVERSITÀ
DEGLI STUDI
FIRENZE

**DOTTORATO DI RICERCA IN
AREA DEL FARMACO E TRATTAMENTI INNOVATIVI**

**CURRICULUM: FARMACOLOGIA, TOSSICOLOGIA E TRATTAMENTI
INNOVATIVI**

CICLO XXXII

***Photobiomodulation and purinergic signaling: in vivo
and in vitro approaches for new and innovative treatments in
skin fibrosis and remyelination***

Settore Scientifico Disciplinare BIO/14

Dottorando

Dott.ssa Giada Magni

Tutori

Prof.ssa Anna Maria Pugliese

Dott.ssa Francesca Rossi

Coordinatore

Prof.ssa Elisabetta Teodori

Anni 2016/2019

INDEX

PART ONE

1 INTRODUCTION	1
1.1 The blue LED device	3
1.1.1 What is Biophotonics	4
1.1.2 The properties of light.....	4
1.1.3 Tissue optical properties	6
1.1.4 Chromophores.....	8
1.1.5 Light-tissue interactions.....	10
<i>Photochemical interactions</i>	11
<i>Photothermal interactions</i>	11
<i>Photomechanical interactions</i>	13
1.2 Effects of blue LED light: <i>in vivo</i> studies on wound healing	14
1.2.1 Effects of blue LED light: <i>in vivo</i> animal model of wound healing	15
1.2.2 Effects of blue LED in human chronic wounds	18
1.3 Photobiomodulation therapy	19
1.3.1 Light in wound healing and in skin fibrosis	21
1.4 Human skin: roles and structure	24
1.4.1 Epidermal layer	25
1.4.2 Dermal layer.....	26
1.4.3 Hypodermal layer	27

1.5 Classification of wounds	28
1.5.1 Acute wound	28
1.5.2 Chronic wound	28
1.5.3 Hard-to-heal wound.....	29
1.6 The wound healing	30
1.6.1 Haemostasis	31
1.6.2 Inflammation.....	34
1.6.3 Proliferative phase	37
1.6.4 Remodeling phase	38
1.7 Fibrosis	39
1.7.1 Fibrosis in skin	41
1.7.2 Hypertrophic scars	42
1.7.3 Keloid scars.....	43
1.7.4 Keloid scars management and treatments.....	46
1.7.5 Pharmacological therapies	46
<i>Corticosteroids</i>	47
<i>5-Fluorouracil (5-FU)</i>	48
<i>Bleomycin</i>	48
<i>Interferon (INF)</i>	49
<i>Mitomycin C (MMC)</i>	49
<i>Onion extract and heparin applications</i>	50
1.7.6 Non-pharmacological therapies.....	50
<i>Compression therapy</i>	50
<i>Silicone gel sheet applications</i>	51

<i>Surgery</i>	51
<i>Cryotherapy</i>	52
<i>Radiotherapy</i>	52
<i>Lasertherapy</i>	53
1.8 Adenosine.....	54
1.8.1 Purinergic receptors	56
<i>P₁ receptors</i>	58
<i>Pharmacology of P₁ receptors</i>	59
<i>Distribution of P₁ receptors</i>	61
<i>Role of P₁ receptors</i>	62
1.8.2 The involvement of adenosine in wound healing and fibrosis processes	63
2 THE AIMS	66
The aims.....	68
3 MATERIALS AND METHODS	70
3.1 <i>In vivo</i> experiments.....	72
3.1.1 Animals procedures	72
3.1.2 Mice models	73
<i>Mice model of acute wound</i>	74
<i>Acute diabetic mice model</i>	74
<i>Chronic diabetic mice</i>	75
<i>Purinergic P₂ receptor antagonist treated</i>	75

<i>Coagulopathies mice model</i>	76
<i>Trpv1 knock-out mice model</i>	76
3.1.3 Summary of mice models.....	77
3.1.4 Haematoxylin and eosin staining.....	77
3.1.5 Immunofluorescence staining.....	77
<i>Epifluorescence microscopy</i>	78
3.1.6 Statistical analysis.....	78
3.1.7 Mice model of chronic wound.....	79
3.1.8 Enzyme-Linked Immunoabsorbent Assay	80
3.2 <i>In vitro</i> experiments	81
3.2.1 Keloid scars.....	81
3.2.2 Healthy skin.....	82
3.2.3 Primary cultures of human fibroblasts	82
3.2.4 Confocal microscopy	83
3.2.5 Blue LED light applications.....	84
3.2.6 Cell viability assay	84
3.2.7 Evaluation of cell apoptosis.....	85
3.2.8 WST-8 assay.....	85
3.2.9 Sulforhodamine B assay	86
3.2.10 Electrophysiological recordings.....	87
3.2.11 Raman spectroscopy measurements.....	88
3.2.12 Drugs.....	89
3.2.13 Statistical analysis	89

4 RESULTS	91
4.1 Results obtained on mice model of acute wound.....	93
4.1.1 Blue LED light irradiation reduces early inflammatory infiltrate in the mouse skin acute wounds	93
4.1.2 Streptozotocin-induced acute diabetic mice	98
<i>Induction of one skin abrasion in acute diabetic mice</i>	98
<i>Induction of two skin abrasions in mice</i>	99
4.1.3 Streptozotocin-induced chronic diabetic mice.....	100
4.1.4 Purinergic P ₂ X and P ₂ Y receptors involvement in wound healing process.....	101
4.1.5 Coagulopathies-induced mice	102
4.1.6 Capsazepine-treated mice	103
4.2 The blue LED light modulates wound healing in mice model of chronic wounds	105
4.3 Confocal microscopy characterization of cultured fibroblasts	107
4.4 Effects of blue LED light on cell metabolism of cultured fibroblasts ...	109
4.4.1 Healthy fibroblasts.....	109
4.4.2 Keloid fibroblasts.....	110
<i>Fibroblasts from keloid tissues</i>	110
<i>Fibroblasts from keloid perilesional tissues</i>	111
4.5 Effects of blue LED light on cell proliferation of cultured fibroblasts...	112
4.5.1 Healthy fibroblasts.....	112
4.5.2 Keloid fibroblasts.....	113
<i>Fibroblasts from keloid tissues</i>	113

<i>Fibroblasts from keloid perilesional tissues</i>	114
4.6 Trypan Blue staining	114
4.7 DAPI staining	116
4.8 Selective adenosine A _{2A} receptors antagonists and fibroblasts proliferation.....	117
4.9 Electrophysiological recordings	119
4.10 Raman Spectroscopy	123
5 DISCUSSION AND CONCLUSIONS	128
Discussion and Conclusions.....	130

PART TWO

1 INTRODUCTION	139
1.1 Introduction	141
1.1.2 Demyelinating diseases: multiple sclerosis	142
1.1.3 Oligodendrogenesis	144
1.1.4 Purinergic signalling in oligodendrogenesis	145
<i>Role of P₁ receptors in Oligodendrogenesis</i>	147
1.1.5 A _{2B} adenosine receptors	149
2 THE AIMS	151
The Aims	153

3 MATERIALS AND METHODS	155
3.1 Cell cultures of OPCs	157
3.2 OPC differentiation	157
3.3 Electrophysiological experiments	158
3.4 Real-Time Polymerase Chain Reaction (Real-time PCR)	159
3.5 Drugs	160
3.6 Statistical analysis	161
4 RESULTS	165
4.1 Selective A _{2B} adenosine receptor stimulation inhibits outward K ⁺ currents in cultured OPCs	166
4.2 The A _{2B} receptor activation modulates oligodendrocyte maturation <i>in vitro</i>	173
5 DISCUSSION AND CONCLUSIONS	176
Discussions and conclusions	178
6 REFERENCES	181

PART ONE

1. INTRODUCTION

1.1 The blue LED device

In this work, we studied the effects of the blue LED device on the wound healing process and skin fibrosis. For this purpose, we performed *in vivo* experiments in mice models and *in vitro* tests on human keloid fibroblasts.

The blue LED device is based on the use of a commercially available LED (Light Emitting Diode), emitting at around 420 nanometers (nm) with 1 Watt (W) optical emission power. The device is fiber-coupled: it consists in a benchtop device furnished with a flexible polymeric fiber, 1.2 meters (m) in length, equipped with a touch screen where it is possible to control all the irradiation parameters (Fig. 1), such as irradiation time and power. The illuminated area corresponded to a circle 5 millimeters (mm) in radius. The resulting power density was 1.2 W/cm². The intensity distribution of the light at the tissue surface was homogeneous, as from a top hat intensity light source.¹



Fig. 1. The blue LED light device

The blue LED light device was designed at the Institute of Applied Physics – Italian National Research Council (CNR) and was originally developed as a photocoagulator, i.e. a device that can induce photoemostasis on superficial abrasions. The underlining mechanism is due to the specific absorption of the blue light by the haemoglobin in the bleeding wound. Indeed, haemoglobin shows narrow absorption peaks in the blue range, i.e. at 410 nm and 430 nm for oxygenated and non-oxygenated haemoglobin, respectively. This particular property of haemoglobin was used to ensure local temperature

increase able to induce haemostasis through a photo-thermo-coagulation process.

The use of the proper irradiation settings in terms of dose or fluence, irradiation time, target spot area and emission pattern allows to induce a local temperature rise above the threshold for protein denaturation within the blood, resulting in a fast coagulation effect.¹

1.1.1 What is Biophotonics

Biophotonics deals with interactions between light and biological matter; it is a multidisciplinary research area, embracing all light-based technologies applied to the life sciences and medicine.

The use of light for medical purpose dates back to ancient Egyptians when phototherapy was empirically prescribed for a number of medical disorders ranging from skin pathologies to asthma, behavioral disorders and wounds. More recently, developments in human physiology, which clarified several of the mechanisms behind the interaction between the organism and light, added many new dimensions to this field.²

Notwithstanding its extensive application, especially in the last twenty years, phototherapy was only recently defined in its several components. This allowed the separation from the utilization relying on the thermal effects of light to the application from the ones that are non-thermal and suggest an interaction of light with endogenous photoacceptors.³ Wound healing was probably one of the first and most important areas of interest in which phototherapy was applied.⁴

1.1.2 The properties of light

In physics, light has been described from either “classical” or “quantum” viewpoint. In classical theory, light is considered to be an oscillating electromagnetic field that can have a continuous range of energies, whereas, in the quantum model, light is considered packets, (quanta) of energy called “photons”.⁵

The electromagnetic waves consist of two waves oscillating perpendicular to one another; one of the waves is an oscillating magnetic field,

the other is an oscillating electric field. Wavelengths have a basic property: a trough, the lowest point, and a crest, the highest point; the vertical distance between the tip of a crest and the central axis of the wave, is known as its amplitude and is associated with the intensity of the wave. The horizontal distance between two consecutive troughs or crests is known as the wavelength of the wave and is measured in nm (Fig. 2). Waves oscillate in space: the number of full wavelengths that pass by a given point in space for every second is known as the frequency of the wave. The wavelength and frequency are inversely proportional: shorter wavelengths have a higher frequency and higher wavelengths have a shorter frequency. The period of the wave is the length of time that employs for one wavelength to pass by a given point in space: from a mathematical point of view, the period is the reciprocal of the frequency.⁶

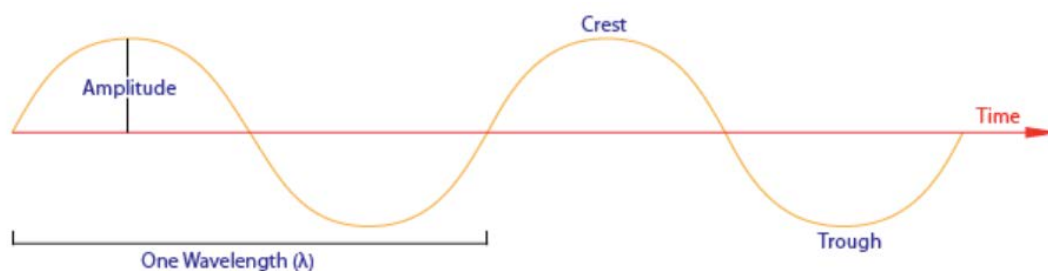


Fig. 2. The basic characteristics of a wave, including amplitude and wavelength. From <https://www.khanacademy.org/> and UC Davis ChemWiki.⁶

The electromagnetic waves can be classified and organized according to their different wavelengths/frequencies; this classification is known as the electromagnetic spectrum (Fig. 3).⁶

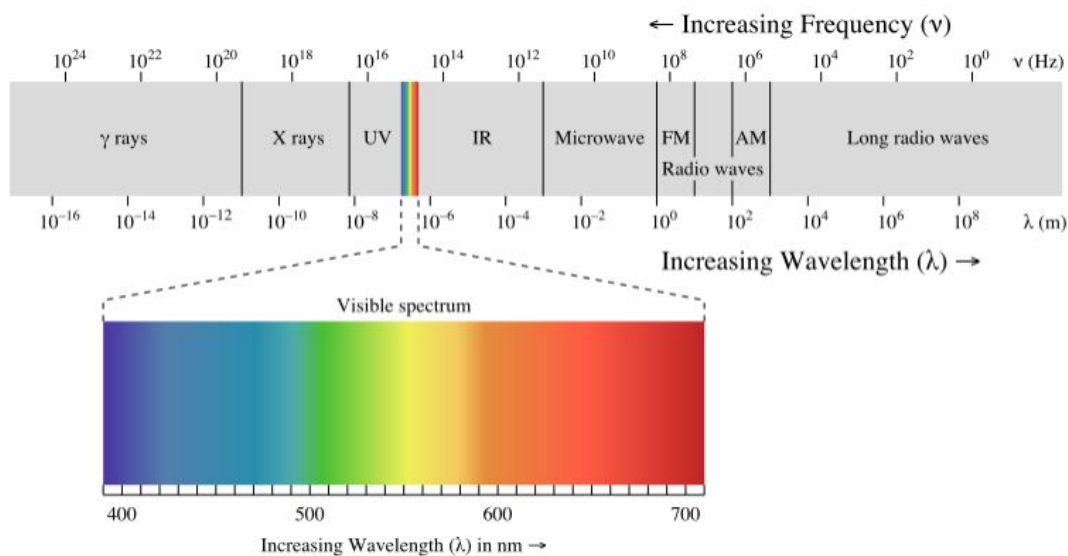


Fig. 3. The electromagnetic spectrum. From <https://www.khanacademy.org/> and UC Davis ChemWiki.⁶

The visible spectrum (VIS), i.e. the light observable with the eyes, is only a little fraction of the different types of radiation that exist. To the right of the VIS spectrum, there are waves lower in frequency and longer in wavelength respect to visible light. These kinds of light include infrared rays, microwaves and radio waves and they are usually referred to as IR spectrum. These wavelengths surround us constantly but, thanks to their lower frequency, corresponding to lower energy, are not dangerous for health. To the left of the VIS spectrum, ultraviolet spectrum (UV) is shown: these types of radiation include ultraviolet rays, X-rays and gamma rays. They present high frequency and thus high energies, making them very health-damaging.⁶

1.1.3 Tissue optical properties

When the matter is exposed to light, three main effects occur, i) reflection, ii) scattering, iii) absorption. These light-effects strongly depend on the properties of tissue and together determine the total transmission of the tissue at a certain wavelength (Fig. 4). Each biological tissue has different optical properties that have important implications on the use of lasers and light-based technologies in the medical field.

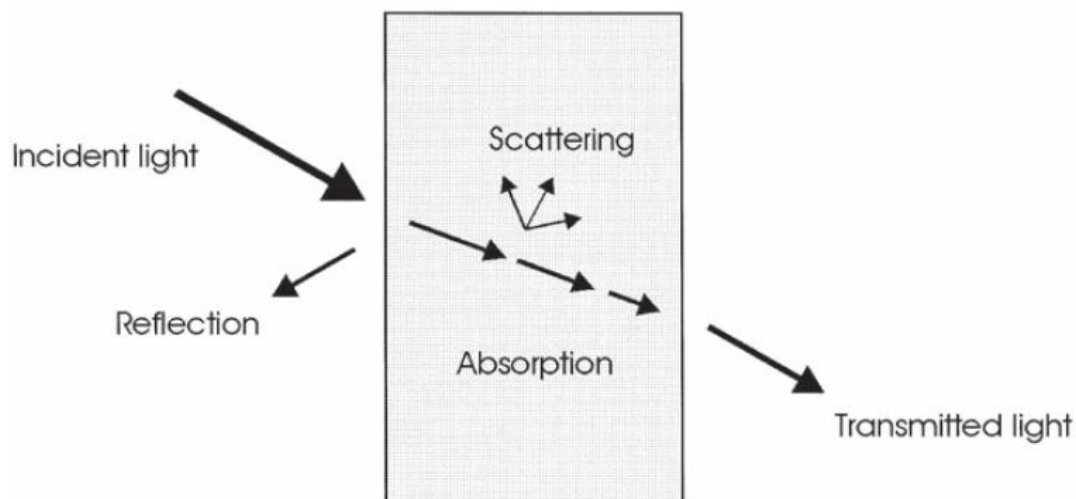


Fig. 4. The geometry of reflection, absorption, scattering and transmission of light. From *"Laser-Tissue Interaction fundamentals and applications"* Niemz, Markolf, 2nd edition, Springer.⁷

Reflection is defined as the returning of electromagnetic radiation by surfaces upon which it is incident; this phenomenon occurs when two materials have two different refraction index, such as air and tissue.⁷

Scattering is a general physical process where some forms of radiation, such as light, sound, or moving particles, are forced to deviate from a straight trajectory by one or more paths, and this is due to localized non-uniformities in the medium through which they pass.⁷

Absorption can be described as the transfer of the energy from an incident electromagnetic wave to matter, as the wave passes through it. In particular, during the passage, the energy of the wave is attenuated by the absorption of the medium. From a physical point of view, absorption is due to a partial conversion of light energy into heat motion or certain vibrations of molecules of the absorbing material. When considering biological tissues, only the cornea is highly transparent to the visible light: meaning that the total radiant energy entering and emerging is almost the same. At the same time, the cornea appears opaque in the infrared spectral region: it means that the terms transparent and opaque are wavelength-dependent.⁷

As regards dermis, the depth of light penetration into this tissue depends on the wavelength and, as previously stated, is limited by scattering and absorption. Moreover, each skin layer has different optical properties, so

that in skin the penetration depth depends on light wavelength and optical properties of the layer. In Fig. 5 it is possible to observe the different penetration depths and that the blue light, i.e. the light in the range from 410 to 430 nm, has a poor penetration capability.

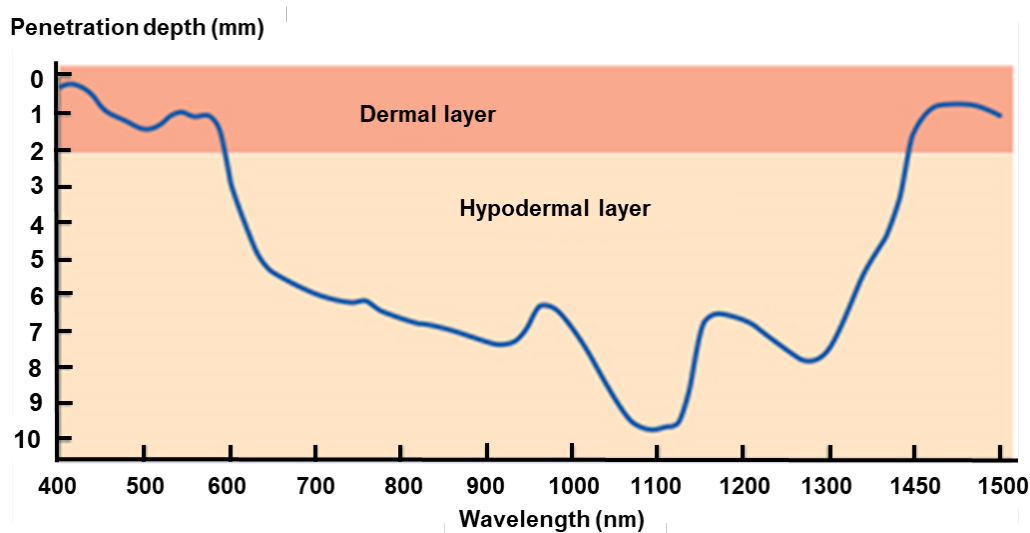


Fig. 5. The blue light penetration capability. From <https://www.bioopticsworld.com>.⁸

1.1.4 Chromophores

In biological tissue, the absorption of light is principally due to specific molecules named chromophores, i.e. molecules which absorb light at specific wavelengths.

Chromophores may be classified as endogenous or exogenous, in respect to the considered biotissue. Moreover, chromophore can absorb in the VIS, in the UV and in the IR spectrum. Chromophores UV-absorber are nucleic acids (deoxyribonucleic acid, DNA, and ribonucleic acid, RNA), some amino acids (such as Tryptophan, Phenylalanine and Tyrosine) and proteins. In the VIS spectrum, the principal absorbers are the molecules which contain Fe-protoporphin IX, a chemical group precursor of Heme group, such as cytochrome C and haemoglobin. Other endogenous chromophores are flavins and additional coloured-natural compounds. In the IR spectrum, the main chromophores are melanin, a pigment contained in skin melanocytes, and water, the major constituent of all biological tissues.

Taking into account the spectra of the main endogenous chromophores, it is possible to identify an optical therapeutic window, ranging from 680 to 1200 nm, exploitable for medical applications of light sources. In this spectral range, the radiation penetrates the biological tissues with a limited energy loss, thus enabling the treatment of deeper tissue structures⁹⁻¹⁰ (Fig. 6). This window is currently a relatively narrow range of the wavelengths that can actually interact with photoacceptors; it is located near the IR portion of the spectrum of the VIS light and is named near-infrared (NIR) light.

Water is one of the most important constituents of the biological tissue and for this reason, plays a fundamental role in absorption phenomenon: in the VIS region, the absorption coefficient of water is low, whereas is higher in the IR region (Fig. 6). Moreover, also oxygenated haemoglobin (Fig. 6) exhibits an absorption peak in the VIS spectrum. In particular, oxygenated haemoglobin shows a narrow absorption peak around 410 nm, while deoxygenated haemoglobin about 430 nm. The absorption peak of human melanin is in the UV region, around 335 nm (Fig. 6) and is almost completely attenuated for wavelengths longer than 700 nm.

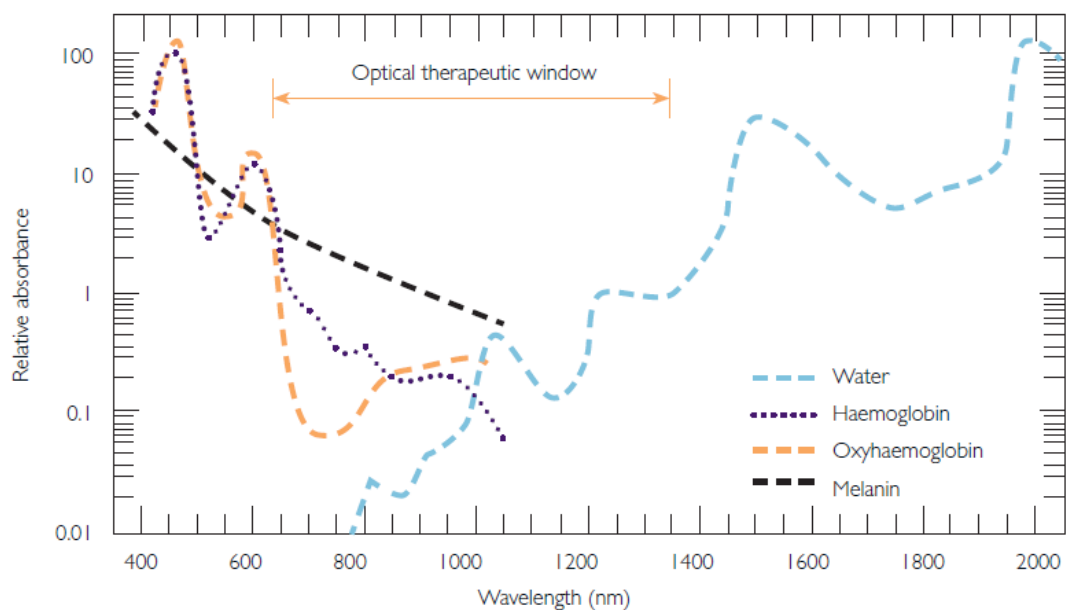


Fig. 6. Optical therapeutic window with reported some of the most important photoacceptors: water, haemoglobin, oxyhaemoglobin and melanin. From Schindl, *et al.*, 2000.⁸

1.1.5 Light-tissue interactions

Several studies were conducted in order to investigate the interaction between lasers and LED sources with targeted-tissue. Beyond the unlimited number of possible combination of the experimental parameters, three categories of interaction types are classified: i) photochemical interactions, ii) photothermal interactions, iii) photomechanical interaction (photoablation, plasma-induced ablation and photodisruption) (Fig. 7). The prevalence of one phenomenon strongly depends on irradiation conditions, and in particular on the light dose, i.e the power density and the interaction duration, that has to be compared with the thermal relaxation time of the tissue.¹¹ Thus, when developing clinical applications of lasers and LEDs, exposure energy, exposure volume, and exposure time shall be selected with very close attention.¹¹

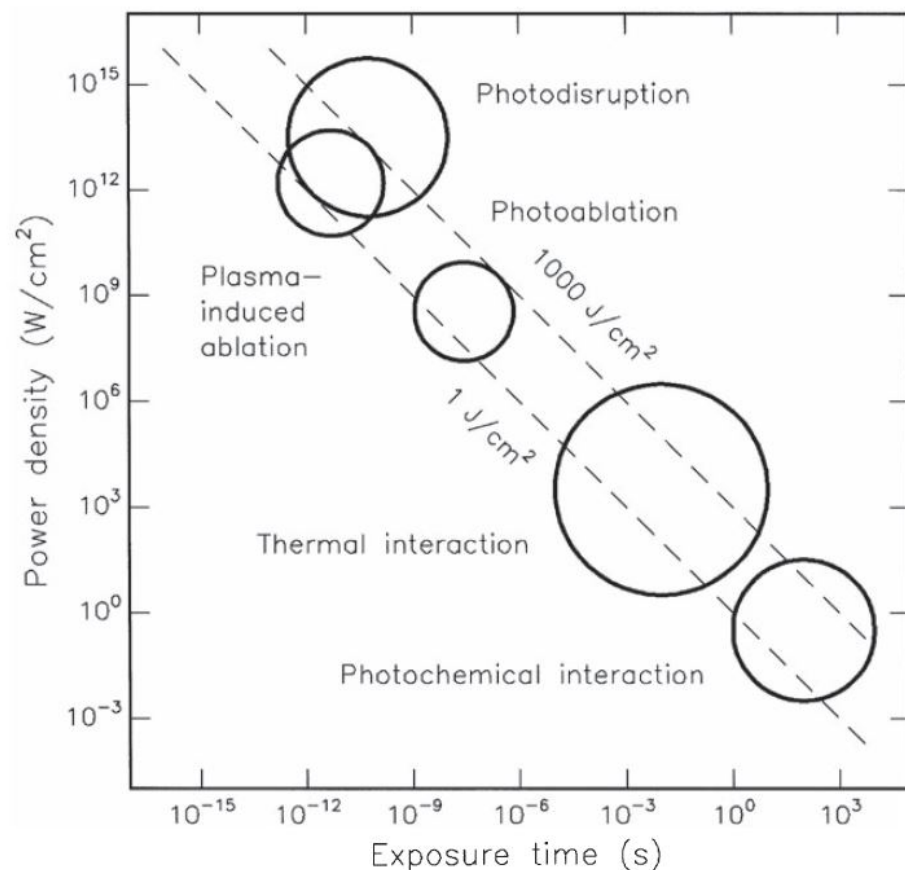


Fig. 7. Map of laser-tissue interactions. From "*Laser-Tissue Interaction fundamentals and applications*" Niemz, Markolf, 2nd edition, Springer. Modified from Boulnois (1986).⁷

Photochemical interactions

This kind of interaction was observed when the light induces chemical effects and reactions in tissues, just like occurs in photosynthesis. Clinically, this type of interaction plays a fundamental role in photodynamic therapy (PDT), a medical application which falls within the larger field of biostimulation.

A new application especially used in esthetic and dermatological fields is photobiomodulation therapy (PBMT), which is most consistently described in 1.3.

Photothermal interactions

In this group are included all the applications where it is possible to observe a local increase of temperature; in particular, depending on the duration and the peak value of the reached tissue temperature, different effects such as coagulation, vaporization, carbonization and melting can be observed. As concern medical applications, it is clear that the provided energy, and consequently the temperature increase, must be chosen very carefully in order to avoid irreversible tissue damages.

The first thermal effect that is observable at low temperature increase can be attributed to changes in molecules structure, in particular bonds destabilization and destruction, and in cells modifications, e.g. in membrane alterations. These kinds of modifications occur when the temperature ranges from 42°C to 50°C, in a state named hyperthermia. When hyperthermia state persists for several minutes, tissues become necrotic. From 50°C to 60°C, measurable reduction in enzyme activity is observed, resulting in reduced energy transfer within the cell. At 60°C, denaturation of proteins and collagen occurs, whereas, at 100°C, water molecules contained in most tissues start to vaporize. The large vaporization heat of water is advantageous since the vapour generated carries away excess heat and helps to prevent any further increase in the temperature of adjacent tissue. Due to the large increase in volume during this phase transition, gas bubbles are formed inducing mechanical ruptures and thermal decomposition of tissue fragments. When temperatures exceed 100°C, carbonization takes place and it is evidenced by

the blackening of adjacent tissue and the escape of smoke. Finally, beyond 300°C melting can occur, depending on the target material (Fig. 8 A and B).

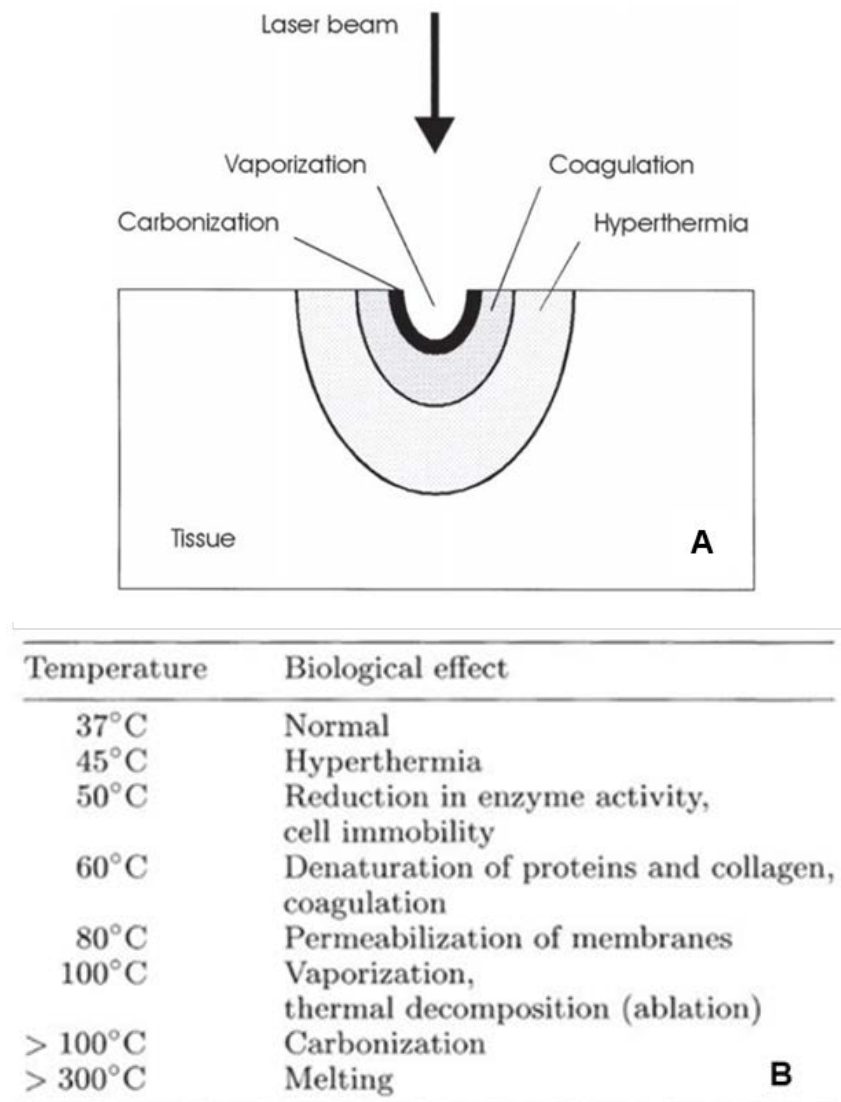


Fig. 8. **A:** Location of thermal effects inside biological tissue. **B:** Association with local temperature and tissue effects. From “*Laser-Tissue Interaction fundamentals and applications*” Niemz, Markolf, 2nd edition, Springer.⁷

Thermal damage not only depends on temperature but also on its temporal duration: e.g. 60°C lasting for at least 6 seconds, provokes irreversible damage. Carbonization, vaporization and coagulation induce irreversible tissue damages, whereas hyperthermia can be both irreversible and reversible process (Fig. 9).

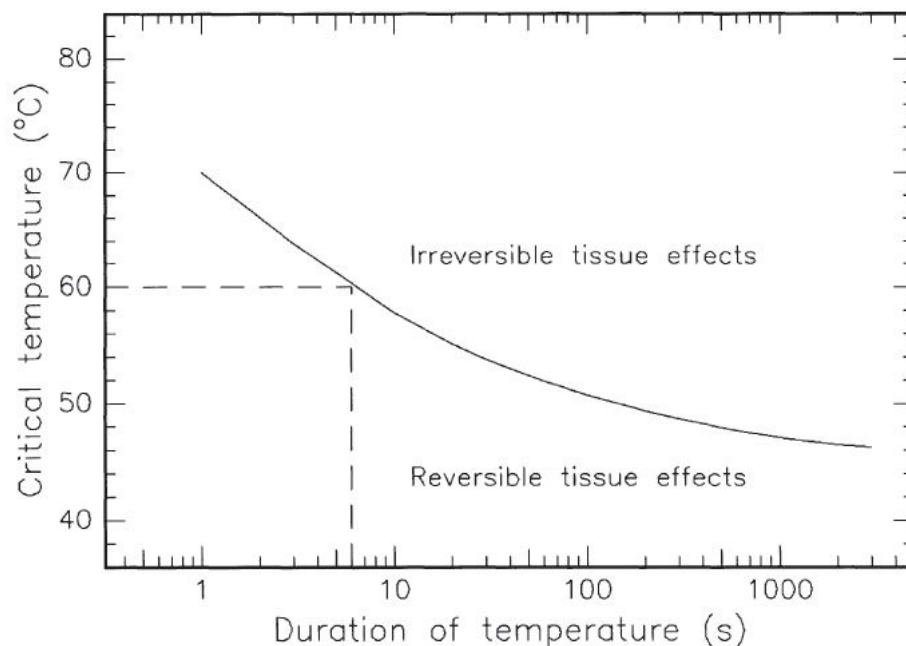


Fig. 9. The critical temperature for the occurrence of cell necrosis. From “*Laser-Tissue Interaction fundamentals and applications*” Niemz, Markolf, 2nd edition, Springer.⁷

Photomechanical interactions

Photomechanical effects become evident when short laser pulses are used to treat biological targets. As the laser pulse duration becomes shorter than a few microseconds, beside the purely thermal effects, there may appear significant photomechanical effects, such as pressure pulses propagating both in the air above the irradiated surface and inside the tissue. Depending on the type of interaction, the pressure pulse can be an acoustic pulse, i.e. a low pressure perturbation propagating at sound speed, or a shock wave, characterized by a high instantaneous pressure peak, propagating at ultrasound speed.¹¹

If tissue irradiation is performed under heat confinement conditions, very high temperatures may develop in a short time within a limited target volume, thus inducing significant photomechanical effects, such as fragmentation of hard tissues as kidney stones, or to enable highly precise cutting of tissues.¹¹

1.2 Effects of blue LED light: *in vivo* studies on wound healing

Ten years ago the research staff from the Biophotonics and Nanomedicine Lab (BPNLab) of the Institute of Applied Physics – Italian National Research Council, started a study on the effects of the blue light in wounds. The project was conducted in close collaboration with the European Laboratory of Nonlinear Spectroscopy (LENS) and the Small-Medium Enterprise Light4Tech.

The first step of the study was to estimate the optimal wavelength and treatment time, in order to obtain an immediate coagulation effect in bleeding wounds. To this aim, a modelling study of the photothermal process was set up. Using Finite Element Model (FEM) it was possible to study the temperature dynamics in the tissue and the characteristics of the device so that at the end of the theoretical study a compact blue LED light device was designed.

After the theoretical study, the identified parameters and light sources were tested on superficial dermoabrasions performed on the back of rats and a thermal camera was used to measure the superficial temperature: during the treatment a temperature enhancement of around 13°C was measured, confined in the bleeding surface. After irradiation, the treated wound regained a temperature below 45°C in about 10 seconds and no thermal damages were observed. Moreover, at eight days after surgery, all the abraded areas were healed (both LED-irradiated and control skin) and in 30% of the treated rats the photocoagulated areas had a reduced healing time when compared to the control areas in the same animal.¹²

The blue LED device was then further optimized (Fig. 10), thanks to the support of Regional and European fundings; the studies were focused on the capability of the blue light to improve the healing process.^{1,13-14-15-16-17-18-19}



Fig. 10. The blue LED light device developed in the framework of different regional and European projects, in order to study the effects of treatment in animal and human and to provide a marketable device.

1.2.1 Effects of blue LED light: *in vivo* animal model of wound healing

The first *in vivo* experiments set up with the purpose to investigate the improvement of the healing process was performed on four abrasions on the back of 10 rats.²⁰ In this experiment, the treatment time was set at 30 seconds, corresponding to a fluence of 20.6 J/cm²: the treatment was performed immediately after the lesion in two wounds, whereas the other two were left naturally recover (Fig. 11 A). After 7 days from the lesion, when the wounds were healed, four biopsies were harvested and the samples were subjected to a different analysis. By haematoxylin and eosin (H&E) staining, an early and complete recovery in the skin was evidenced in the treated wounds in respect to the untreated ones (Fig. 11 B), 7 days after the treatment: while in the treated wound group every layer of the epidermis was totally regenerated (Fig. 11 F), in the untreated group the stratum corneum was still to be formed (Fig. 11 G).

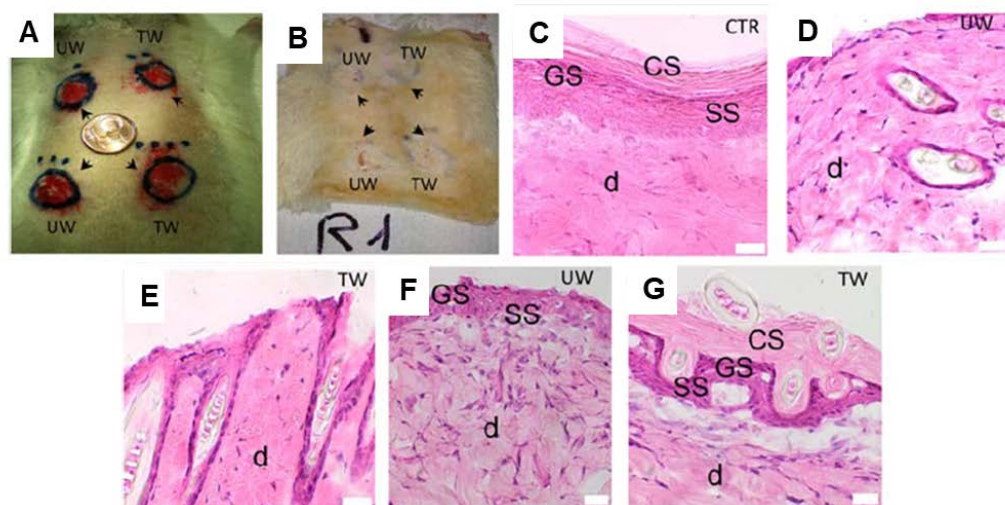


Fig. 11. **A:** Representation of different steps during the study of epithelialization: grossly evaluation of wounds soon after the treatment. **B:** Representation of different steps during the study of epithelialization: grossly evaluation of wounds 7 days after treatment. **C.** H&E images of control. **D, E:** H&E images of an abrasion evoked by initial treatment with a consequent disappearance of the epidermis in the untreated or treated wound. **F, G:** H&E images of the appearance of the epidermis in treated but not in the untreated wound. Corneum stratum (CS), granular stratum (GS) and spinous stratum (SS) are evident in **C** and **G**, only GS and SS in **F**. Modified from Cicchi *et al.*, 2016.²⁰

Similar results were obtained by the evaluation of the cellular infiltrate: the stained-section of the dermis in the untreated tissue showed a rich cellular infiltrate (Fig. 12 B-D) in comparison to the treated wound tissue which showed a significant decrease of inflammatory cellular infiltration (Fig. 12 C-E).²⁰

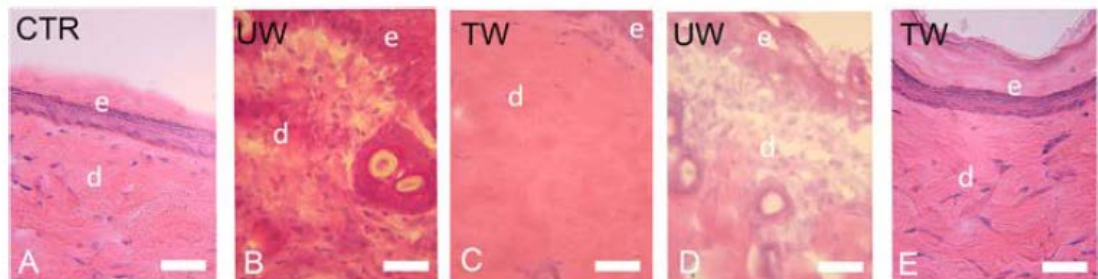


Fig. 12. Histological examination. **A**: H&E images of the subpapillary cell infiltrate in control. **B-D**: H&E images of the subpapillary cell infiltrate in the wounds. **C-E**: H&E images of the subpapillary cell infiltrate in the treated skin. In the images both epidermis (e) and dermis (d) are visible. From Cicchi *et al.*, 2016²⁰

The Authors demonstrated also that in the treated wound the number of fibroblasts and myofibroblasts were similar to that found in healthy skin (Fig. 13 A) but reduced in comparison to untreated wound (Fig. 13 B).

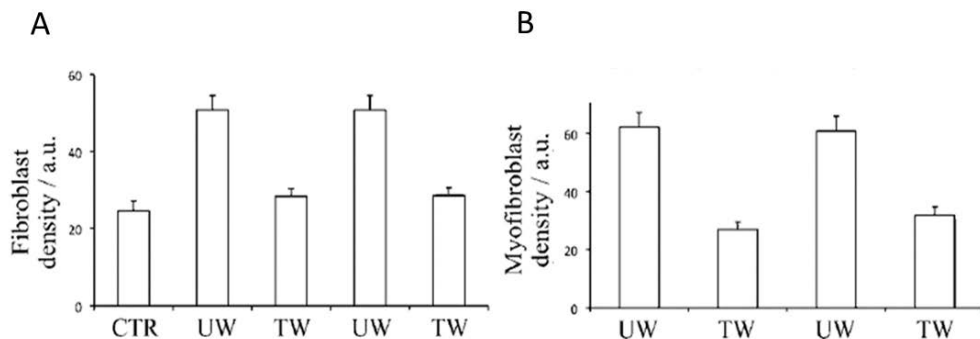


Fig. 13. **A**: Bar graphs representing mean \pm standard error (SE) of heat shock protein-47 (HSP47) in untreated or treated wounds. **B**: Bar graphs representing mean \pm SE of alpha-smooth muscle actin (α -SMA) in untreated or treated wounds. From Cicchi *et al.*, 2016.²⁰

Furthermore, by using two-Photon Fluorescence (TPF) microscopy coupled with Second-Harmonic Generation (SHG) microscopy it was possible to point out that collagen distribution is more sparse in the untreated wound area, whereas is more uniform in the treated wound area, where collagen almost fill the dermal space, as commonly occurs in the healthy dermis (Fig. 14 G)²⁰. Moreover, collagen orientation in the treated wound showed more

isotropic distribution of collagen fiber bundles with several intersections in comparison to the untreated wound where intersections are not clearly identifiable.²⁰

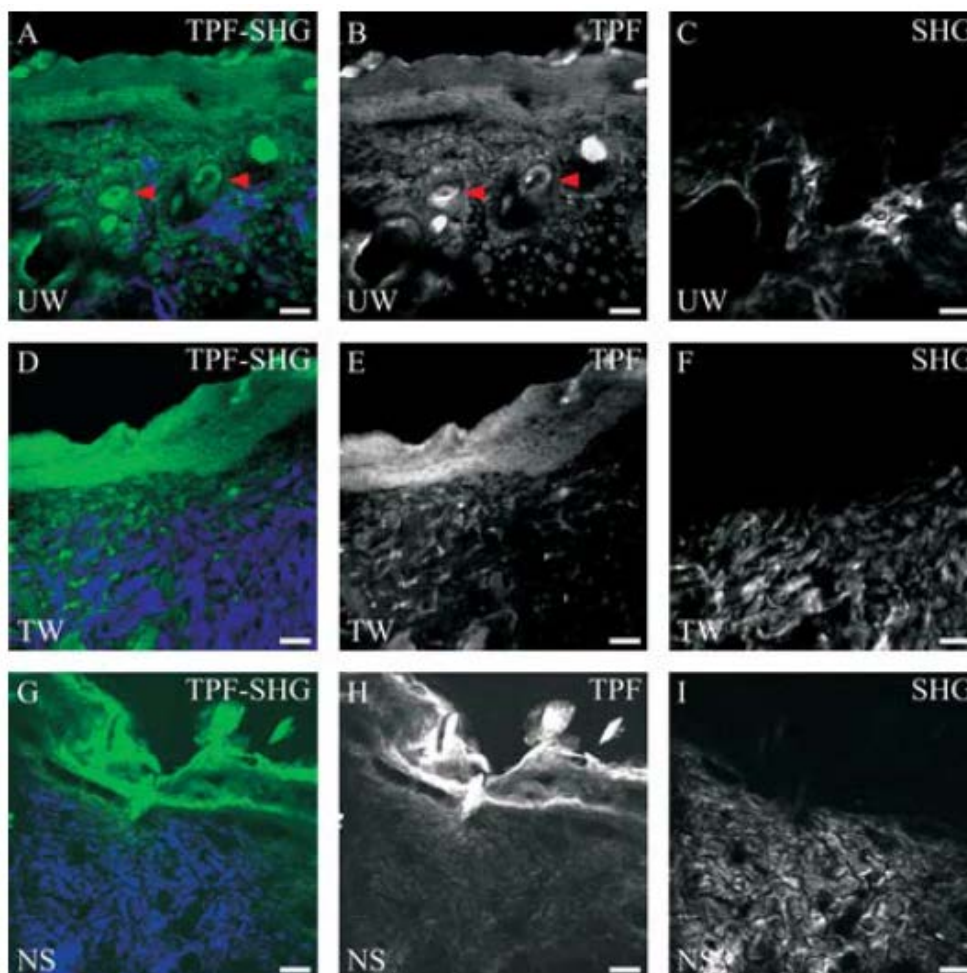


Fig. 14. Combined TPF-SHG imaging. **A, D, G**: Combined TPF-SHG images of thin tissue cross-sections excised from untreated wound areas (**A**), treated wound areas (**D**), and normal skin (**G**). Fluorescence is coded in green colour scale and SHG is coded in the blue colour scale. **B, E, H**: TPF images of thin tissue cross-sections excised from untreated wound areas (**B**), treated wound areas (**E**), and normal skin (**H**). **C, F, I**: SHG images of thin tissue cross-sections excised from untreated wound areas (**C**), treated wound areas (**F**), and normal skin (**I**). Scale bars: 40 μm . From Cicchi *et al.*, 2016.²⁰

All together, these results suggest that fibroblasts appear as a cellular type very sensitive to the blue LED light irradiation. Starting from these bases, part of the present study was dedicated to the investigation of the effects of the same blue LED light in human cultured fibroblasts cells isolated from keloid scars, a form of skin fibrosis.

1.2.2 Effects of blue LED in human chronic wounds

Recently, the results obtained by an Italian multi-centric study demonstrated the beneficial effects of the blue LED light on inferior limbs ulcers, unresponsive to standard care.²¹ In this study, the clinician applied a standard cleansing procedure to the lesion, and then the patient was treated with the blue LED light for 1 minute covering the entire wounded skin area.²¹ Soon after the blue LED light treatment, the appropriate medication and dressing for the type of lesion were applied according to the required standard.²¹ The blue LED light treatment on these patients was well accepted and tolerated, and there were no reports of side effects or other adverse events.²¹ Moreover, dermatologists reported the improvement of the wound bed, a reduction of the lesion depth and a revitalization of the perilesional skin with a general increase of patients compliance²¹ (Fig. 15).

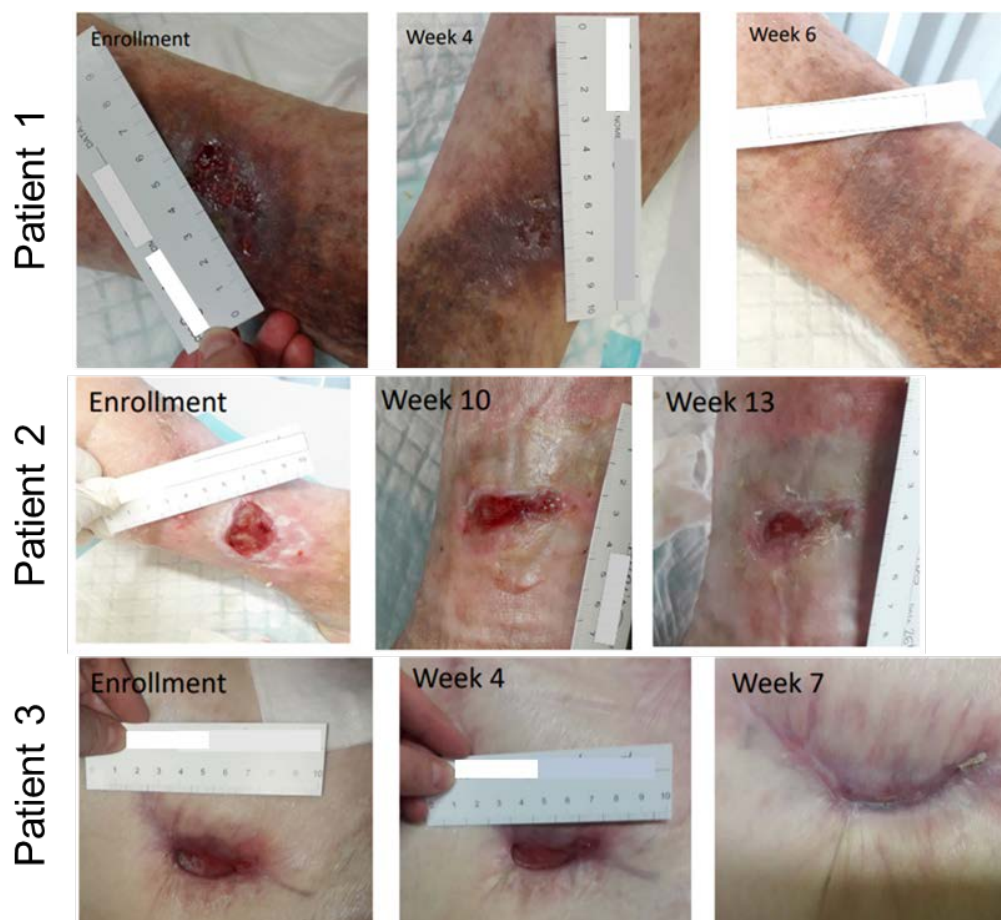


Fig. 15. Three patients treated with the blue LED light device. From Lasagni, *et al.*, "Blue LED light medical device therapy in the treatment of unresponsive leg ulcers: case series". Poster presented at the European Wound Management Association Congress 2019, Gothenburg, Sweden.

1.3 Photobiomodulation therapy

Recently, physical therapy regained an important role in the management of wounds, and new technologies and devices have been developed. “Physical therapy”, refers to the interaction between the wound and a physical system in which there is a transfer of energy to/from the wound and this can translate into observable and measurable modifications in the system as well as in the wound. Among these new therapies, shock waves, electromagnetic fields and photobiomodulation therapy are considered.

In 2015, the terms “photobiomodulation therapy” have been included in the Medical Subject Headings (MeSH) index of the National Library of Medicine.³ PBMT is defined as “a form of light therapy that utilizes non-ionizing forms of light sources, including lasers, LEDs and broadband light, in the visible and infrared spectrum. It is a non-thermal process which involves endogenous light-absorbing molecules (chromophores, see 1.1.4 paragraph) that elicit photophysical and photochemical events at various biological scales. This process results in beneficial therapeutic outcomes including, but not limited to, alleviated pain or inflammation, immunomodulation, and promoting of wound healing and tissue regeneration” (From the Journal of Wound Care vol 27 no 6 EWMA document 2018).³

Some authors reported that photobiomodulation, especially using a red light source, has also been shown to stimulate hepatocyte proliferation and metabolism,²²⁻²³ fibroblast proliferation, and wound healing²⁴ in animal models or human trials.²⁵

Although the underlying mechanisms of red light photobiomodulation are not well understood, it had been postulated that mitochondrial Cytochrome C Oxidase is activated due to its preferential absorption of red light,²³ and the increased cyclooxygenase (COX) activity leads to increase of adenosine triphosphates (ATPs), cyclic adenosine monophosphates (cAMPs), mitochondrial membrane potential, nitric oxide (NO), and calcium ion concentration.^{26-22-23,27} ATPs and cAMPs participate in G-protein-coupled receptor signalling pathways and activate the downstream cAMP-dependent protein kinase A, leading to upregulation of responsive genes.²⁷⁻²⁸

Among the several factors which influence the interaction between light and biological tissue, a fundamental role is played by the source of light. The light sources for medical purposes may be either LED or LASER. In the case of LED-generated light, the emission is not unidirectional while LASER-generated light is unidirectional and coherent, reaching much higher intensity with the same amount of energy, concentrating the area of application.²⁹

To exert its effect, light has to interact with the structures of our cells. Although there are still some controversies regarding the possible targets for this interaction, cytochrome C (Cyt C) oxidase appears to be the best candidate as the principal photoacceptor. This is due to its conformation with four possible sites of photoacceptance, the two copper centres (CuA and CuB) and the two iron centres (HemeA and HemeB). These are all involved in the transfer of electrons in the respiratory chain on the mitochondrial membrane of the eukaryotic cells.³⁰ Other candidates, possibly with complementary roles, are flavoproteins and porphyrins, which are implicated in the generation of reactive oxygen species (ROS) after an interaction with photons.³¹ In all these cases, and eventually, in the other cases, in which light may interact with biological structures, this has to be considered a so-called primary reaction.

The secondary reactions include the effects that the first interaction induces within the metabolism of the cells and the tissue by transduction and amplification of the original signal, leading to a photoresponse.³² Secondary reactions consist of the production of NO, the intracellular increase of ROS, the increase in permeability of cell membrane, the increase of intracellular calcium levels, the increase in cell metabolism, the increase of acids nucleic synthesis, fibroblast proliferation, activation of lymphocytes, macrophages and mast cells, and increased synthesis of interleukins and growth factors.³³

Photobiomodulation therapy has now accumulated evidence of positive action on all phases of wound repair from the first inflammatory phases to the remodeling phase.¹⁰

A non-secondary positive aspect of the PBMT is the reduction of the number of applications and the time required for effectively obtaining a therapeutic effect on wound healing, which allows for containment of the costs of management for these typically very costly chronic pathologies. This is both in terms of reduced use of antibiotics and of a better use of resources.³⁴

Despite the fact that the field of PBMT is one of the most stimulating and rich among the physical therapies for wound healing, some debates and reservations remain both from a methodological and a clinical point of view. There are numerous reasons for this: among them, the main reasons are referred to the partial understanding of the PBMT mechanism of action and the great variability as regards the use of the optical parameters in different studies that makes difficult the comparison between results.

1.3.1 Light in wound healing and in skin fibrosis

Currently, it is well documented that the treatment with red or infrared light with less than 200 mW/cm² irradiance and with wavelength in the range of 600 nm to 1000 nm promotes the repair process of the skin in experimental animal and human wounds.³⁵⁻³⁶⁻³⁷⁻³⁸ The evidence indicates that red and NIR light advance tissue repair by enhancing fibroblast migration and proliferation, collagen synthesis,³⁹⁻⁴⁰⁻⁴¹⁻⁴² and by modulating the timing and release of growth factors and cytokines, including basic fibroblast growth factor (bFGF), interleukin (IL)- 6 and IL-10.⁴³

At the same time, accumulating evidence indicates that light in the wavelength range from 400 to 480 nm, commonly referred to as blue light, is antimicrobial at long irradiation times, and has been shown to suppress *Staphylococcus aureus*, including methicillin-resistant *Staphylococcus aureus*,⁴²⁻⁴³⁻⁴⁴⁻⁴⁵ *Propionibacterium acnes*,⁴⁶⁻⁴⁷ *Pseudomonas aeruginosa*,⁴³ *Salmonella Entiriditis*, *Serovars*, *Typhimurium* and *Heidelberg*⁴⁸ and other bacteria.^{47,49-50} Also, blue light has been shown to improve tissue perfusion by the release of NO from nitrosyl complexes with haemoglobin in a skin flap model in rats.⁵¹ Since NO formation leads to vasodilatation and subsequent increase microcirculatory blood flow, the use of blue light might be of great importance for wound healing of diabetic and venous ulcers.⁵² Moreover, blue light has been shown to enhance angiogenesis⁵³ and to be anti-inflammatory.^{46,54}

These findings suggest that the combination of red/NIR light and blue light could promote healing and suppress wound infection simultaneously.

Other studies reported that VIS and NIR light can induce a significant and versatile range of changes in cell transcriptome, with numerous gene expression pathways affected, leading to alterations in proliferation, differentiation, and collagen production.⁵⁵⁻⁵⁶⁻⁵⁷⁻⁵⁸⁻⁵⁹⁻⁶⁰

However, the full spectrum of cell biological effects triggered by light still remains to be elucidated: the main reason is that they are highly dependent not only on the wavelength and dose of light but also on other biological factors such as the extracellular environment.⁶¹⁻⁶²⁻⁶³

One conclusion seems to be widely accepted: long VIS and NIR wavelengths are associated with neutral and stimulatory effects, while short visible wavelengths are most frequently reported to exert inhibitory effects.^{56,63-64-65} This statement is confirmed by several studies, in which blue light was applied *in vitro* experiments to analyze the effects on viability, metabolism, migration and proliferation rate and, in general, the effects on the wound healing process.

Mignon *et al.*,⁶⁶ demonstrated that repeated exposures to light at 450, 500, and 530 nm have a remarkably similar modal shape: an inhibitory phase, where metabolic activity was reduced to low- to mid-level doses ($\leq 30 \text{ J/cm}^2$), and a steep decrease of metabolic activity associated with cytotoxic effects at higher dose levels ($> 30 \text{ J/cm}^2$). The dose-response curve at 450 nm was qualitatively similar to a biphasic dose-response model with two inflexion points, i.e. a classical dose-response curve models from chemical drug research,⁶⁷ suggesting similarities between the action of light and chemical drugs on cells. Moreover, the obtained dose-curves had a very strong dependence on the energy of photons: the shorter the wavelength, the higher the impact on metabolic activity, at one fixed-dose parameter.

Studies conducted by Masson-Meyers group,⁶⁸ indicate that irradiation with 470 nm blue light at low fluences of 3, 5 and 10 J/cm^2 does not adversely affect healing in an *in vitro* scratch model of wound healing. Whereas fluences as high as 55 J/cm^2 may slow the rate of wound closure, lower fluences, such as 5 J/cm^2 promote cell migration and faster fibroblast repopulation of the scratch wound. Furthermore, fluences in the range of 3 to 10 J/cm^2 significantly diminished IL-6 concentration.

Chronic wounds and skin fibrosis are two sides related to an aberrant wound healing: they are often associated with abnormal cytokine profiles, which may interfere with Alpha-Smooth Muscle Actin (α -SMA) induction by Transforming Growth Factor Beta (TGF- β).⁶⁹ In addition, ischaemic and hypoxic conditions induced impaired myofibroblast differentiation.⁷⁰ As concern myofibroblasts, these cells are considered to be the final effector cell responsible for scarring, contraction and excessive collagen production,⁷¹ in all fibrotic conditions. Thus, blocking myofibroblast differentiation, proliferation and activity may represent a useful strategy for the prevention or reduction in pathological fibrotic conditions. Taflinsky *et al.*,⁷² demonstrated that myofibroblast differentiation can be blocked *in vitro* by blue light.

In vitro studies conducted by Mamalis *et al.*,⁵⁸ show that blue LED light at 415 ± 15 nm can inhibit fibroblast proliferation in a dose-dependent manner without causing significant effects on viability at fluences of 10, 15, 30, and 80 J/cm². These alterations in final cell count may have resulted from modulation of cell cycle, increase in autophagy, and/or apoptosis. Furthermore, the blue LED irradiation with fluences of 5, 30, 45 and 80 J/cm² decreased fibroblasts migration speed compared to matched bench control in a dose-dependent manner. This evidence takes on an important meaning in the pathogenesis of skin fibrosis.⁷³⁻⁷⁴ Specifically, the increased migration speed of fibroblasts may contribute to increased local recruitment of fibroblasts to the affected skin and recurrence or maintenance of fibrotic conditions.⁷³⁻⁷⁴

Soo Lee *et al.*,⁷⁵ demonstrated that irradiation at 410 nm light using 10 J/cm² fluence inhibited collagen synthesis in keloid fibroblasts *in vitro* and suggested that photobiomodulation might be effective in preventing keloid formation at the initial stage.

Taken all data together, it is quite difficult to compare various studies and truly discriminate the biological effects of different wavelengths within the visible light spectrum, considering all possible light sources.

1.4 Human skin: roles and structure

Skin is the largest organ of the integumentary system and covers the entire external surface of the human body. It is a dynamic, complex and regenerating organ that comprises about 15% of the total body weight.⁷⁶ Skin has a remarkable plasticity and provides key roles including protective functions such as mechanical, photoprotection and immunosurveillance, but it is responsible also of sensation, temperature regulation, and insulation from environmental agents.⁷⁷ Despite the constant exposure to physical, biochemical, and radiation injury, a functional integumentary system is able to counteract these forces and maintain a dynamic balance that leads to a relative state of homeostasis.⁷⁷

From the anatomical point of view, the skin is divided into three functionally interdependent layers: epidermis, dermis and hypodermis whose composition and thickness depend by anatomical site, the level of hydration and other factors including sex, age and ethnicity (Fig. 16).⁷⁸

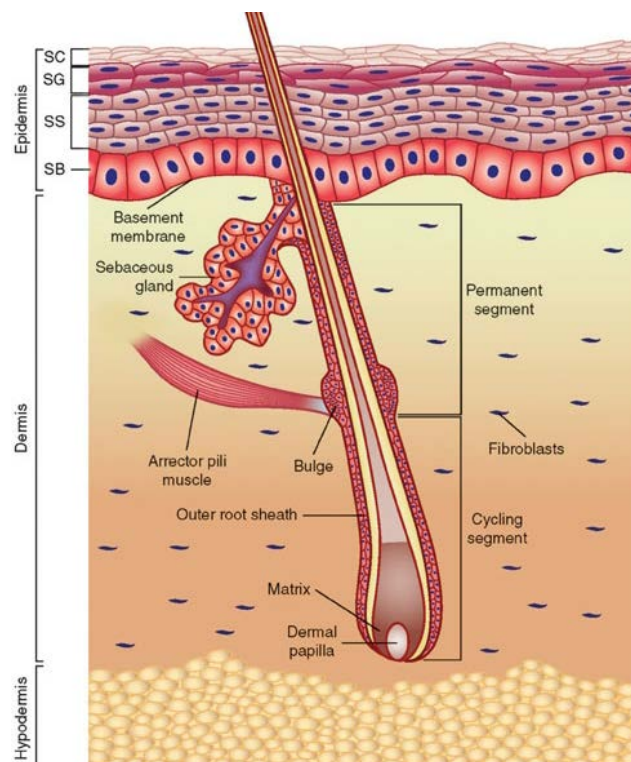


Fig. 16. Anatomy of the skin. Skin is composed of three layers, starting with the outermost layer: the epidermis, dermis, and hypodermis. The epidermis is a stratified squamous epithelium that is divided into four layers, starting with the outermost layer: stratum corneum (SC), stratum granulosum (SG), stratum spinosum (SS), and stratum basale (SB). Outer root sheath of the hair follicle is contiguous with the basal epidermal layer. Stem cell niches include the basal epidermal layer, base of the sebaceous gland, hair follicle bulge, dermal papillae, and dermis. From Wikicommons. Author: Wong, *et al.*, *Skin tissue engineering* (March 31, 2009). Derivative work: Anka Friedrich

1.4.1 Epidermal layer

The epidermis is a stratified squamous epithelium with a thickness varying from 0.04 mm on the eyelids to 1.6 mm on the palms and soles of the feet, with a turnover rate of about twenty-eight days.⁷⁶

The majority of the epidermis (at least 80%) is composed by keratinocytes. These cells originate from the basal layer and produce keratin, a protein responsible for the formation of epidermal water barrier by lipid secretion; moreover, keratinocytes also regulate the calcium absorption modulating the activation of cholesterol precursors. The remains of the epidermis consist in a small subpopulations of melanocytes (cells with neural crest origin that produce a pigment called melanin), the Langerhans cells (the first line defenders and dendritic antigen-presenting cells), and the Merkel cells (cells with both neuroendocrine and epithelial features that synapse with the unmyelinated dermal sensory axons that are sensitive to mechanical stimuli, especially pressure). In addition to the epidermal layer, there are three different types of appendages: the sweat glands (which serves as thermoregulators), the pilosebaceous follicles (that produce the hair and sebaceous excretions), and the nails which cover the distal phalanges.⁷⁹

The keratinocytes move progressively from the attachment to the epidermal basement membrane towards the skin surface; this event produces five histologically-subdivided layers: from the deepest portion, *stratum basale*, *stratum spinosum*, *stratum granulosum*, *stratum lucidum* and *stratum corneum*, the outer layer⁸⁰ (Fig. 17).

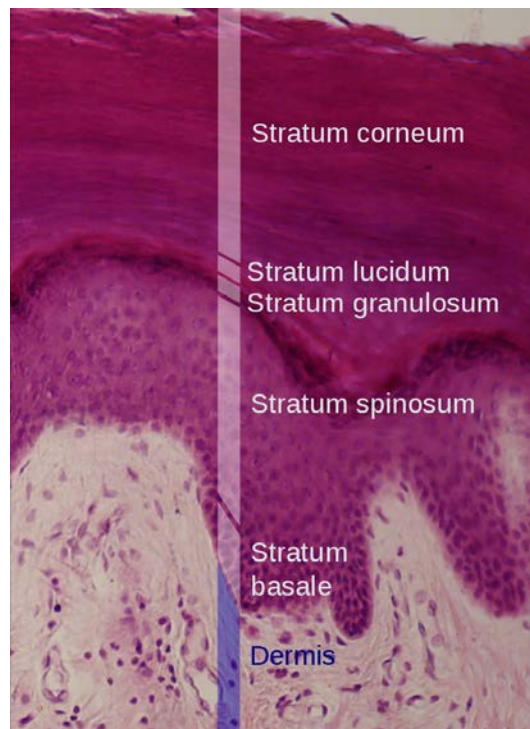


Fig. 17. Epidermidis subdivided into five layers and dermis. From the outer to deepest. *Stratum Corneum*, *Stratum Lucidum*, *Stratum Granulosum*, *Stratum Spinosum* and *Stratum Basale*. From Wikicommons. Author: Wbensmith.

1.4.2 Dermal layer

The dermis is an integrated system of fibrous, filamentous and amorphous connective tissue, it provides pliability, elasticity and tensile strength of the skin and overall is 15 to 40 times thicker than the epidermis, depending on the anatomic site. Structural components of the dermis are collagen, elastic fibers and extracellular matrix (ECM); moreover, the dermis houses the sweat glands, hair, hair follicles, muscles, sensory neurons, and blood vessels.⁸¹ Due to its architecture, the dermal layer governs the general mechanical behaviour of skin.⁸²

The principal component of the dermis is collagen with at least fifteen genetically distinct types in human skin. The predominant form of collagen that we found in the human dermis is type I collagen (about 70% of overall).⁸³

The dermis is connected with the epidermis by basement membrane and is composed of two histologically-identified layers: the papillary dermis and reticular dermis which merge together without clear demarcation. The papillary dermis is the superficial area adjacent to the epidermis; it is thin and has a

loosely arranged fine meshwork of connective tissue fibers. The reticular dermis is the deeper layer, it is thick, less cellular, and consists of dense connective tissue/bundles of collagen fibers much thicker and has coarser, more compacted connective tissue fibers that run in various directions, but in a general plane parallel with the skin surface.⁸⁴

In the papillary dermis there appear to be more fibroblasts than in the reticular dermis, and these papillary fibroblasts seem to be more active.⁸⁵ Recent studies have pointed out what accounts for the differences in the papillary dermis and reticular dermis:⁸⁶ the two layers of the dermis are formed by two different families of dermal fibroblasts. The first family of fibroblasts originated from the dermal papillae which regulate the growth of hair follicles and erector pili muscles, whereas the second family form the reticular dermis and the underlying adipose layer called hypodermis.

Reticular fibroblasts are generally described as being essentially quiescent despite exhibiting significant metabolic activity. This is in contrast to the papillary fibroblasts, depicted as potentially proliferative but less metabolically active.⁸⁶⁻⁸⁷ Additionally, while the reticular and papillary fibroblasts belong to the same histological cell type, they are known to have significant differences in functions reflected by their transcriptome.⁸⁸

As such, photobiomodulation might have a differential effect on these cell subpopulations, potentially leading to specific treatments targeting reticular and papillary fibroblasts differently: e.g. some evidence suggests that scarring occurs due to the dominant action of the reticular fibroblasts and suppressed activity of the papillary fibroblasts during the first wave of wound healing,⁸⁹ which highlights a need in differential treatment.

1.4.3 Hypodermal layer

The hypodermis is the innermost layer of the skin, and indeed it is named also “subcutaneous tissue”. This layer is composed by adipocytes, which originate from lobules of fat tissue, and house large blood vessels, nerves and hair follicle roots. The connective tissue is poor and the major part is involved in the separation of the fat lobules. The thickness is very different

among people and fully depends on nutritional habits and diet; moreover, also the distribution depends on the gender.⁹⁰

The principal function is fat storage and energy reserve: its adipocytes shrink or swell depending on the needs. Other important functions of the hypodermal layer are the regulation of the body temperature, by insulating the body, and the protection of bones, muscles and deep organs from external trauma. From a clinical point of view, the hypodermis represents an important route of drug administration.⁹¹

1.5 Classification of wounds

The “wound” is defined as an interruption of a typical anatomical structure and function.⁹²⁻⁹³⁻⁹⁴

There is no standard classification for wounds, but there are several ways in which wounds can be categorized. The issues of greatest relevance in the assessment are the following: i) the nature of the injury leading the wound, ii) the timing, iii) acute or chronic wound and iv) the depth of injury and underlying tissues involved in the wound.⁹⁵

1.5.1 Acute wounds

The term “acute” refers to those wounds such as burns, surgical and traumatic injuries that heal with a physiological healing process without interruption and in a relatively short time. In human, the inflammatory phase typical of acute wounds lasts for around two weeks and the recovery is full. The healed-tissue shows a characteristic scar consisting of newly synthesized type I collagen and lighter surface colour than the surrounding unwounded skin.

1.5.2 Chronic wounds

In this category of wounds, the inflammation persists for months or years and assumes the characteristics of chronicity. Some types of wounds which belong to this group are diabetic wounds, such as diabetic foot, and venous wounds, such as ulcers at the inferior limbs. These not-healing lesions

provoke a prolonged inflammatory response into the wound site and abrogate tissue repair.

Chronic inflammation often occurs when a wound is contaminated with pathogens or covered by foreign material that cannot be phagocytized or solubilized during the cellular response. The chronic inflammatory response may not be characterized by the canonical signs of inflammation, but in some cases, the body responds to the presence of persistent foreign material and possible infection by local proliferation of mononuclear cells. In particular, macrophages with ingested exogenous material become able to attract fibroblasts that produce collagen, leading to a slowly forming encapsulated mass of fibrous tissue, a granuloma.

1.5.3 Hard-to-heal wounds

The hard-to-heal, are wounds in which the standard management and appropriate care fail. In this case, the main objective is to identify as early as possible when a wound is slow to heal. Indeed, despite the advances and increasing knowledge in the healthcare and management of wounds, the clinicians often encounter wounds where the healing is prolonged or never achieved. This event depends by a complex combination and interaction of four factors, inside and outside the wound: i) patient-related factors, ii) wound-related factors, iii) healthcare professional and iv) resource treatment-related factors.⁹⁶ The last two factors are beyond the purpose of this work and are not further considered.

The patient-related factors are the issues that can affect the wounded patients, such as diabetes mellitus, obesity, malnutrition, old age, decreased perfusion, organ failure etc; all these factors can delay the healing process.

Among the wound-related factors, which can increase the failure of the typical care, we found: wound healing duration and/or senescence, size, wound bed condition, ischemia, inflammation and/or infection, anatomical site and treatment response. In particular, the measurement of the area and depth of the wound, by evaluating the epithelial advancement (also called “wound edge effect”) is important to predict potentially hard-to-heal wounds.

1.6 The wound healing

From a clinical point of view, a wound can manifest itself with several different appearances: from a simple break in the epithelial integrity in the skin, such as a scratch, until an injury at subcutaneous tissue, with damages to other structures, not only muscles, tendons and vessels but also organs.

Skin represents a protective barrier against several environmental agents: for this reason, solution of continuity in it must be repaired in a fast and efficient way; indeed, a loss of integrity of skin or deficiency in wound closure leads to severe pathologies and even death.

Wound healing is a dynamic and complex process, but at the same time interactive and it is composed of four coordinated and overlapped phases i) haemostasis, ii) inflammation, iii) proliferative stage and iv) tissue remodeling (Fig. 18). In each of these phases, different types of cells, several kinds of soluble mediators, blood cells, extracellular matrix and tissues play a fundamental and established role (Fig. 19).

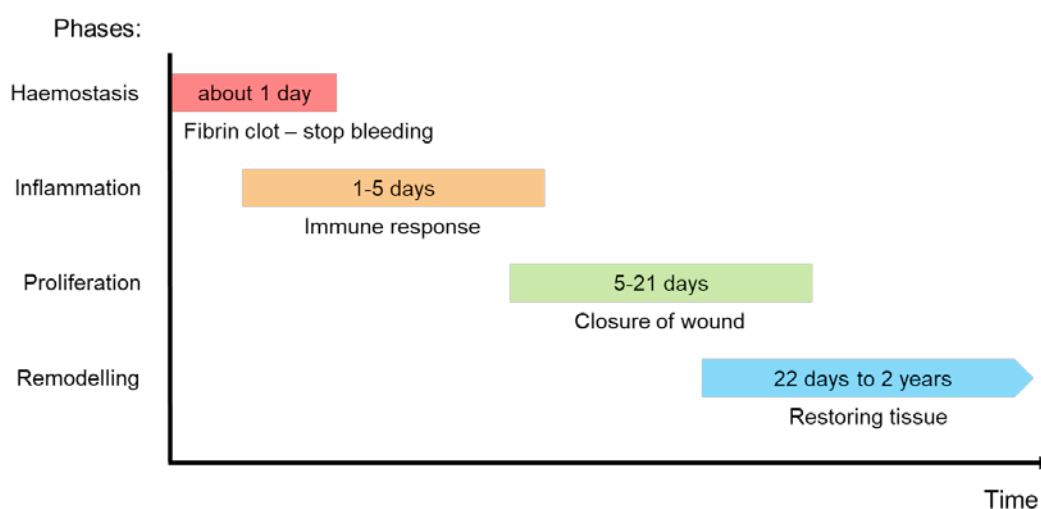


Fig. 18. Physiological wound healing phases

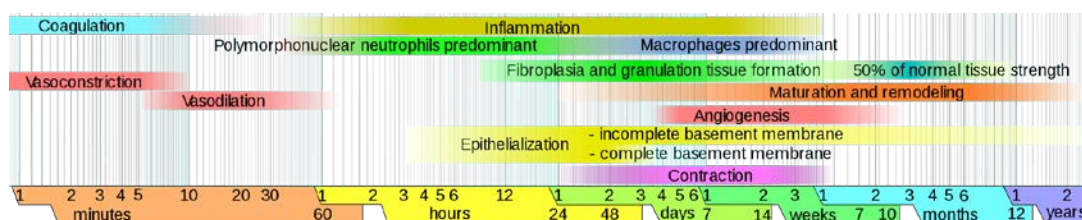


Fig. 19. Phases of physiological wound healing. Limits vary within faded intervals, mainly by wound size and healing conditions. From Wikicommons, Author: Häggström, 2014.

Beyond the canonical description of the wound healing process, it's a matter of fact that the process of repair starts immediately after an injury, independently on injury site and that all wounds go through similar phases of healing. Only specialized organ such as the liver and the eye, or tissue such as the skeletal tissue have distinctive forms of regeneration and repair and follow a separate pathways.⁹⁷⁻⁹⁸⁻⁹⁹

1.6.1 Haemostasis

Usually, a tissue injury provokes blood vessels damage, their disruption and haemorrhage, resulting in extravasation of blood constituents; the haemostasis is the physiological process to induce stop bleeding after wound injury (Fig. 20). Haemostasis is a highly adaptive and self-defence process having two principal aims: the one is preventing the exsanguination, protect the vascular system keeping it intact and avoid damage to vital organs throughout the formation of an aggregate of thrombocytes and platelets in a fibrin network. The second aim is providing a matrix for invading cells that are needed in the later phase of healing¹⁰⁰⁻¹⁰¹⁻¹⁰² and, at the same time, forming a barrier against the invasion of microorganism.¹⁰³ The phase of haemostasis is divided into three distinct part: i) primary haemostasis, ii) plasma coagulation and iii) fibrinolysis.¹⁰⁴

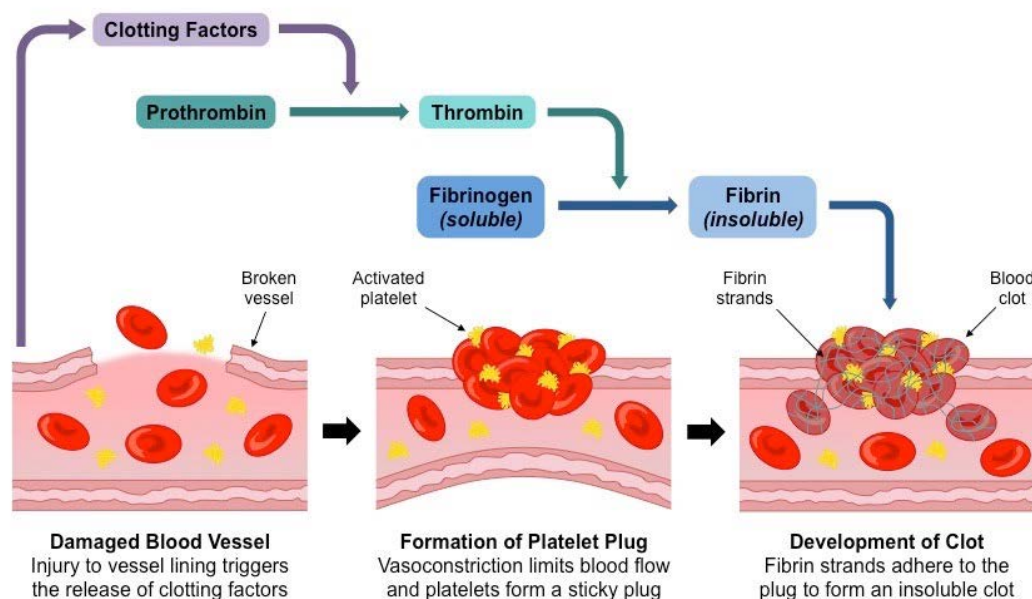


Fig. 20. The platelet activation, the formation of platelet plug and its development in a clot. From <http://ib.bioninja.com.au>.¹⁰⁵ Author: Cornell, B.

Primary haemostasis is the result of numerous and complex interactions among the vascular walls, platelets and adhesive proteins (Fig. 19-20). The vascular wall is a non-interrupted monolayer of hexagonal endothelial cells, which controls selective exchanges between blood molecules and extravascular tissues.¹⁰⁶ The luminal surface of blood vessels shows antithrombotic properties, such as i) expression of negatively charged heparin-like glycosaminoglycans, ii) synthesis, exposure and secretion of platelet inhibitors and iii) coagulation inhibitors and fibrinolysis activators. In case of activation, usually by thrombin or inflammatory cytokines, endotoxin or hypoxia, the antithrombotic properties of endothelial cells convert to prothrombotic ones, characterized by i) exposure of anionic phospholipids on the outer of the cell membrane, ii) secretion of platelet-activating agents, exposure of coagulation factor receptors and secretion of inhibitors of fibrinolysis.¹⁰⁴ By contrast, the layer underlying the endothelium contains highly thrombogenic components and other molecules involved in platelet adhesion.

After an injury, the muscular contraction in the endothelial layer is the first response which compromises the integrity of blood vessels (Fig. 20). At the same time, activated platelets adhere to various substrates, such as

collagen exposed to blood, fibrin and atherosclerotic plaques. After platelets adhesion, a series of events that lead them to shape-modified are started: from discoid, platelets became spherical, the internal granules migrate at the centre of platelet and pseudopodia emerge to help the anchoring of the platelets to substrate on the endothelial wall. In the granules, platelet synthesizes several pharmacological-active molecules, such as thromboxane A₂ and platelets-activating factor: these molecules can bind to a specific receptor site on the membrane of other platelet and allow a new platelets recruitment.

The fundamental event that leads to platelet aggregation and fibrin clot forming, is the expression and activation of GPIIb-IIIa receptors, which can bind fibrinogen, a precursor of fibrin molecule.¹⁰⁷ During this time, the phospholipids on platelets membrane translocate and negatively charged of phosphatidylserine is expressed on the outer membrane: these negative charges create a catalytic point on platelet membrane surface to stimulate the coagulation factors to work.¹⁰⁸ Moreover, the accumulation of phosphatidylserine induces an increase of microvesicles release which probably plays a role in the disseminating platelets procoagulant activity.¹⁰⁹

The modifications occurred in platelet contribute to induce plasma coagulation by coagulation cascade. This event is more complicated and there exist two distinct ways that gather at the end: extrinsic and intrinsic pathways.

Many pathologies can lead to a coagulation disorder acting on one of these ways or both, however, the plasma coagulation is finely regulated by some factors, mainly synthesized in the liver and circulating in the bloodstream as zymogens. The inactive zymogens can be processed by a specific enzyme with serine-protease cleavage activity that leads the molecule into an active form: e.g. the conversion of prothrombin in thrombin and the polymerization of fibrinogen into fibrin, both necessary to form the haemostatic plug. Moreover, some of these factors need vitamin K to be fully active.¹⁰⁴

The last step of haemostasis is fibrinolysis. This is an enzymatic process leading to fibrin clot solubilization by plasmin originating from fibrin bound plasminogen.¹¹⁰ Plasminogen is synthesized by hepatocytes and has a high affinity for fibrin, through peptidic loops called "kringles". Plasmin is generated by cleavage of a peptide bond by plasminogen activators. The principal plasminogen activator is tissue plasminogen activator (t-PA or PLAT),

which also exhibits two kringle loops. The fibrinolytic system is not only able to proteolyze fibrin clots but also plays a critical role in vessel wound repair, in the remodeling processes and in angiogenesis, through the degradation of the ECM.

In the cytoplasm, platelets contain α -granules filled with growth factors and cytokines, such as TGF- β , platelet-derived growth factor (PDGF), epidermal growth factor (EGF) and insulin-like growth factors (IGFs).⁹⁷ These molecules act as promoters in the wound healing process by triggering and attracting neutrophils, macrophages, endothelial cells and fibroblasts.¹⁰¹⁻¹⁰²⁻¹¹¹ Platelets also contain vasoactive amines, such as serotonin, that cause vasodilation and amplified vascular permeability and the migrations of cells and growth factors in the site of the lesion.¹¹²⁻¹¹³

1.6.2 Inflammation

The cellular inflammatory response in wounds follows the haemostasis step and coincides with the classical signs of inflammation: swelling, redness and heat.¹¹⁴ It is a highly ordered process orchestrated by numerous cytokines, growth factors and cells types, including neutrophils, leukocytes, macrophages and fibroblasts. The inflammation process aimed at destroying pathogens, fighting local infections and phagocytosing local debris and damaged connective tissue, with the purpose to restore healthy functional conditions and improve wound healing outcomes.¹¹⁵⁻¹¹⁶⁻¹¹⁷ The inflammatory response is divided into two distinct separate phases: an early inflammatory and late inflammatory phase.⁹⁸

The early inflammatory phase starts when haemostasis is near to the conclusion. This step has several functions, the first of which is the recruitment of neutrophils in the site of the lesion. Neutrophils are attracted in the wound site within 24-36 hours after injury and play the fundamental role to phagocytise bacteria and remove not only the residue of damaged tissue but also exogenous fragments (Fig. 21). The main chemoattractive agents including TGF- β , some peptides generated by bacteria and platelet products.¹¹⁸ In this early phase, the adhesion molecules on the neutrophils surface are subject to alterations: the cells become sticky and can adhere to

the endothelial cells surrounding the wound.⁹⁷⁻⁹⁸ After that, the neutrophils roll along the endothelium driven by the blood flow. Both adhesions and rolling mechanisms are led by selectin-dependent interactions that provoke a weak attachment.⁹⁸⁻¹¹² This event induces the endothelial cells to secrete chemokines that quickly stimulate a stronger adhesion of neutrophils, in this case, integrins-mediated⁹⁹⁻¹¹² neutrophils break rolling and migrate out of the venules, squeezing between the endothelial cells by a process named “diapedesis”. The neutrophils activity progressively reduces within a few days after injury and at the end of their activity, the residual neutrophils are eliminated from the wound both by apoptotic mechanism and phagocytosis by macrophages.¹¹⁹⁻¹²⁰⁻¹²¹⁻¹²²⁻¹²³

Another important type of cell which plays a pivotal role in this phase are the mast cells. Mast cells are essential not only in inflammatory phase but also in haemostasis, angiogenesis, fibroblasts proliferation, wound contraction and remodeling. In the inflammatory phase, resident mast cells released chemokines and cytokines that are important to recruiting neutrophils and monocytes,¹²⁴ while, in early wound healing, during their degranulation process, are responsible for the release of histamine, prostaglandins and leukotrienes. Histamine acts on histamine receptor 1 and provokes the dilatation of arterial and increased permeability of venules,¹¹⁴ leading to increasing the infiltration of neutrophils and other inflammation mediators.¹²⁵ Mast cells are also implicated in disease processes where there is excessive fibrosis of the dermis where it resides, such as scleroderma¹²⁶ and hypertrophic scars.¹²⁷

Late inflammatory phase began at 48-72 hours after lesion when macrophages appear in the wound site attracted by several chemoagents, (Fig. 21) such as TGF- β , PDGF, Tumor Necrosis Factor-alpha (TNF- α) and IL-4 and IL-13. Macrophages released a potent tissue growth factors, in particularly TGF- β , transforming growth factor-alpha (TGF- α), heparin - fibroblasts growth factor (FGF) and activated keratinocytes, endothelial cells and fibroblasts.¹²⁸⁻¹²⁹⁻¹³⁰⁻¹³¹

Macrophages are heterogeneous and versatile cells; during healthy conditions, resident macrophages play a key role in tissue development, in the immune response to pathogens and surveillance about tissue changes,

maintaining the homeostasis.¹³² On the basis of the genic expression profile, macrophages can be classified into two distinct subpopulations: M1 or “classically activated” and M2 or “alternatively activated”. The M1 phenotype is characterized by the expression of high levels of proinflammatory mediators and cytokines, such as IL-1 and TNF- α . Moreover, shows also a high production of reactive nitrogen and oxygen intermediates and promotion of T-helper1 (Th1) response.¹³³ After the acute phase of tissue injury, M1 phenotype switch in M2 thanks to the signalling mediated by IL-4 and IL-13, also recognized as immunomodulatory and profibrotic signal.¹³⁴

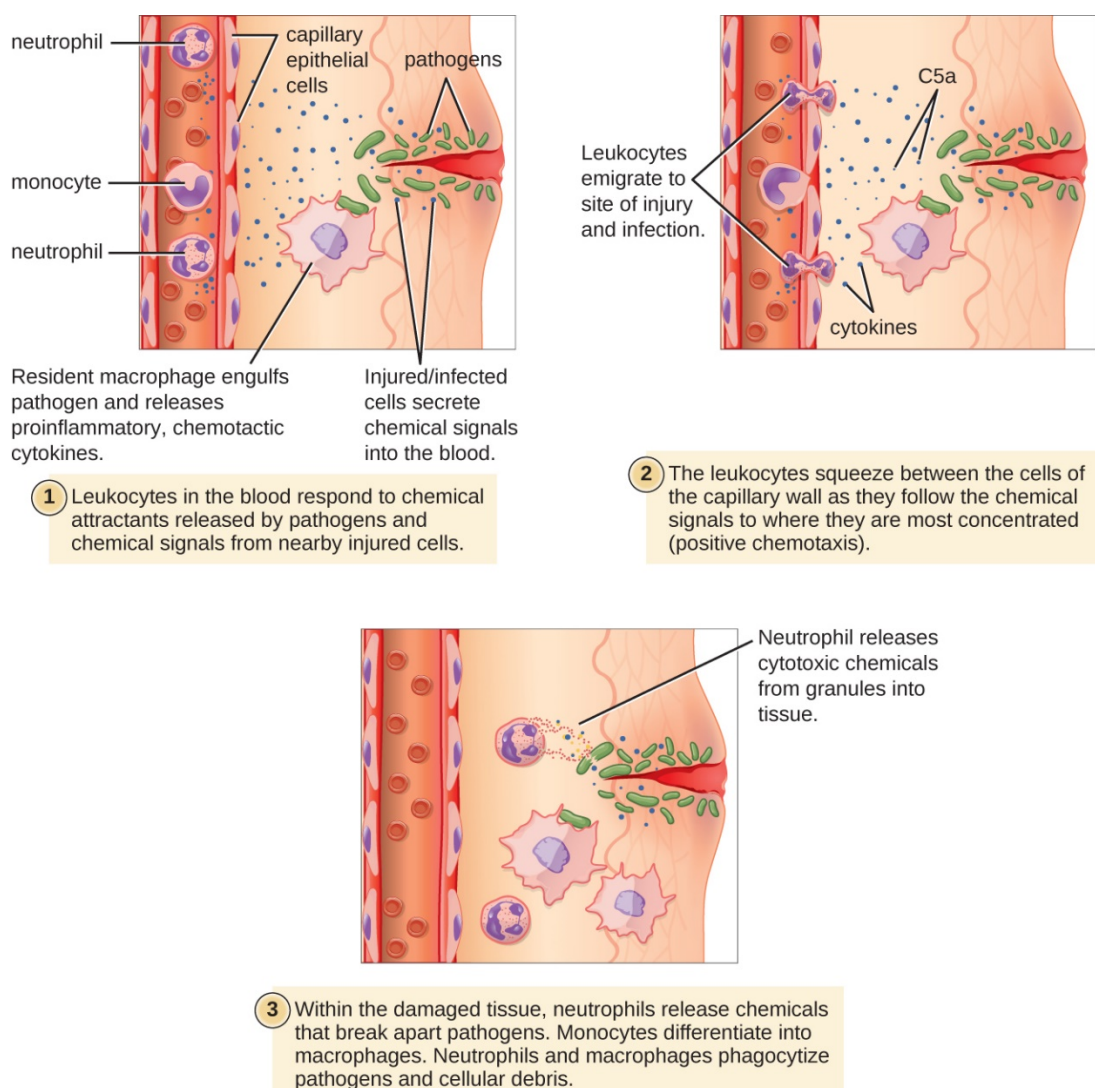


Fig. 21. Summary of early inflammation phase, with activation of leukocytes, neutrophils and macrophages. From Wikicommon.

1.6.3 Proliferative phase

The proliferative phase starts on the third day after injury and lasts for the two weeks thereafter; during this time the wound goes towards tissue repair. The main events that occur in this stage are i) the restoring an intact epidermis after injury, in a process named reepithelialization, ii) the establishment of adequate blood source through angiogenesis and iii) the strengthening of the injured dermal tissue (named fibroplasia).¹¹⁴ (Fig. 19).

Re-epithelialization is a complex process that involves several steps, including the migration of keratinocytes into the wound, their proliferation and the differentiation in a stratified epidermis. About 12 hours after injury, keratinocytes are subject to several events, such as changes in shape, expression of lamellipodia, loss of cell-to-cell junctions and matrix contacts; moreover, during the migration, keratinocytes inhibit their proliferative potential. Using the integrin receptor on the surface, keratinocytes are able to connect with the temporary fibrin matrix; throughout this time, keratinocyte produces metalloproteinases (MMPs), a proteolytic enzyme, in particularly MMPs-9 and MMPs-1, which are able to degrade type IV collagen and laminin in the basement membrane.^{114,135} Once reached the wound site, keratinocytes recover their proliferation activity, stimulated by EGF, keratinocytes growth factor (KGF) and TGF- α .

Dermal reconstitution begins approximately four days after damage and it is characterized by granulation tissue formation, angiogenesis and fibroplasia, the accumulation of fibroblasts.

Fibroplasia is described such as a process in which fibroblasts proliferate and migrate into the fibrin clot, where they produce new collagen and other matrix protein to originate the granulation tissue. The collagen deposition is performed by an activated phenotype of fibroblasts: the myofibroblasts, specialized contractile cells characterized by the expression of α -SMA, a splice variant of fibronectin.^{117,136-137} These cells can migrate in the wound site from the healthy surrounding tissue attracted by TGF- β and PDGF released in the previous phases.¹³⁰

Fibroblasts cells are responsible of the type III collagen deposition, in order to synthesize the granular tissue, a new and temporary stroma, that will

be substituted with a definitive new ECM composed by type I collagen.¹⁰³ Around two weeks after damage, the remodeling of the ECM starts. During this time, excess collagen fibers are removed and the residual are re-organized in order to promote wound contraction.^{92,138} Initial collagen degradation is performed by collagenase enzyme and, after partial degradation, collagen fragments undergo additional breakdown by MMPs. These enzymes are secreted by fibroblasts, macrophages, endothelial cells and epidermal cells. Elevation in MMP levels may lead to excess collagen breakdown, resulting in the development of chronic wounds.¹³⁹⁻¹⁴⁰ Another way to reduce the fibroblasts in excess is via the apoptotic way. Dysregulation of these processes occurs in fibrotic pathologies, such as keloids, scleroderma and morphea.¹⁴¹

Another important event achieved in this third phase of the wound healing process is angiogenesis, a growth of new vessels by the sprouting of preexisting ones in the healthy tissue adjacent to the wound. Several pro-angiogenic factors, such as FGF, vascular endothelial growth factor (VEGF), PDGF and other ones, are released during the haemostatic and inflammatory phase and act on endothelial cells. All these factors give a contribution to promoting endothelial cells proliferation and their migration in the wound site.¹⁴²⁻¹⁴³⁻¹⁴⁴⁻¹⁴⁵⁻¹⁴⁶ The endothelial cells can produce proteases in order to degrade the basal lamina of the vessel, induce chemotaxis, proliferation from an injured surrounding vessel, differentiation and remodeling. After these series of events, within a few days, a new microvascular network composed of several capillaries is originated. Newly formed vessels participate in granulation tissue formation and provide nutrition and oxygen to growing tissues.¹¹⁴

1.6.4 Remodeling phase

Remodeling phase is the last stage of the wound healing process, in which a new epithelial layer is synthesized and scar tissue is formed. The synthesis of the new ECM is has begun in the previous phase, and correspond with the granulation tissue production.

The remodeling of the wound is closely controlled with the purpose of preserving a delicate equilibrium among degradation and synthesis, leading to

normal healing. The collagen degradation process is due to the MMPs enzymes, produced in the previous phases not only by neutrophils and macrophages, but in particular from fibroblasts cells. The activity of MMPs are finely regulated and are significantly involved also in ECM remodeling.

The bundles of initial collagen deposition are highly disorganized and the new collagen matrix becomes more and well oriented over time. Towards the final step of the remodeling phase, the wound completes the contraction and the underlying connective tissue allows the closing of the wound edges of the wound. This process is regulated by several factors, such as PDGF, TGF- β and bFGF.¹⁴⁷⁻¹⁴⁸⁻¹⁴⁹

When the wound healing process reaches the end, the density of fibroblasts and macrophages is reduced by apoptosis, the growing of capillaries is blocked, blood flow to the area decays and metabolic activity at the wound site decreases.^{147,150-151} Collagen fibers can recover nearly 80% of the original strength compared with unwounded tissue and the final strength depends on the site of the repair and its duration, but the original strength of the tissue can never be regained.¹⁴⁷⁻¹⁴⁸

The end of the remodeling phase is a fully matured scar with a decreased number of cells and blood vessels and a high tensile strength¹⁵² (Fig. 19).

Clinically, this phase is manifested as a palpable softening of the scar and the changing of its hue from pink to pale.^{117,153}

1.7 Fibrosis

As described above, after skin wounding, the repair begins immediately. Several factors can bring to interferences with the healing process and when the fragile equilibrium of the reparative process has been disturbed, the wound healing process can migrate towards two radically different extremes. On the one hand, in the poor healing process, the injury stops the restorative development and becomes a chronic wound or classified such as a hard-to-heal wound. On the other hand, in excessive healing, an exaggerated matrix deposition can lead to scar ranging from hypertrophic scar to keloid⁹⁴ (Fig. 22).

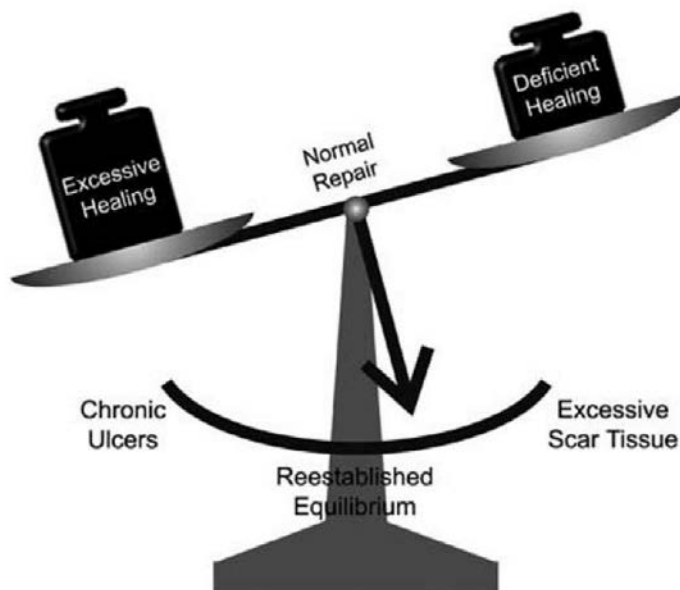


Fig. 22. Any disturbance of the delicate balance of normal wound repair leads to a disruption of anatomical structure and function. From Bran *et al.* 2009.⁹⁴

Fibrosis is described as the degeneration of connective tissue in which excessive accumulation of fibrillary, collagen-rich ECM replaces functional tissue, can occurs in organs or body tissues not only after lesion but also subsequently to a pathologic condition. In both cases, the typical structure and architecture about organs parenchyma or tissue are subject to changes and accompany a loss of function.¹⁵⁴⁻¹⁵⁵

Even if we gained a great knowledge about fibrotic disorders and their several effects, the mechanisms of fibrosis are still partially unclear and the need for anti-fibrotic treatment remains. Despite that, the hypothesis on the general mechanism of fibrosis are reported in the scientific literature: the principal mechanisms are described in the followings. The injured cells recruit several regulators of fibrosis such as cytokines, chemokines, PDGF, VEGF and caspases. These regulators recruit endogenous cells such as neutrophils, macrophages, T and B-lymphocytes that release profibrotic growth factors, for instance, TGF- β , PDGF and connective tissue growth factor (CTGF).¹⁵⁶

T helper cells, also known as CD4⁺ cells or Th cells, produce some cytokines and were the first to be documented to have strong profibrotic features. Typical cytokines released from Th-2 cells are IL-4, IL-5, IL-10, IL-13 and IL-21. Four of them, IL-4, IL-5, IL-13 and IL-21, are related to fibrosis

development. Moreover, IL-4 cytokine is closely associated with myofibroblasts collagen deposition to form ECM.¹⁵⁶⁻¹⁵⁷

Myofibroblasts are the key cellular mediator of fibrosis and are activated not only by cytokine but also by paracrine signals derived from i) lymphocytes and macrophages, ii) autocrine molecules released by the same myofibroblasts and iii) pathogens-associated molecular patterns produced by pathogenic organisms that interact with toll-like receptors on fibroblast cells. Myofibroblasts can be derived from multiple sources. Today two mechanisms are known: the epithelial-mesenchymal transition (EMT) and, most recently, endothelial-mesenchymal transition (End-MT). Moreover, fibroblast-like cells derive also from bone marrow stem cells and expressed a myofibroblasts-phenotype.

This scenario suggests that several subpopulations of myofibroblasts exist, and these are activated and/or recruited by different pathways that involve cytokines and play a fundamental role in different fibroproliferative disease. The possibility to interrupt their development, activation or enrollment, could be a potential therapeutic approach in the treatment and management of various fibrotic diseases.¹⁵⁶

1.7.1 Fibrosis in skin

The basics of wound healing process appear to be deciphered, but the precise mechanism in which the wound healing process is regulated is still enigmatic.

In adult human wounded tissue, the normal repair occurs when there is a re-established equilibrium between scar formation and scar remodeling: in healthy subjects, this reaction represents the typical response to skin injuries. The perfect scar should be comparable to a thin line with a similar pigmentation about to the neighbouring unwounded tissue.

From a clinical point of view, scars ranging from asymptomatic to scars with evident issues may be accompanied by functional limitation and frequently cause significant cosmetic problems.

Scars are categorized in plastic surgery literature describing main groups of wounds ranging from normal mature scars to major keloids, with

linear and widespread hypertrophic scars placed somewhere near the middle.⁹⁴⁻¹⁵⁸⁻¹⁵⁹ Despite the obvious clinical manifestations, pathological and biochemical differences, hypertrophic scar and keloid remain a therapeutic challenge. Until a few years ago, was popular to think that hypertrophic scars and keloids represent two different manifestations about the same skin problem and the terms were often used interchangeably.

Actually, as concern the scar management, one of the first challenges is the differential diagnosis, clinical instruments to clearly define the hypertrophic scar from keloid, in order to apply specific clinical approaches.

There are also other fibrotic pathologies that affect the skin, such as systemic sclerosis and scleroderma, but they are out of the scope of the present work.

1.7.2 Hypertrophic scars

Hypertrophic scars are a frequent complication of burn injuries, but can also originate after a piercing, tattoo or even acne. In women, one of the major causes is the caesarian section. However, extensive data are lacking.¹⁶⁰

This kind of scars are typically hoisted, light red or pink in colour and usually can be itchy, painful and in the worst cases, lead to the restriction of the movements. Usually, this kind of scar occurs soon after injury, evolves over a limited period of time that is longer than normal scar, but usually less than a year and often spontaneously regress without recurrence.

From a histological point of view, the hypertrophic scar contains chiefly type III collagen. This collagen is organized in flatter and less demarcated bundles with a wavier pattern; the orientation is parallel to epithelial surfaces, such as in unwounded tissue. Moreover, they exhibit nodular structures that inclose collagen, fibroblasts and myofibroblasts α -SMA⁺, which play a fundamental role in the pathogenesis of contraction.¹⁵⁵⁻¹⁵⁷ Studies conducted between the years 1970 and 1990, comparing hypertrophic scars and keloids from a morphological and histological point of view, showed that only in the hypertrophic scar myofibroblasts were present.^{94,161-162} More recent studies, as this work, show instead that myofibroblasts are also present in keloid tissue.¹⁶³⁻¹⁶⁴⁻¹⁶⁵

Hypertrophic scars do not grow beyond the margins of the original wound: this is the principal characteristic of hypertrophic scars and one of the most important features to distinguish them from keloids¹⁶⁶ (Fig. 23).

A wide range of therapeutic options is available. The majority of the current treatments aim at help flatten and shrink the scar and the most lesions are responsive to treatment.



Fig. 23. Four weeks hypertrophic scars. From Wikicommons. Author Cgomez447.

1.7.3 Keloid scars

In 1817 Alibert was the first one to use the term “keloid” to describe the lesions as cancrroid and later “crab claw-like appearance”, as the original meaning in ancient greek, to define the lateral expansion of an excessive scar into the surrounding healthy tissue (Fig. 24).¹⁶⁶⁻¹⁶⁷ Many years later, Mancini (1962) and Peacock (1970) described in different manner keloids and hypertrophic scars, distinguished from each other.¹⁶⁸

Today keloids are classified such as benign fibro-proliferative dermal tumours and, as a contrary of hypertrophic scar, grow beyond the boundaries of the original wounded tissue and do not exhibit a tendency to regress. In literature it is also used a time-scale to define the types of scarring: at least twelve months-scar, with an extension of the original site, can evolve into a keloid.¹⁶⁹ From a clinical point of view, keloid scars are refractory to the treatments and have a high rate of recurrence.

Regarding epidemiology, keloids are closely related to dark-skinned people, which is fifteen times more likely to develop keloids than those with lighter skin. Indeed, the incidence peak is 4.5-16% in south Americans and Hispanic populations,^{170,160} while the frequency is equally distributed in both sexes¹⁷¹⁻¹⁷² at any age.¹⁷³⁻¹⁷⁴

Keloid manifests peculiar features: the dimension can be ranging from millimetres to several centimetres, also depending on the site of the lesion. The surface is smooth and shiny, with different thickness, with compactness ranging from mildly tender to the firm. The borders are well-demarcated, but irregular in outline. The colour can vary from purple to pink, generally it is always more pigmented respect the healthy surrounding skin; moreover, keloids are associated with persistent itching, intermittent pain and a contraction sensation. Excessive scarring also affects the quality of life of patients, not only physically, (e.g. impending facial muscular movement) but also from the physiological perspective, causing cosmetic annoyance.

The anatomic sites most involved in keloids formation include ears, back, chest, shoulders, upper arms, upper back and cheeks. Many authors also refer to the importance of the mechanical skin tension,¹⁷⁵⁻¹⁷⁶ in particular, the attention has focused on the distinct site-specific shapes that reflect the predominant direction of the mechanical forces on the wound. Nevertheless, other authors have different opinions.¹⁷⁷

The aetiology is still partially unclear. Several factors including the anatomic site of the lesion and the genetic background may predispose subjects to develop keloids. Numerous types of injuries can lead to keloid scars in incline individuals: surgery, burns, tattoo, piercing, needle sticks, vaccinations, insect bites, but also some skin inflammatory process such as varicella, folliculitis, acne and herpes zoster infection. Infrequently, keloid can occur also spontaneously. The inflammation in keloids, and in scars generally, is incessant. Moreover, is confined for the major part in the reticular dermis, where it is also accelerated the angiogenetic process and collagen deposition. These findings suggest that the cause of keloid is an aberration of the physiological wound healing process in dermal skin layer.¹⁷⁸

Keloid formation is also associated with endocrine factors: indeed, frequently keloid seems to appear during puberty, and in women an onset or increase during pregnancy has been reported.¹⁷⁹⁻¹⁸⁰

Keloid-derived fibroblasts show an increased level of fibronectin biosynthesis compared to normal skin fibroblasts. Fibronectin is involved and plays a fundamental role in the development of the granulation tissue and re-epithelialization process.¹⁸¹⁻¹⁸² As concern the collagen type, the predominant one in keloids are type I and type III, with minor quantities of type IV and type V. Regarding the collagen synthesis in keloids, it is estimated to be twenty times higher than in unwounded tissue and three times greater in respect to hypertrophic scars.¹⁶⁰ To explain this evidence, in literature it is reported that both pre-transcriptional and post-transcriptional mechanisms of type I collagen expression and synthesis do not work efficiently.¹⁸³

As described above, during scar formation and contraction an essential contribution is due to growth factors. In particular, TGF- β and PDGF. Transforming growth factor- β is the major factor that stimulates fibroblasts to secrete protein of ECM in the site of the lesion. Typically, the TGF- β activity is extinguished when the healing process is complete, but not in fibrotic diseases, where the TGF- β synthesis is poorly regulated. Indeed, it was demonstrated that keloid fibroblasts secrete increased levels of TGF- β .¹⁸⁴

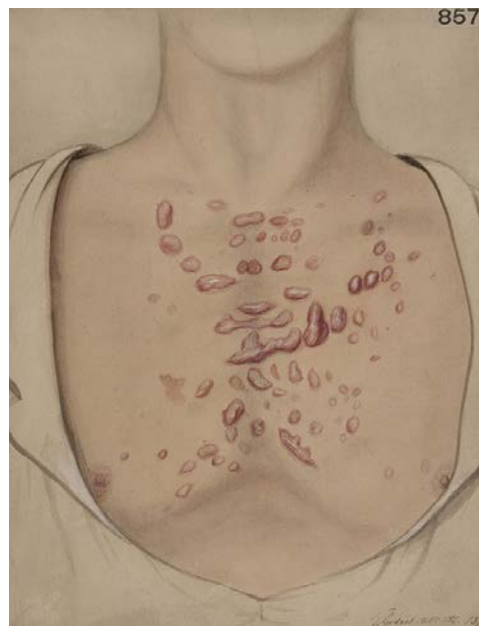


Fig. 24. Watercolour drawing of keloid of Alibert on the chest, in the site of scars of acne vulgaris. From Wikicommons.

1.7.4 Keloid scars management and treatments

Nowadays, efficient keloids treatment is still a challenge. The reasons are probably due to several factors, such as the long therapy duration, the lack of guarantee of good results and the clinical difficult to obtain an early and clear diagnosis.

There is a wide range of therapies that are used in keloid treatment, some of which are applied also in hypertrophic scars, others are selective for keloids. Keloid approaches can be grouped into three main categories: pharmacological therapies, non-pharmacological therapies and new therapies under investigation.^{117,185}

Given the large number of existing treatments and also the possibility of using them in combination, a need for clinicians to elucidate the treatment to be applied depending on the type of lesion was manifested. In 2014, international guidelines based on an algorithm were published: in this work, preferential treatment has been correlated to manage a specific type of keloid or hypertrophic scar. For a minor keloid, the first choice is the treatment with silicone gel/sheet application with corticosteroids injection, followed by the use of an ablative pulsed-dye laser. In case of unresponsiveness, the second choice is surgical excision with the use of intralesional injections or antiproliferative agents. As concern a large keloid o hypertrophic scars, the treatment starts with corticosteroids injection followed by the use of antiproliferative agents and finally the pulsed-dye laser. If the lesion is unresponsive, surgery is recommended.¹⁸⁶

1.7.5 Pharmacological therapies

These treatments have the purpose to reduce scar tissue and revert collagen architecture, also trying to prevent the scar recurrence. In this group there are the most traditional intralesional-administered treatments, such as corticosteroids, 5-Fluorouracil, Bleomycin, and Interferon, but also topically drugs, like Mitomycin C, onion extract and heparin applications.

The therapies mentioned above are just some of the numerous pharmacological treatments available for the management of keloids and hypertrophic scars. Indeed, other drugs are also used in the clinic such as

Imiquimod, Tacrolimus, Sirolimus, Doxorubicin, Verapamil, retinoic acid, Tamoxifen, and botulinum toxin.

Due to the lack of complete and in-depth studies, or to unsatisfactory results, these treatments are not used as a single therapy but are often administered in combination, after surgery or in association with the use of compression dressings.

Corticosteroids

The first-line therapy is certainly corticosteroids, such as hydrocortisone acetate, dexamethasone, methylprednisolone and triamcinolone (TAC),¹⁸⁷ that are able to induce the flattening of the keloid and symptomatic relief. The injection is made directly inside the scarred tissue and represents the traditional therapy since the second half of the 20th century; previously, topical administrations were used, but the efficacy was lower.¹⁸⁸⁻¹⁸⁹

The principal pharmacological effect of corticosteroids is to suppress the inflammatory response by acting on the immune system of the patient; moreover, they can reduce both the collagen and glycosaminoglycan synthesis, through activation of the nuclear receptor, and the proliferation rate of fibroblasts, modulating their gene transcription.¹⁸⁷⁻¹⁹⁰⁻¹⁹¹ Despite the long-time of clinical utilization in keloid scars, the mechanism of action of corticosteroids is still partially unclear, just like the correct preparation and dosage. The approaches employ different concentrations, depending on the size and the site of the keloid besides the age of the patients. Typical concentration are 10, 20, 30 and 40 mg/mL, to repeat for subsequent treatments at intervals of three or four weeks until clinical resolution is achieved or the side effects prohibit the use.¹⁹²

Corticosteroids show side effects such as the atrophy and hyper- or depigmentation of the surrounding unscarred tissue; to avoid this event the injection should be made in the middle dermis. Moreover, it can lead to glucose intolerance and rare cases of Cushing's syndrome are reported. Other side effects are osteoporosis, glaucoma, necrosis of tissue, telangiectasias and ulcerations; it is also known that it provokes painful sensations in the site of

the injection and topical anaesthesia by lidocaine is frequently needed.¹¹⁷⁻¹⁸⁹⁻¹⁹⁰

5-Fluorouracil (5-FU)

This antineoplastic agent is used in clinics since 1990, in order to counteract the hypermetabolic state that characterized keloids.

5-FU is a fluorinated pyrimidine analogue with antimetabolite activity: intracellularly, this molecule is incorporated into DNA, thus inhibiting DNA synthesis and cell proliferation. Cells with fast metabolism and proliferation, such as keloid fibroblasts, are preferentially targeted and have led to apoptosis without provoking tissue necrosis.^{185,193}

Several studies have confirmed that 5-FU is effective in the treatment of keloid scars.¹⁹⁴⁻¹⁹⁵ Among them, in 1999, Fitzpatrick was the first one to describe the results of a 9 years study on the effects of the 5-FU on 1000 patients, showing the successful results obtained with the intralesional use of this molecule, in association or alone.^{168,196} When used with other therapies, 5-FU is administrated in association with corticosteroids injection: after keloid excision, the use of 45 mg/mL of 5-FU in association with 4 mg/mL of TAC, for eight times, reduces the recurrence rate to 4-19%.¹⁹⁷

In the other randomized clinical trial, weekly intralesional injections of 50 mg/mL of 5-FU for twelve weeks, induces a reduction of the scar size of at least 50% of the majority of patients, without symptoms recurrence in a period of two years.^{168,198} Adverse effects are rare, but include superficial skin irritation, ulceration, often accompanied by burning and painful sensations.

Despite the scientific debate regarding its use, the intralesional treatment with 5-FU is considered safe, indeed the toxic effects are associated only with intravenous administration and not with subcutaneous injections.

Bleomycin

Bleomycin was obtained from *Streptomyces verticillus* and in its sulfate form it is used to anticancer treatments in several types of malignancy. It was firstly investigated as a scar reducing agent in the mid of 1990.¹⁹⁹ This molecule can inhibit collagen synthesis by the reduction of TGF- β 1 trigger and

other findings have shown the capability to block the cell cycle in G₂ phase.²⁰⁰ The use of Bleomycin is still poor clear in keloid clinical management, but the recommended dosage starts at 0.1 mL (1.5 units/mL) until 6 mL to repeat from three to five times per month. With this treatment, a regression of the 69.4% of keloids was observed.²⁰¹ The side effects of Bleomycin derived both from its toxicity, even if the systemic toxic effects with intralesional injections seem to be rare, and occasionally can also induce hyperpigmentation and dermal atrophy.

Interferon (INF)

This cytokine is secreted by T-helper cells and different forms are used in keloid treatment, in particular, INF- α , INF- β and INF- γ . INF is involved in several scars originated-processes and has antiproliferative, antifibrotic and antiviral effects. In particular, in keloid scars, IFN can reduce fibroblasts proliferation rate, collagen synthesis and ECM production modulating TGF- β 1 signalling.²⁰²

From a clinical point of view, the results obtained with intralesional injections of INF are inconclusive and the improvements are minimal. Moreover, the therapy is often expensive and side effects such as flu symptoms and pain in the site of the injections are frequently.

Mitomycin C (MMC)

Mitomycin C is a derivate from *Streptomyces caespitosus*, isolated in 1958 by Wakaki. MCC is an antibiotic molecule with antiproliferative and antineoplastic property and the first application is against pterygium. MCC is an alkylating agent and can form crosslinking at guanine and adenosine nucleotides in DNA molecules.

Several studies have performed on this molecule: both *in vitro* and *in vivo* findings show that MCC can suppress the proliferation in cultured fibroblasts and reduce the percentage of wound contraction in mice.

In the study performed by Bailey on a group of 10 patients, 1mg/ mL of MCC was topically applied for 3 minutes on keloids and the treatment was repeated after three weeks. During a six months follow-up, in which the keloid

scars were photographed, a satisfaction questionnaire was proposed and about the 80% of the patients were satisfied by the results.²⁰³

Onion extract and heparin applications

The exact mechanism through which this therapy reduces scar formation and development is still unclear. The onion extract has fibroblasts-inhibiting activities and increases the expression of MMPs. Moreover, the onion extract containing Quercetin and Kaempferol flavonoids reduces the synthesis of collagen.²⁰⁴ Heparin, instead, have a robust capability to bind collagen molecules, forming intramolecular interaction and weakening the molecule.

1.7.6 Non-pharmacological therapies

This kind of treatment has more advantages, and most of all this therapy is delimited in the skin fibrosis area.

The main treatments included in this category are compression therapy, silicone gel sheet applications, surgery, cryotherapy, radiotherapy, laser therapy. Also in these cases, fibroblast cells are the principal targets and they have to reduce their proliferation rate, as collagen synthesis is the main goal.

Compression therapy

Compression therapy became a popular treatment in the 1970s and was used as a standard option in the management of hypertrophic scars due to burns. Currently, it is still the preferred conservative management for prophylaxis of hypertrophic scars and keloids.

The mechanism of action of pressure therapy is still poorly understood, but a plausible hypothesis is that the permanent pressure limit the supply of blood, nutrients and oxygen to the scar tissue inducing a decrease in collagen synthesis and increase in fibroblasts apoptotic process.²⁰⁵⁻²⁰⁶⁻²⁰⁷

Special garments are designed for an individual patient with the purpose to guarantee a direct and continuous pressure on the scar for 8-24h a day for at least the first six months of the wound healing process, but to obtain more satisfactory results, the treatment must be applied continuously up to one year

or even more. The recommended pressure is 15-40 mmHg, but for several reasons this value is not always achieved in all the anatomical districts.^{175,208}

Unfortunately, this type of treatment often creates many discomforts for the patient, and this determines poor diligence in following the therapy and a compliance reduction.^{190,209-210-211}

Silicone gel sheet applications

Liquid silicone was introduced in the 1970s to treat both hypertrophic scars and keloids. In the early 1980s, the liquid formulation has been replaced with silicone sheets and the clinical efficacy was improved.²¹² The mechanism of action is still partially unclear, but the evidence suggests that silicone probably forms an impermeable membrane that keeps the skin hydrated, as well as it might the *stratum corneum*, reducing both capillary hyperemia, oedema and fibroblasts activity.²¹³⁻²¹⁴ Other authors, instead, support the idea that the silicone is inert with no effects on fibroblasts, but rather that acts on keratinocytes increasing the release of growth factors that would stimulate fibroblasts and modulate collagen synthesis.^{208,212,215}

Currently, topical silicone gel either as a topical gel or as an impregnated elastic sheet is widely used, particularly in the management of hypertrophic scars with daily applications ranging from 12 to 24 hours from one month until one year. This treatment plan can improve the colour and thickness, pain and itching due to the scar, while no significant results are obtained for elasticity. The side effects are a few: for these reasons, this kind of therapy is recommended as prophylaxis and in case of a scar younger than three months, in which it is easier to obtain satisfactory results.

Surgery

Surgery is still the traditional treatment to remove keloids and hypertrophic scars, but with a fundamental difference between them.

In case of keloid-prone patients, it is well-known that if surgical excision is provided alone, the recurrence rate ranges from 45 to 100%: adjuvant therapies, such as intralesional corticosteroids, radiotherapy or cryosurgery are typically used in order to obtain a more pleasing results.^{190,216-217} Indeed,

recent studies have demonstrated that the combination of surgery with steroid treatment reduces the recurrence rate to less than 50%.¹⁸⁵

As concern the type of surgical removal, different opinions are reported: the total excision of keloid, could increase the collagen synthesis and induces a rapid regrowth of a larger keloid; as a contrast, an intramarginal excision does not stimulate collagen synthesis and the recurrence rate is lesser.²¹⁸⁻²¹⁹ However, the surgery of keloids remains the second-line therapy for lesions unresponsive to pharmacological treatments or compressive therapies.¹⁶⁰

Cryotherapy

Cryotherapy is used as monotherapy and owes its success on changes in the microcirculation provoked by freezing: the extremely low temperatures induce vascular damage, and blood stasis in the keloid tissue lead to cellular hypoxia.

In association with TAC, cryotherapy is the most popular treatment of small keloids and hypertrophic scars, such as acne scars. Quickly and repeatedly applications of NO Liquid are typically used with success rate ranging from 30 to 75%, but a hypopigmentation and different degree of atrophy are common side effects.¹⁹²

Recently, an intralesional-needle cryoprobe method has assessed: a cryo-needle is introduced into the long axis of the scar in order to maximize the volume of the scar tissue needed to be frozen. The inserted cryo-needle is connected to a cryogun filled with NO and introduced into a cryoprobe, which leads to freezing scar. This method gives the surgeons the ability to freeze any hypertrophic or keloid scar to an adequate depth.^{185,220}

Radiotherapy

The principal use to radiotherapy is as an adjunctive measure after surgical excision. In this case, the success rate is between 65 and 99% when compared to excision alone. The effects of radiotherapy are mediated through inhibition of fibroblasts proliferation and inducing apoptosis. This event leads to decreased collagen synthesis.

The recommended dose is 15-20 Gray (Gy) to be administered in five or six treatments. This procedure may decrease the fibroblasts number, such as in physiological wound healing process, and prevent the adverse effects such as telangiectasia, atrophy and erythema. Although cancer development post-radiotherapy on keloid scars is uncommon, the risk to induce malignancy, particularly in breast and thyroid area, discourage this kind of treatment that should be handled with caution from specialized operators.^{168,185,190}

Lasertherapy

The introduction of laser in the treatment of keloid is dated in the mid-1980s and starting from this period, the therapeutic use of the laser with different wavelengths was intensively investigated.

In one of the first study in which the laser was used on keloid scar, conflicting results were reported: using a CO₂ laser, only one out of thirteen patients showed improvement.²²¹⁻²²²

Other studies show that the keloid excision alone with CO₂ laser does not provide an advantage in respect to surgical removal. Moreover, the recurrence rate, about 50%, is similar in both techniques.²²³⁻²²⁴

Another type of laser which is used both in keloids and hypertrophic scars management is the pulsed dye laser (PDL). In particular, in studies with a 585 nm PDL, they demonstrated a reduction in collagen synthesis and fibroblast proliferation rate in keloids.²²⁵ However, the high absorption by melanin limits the use of the PDL in darker-skinned subjects, the same which have the major risk to form keloids.¹⁹²

Currently, the laser therapy treatment recommends fluences ranging from 6.0 to 7.5 J/cm² or from 4.5 to 5.5 J/cm², with 7 mm and 10 mm in spot dimension respectively.²²⁶ From two to six treatments are necessary to improve the scar colour, pliability and texture.²²⁷ The common side effects are hyper- or hypopigmentation and postoperative purpura, which can persist until seven days.

1.8 Adenosine

Adenosine is a purine nucleoside indispensable for DNA synthesis: it is formed by an adenine and ribose molecule joined through an N9-glycosidic bond, which, in the nervous system, is continuously formed both at intracellular and extracellular level (Fig. 25).

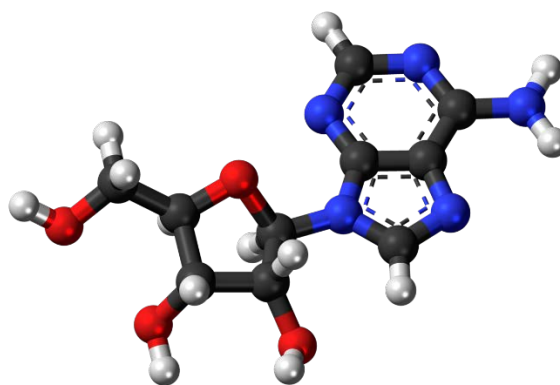


Fig. 25. Ball-and-stick model of the adenosine molecule. Black: carbon (C). White: hydrogen, (H). Red: oxygen (O). Blue: nitrogen (N). Author Jynto. From Wikicommons.

Adenosine plays an essential role as neuromodulator also in biochemical processes and signal transduction, correlating with molecules such as ATP, ADP (adenosine diphosphate) and AMP (adenosine monophosphate). At the central level, it carries out numerous actions: acts as an endogenous anticonvulsant, influences control of motility, pain, learning and memory.²²⁸ Moreover, adenosine has a further crucial role in the modulation of emotional states, conditioning social interactions and aggressive behaviours.

In physiologic conditions, extracellular adenosine exercises an inhibition on synaptic transmission and this makes adenosine a highly protective neuromodulator. At the extracellular side, adenosine is produced from AMP which is dephosphorylated by the enzyme 5'-nucleotidase (5'-NT). Adenosine can also be formed through the breakdown of nucleotides which are released into extracellular space. The 5'-NT is inhibited by ATP and it has an elevated affinity towards AMP: for this reason, when the cell is exposed to an intense metabolic activity with increased ATP consumption and consequent elevated production of AMP.²²⁸ Adenosine is a paramount chemical mediator

which can activate determined biologic responses and its action mainly occurs through purinergic receptors activation. These every receptor is structurally composed of seven amphipathic α -helices (TM 1-7), which consist of a sequence of 20-25 hydrophobic amino acids (Fig. 26).

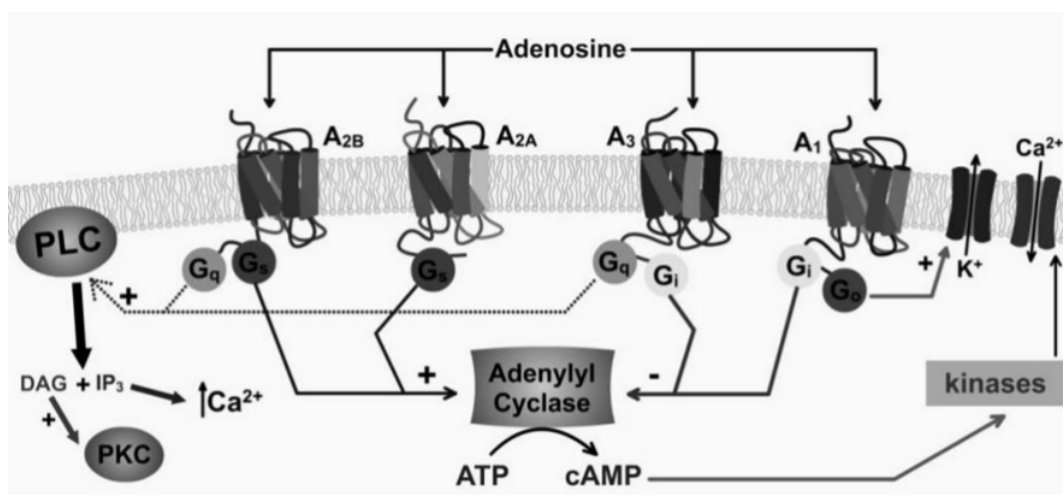


Fig. 26. Seven transmembrane domain receptor (TM) coupled with a G-protein. The G_{α} , binding GTP, release itself and activates a biologic response. From Cristalli, G. *et al.* 2008.²²⁹

The N-terminal portion is located at the extracellular level whereas the C-terminal exposes toward the intracellular side; all the 7 domains are strictly interconnected via 3 intracellular (IL 1-3) and 3 extracellular loops (EL 1-3).²²⁹ The seven transmembrane domain receptors are always associated, at the intracellular side, with specific transduction heterotrimeric protein, defined G protein, which is activated after the interaction between the receptor and substrate.

The purine receptors have been classified into two categories by Burnstock in 1978, P₁ and P₂ (X, Y) receptors, the latter ones activated by ATP.²³⁰ This distinction helped to clarify the incredible variety and complexity of purine-mediated effects observed till then and the ubiquitous presence of ecto-ATPases, enzymes catalysing extracellular nucleotides degradation. The presence of these enzymes on cell membranes incredibly complicated the scenario by forming ADP, AMP and adenosine from extracellular ATP,²³¹ so that some of the actions of ATP were directly due to P₂ receptor activation, whereas others were due to the indirect action of adenosine on P₁ receptors.

Both P₁ and P₂ subfamilies which later recognised to be further divided into different subtypes. P₁ receptors were initially distinguished into two classes (A₁ and A₂ receptors) on the basis of their excitatory or inhibitory actions on adenylyl cyclase.²³² Later work defined four different subtypes of P₁ receptors: A₁, A_{2A}, A_{2B} and A₃.²³³ P₂ receptors appeared to be more heterogeneous, with P_{2T}, P_{2Z} and P_{2U} subtypes being proposed from different authors.²³⁴⁻²³⁵ The definitive classification came from Abbracchio and Burnstock²³⁶ who proposed that P₂ purinoceptors should belong to two major families: P_{2X} ligand-gated ion channel receptors and P_{2Y} G-protein-coupled receptors (GPCR). Cloning experiments supported this classification and helped to subdivide P₂ receptors into seven P_{2X} and eight P_{2Y} subtypes.²³⁷

To date, it is well recognised that purinergic signalling plays a fundamental role in several biological systems, from invertebrates to mammals, and purinergic-mediated effects including both short-term - neurotransmission, endothelial-mediated vasodilatation, platelet aggregation - and long-term - cell proliferation, differentiation, migration and death - phenomenon have been demonstrated.

1.8.1 Purinergic receptors

Receptors for both ATP and adenosine are widely distributed in the nervous system as well as in other tissues. The notion that there are purinergic receptors, that is, proteins on the surface of cells that bind and respond to purines, was slow to evolve. The first evidence was the observation of the cardiovascular physiological effects of purines. Drury and Szent-Gyorgyi,²³⁸ first noted effects of adenine nucleotides on cardiac and vascular tissues in 1929. Thirty-four years later, Berne²³⁹ identified a physiological role for adenosine as a mediator of coronary vasodilation in response to myocardial hypoxia. In the 1970s, adenosine was found to stimulate cyclic adenosine monophosphate (cAMP) formation in brain slices. Subsequently, the physiological effects of adenosine on almost all tissues have been described. Based on the responses of various tissues to purines, Burnstock²³⁰ proposed that there are distinct receptors that bind adenosine or ATP, designated P₁ and P₂ receptors, respectively (Fig. 27). The existence of adenosine receptors was

not widely accepted until the 1980s when saturable binding sites for radioactive adenosine analogues were demonstrated in brain. The existence of adenosine receptors was proved unequivocally when the first adenosine receptors were cloned in 1990.²⁴⁰

Originally, the “P” in P₁ and P₂ was meant to designate purinergic receptors. However, it has been discovered that some of the P₂ receptors bind pyrimidines, UTP or UDP, preferentially over the purine, ATP. Hence, the “P” in P₂ is now used to designate purine or pyrimidine. Despite these exceptions, P₁ and P₂ receptors collectively are still generally referred to as purinergic receptors. In addition to adenosine, various synthetic adenosine analogues activate P₁, but not P₂, receptors and synthetic ATP or Uridine Triphosphate (UTP) analogues activate P₂, but not adenosine, receptors. However, not all purines activate P₁ or P₂ receptors. For example, adenine, guanosine and uric acid do not activate P₁ receptors. Inosine, the purine nucleoside product of adenosine deamination, generally has weak activity at P₁ receptors but does activate A₃ adenosine receptors in ischemic tissues, particularly in rodent species.²⁴¹ The development of synthetic compounds that activate P₁ or P₂ receptors has been important for elucidating how these receptors function because some of these compounds are more powerful and selective than the parent purines and most are more stable than the short-lived endogenous compounds adenosine and ATP.

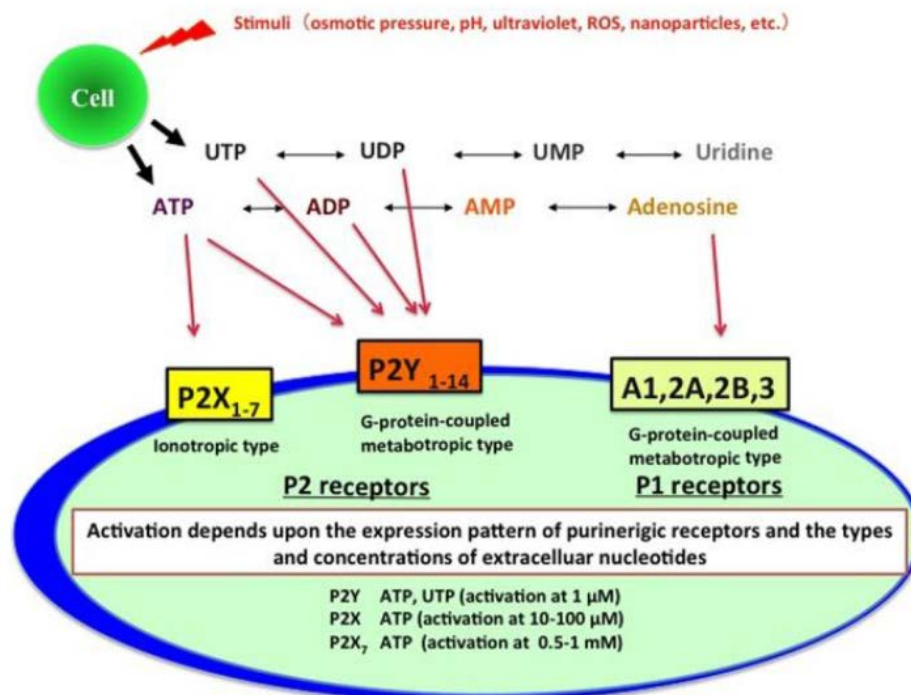


Fig. 27. Schematic overview of purinergic/ATP signalling. Intracellular ATP is released into the extracellular space in response to various stimuli. The released ATP is rapidly metabolized to ADP, AMP, and adenosine, and these metabolites bind with P₂X, P₂Y, and/or P₁ receptors, respectively, and activate receptors with a different concentration, leading to downstream signalling. ATP indicates adenosine triphosphate; ADP, adenosine diphosphate; AMP, adenosine monophosphate; P₂, purine 2. From Kojima *et al.*, 2017.²⁴²

P₁ receptors

Molecular cloning and pharmacological studies have identified four subtypes of adenosine P₁ receptors: A₁, A_{2A}, A_{2B} and A₃ receptors.²³³ All of them have already been cloned at least from rat, mouse and human. Structural data report a close similarity between adenosine receptors of the same subtype among mammalian species, except for A₃ receptors. This subtype is the most recently discovered one, being cloned only in the last 15 years,²⁴³ and presents the largest variability. For instance, almost 30% difference in the amino acid sequence is found between humans and rats.²³³

All P₁ receptors are metabotropic GPCR. Hence, A₁ and A₃ subtypes are associated with G_i activation, adenylyl cyclase inhibition and decrease of intracellular cAMP levels, while A_{2A} and A_{2B} receptors are linked to G_s proteins that activate the same enzyme increasing cAMP concentration in the cytosol. However, adenosine receptors have also been reported to couple to other G-

proteins than Gs, modulating different second messenger systems. For instance, in addition to their effects on adenylate cyclase (and contrary to adenosine A_{2A} receptors) adenosine A₁, A_{2B} and A₃ receptors are also characterized by their stimulatory effect on phospholipase C (PLC).²⁴⁴⁻²⁴⁵ Furthermore, A₁ and A₃ receptors can also activate phospholipase D (PLD).²³³ Several types of Ca²⁺ and K⁺ channels are also activated (either by a direct G protein-channel interaction or by second messenger systems) after adenosine receptor stimulation, such as the G-protein-coupled Inwardly Rectifying Potassium (GIRK) channel Kir3.0 that is positively modulated by adenosine A₁ receptor activation.²⁴⁶ The A₁, A_{2A} and A₃ receptors present a particularly high affinity for the endogenous ligand, being activated by nanomolar concentrations of adenosine.²³³ On the other hand, the affinity values of A_{2B} receptors for adenosine in binding and functional experiments are higher than 1 μM.²⁴⁷ Under physiological conditions, extracellular adenosine concentrations are estimated to be in the range of 30 to 200 nM.²⁴⁸⁻²⁴⁹ These levels are sufficient to activate A₁, A_{2A} and A₃ receptors subtypes, but not A_{2B}, which require higher concentrations (micromolar range) of adenosine to be activated. Such higher adenosine concentrations are only reached under pathological conditions, such as during hypoxia or ischemia *in vivo*²⁵⁰ and *in vitro*.²⁵¹

Pharmacology of P₁ receptors

Since adenosine receptors have been studied for a long time, there are several useful pharmacological tools available at present. Numerous adenosine analogues have been developed that selectively bind one of the four different subtypes of P₁ receptors. In human, rat and mouse tissues, the A₁ full agonist 2-Chloro-N-cyclopentyladenosine (CCPA) (and to a lesser extent CPA) and the antagonist 8-Cyclopentyl-1,3-dipropylxanthine (DPCPX) are highly selective compounds active at nanomolar concentrations. Allosteric enhancers for this receptor subtype (such as PD81723 and analogues) are also available and increase the agonist binding and its effects.²⁵²⁻²⁵³

The 5'-N-Ethylcarboxamidoadenosine (NECA) was long considered to be a selective A₂ agonist but it has been largely demonstrated that it is an

unselective agonist at all P₁ receptors, only slightly preferring A_{2A} subtypes.²³³ However, based on evidence that 2-substitution of NECA molecule increased selectivity, the 2-(4-(2-Carboxyethyl)phenethylamino)-5'-N-ethylcarboxamidoadenosine (CGS21680) was developed as an A_{2A} selective agonist.²⁵⁴ This compound is less potent and selective in humans than in rats,²⁵⁵ but it has been replaced by another recently developed A_{2A} agonist, the 4-(3-[6-amino-9-(5-ethylcarbamoyl)-3,4-dihydroxy-tetrahydro-furan-2-yl]-9H-purin-2-yl]-prop-2-ynyl)-cyclohexanecarboxylic acid methyl ester (ATL-146e), which is 50 fold more potent than CGS21680 at the human receptor.²⁵⁶ Among the numerous A_{2A} antagonists, the most selective so far are the 2-(2-Furanyl)-7-(2-phenylethyl)-7*H*-pyrazolo[4,3-*e*][1,2,4]triazolo[1,5-*c*]pyrimidin-5-amine (SCH58261) and SCH442416 and the structurally related ZM241385.²⁵⁷

Potent A_{2B} agonists with affinity values in the low nanomolar range have been lacking till recently, when a new class of non-adenosine compounds (pyridine derivatives) has been synthesised by Beukers and colleagues.²⁵⁸ Among them, the 2-Amino-4-(4-hydroxyphenyl)-6-[(1*H*-imidazol-2-ylmethyl)thio]-3,5-pyridinecarbonitrile (LUF5835) is a full agonist with an EC₅₀ of 10 nM at human A_{2B} adenosine receptors expressed in CHO cells. Unfortunately, its selectivity towards A₁ adenosine receptors and A_{2A} adenosine receptors is not adequate to discriminate between them in native tissues. The situation is somewhat more favourable for antagonists, as some potent and relatively selective compounds have been found among anilide derivatives of xanthines with K_i values in the low nanomolar range, such as the *N*-(4-Cyanophenyl)-2-[4-(2,3,6,7-tetrahydro-2,6-dioxo-1,3-dipropyl-1*H*-purin-8-yl)phenoxy]-acetamide (MRS1754),²⁵⁹ that is over 200-fold selective for A_{2B} vs all other P₁ receptors.²⁶⁰

An emblematic feature of the adenosine A₃ adenosine receptors, the most recently discovered one, is its insensitivity to the antagonistic actions of methylxanthines, such as caffeine and theophylline, the traditional blockers of adenosine receptors.²⁶¹ Hence, most A₃ antagonists are dihydropyridines, pyridines and flavonoids.²⁶² Another class of highly selective compounds are isoquinoline and quinazoline derivatives, such as the *N*-(2-Methoxyphenyl)-*N*-[2-(3-pyridinyl)-4-quinazoliny]-urea (VUF5574) that presents a K_i value of 4 nM vs human A₃ adenosine receptors but not vs the rat isoform.²⁶³ In this

regard, it is worth noticing that significant species differences in the affinity of adenosine A₃ receptor antagonists have been noted, as expected from the high structural inter-species variability already mentioned. The affinity values of several A₃ blockers are typically more than 100-fold greater on human than rat receptors, as described for *N*-[9-Chloro-2-(2-furanyl)[1,2,4]-triazolo[1,5-c]quinazolin-5-yl]benzene acetamide (MRS1220). The unique rat-selective compound is the A₃ agonist propyl 6-ethyl-5-ethylsulfanylcarbonyl-2-phenyl-4-propylpyridine-3-carboxylate (MRS1523). In contrast, the affinity of the most widely used A₃ agonist, the 1-[2-Chloro-6-[(3-iodophenyl)methyl]amino]-9*H*-purin-9-yl]-1-deoxy-*N*-methyl-β-D-ribofuranuronamide (2-Cl-IB-MECA), does not vary beyond an order of magnitude between the species examined, at least among mammals. The high affinity (low nanomolar range) and selectivity (more than 100-fold vs A₁ adenosine receptors and A_{2A} adenosine receptors) of this compound towards A₃ adenosine receptors turns it into the most used pharmacological tool for investigating A₃-mediated effects.²⁶⁴

Distribution of P₁ receptors

Receptor distribution provides helpful information on whether the endogenous agonist will exert significant effects in the intact organism. Thus, in this case, the rather low levels of adenosine present under basal physiological conditions and the 3-fold difference in receptor affinity for the agonist between the four P₁ subtypes might suggest adenosine acts as a tonic modulator of normal cell functions or whether its role only becomes relevant during pathological conditions. Highest levels of A₁ adenosine receptors are present in the central nervous system (CNS)²⁶⁵ with well known regional distributions²⁶⁶ that will be examined in detail. High levels are also found in adrenal glands, eye and atria. Intermediate levels are also found in skeletal muscles, liver, kidney, adipose tissue, gastrointestinal smooth muscles and bronchi. Lung and pancreas present low level of A₁ adenosine receptors expression.²³³

The A_{2A} adenosine receptors are highly present in spleen, thymus, immune cells (leukocytes and granulocytes) and platelets. Lower levels are also found in the heart, lung and blood vessels. The A_{2B} subtype is particularly

abundant in the gastrointestinal tract, mainly in caecum, colon and urinary bladder. Other regions are lung, blood vessels and adipose tissue.

The A_3 subtype is mainly found in rat testis²⁶⁷ and mast cells, in accordance with the fact that for a long time the unique role assigned to this receptor have been mast cell degranulation and histamine release. Intermediate levels are also found in the lung, spleen, thyroid and liver.²⁶⁸⁻²⁶⁹ Low levels of A_3 adenosine receptors are found in the brain.²⁶⁵

Role of P_1 receptors

P_1 receptors exert important pathophysiological roles in a variety of tissue, from the cardiovascular system to the brain. At systemic level, adenosine acts as a negative chronotropic, inotropic and dromotropic modulator on heart functions by activating A_1 adenosine receptors. These effects are mainly due to the attenuation of the stimulatory actions of catecholamines on the heart functions carried on by A_1 adenosine receptors activation.²⁷⁰ In contrast, the hypotensive effects exerted by adenosine in the periphery are attributed to A_{2A} adenosine receptors activation, causing vasodilatation of blood vessels²⁶⁹ and led, in the '60s-'70s, A_{2A} agonists to be tested in clinical trials as antihypertensive drugs. In addition, A_{2A} adenosine receptors receptor stimulation also inhibits platelet aggregation and exhibits marked anti-inflammatory activities by inhibiting T-cell activation and proliferation, by reducing pro-inflammatory cytokine production and enhancing anti-inflammatory cytokine levels.²⁷¹⁻²⁷²

Less is known about the roles of A_{2B} and A_3 adenosine receptors in the periphery. One of the first described biological effects of adenosine A_3 adenosine receptors stimulation was degranulation of mast cells,²⁷³ suggesting a pro-inflammatory role of this receptor subtype. This hypothesis has been confirmed by subsequent studies demonstrating that A_3 adenosine receptors activation facilitates antigen-dependent histamine release from mast cells.²⁶⁹ In addition, it has a demonstrated irritant effect in asthmatic lung mediated by A_3 adenosine receptors stimulation,²⁷⁴ probably partnered, in eliciting this effect, by A_{2B} adenosine receptors stimulation, that also mediates

bronchoconstriction.²⁷⁴ For this reason, mixed A_{2B} and A₃ antagonists have been proposed as candidates for the treatment of asthma.²⁷⁵

1.8.2 The involvement of adenosine in wound healing and fibrosis processes

Adenosine, acting on its receptors, promotes the formation of granulation tissue²⁷⁶⁻²⁷⁷⁻²⁷⁸ and is implicated in normal or aberrant wound healing as well as in fibrosis (for a review see: Shaikh and Cronstein 2016).²⁷⁹ In particular, the Gs-coupled A_{2A} and A_{2B} subtypes are the most involved in fibrosis, as demonstrated by the fact that A_{2A} receptor deletion in transgenic mice causes the formation of more disorganized granulation tissue and a reduction in new vessel formation in the wounds, while A_{2A} agonists promote neo-angiogenesis in wild type littermates.²⁷⁸

Stimulation of A_{2B} receptors increases VEGF, bFGF and IL-8 in human microvascular endothelial cells (HMEC-1) through phospholipase C activation.²⁷⁶ In addition, A_{2A} receptor blockade reduces thrombospondin-1 (TSP-1) expression in endothelial cells and the latter suppresses *in vitro* angiogenesis in endothelial cells.²⁸⁰ Recently, knowledge has been added to this issue by showing that A_{2A} and A_{2B} receptor stimulation promotes angiogenesis through enhanced TSP-1 production by human macrophages.²⁸¹

Collagen is the main constituent of the extracellular matrix. The deposition of collagen from fibroblasts is an essential part of wound healing and also contributes to the pathological remodeling of organs; however, excessive cell stimulation can lead to aberrations. A_{2A} receptors stimulate fibroblasts in the production of type I and type III collagen and at the same time regulate the MMPs 9, 2 and 14, involved in the breakdown of collagen.²⁸² In bleomycin-induced fibrosis in the mouse, A_{2A} stimulation promotes widespread production of collagen and this effect is abolished in A_{2A} knockout mice or in wild type mice treated with A_{2A} selective antagonist;²⁸² again with respect to adenosine, mice genetically deficient of the adenosine degradation enzyme adenosine deaminase are also protected by dermal fibrosis.²⁸³

Overall, these data suggest that adenosine and the A_{2A} and A_{2B} receptors are involved in the pathogenesis of fibrosis. Modulation of these

receptors could help in reducing inflammation and promoting wound healing, but their excessive activation could lead to architectural disturbances and loss of tissue integrity in a variety of fibrosis disorders. So, another objective of this research project will be to characterize the possible involvement of purinergic P₁ receptors in fibrosis processes.

2. THE AIMS

The blue LED light device was developed about 10 years ago as a photocoagulator, in order to induce haemostasis on superficial skin abrasions. It proved to be effective in accelerating the wound healing of skin tissues from patients and animal models.

Starting from these bases, in the first part of this work we decided to extend this knowledge by studying the effects of blue LED light irradiation on the healing process of acute wounds. To this aim, the effects of blue LED light were investigated, by studying the expression of several markers of inflammation in the irradiated (treated) or untreated skin abrasion in different strains of mice using histological analysis and immunofluorescence staining. In the next series of experiments, the effects of the blue LED light irradiation were also evaluated in an animal model of chronic wound. The effects on several markers of inflammation, such as TNF-alpha, bFGF, MMPs 1 and 9, VEGF and EGF, were investigated by using a multiparametric ELISA assay.

It has been observed in a previous study²⁰ that the blue LED light effects are mediated by direct modulation of fibroblasts and myofibroblasts activity and inflammatory infiltrate at the tissue level. In the second part of this work, in order to better clarify the cellular mechanism underlying the beneficial effects of the blue LED light on wound healing, we studied the effects of the blue LED light irradiation on human fibroblasts cells, isolated from keloid scars, a type of skin fibrosis. Keloids are due to an exaggerated collagen deposition by fibroblast cells; up to now no definitive treatment for this pathology is available. The results were compared to those obtained in experiments performed on fibroblasts isolated from healthy or keloid perilesional tissues. To this purpose, we used biochemical, electrophysiological and Raman spectroscopy techniques.

3. MATERIALS AND METHODS

3.1 *In vivo* experiments

3.1.1 Animal procedures

All animal procedures were conducted according to the Italian Guidelines for Animal Care, DL 116/92, application of the European Communities Council Directive (86/609/EEC), and approved by the Committee for Animal Care and Experimental Use of the University of Florence. All the adult male mice (15-20 g, Envigo, Milan, Italy) were held under controlled conditions, including constant temperature, allowing free access to regular chow and 3-stage filtered water.

After 1 week of acclimatization, mice were randomized, weighted and anaesthetized by Ketamine (80-100 mg/kg i.p.) and Xylazine (10 mg/kg i.p.) that were purchased from Sigma-Aldrich (Milan, Italy). After anaesthesia, the dorsal skin was gently stretched to required dimensions and one or two superficial wounds, about 1 cm in diameter, were produced with an abrasor in each animal. The abrasor consists of a drill with an extension for manual work that mounts a cylinder head of commercial sandpaper (KWH Mirka Ltd, Jeppo, Finland, 68 μm particle size). The wounds have been realized with the abrasor set at a speed of 200 rpm. The rotating abrasive cylinder was brought into contact with the skin of the mice to remove it without exerting any pressure. We stopped the procedure when the underlying layer of the skin with its gaping and gushing capillaries could be observed.

After the experimental procedure, the animals were housed in regulation cages in controlled lighting (12/12 light and dark) and temperature facility and had free access to water and standard rodent diet *ad libitum*.

In all cases, the wound was immediately treated after the end of surgical intervention, as following described: the blue LED light energy density was set at 20.6 J/cm² (corresponding to 30 seconds of treatment) keeping the fiber tip at a constant distance (about 2 mm) from the target, in continuous slow motion. During the whole experiment, the animals were kept at a constant temperature (37.5 °C) to reduce stress due to anaesthesia. A topical application of a small amount of Streptosil (Boehringer Ingelheim Italia spa, Milan, Italy) was applied after treatment to each induced-wound in order to prevent the onset of

infections. With the purpose to avoid accidental thermal damages and to control the temperature dynamics during the treatment, the entire procedure was monitored by an infrared thermal camera (InfReC, Nippon Avionics Co., Ltd., Japan).

At specific follow up times, the animals were sacrificed and the dorsal skin promptly excised, as described in Table I. The excised patches (1 cm, as shown in paragraph 1.3) were immediately included in a cryopreserved matrix (Killik, Bio-Optica, Milan, Italy) and frozen at -80 °C. Each biopsy was cut by the use of the cryostat (Leica AgProtect 1950, Milan, Italy) and the obtained sections, 10 µm in thickness, were collected on a microscope slide (Superfrost Plus, Thermo Fisher Scientific, Bio-Optica, Milan, Italy), post-fixed in cold acetone and stained with haematoxylin and eosin (H&E) for microscopic examination or stored at -20°C for successive analysis.

3.1.2 Mice models

In order to investigate the wound healing process in healthy and pathologic conditions and the possible involvement of TRPV1 channel and Adenosine in the blue LED light mechanism of action, five different mice models were used. In particular, we examined acute wounds in healthy mice, acute and chronic diabetes in diabetes-induced mice, a coagulopathic mice model, *Trpv1* knock/out and capsazepine-treated mice and Suramin treated mice.

Model	Mice strain	N° of wounds	Follow-up
Acute wound	CD1	2 (rostral and caudal)	0-1-3-6-12-18-24 hours
Acute diabetes	CD1	1 (central)	6-15 days
		2 (rostral and caudal)	3-7 days
Chronic diabetes	CD1	1 (central)	3-15 days
P ₂ antagonists treated	CD1	1 (central)	6 hours
Coagulopathies	CD1	1 (central)	6-24-72 hours

Table I. Mice models used to study the effects of blue LED light in wound healing.

Mice model of acute wounds

Twenty-seven mice were used. All the procedures were performed as previously described in 1.1 paragraph of this section and shown in Fig. 28.

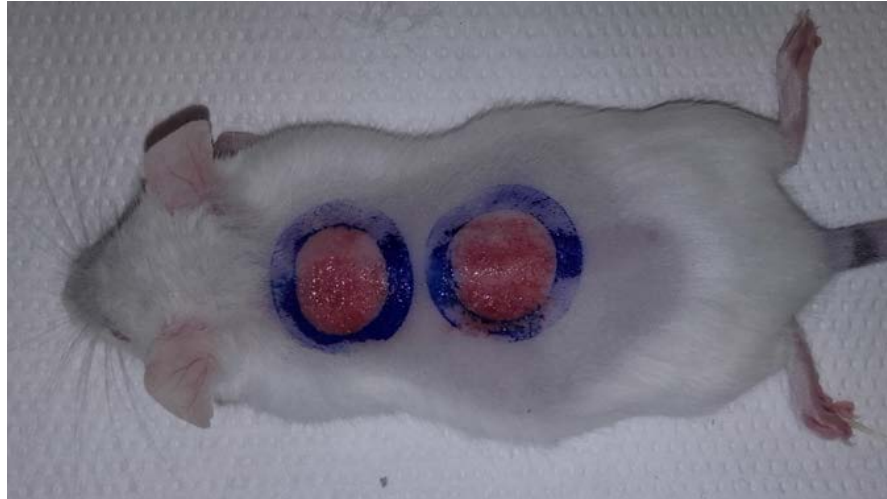


Fig. 28. CD1 mice model of superficial abrasion. The image represents CD1 mice with two wounds.

Acute diabetic mice model

Twenty-four mice were used. Diabetes was induced by injections of 40 mg/kg i.p. of Streptozotocin (STZ) (Sigma-Aldrich, Milan, Italy) for five consecutive days. Glycaemia was measured every day with a blood glucose monitor and specific strips (GL 50, Beurer Medical Italia, Milan, Italy) in order to maintain the values higher than 270 mg/dL. Mice were considered acute diabetes-affected when glycaemia was above the value of 270 mg/dL. The animals were used for the experiments immediately following the end of the treatment with STZ.

As reported in Table I, we performed two different groups of acute diabetic model: 12 mice with one wound and other 12 mice with two wounds. In Fig. 29 an example of an animal with one wound is depicted.



Fig. 29. CD1 acute diabetic mice model with one superficial wound.

Chronic diabetic mice

Twelve mice were used. Chronic diabetes in mice was induced by STZ likewise in an acute diabetic model. These mice were considered chronic diabetes-affected when glycaemia remained above 270 mg/dL for at least one week after induction.¹⁹ Thus, the experiments were performed not until one week after the last dose of STZ.

Purinergic P₂ receptor antagonist treated

Fifteen mice were used to investigate the possible involvement of purinergic receptor in the wound healing process. Suramine (Tocris Bioscience, Milan, Italy) were used. The compound was intraperitoneal administered (25 mg/Kg) one hour before irradiation. Mice were randomized and subdivided into 4 different groups on the basis of wound treatment:

1. Untreated
2. 20.6 J/cm² of blue light application
3. Suramin
4. Suramin + 20.6 J/cm² of blue light application

Coagulopathies mice model

Nine mice were used to evaluate the effect of the blue LED light when coagulopathies occur. Mice were administered intraperitoneal sterile and nonpyrogenic heparin (Sigma-Aldrich, Milan, Italy) at 200 units/kg or diluent (placebo) 25 minutes before the induction of abrasions. Abrasion procedure and anaesthesia were administered as previously described.

The animals were divided into three groups and underwent a different sacrifice-time: i) 6 hours, ii) 24 hours, iii) 72 hours after treatment, respectively.

Trpv1 Knock-out mice model

In this work, we tested the TRPV1 channel using Capsazepine (CZP) (Sigma-Aldrich, St. Louis), a competitive antagonist of the TRPV1 receptor.¹⁹ Thirty mice were used with the purpose of evaluating a possible role of vanilloid channel family in a blue light-mediated faster healing. To this purpose, the animals were treated 30 minutes before the blue LED light treatment with 3 mg/Kg i.p of Capsazepine.

The animals were randomized and divided into 3 groups (Fig. 30):

1. Trpv1 knock-out
2. Capsazepine treated
3. Control group, in which a physiological solution was administered



Fig. 30. C57BL/6 Trpv1 knock-out mouse with two wounds.

3.1.3 Summary of mice models

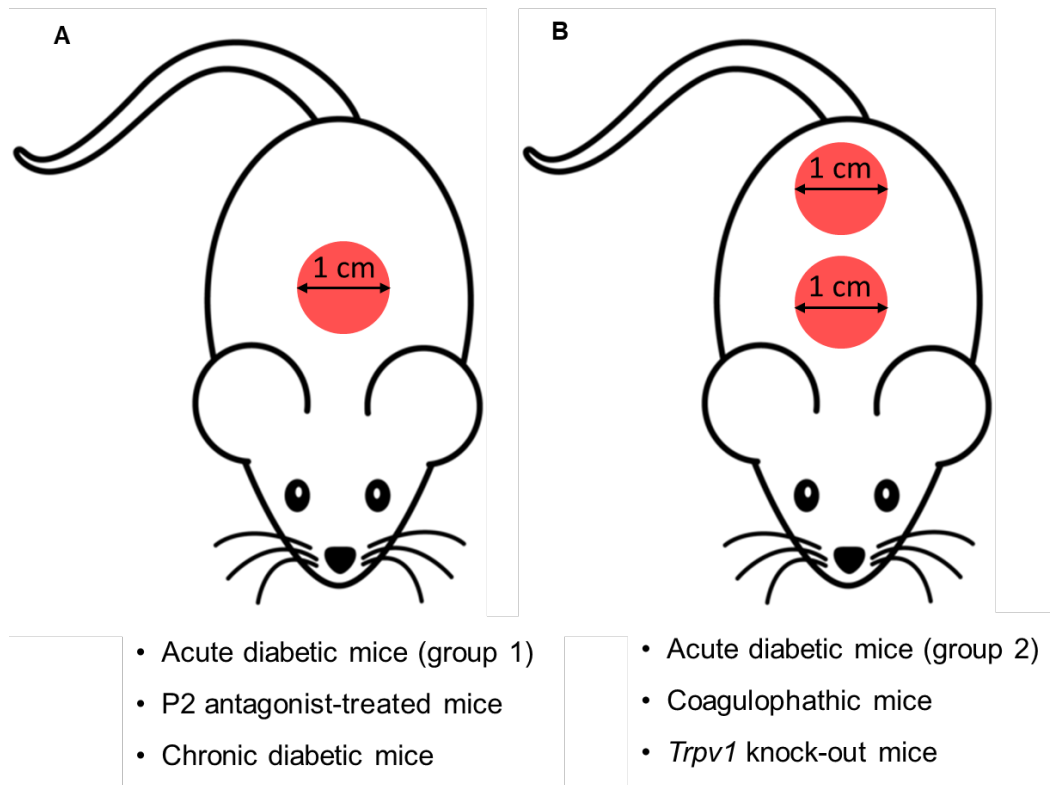


Fig. 31. **A**: Schematic drawing of a mouse with one wound and corresponding groups under investigation. **B**: Schematic drawing of a mouse with two wounds and corresponding groups under investigation.

3.1.4. Haematoxylin and eosin staining

Haematoxylin and eosin ready-to-use solutions (Sigma-Aldrich, Milan, Italy) were used to study the inflammatory infiltrate and to perform qualitative investigations on different mice models.

Images were taken with a Leica optical microscope DM500 (Milan, Italy), equipped with a camera (Leica, IC50, Milan, Italy) connected to a PC, and images visualized with ProgRes Capture Basic software (Jenoptik, Jena, Germany) or a WWR international PBI light microscopy plugged with a tablet camera system (Bergamo, Italy).

3.1.5 Immunofluorescence staining

All these experiments were conducted in the laboratory of the Department of Clinical and Experimental Medicine, Research Unit of Histology and Embryology, University of Florence, directed by Doctor Stefano Bacci.

Immunofluorescent stains were also performed to assess expression levels of different inflammatory markers during wound healing.

Sections from each wound (one section per staining, ten microscopic fields for each sample) were labelled with the following antigens: anti-Ly6g for granulocytes, anti-CD68 for M1 macrophages, anti-CD206 for M2 macrophages (purchased from Abcam, Cambridge, UK) and rhodaminated avidin to stain mast cells and their granules (Sigma-Aldrich, Milan, Italy). All these monoclonal antibodies were diluted 1:50. Appropriate fluorescein isothiocyanate labelled polyclonal antibodies from rabbit or mouse, diluted 1:32 (Sigma-Aldrich, Milan, Italy) were used as secondary ones. Primary antibodies were applied overnight at 4 °C, secondary ones for 2 hours at 37°C. Control samples from healthy back mice skin were also used for immunofluorescence examination. The omission of the primary antibody and substitution with an irrelevant one was used as a control for the immunofluorescence reactions.

Epifluorescence microscopy

Photomicrographs were taken with an Axiophot microscope (Zeiss, Berlin, Germany) equipped with epifluorescence, through a digital photo camera (Zeiss, Berlin, Germany) connected with a personal computer (ED, Rome, Italy) hosting the software Axiovision 4 (Zeiss, Berlin, Germany).

All measurements were performed at the end of the experiment in a blinded manner by researchers not involved in wound preparation and treatment.

3.1.6 Statistical analysis

Cellular infiltration as shown in H&E-stained sections was graded on a 0-3 arbitrary scale for each biopsy site.²⁸⁴

Immunostained sections were placed on the microscopic stage; adjacent, not overlapping fields were photographed separately for the dermis, at magnification 40X. Positive cells were counted using the software image analysis ImageJ (imagej.nih.gov/ij) as it follows. The background grey level was measured, the threshold was set at 1.5 times the background and the

structures in the dermis that were brighter (i.e. more intensely fluorescent) than the threshold were counted by the software. Each image of the shape of positive cells was subtracted from a background image to compensate for any unevenness in the illumination and camera response. The resulting image was converted into a binary image by selecting a threshold level. The image was then compared with the original optical image and any selections not corresponding to single cells were removed.²⁸⁵ The counts were obtained for spots larger than 50 pixels, which were assumed to represent whole cells. For each comparison, the average value for each specimen was assumed as a sample unit. Data obtained was expressed mean \pm SEM (standard error of mean). All differences were subjected to analysis of variance (including Bonferroni-corrected t-tests or Tukey HSD tests), assuming $p < 0.05$ as significant, using StatView 512+ (Abacus Concepts, Berkeley, CA) or StatPlus (AnalystSoft, Walnut, CA) programs. In case of significant result of the analysis of variance among all experimental groups, the values at each time point were compared with controls by Student t-test for unpaired values with two tails, assuming $p < 0.05$ as significant.²⁸⁶

Data obtained from ELISA assay was expressed as mean \pm SD (standard deviation). Each measure is repeated in triplicate. Statistical analysis was performed using unpaired T-test between corresponding treated or untreated samples.

3.1.7 Mice model of chronic wounds

Sixty-three mice were used. Each mouse was randomized and weighed before the treatment. The anaesthesia was performed by Ketamine (80-100 mg/kg i.p.) and Xylazine (10 mg/kg i.p.). All the animals were randomized and divided into three groups: GI, GII and GIII. In GI and GII groups one full-thickness wound was performed on the shaved back, with a 4 mm large punch (Paramount Surgical Ltd, Delhi, India), while in GIII group two full-thickness wounds were induced (Fig. 32).²⁸⁷

The animals of the GI group and only one lesion of GIII group were treated with a single application of 20.6 J/cm² blue LED light, while the GII group were left to naturally recover.

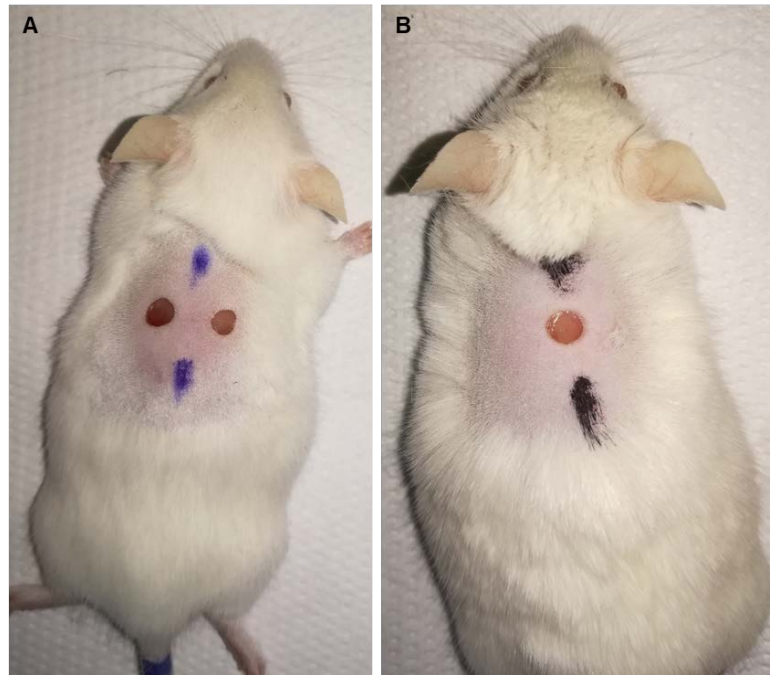


Fig. 32. CD1 mice model of a chronic wound. **A:** Mouse with two full-thickness wounds. **B:** Mouse with one full-thickness wound.

The animals were sacrificed at different times after the induction of the wound; the selected times were: 1, 3, 6, 9, 24 hours and 7 and 14 days.

Immediately after the sacrifice, skin biopsies from the back were obtained. When the healing process was still incomplete and the regenerated tissues were also absent, the perilesional tissue was harvested. This happened at all follow-up times, with the exception of 7 and 14 days.

3.1.8 Enzyme-Linked Immunosorbent Assay

An Enzyme-Linked Immunosorbent (ELISA) assay enabled to study bFGF, EGF, TNF- α , VEGF, MMP-2 and MMP-9 at different postoperative time points. This multiplex sandwich ELISA-based quantitative platform (Quantibody[®] Custom Array, RayBiotech, Norcross, GA, USA) enabled us to accurately determine the concentration of multiple cytokines simultaneously. Each skin sample was homogenized by TissueLyzer II[®] (Qiagen, Milan, Italy) in Radioimmunoprecipitation assay buffer (RIPA buffer) in which an appropriate dilution of Protease Inhibitor Cocktail (Sigma-Aldrich, Milan, Italy) was added, to inhibit serine, cysteine, acid proteases, and aminopeptidases.

After that, the samples were centrifugated and the supernatant was used to measure the total proteins contain using the bicinchoninic acid assay (BCA) (Thermo-Fisher Scientific, Waltham, MA USA), in accordance to manufacturer instructions. The determination of the protein concentration was obtained by absorbance measured at 570 nm, using a 96-well spectrophotometer (LT-4000 Labtech, Heathfield, East Sussex, England) compared to a standard curve obtained with serial dilutions with BSA. The ELISA assay was performed in accordance with manufacturer instructions.

3.2 *In vitro* experiments

3.2.1 Keloid scars

Keloid samples were obtained from seven patients subjected to aesthetic surgeries performed at the AOU Città della Salute e della Scienza in Turin (Italy). From four out of seven patients, we also obtained keloid perilesional tissue. This study was approved by the Local Hospital Ethical Board (protocol n° 0073787 on 25th July 2017). All the experiments were performed in accordance with the Helsinki declaration and in conformity with Good Clinical Practice (GCP).

The general characteristics of excised-keloid tissues are depicted in Table II.

	ID Patient/ Fitzpatrick scale	Date of birth/sex	Dimension (cm)	Onset/ethiology	Date/type of surgery
	1 / IV	2004/M	8x4 cm + <u>boundary</u> <u>tissue</u>	2012/skin burn	2017/ surgical removal and cover with INTEGRA™, followed by dermal skin grafting (IDE)
	2 / II	1972/M	1.5x1 cm	2016/piercing → granuloma by foreign body → surgical removal → keloid	2017/ cryoexcision

	3 / II	1975/F	1x1 cm	2016/piercing → granuloma by foreign body → surgical removal → keloid	2017/ cryoexcision
	4a / II	1987/M	6x7 cm + <u>boundary tissue</u>	2012/spontaneous growth → 2014 surgical removal and suture → keloid	2017/ surgical removal and application of skin from the Skin Bank
	4a / II	1987/M	5x5 cm + <u>boundary tissue</u>	2012/spontaneous growth → 2014 surgical removal and suture → keloid	2017/ surgical removal and application of skin from the Skin Bank
	5 / V	1980/F	4x2 cm + <u>boundary tissue</u>	2001/piercing → keloid → 2011 surgical removal and suture → new keloid tissue	2017/ cryoexcision
	7/ V	1980/M	12x7 cm 7a: <i>pars distale</i> 7b: <i>pars intermedia</i> 7c: <i>pars prossimale</i>	2010/piercing → surgical removal → 2017/keloid relapse	2017/excision and application of INTEGRA™ dual layer
	8 a/VI	1989/M	1x1.5 cm	2015/Spontaneous growth → 2016 laser removal → 03.2017 keloid relapse	2017/ cryoexcision
	8 b/VI	1989/M	1x1 cm	2015/Spontaneous growth → 2016 laser removal → 03.2017 keloid relapse	2017/ cryoexcision
	8 c/VI	1989/M		2015/Spontaneous growth → 2016 laser removal → 03.2017 keloid relapse	2017/ cryoexcision

Table II. Characteristics of keloid and perilesional tissue used to prepare primary cultures of human fibroblasts.

3.2.2 Healthy skin

The healthy human skin samples were obtained from two patients subjected to aesthetic surgeries performed at the AO in Perugia. The study was approved by the Hospital Ethical Board (protocol n° 16806/19/AV on 17th/07/2019). All the experiments were performed in accordance with the Helsinki declaration and in conformity with GCP.

3.2.3 Primary cultures of human fibroblasts

Keloid, perilesional and healthy tissues were maintained in Dulbecco Modified Eagle Medium (DMEM) at 4°C and used within 5 hours from the excision. Each sample was subjected to eight vigorous washes, in order to remove hair and blood residue. Then, dermal and epidermal portions were dissected with scalpels or scissors to obtain sections of about 4-6 mm diameter. Fragments were disposed on scratch-Petri dishes and were maintained semi-opened into the laminar flow for 40 minutes to allow adhesion to the dish.²⁸⁸ After this procedure, DMEM low glucose (1.5 g/L) medium (Pan-React Applichem, Milan, Italy) supplemented with 10% Foetal Bovine Serum (FBS), 1% of Glutamine and 1% Penicillin-Streptomycin (EuroClone, Milan, Italy) was added and cells maintained at 37°C and 5% CO₂ (Fig. 33 A). Within three weeks from the preparation, fibroblasts migrated from the tissue to the bottom of the dish (Fig. 33 B-D). When an adequate number of cells were obtained, fibroblasts were detached by Trypsin-EDTA solution (Sigma-Aldrich, Milan, Italy), collected in a centrifuge tube, centrifuged and pellet seeded in T75 flask (Greiner Bio-One, GmbH). Fibroblasts were maintained under standard culture conditions (37°C; 5% CO₂), medium refreshed every 48 hours. Cells were splitted when reaching about 80% of confluence.

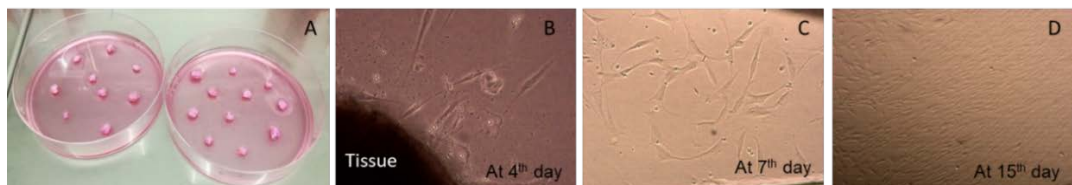


Fig. 33. **A:** Preparation of human fibroblasts primary cultures. **B-D:** Human cultured fibroblasts at different times.

3.2.4 Confocal microscopy

Confocal analysis was performed with a 63x (NA 1.40 Plan) oil immersion objective using a confocal laser scanner microscope (TCS SP8, Leica Microsystems CMS, GmbH, Mannheim, Germany). LASX (Leica Microsystems CMS, GmbH, Mannheim, Germany) software was used to visualize and process acquired-images.

Cells were seeded in treated-glass bottom dishes (Ibidi, GMBH, Martinsried, Germany) and an immunostaining protocol was performed as follows. Cells were permeabilized using 0.25% Triton X100 (Sigma-Aldrich, Milan, Italy) in PBS (Pan-React Applichem, Milan, Italy). Unspecific sites were blocked by incubation in 1% of BSA (Sigma-Aldrich, Milan, Italy) in PBST (PBS plus 0,1% of Tween20) (Sigma-Aldrich, Milan, Italy). Anti-Alpha-smooth muscle actin (α -SMA), anti-HSP47 and anti-cytokeratin antibodies were diluted 1:250, while anti-type I collagen antibody was diluted 1:500. All secondary antibodies, AlexaFluor555, AlexaFluor488 and AlexaFluor647, were diluted 1:400. All antibodies were purchased from AbCam (UK, Cambridge) and used accordingly to the manufacturer instructions. DAPI (Sigma-Aldrich, Milan, Italy) was added to stain cell nuclei.

3.2.5 Blue LED light applications

All the experiments were performed applying the blue LED light with the fiber-device previously described in 1.1. The fluence values which correspond to different doses of blue light directly applied to cultured cells are reported in Table III.

Fluence values were calculated taking into account the dimension of the well and of the irradiation spot, at the maximum energy provided by the device. All the irradiation parameters were measured using a photodiode energy sensor (Ophir, Darmstadt, Germany).

Time (s)	Fluence (J/cm ²)
5	3.43
10	6.87
20	13.7
30	20.6
45	30.9
60	41.2

Table III. Doses of blue light used to perform the experiments.

3.2.6 Cell viability assay

Cell viability was assessed by using Trypan Blue solution 0.4% (Sigma-Aldrich, Milan, Italy), a dye used to label dead cells. Trypan Blue is not absorbed by healthy and viable cells, but stains, in blue or light blue, cells with a damaged membrane. This technique was used to discriminate the presence of necrotic cells in the culture after blue LED light treatment. Fibroblasts were seeded in four p35 dishes for each experimental condition and maintained in low glucose DMEM for 24 h. The day after, two out of the four dishes prepared were treated with the blue LED light applying 41.2 J/cm², the remaining two dishes were used as control (untreated cells). The treatment was performed in DMEM SFM. Dishes were divided into two groups and Trypan Blue staining was evaluated 24 or 48 hours after irradiation. After removal of SFM DMEM, two washes in PBS were performed and Trypan Blue diluted 1:4 in PBS was applied for 6 min to all the dishes. After two additional washes in PBS, cells were observed under an inverted optical microscope and images were acquired by using a 5-megapixel photo-camera (Eurotek Orma, INV100T).

3.2.7 Evaluation of cell apoptosis

In order to evaluate apoptosis induced by blue LED light treatment, DAPI staining was performed to analyze eventual nuclear fragmentation.

Fibroblasts, irradiated following the procedure described above, were fixed at 24 or 48 hours after irradiation by paraformaldehyde 3.6% in PBS for 6 minutes. After two washes in PBS, cells were permeabilized by Triton X-100 for 10 minutes on a mechanical shaker. After two washes in PBS, one drop of DAPI was applied on each sample before mounting on a coverslip. Quantification of fragmented, picnotic, nuclei was performed by using a confocal microscope (TCS SP8, Leica Microsystems CMS, GmbH, Mannheim, Germany) with 40x objective (NA 0.75 Plan) water-immersed and images were processed by ImageJ software.

3.2.8 WST-8 assay

The tetrazolium reduction assay measures some aspects of general metabolism or an enzymatic activity as a marker of viable cells.²⁸⁹

CCK-8 was purchased from Sigma-Aldrich (Milan, Italy). CCK-8 use WST-8 (2-(2-methoxy-4-nitrophenyl)-3-(4-nitrophenyl)-5-(2,4-disulfophenyl)-2H-tetrazolium, monosodium salt), which produces a water-soluble formazan dye upon bioreduction in the presence of an electron carrier, 1-Methoxy PMS. WST-8 is bioreduced by cellular dehydrogenases to an orange formazan product that is soluble in the tissue culture medium.

Fibroblasts were counted by using Neubauer chamber and 5×10^3 cells were seeded in 96-multiwell plate (Greiner Bio-One, GmbH) and maintained for 24 hours in standard culture conditions, before the experiments. The day after, DMEM was replaced with SFM (Serum-Free Media) before treatment and then cells were irradiated (3 replicas considered) by blue LED light at 3.43 – 6.87 – 13.7 – 20.6 – 30.9 and 41.2 J/cm². This protocol enabled us to study the dose of irradiation that can provide the best modulation of fibroblasts if any. For each experiment, three wells were left untreated and used as a control. The irradiation was performed by holding the fibre steadily 1 cm far from the bottom of each well. Each treatment was performed in SFM without red phenol to avoid light absorption from the cell medium. Measurements were performed 24 and 48 hours after irradiation: absorbance at 450 nm was read and a reference wavelength at 630 nm was used, with an automatic microplate absorbance reader (LT-4000 Labtech, Heathfield, East Sussex, England), processing the values with a specific commercial software (GraphPad Prism, San Diego, CA, USA). Each experiment was independently performed in triplicate.

3.2.9 Sulforhodamine B assay

Cell proliferation was measured by SRB (Sulforhodamine B) based Assay purchased from Sigma-Aldrich (Milan, Italy) which binds stoichiometrically to proteins under mildly acidic conditions and then can be extracted under basic conditions; thus, the amount of bound dye can be used as a proxy for cell mass, which can then be extrapolated to measure cell proliferation.²⁹⁰⁻²⁹¹⁻²⁹²

Experiments were performed as described in 2.8. Measurements were performed 24 and 48 hours after irradiation: the absorbance at 570 nm,

coupled with a reference wavelength at 630 nm was used, and with an automatic microplate absorbance reader (LT-4000 Labtech, Heathfield, East Sussex, England), processing the values with a specific commercial software (GraphPad Prism, San Diego, CA, USA). Each experiment was independently performed in triplicate.

3.2.10 Electrophysiological recordings

Whole-cell patch-clamp recordings were performed in -60 mV clamped-cells as described ²⁹³⁻²⁹⁴. The following solutions were used: standard K⁺-containing extracellular solution (mM): NaCl 147; KCl 4; MgCl₂ 1; CaCl₂ 2; HEPES (4-(2-hydroxyethyl)-1-piperazineethanesulfonic acid) 10; D-glucose 10 (pH 7.4 with NaOH). Standard K⁺-based pipette solution (mM): K-gluconate 130; NaCl 4.8; KCl 10; MgCl₂ 2; CaCl₂ 1; Na²-ATP 2; Na²-GTP 0.3; EGTA 3; HEPES 10 (pH 7.4 with KOH). For K⁺-replacement experiments, extracellular and intracellular K⁺ were substituted with equimolar Cs⁺.

Confluent cells were suspended, plated into 13 mm diameter coverslips and allowed to adhere for at least 2 hours before starting electrophysiological recordings. Each coverslip was then transferred to a 1 ml recording chamber mounted on the platform of an inverted microscope (Olympus CKX41, Milan, Italy) and superfused at a flow rate of 1.5 ml/min by a three-way perfusion valve controller (Harvard Apparatus). Borosilicate glass electrodes (Harvard Apparatus, Holliston, MA) were pulled with a Sutter Instruments puller (model P-87) to a final tip resistance of 3–5 MΩ. Data were acquired with an Axopatch 200B amplifier (Axon Instruments, CA), low-pass filtered at 10 kHz, stored and analysed with pClamp 9.2 software (Axon Instruments, CA).

All the experiments were carried out at room temperature (RT: 20–22°C) and the treatment with Blue LED light was carried out for 30 s. Series resistance (R_s), membrane resistance (R_m), and membrane capacitance (C_m) were routinely measured by fast hyperpolarizing voltage pulses (from -60 to -70 mV, 40 ms duration). Only cells showing a stable C_m and R_s before, during, and after Blue LED light application were included in the analysis. Immediately after seal breaking-through, cell resting membrane potential was determined by switching the amplifier to the current-clamp mode. A voltage ramp protocol

(800 ms depolarization from -80 to +80 mV) was used to evoke overall voltage-dependent currents before, during, and after Blue LED light treatments. The equilibrium potential for K^+ (E_K) and Cl^- (E_{Cl}) ions was calculated by applying Nernst equation as follow: $E = E_0 - (RT/nF) \ln([K^+]_o/[K^+]_i)$; where R = ideal gas constant = 8.314 J/mol(K); F = Faraday's constant = 95,484.56 C/mol; $\ln([K^+]_o/[K^+]_i)$ = natural log of the ion concentration quotient across cell membrane. Data were expressed as mean \pm SEM.

3.2.11 Raman spectroscopy measurements

Raman spectroscopy can serve as an efficient and rapid tool to determine the redox state of the photosensitive species in the cell, before and after the blue LED light exposure. In particular, through proper choice of the excitation wavelength, Raman spectroscopy can be used to reveal the redox conditions of the biomolecular species throughout the mitochondrial electron chain transport, i.e. the cytochromes, directly from cells or tissues.²⁹⁵

Raman experiments were carried out on a micro-Horiba Xplora coupled to a 532 nm wavelength laser for the excitation. The spectrograph used 1200 grooves mm^{-1} grating with a confocal microscope in backscattering geometry and a 2D-CCD camera. The backscattered light was collected by a 100X microscope objective with 0.9 NA, which generated a $\approx 1 \mu m$ large laser beam waist. An integration time of 5 seconds and a laser power value of 5 mW on the sample were employed for Raman measurements on fibroblast cells.

Firstly, we performed experiments on Cyt C pure solutions (Sigma-Aldrich, Milan, Italy), in order to obtain information about the possible effect of blue light on the redox state of this molecule. Samples were prepared by drop-casting of 3 μl of an aqueous Cyt C solution at 0.1 mM concentration on the gold mirror support (ME1S-M01; Thorlabs, Inc., Newton, NJ). Upon evaporation of the solvent, a circular coffee-ring stain of Cyt C was formed on the support. Raman measurements were performed on 5 different points of the Cyt C ring stain for each sample. Raman spectra were recorded on samples without treatment and after the irradiation with 20.6 J/cm^2 and 41.2 J/cm^2 blue LED light.

After that, fibroblasts were detached by using Trypsin EDTA, centrifugated (1000 rpm for 6 minutes) in PBS and the pellet was used to Raman analysis. Typically, for a single Raman measurement, a volume of 2 μ l of the pellet was drop-casted onto a gold mirror support and Raman spectra were immediately recorded on samples without treatment (control) after 20.6 J/cm² and 41.2 J/cm² of blue LED irradiation. For each sample at least 5 individual cells were inspected while carefully avoiding cell dehydration.

3.2.12 Drugs

We used two selective adenosine A_{2A} receptor antagonists: 4-(2-(7-amino-2-(furan-2-yl)-[1,2,4]triazolo[1,5-a][1,3,5]triazin-5-ylamino)ethyl)phenol (ZM241385, Tocris, Milan, Italy) and NPD150, a new A_{2A} selective antagonist synthesized by the group of pharmaceutical chemists directed by Professor Vittoria Colotta, Dept. of NEUROFARBA, Section of Farmaceutica e Nutraceutica, University of Florence. The compound was recently identified as belonging at the class of 8-amino-1,2,4-triazolo[4,3-a]pirazin-3-oni series. All drugs were dissolved in dimethyl sulphoxide (DMSO). Stock solutions, of 1000–10.000 times the desired final concentration, were stored at -20°C. The final concentration of DMSO (0.1%) used in our experiments did not affect cell proliferation (data not shown). Each drug was applied at the desired concentration directly in the culture medium for 15 minutes at 37°C and maintained for all the experiment.

3.2.13 Statistical analysis

Data were expressed as mean \pm SEM. Student's paired or unpaired t-tests and one-way ANOVA followed by Dunnett's multiple comparison test analysis were performed. Statistical significance was set at * $p < 0.05$. Data were analysed by using software package GraphPad Prism (GraphPad Software, San Diego, CA, USA).

4. RESULTS

4.1 Results obtained on mice models of acute wound

The skin inflammatory infiltrate is a typical response to wound healing which is possible to study using histological analysis. Indeed, each inflamed tissue shows typical histological characteristics, as demonstrated in many animal models and human subjects.²⁹⁶

4.1.1 Blue LED light irradiation reduces early inflammatory infiltrate in the mouse skin acute wounds

These series of experiments aim to investigate the role of different inflammatory cells in the process of wound healing in CD1 mice subjected to superficial abrasions. In particular, we carried out two abrasions on the skin. One was treated by applying a dose of 20.6 J/cm² of blue LED light, while the other one did not receive any treatment. Microscopic evaluation^{20,297} of histological samples colored with H&E indicates a more pronounced inflammatory infiltrate in treated wounds if compared to corresponding untreated wounds at 3 and 18 hours from the wound induction (Fig. 34). At a longer follow up, the differences in the inflammatory infiltrate level in treated and not treated wounds decreases.

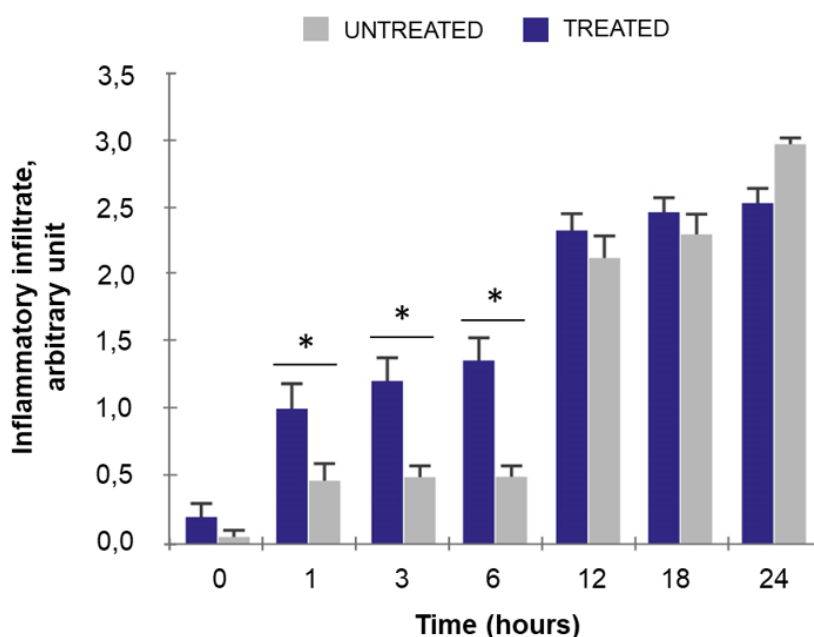


Fig. 34. Changes in the level of inflammatory infiltrate in mouse biopsies of acute wounds in the absence or after blue LED light exposure. Data, calculated at different times from wound induction, are expressed as mean \pm SEM. N=3 for each experimental condition. Statistical analysis: * p < 0.05, unpaired T-test between corresponding treated or untreated groups.

We further analyzed in more detail the cell types involved in the formation of the inflammatory infiltrate in untreated and treated wounds.

Since the granulocyte neutrophils show high motility, the phagocytic activity was first considered. This population of cells was identified by the use of the anti-Ly6G antibody revealed by epifluorescence microscopy. As shown in Fig.35, the number of Ly6G⁺ cells was similar along different times, both in treated and untreated wounds, while at 24 hours from skin abrasion, a significant increase in the number of Ly6G⁺ cells was observed only in the untreated groups (Fig. 35). These results suggest that at 24 hours the treated wound shows a modest level of these cells that could represent a more controlled inflammatory response to injury.

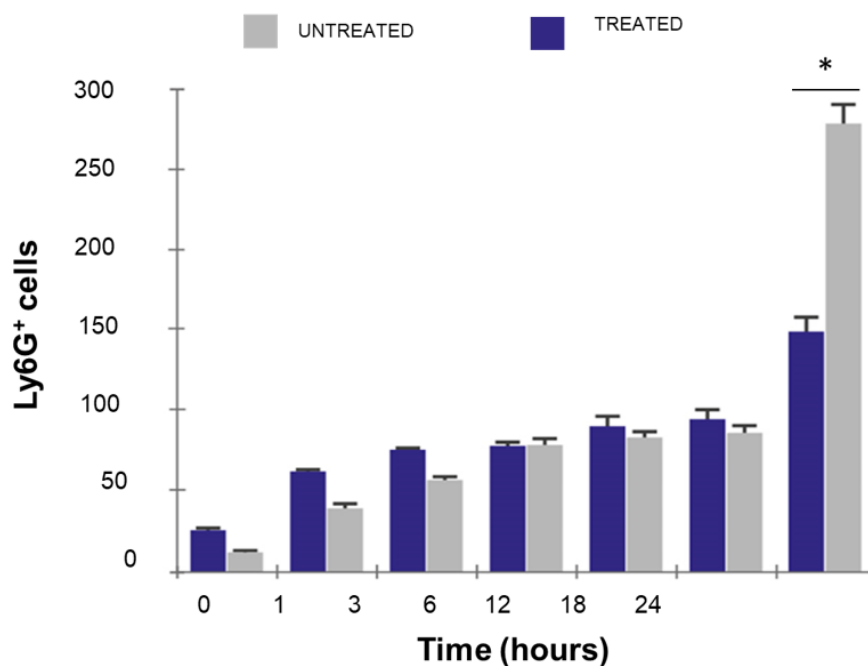


Fig. 35. Quantitative analyses of granulocytes neutrophils (Ly6G⁺ cells) in mouse biopsies of acute wounds in the absence or after blue LED light exposure at different times from skin abrasion. Data are expressed as mean±SEM, calculated at different times from wound induction. N=3 for each experimental condition. Statistical analysis: * $p < 0.05$, unpaired T-test between the treated and corresponding untreated group at 24 hours time point.

Another type of cells which play a role in inflammatory infiltrate are mast cells. They are involved in the first stages of inflammatory infiltration and organization of tissue repair processes. Mast cells, by the release of various mediators, regulate the functions of many cell types, such as dendritic cells, macrophages, T and B lymphocytes, fibroblasts, endothelial cells and

epithelial cells.²⁹⁸ Thereafter, mast cells represent a key-regulators in the control of wound healing events.²⁹⁸

In the first inflammatory phase, the blue LED light irradiation did not significantly affect mast cells density in the treated wounds in comparison to corresponding untreated (Fig. 36).

As a contrast, mast cells degranulation index is significantly increased by blue light in the range from 1 to 3 hours from skin abrasion (Fig. 37).

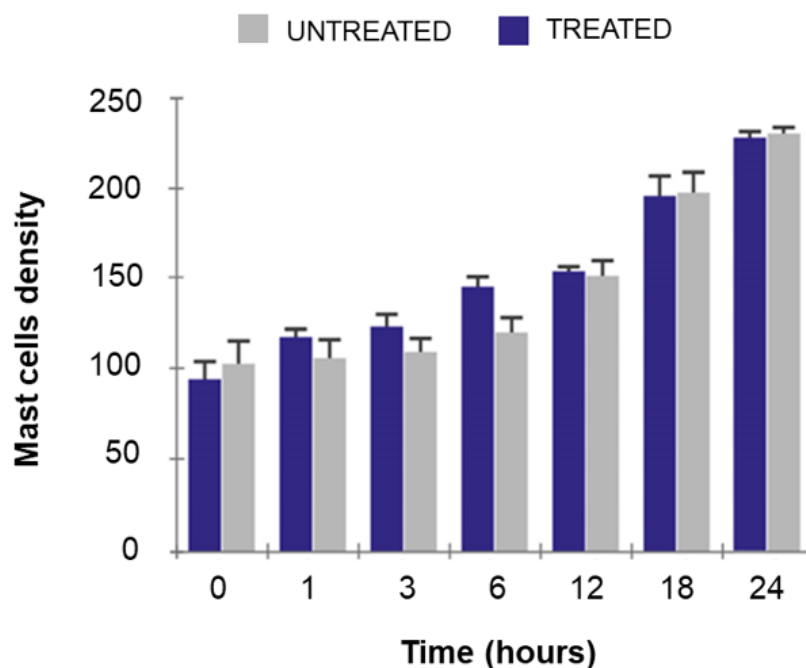


Fig. 36. Changes in the mast cell density in mouse biopsies of acute wounds in the absence or after blue LED light exposure. Quantitative analyses of avidin-rhodamine conjugated positive cells in the two experimental groups at different times from skin abrasion. Data are expressed as mean \pm SEM. N=3 for each experimental condition.

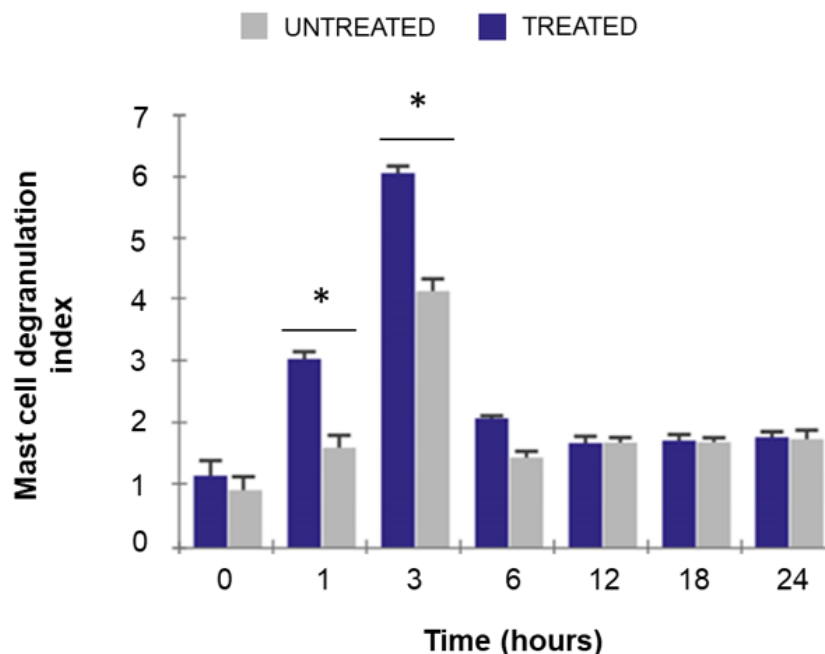


Fig. 37. Changes in the mast cell degranulation index in mouse biopsies of acute wounds in the absence or after blue LED light exposure. Quantitative analyses of avidin-rhodamine conjugated positive cells in the two experimental groups at different times from skin abrasion. Data are expressed as mean \pm SEM. N=3 for each experimental condition. Statistical analysis: * p < 0.05, unpaired T-test between the treated and corresponding untreated groups at 1 and 3 hours time point.

Macrophages are one of the most important cells involved in the inflammatory response in wound healing. Two different macrophages phenotypes, i.e. M1 or pro-inflammatory and M2 or pro-healing, have been described. The investigation about the polarization of these cells gives important information about the wound environment. For these reasons, we carried out a morphological examination on macrophages populations and specific fluorescent markers were used to localize the morphofunctional passage of these cells. In particular, anti-CD68 and anti-CD206 antibodies were used to reveal macrophages density per unit of the surface with epifluorescence M1 and M2 subpopulation respectively.

In untreated samples, the M2 subpopulation increased in a closely related manner during the 24 hours from the lesion (Fig. 38), while in treated samples, this macrophage phenotype reached two peaks at the 6th and the 9th hours after treatment (Fig.39). In particular, these increases are accompanied by a reduction in M1 phenotype only in treated tissue compared to untreated (Fig. 39 and Fig. 38, respectively). In any case, after 24 hours from the

induction of the wounds, M2 subpopulation density is increased in all, treated and untreated, tissues.

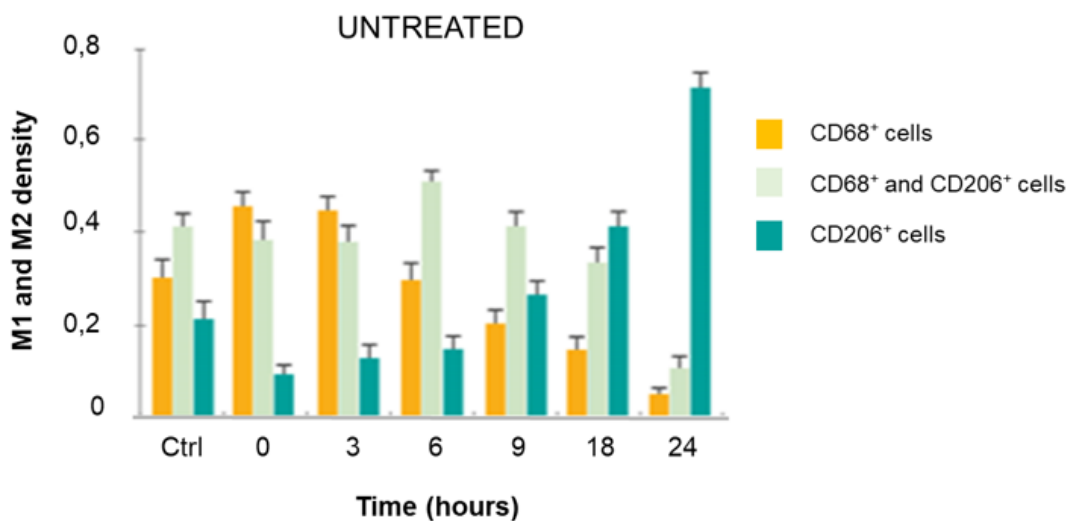


Fig. 38. Immunofluorescence analysis indicating the switch of macrophages from M1 to M2 phenotype in the untreated sample of mouse biopsies of acute wounds after different times from wound induction. Data are expressed as mean \pm SEM. CD68⁺ cells (orange column) represents M1 phenotype; CD206⁺ cells (green column) represents M2 phenotype. CD68⁺ and CD206⁺ cells are macrophages with both stainings. M1 appears more abundant in the early inflammatory phase (0, 3, 6 hours) while M2 predominates in the late phase (18, 24 hours). N=3 for each experimental condition.

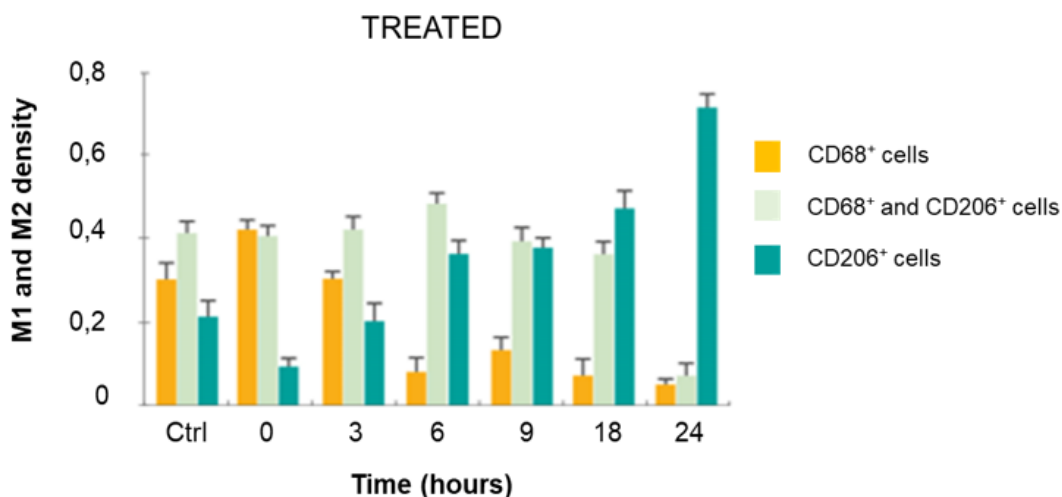


Fig. 39. Immunofluorescence analysis indicating the switch of macrophages subpopulations from M1 to M2 phenotype in blue LED light treated sample of mouse biopsies of acute wounds after different times from wound induction. Data are expressed as mean \pm SEM. CD68⁺ cells (orange column) represents M1 phenotype; CD206⁺ cells (green column) represents M2 phenotype. CD68⁺ and CD206⁺ cells represent macrophages with M1 and M2 characteristic. M2 phenotype is evident from 6 hours from wound induction. N=3 for each experimental condition.

We conducted a new series of experiments to evaluate the wound healing process after the blue LED light irradiation, in different pathological models. For reaching this purpose, we decided to use histological investigations and to compare skin biopsies obtained from untreated mice with the biopsies from treated mice.

4.1.2 Streptozotocin-induced acute diabetic mice

Induction of one skin abrasion in acute diabetic mice

Haematoxylin and eosin staining performed on acute diabetic mice biopsies enabled us to observe qualitative differences into the wound healing process between wounds in which 20.6 J/cm^2 were applied and untreated mice. In this model, we evaluated the healing process in a time range from three days to seven days.

In this set of experiments, the effects of the blue LED light were observed on a skin abrasion and compared to the healing process in an untreated abrasion in the same animal (Fig. 40 A-D). As shown in Fig.40, at the 3rd day post-treatment, the treated tissue (Fig. 40 C) exhibits a better collagen disposition respect to the untreated tissue (Fig. 40 A). Seven days after the lesion, both the treated (Fig. 40 D) and the untreated tissue (Fig. 40 B), show a restored collagen morphology and similar skin tissue architecture.

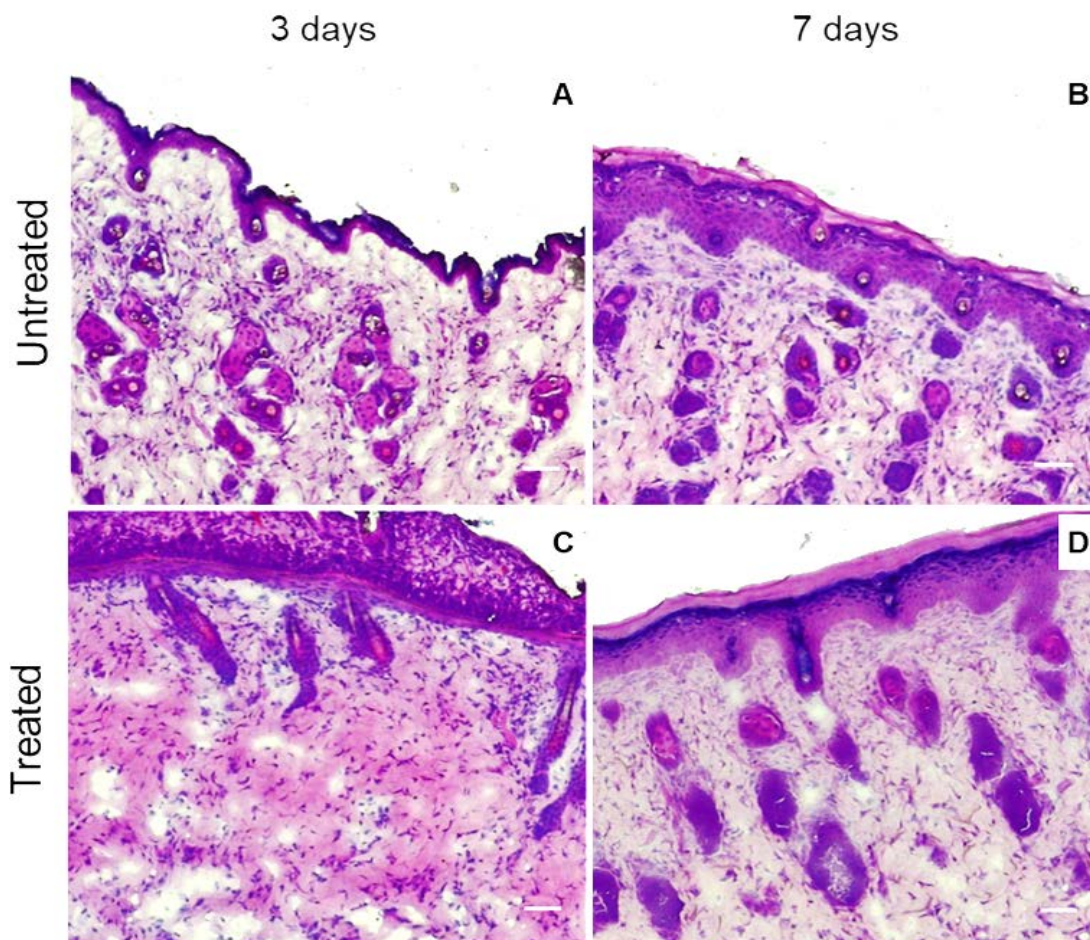


Fig. 40. H&E staining of skin sample of mouse acute wounds biopsies obtained from acute diabetic mice (10X magnification) in different experimental conditions. **A, B**: Untreated samples analyzed at 3 and 7 days after wound induction, respectively. **C, D**: Wounds treated with a single dose of blue LED light, 3 and 7 days after treatment, respectively. Scale bar calibration: 50 μ m.

Induction of two skin abrasions in mice

In this set of experiments, the effects of the blue LED light were observed on a skin abrasion and compared to the untreated lesion, in the same animal. (Fig. 41 A-D). Histological analysis did not evidence remarkable differences in tissue architecture and collagen morphology (Fig.41).

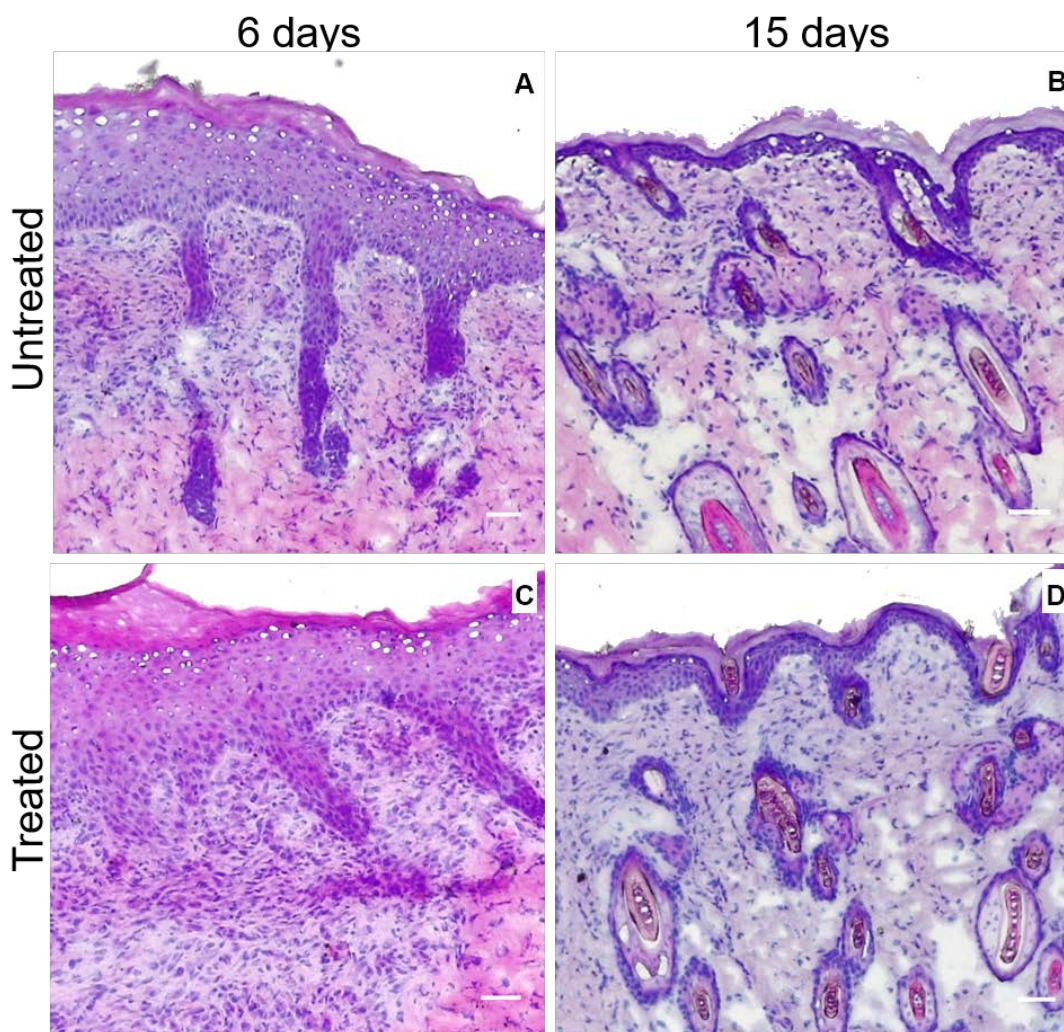


Fig. 41. Haematoxylin and eosin staining of skin sample of mouse acute wounds biopsies obtained from acute diabetic mice (10X magnification) in different experimental conditions. **A, B:** Untreated samples analyzed at 3 or 7 days after wounds induction. **C, D:** Analysis performed at the same time in the corresponding wound treated by a single dose of Blue LED light. Scale bar calibration: 50 μ m.

4.1.3 Streptozotocin-induced chronic diabetic mice

Haematoxylin and Eosin staining analysis, performed on chronic diabetic mice, demonstrated that at the 3rd day from the abrasion there are no evident changes either in the untreated or in the treated samples (Fig. 42 A, C). On the contrary, the morphology of the dermal layer after 15 days from the lesion appeared more organized than the corresponding untreated wound (Fig. 42 B, D).

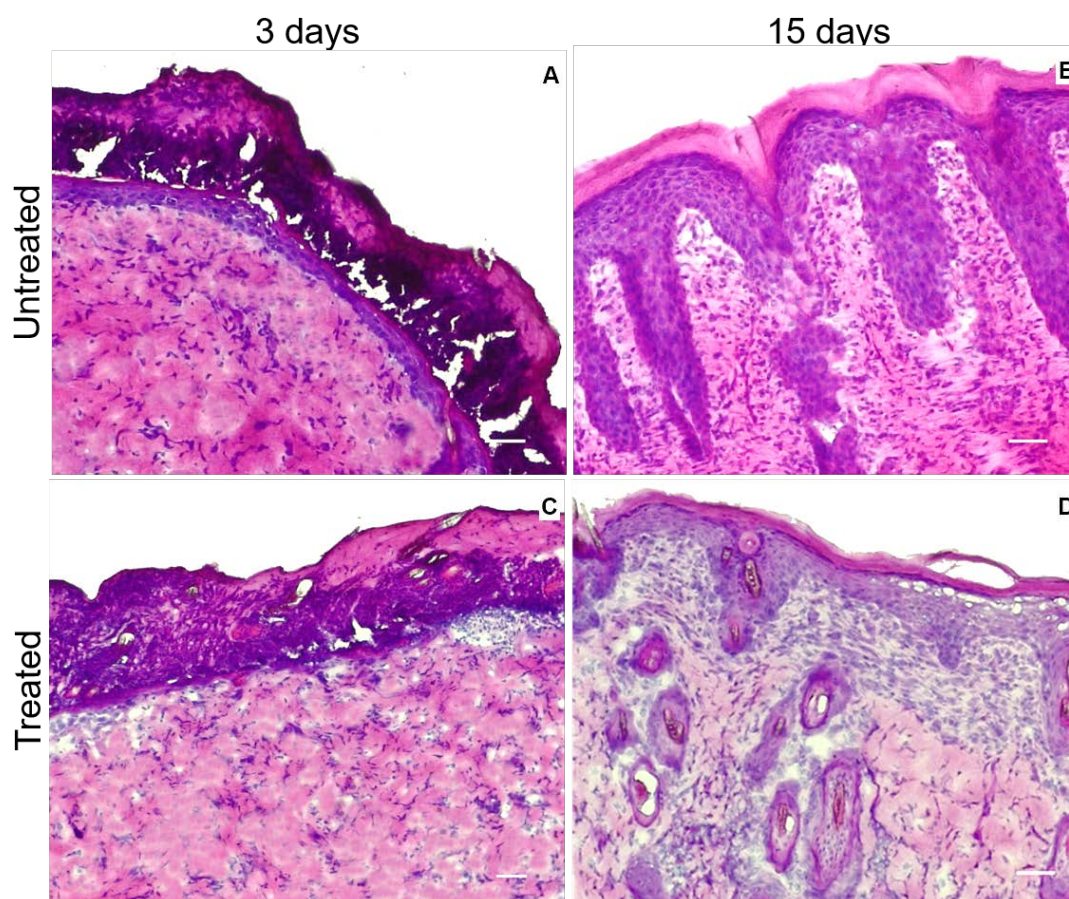


Fig. 42. Haematoxylin and eosin staining of skin sample of mouse acute wounds biopsies obtained from chronic diabetic mice (10X magnification) in different experimental conditions. **A, B:** Untreated samples analyzed at 3 and 15 days after wound induction, respectively. **C, D:** Analysis performed at the same time in the corresponding wound treated by a single dose of blue LED light, at 3 and 15 days after abrasion. Scale bar calibration: 50 μ m.

4.1.4 Purinergic P₂X and P₂Y receptors involvement in wound healing process

The role exerted by ATP in the wound healing process has been clearly established²⁹⁹ and recent studies demonstrated that suramin, non-selective P₂ purinergic receptor antagonist, suppresses the expression of proinflammatory cytokines³⁰⁰ suggesting a role of P₂ receptors in inflammation during the healing process. In our work, mice were intraperitoneally treated with suramin (25mg/Kg) (Fig. 43) or with PPADS, another unselective P₂ receptors antagonist (25mg/Kg, not shown). Thereafter, the two superficial abrasions were produced and the effects of light were observed after 6 hours, when the maximal inflammatory infiltrate in treated tissue was reached (Fig. 34).

It appears that the tissue treated with a combination of suramin and blue LED light showed a less inflammatory infiltrate (Fig. 43 D) when compared with the other images (Fig. 43 A-C). However, additional experiments will be necessary to confirm these results.

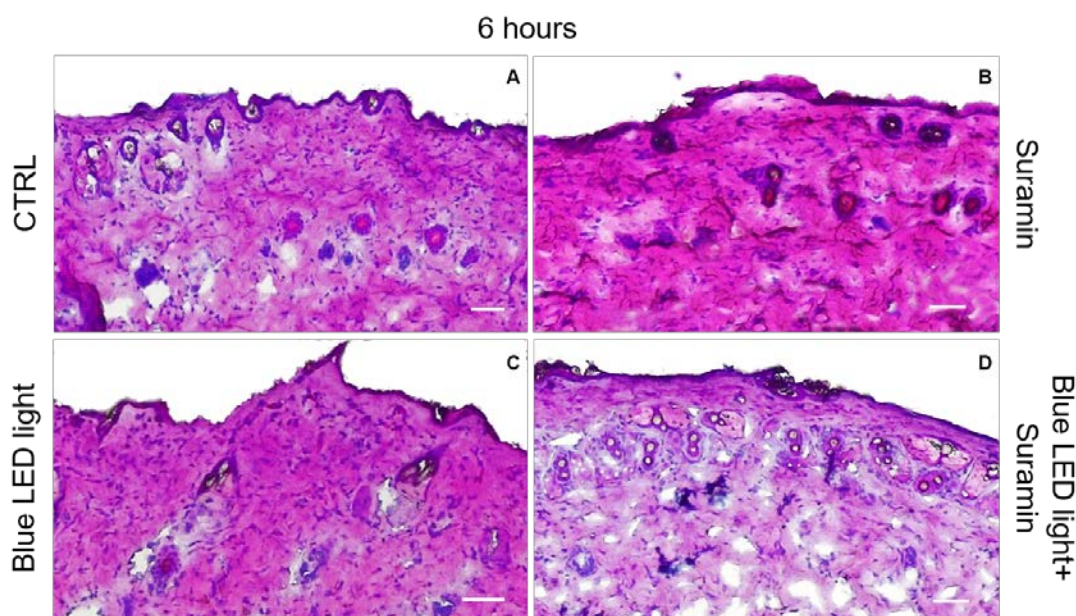


Fig. 43. H&E staining of skin sample of mouse biopsies of acute wounds (10X magnification) obtained after 6 hours from skin abrasion in different experimental conditions. **A:** Staining was performed in tissue taken from control mice (in the absence of any pharmacological or light treatments). **B:** Staining was performed in tissue taken from mice pre-treated with suramin. **C:** Staining was performed in tissue taken from Blue LED light treated- mice. **D:** Staining was performed in tissue taken from mice pre-treated with Suramin which also received light treatment. Scale bar calibration: 50 μ m.

4.1.5 Coagulopathies-induced mice

As described in the introduction (see paragraph 1.1), the blue LED light having a wavelength in the range 410-430 nm acts on protoporphyrin IX contained in haemoglobin molecules and its photothermal effects are revealed by the coagulation of blood in superficial abrasions. On these bases, we performed the heparin-induced coagulopathy in mice with the purpose to observe the possible interactions with early haemostasis and improving wound healing.

From H&E staining, we can observe differences in the early phase of the wound healing process, in particular in a time range from 6 to 72 hours in not-irradiated and in irradiated tissues. After 6 hours from treatment (Fig. 44

B), an increased number of cells appeared enrolled in the healing process in comparison to untreated tissue at the same time (Fig. 44 A). At the following considered times (Fig. 44 C-F) treated and untreated wounds showed a similar healing process, both ending with new epithelial layer formation under the crust (Fig. 44 C-F).

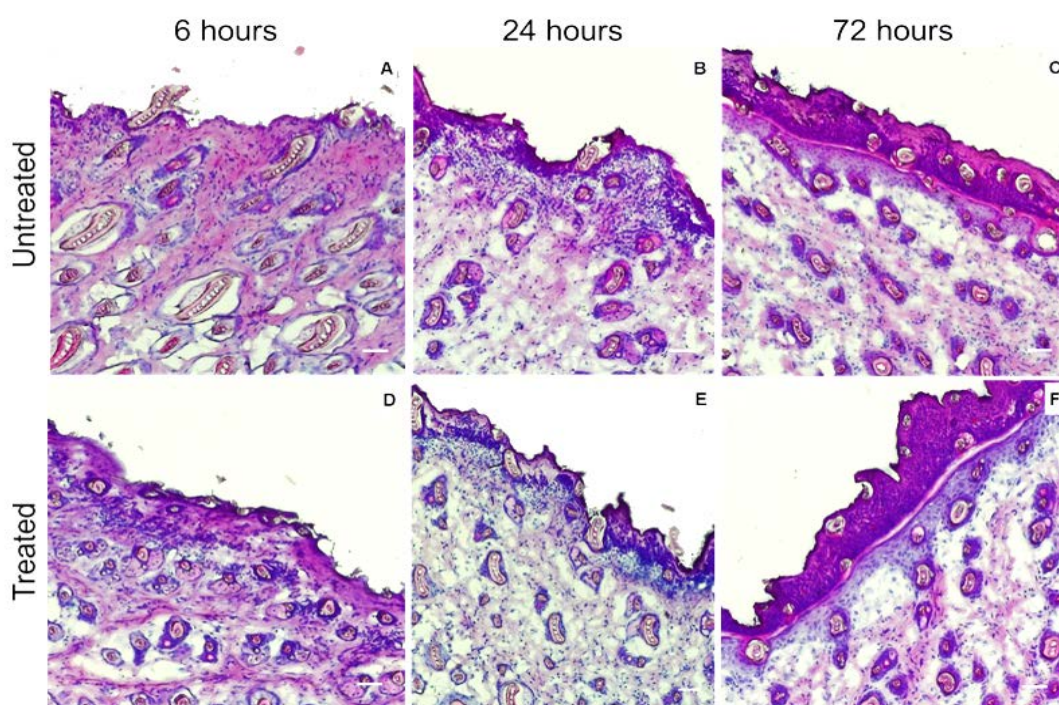


Fig. 44. H&E staining of skin sample in coagulopathy mice (10X magnification). **A-C:** Histology of skin taken from untreated wounds after 6, 24 and 72 hours from abrasion. **D-F:** Images taken from corresponding treated wounds with blue LED light at the same times. Scale bar calibration: 50 μm .

4.1.6 Capsazepine-treated mice

Transient Receptor Potential cation channel (TRP channels) are a large group of ion channels consisting of six proteins family sensitive to different range of temperature. Recently, one of these receptor families was discovered to be involved in inflammation due to atopic dermatitis.³⁰¹

In order to study the possible involvement of TRPV1 channel in the signalling pathway of the blue LED light, we used *Trpv1* knock-out mice (*Trpv1* -/-) and Capsazepine, a selective TRPV1 receptor antagonist. We also tested the vehicle, a standard physiologic solution in which both drugs are diluted. The histology at 6 days after the wound induction in the untreated and the treated

samples, did not show significant differences in the vehicle and transgenic mice groups (Fig. 45 A, B and E, F respectively). On the contrary, only in the Capsazepine-treated mice coupled with the blue LED light treatment, a new epithelial layer was evident, when compared with the capsazepine-treated animals, but in the absence of the blue LED (Fig. 44 C, D).

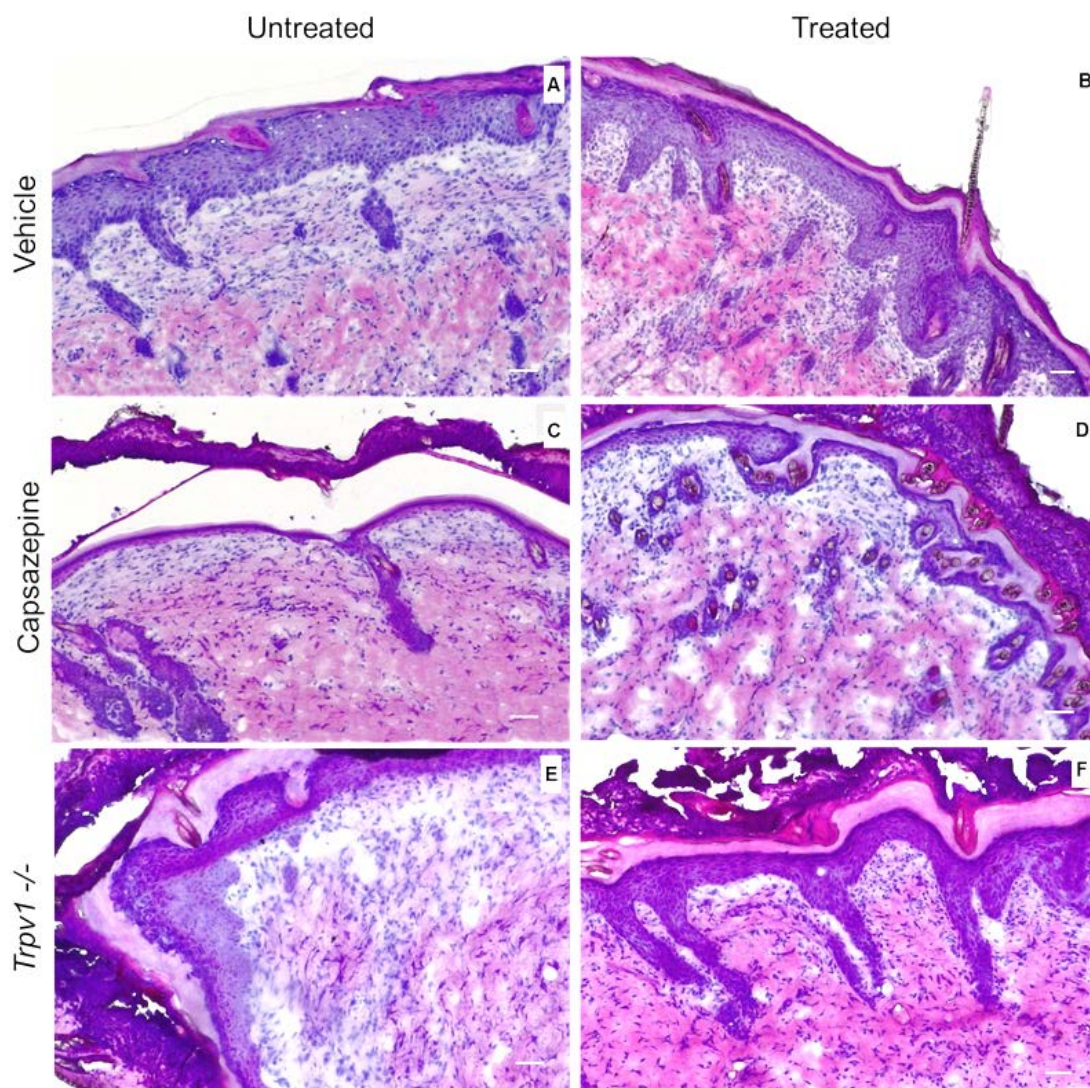


Fig. 45. H&E staining of skin sample in Capsazepine-treated mice (10X magnification). **A**: **B**: untreated and treated wounds with mice injected with vehicle. **C**, **D**: untreated and blue LED light application in mice Capsazepine-treated wounds, respectively. **E**, **F**: untreated and blue LED light application in transgenic mice (*Trpv1* *-/-*)-treated wounds, respectively. Scale bar calibration: 50 μ m

4.2 The blue LED light modulates wound healing in mice model of chronic wounds

Biological markers are usually used as a clear indicator of normal biological processes, pathogenic processes, or pharmacologic responses to a therapeutic intervention.³⁰² On these bases, in this work, we analyzed the levels of bFGF, EGF, TNF- α , VEGF, MMP-2 and MMP-9 involved in wound healing process (Table IV) in mice in which full-thickness²⁹⁷ wounds were performed.

Wound (W)	Time from wounds induction (hours)							
	1		6		24		168	
	UTW	TW	UTW	TW	UTW	TW	UTW	TW
bFGF	290.71 \pm 133.40	263.05 \pm 120.22	266.13 \pm 82.45*	223.22 \pm 66.31*	243.45 \pm 53.21***	176.64 \pm 59.05***	167.61 \pm 185.50	160.37 \pm 144.78
EGF	209.88 \pm 233.76	144.9 \pm 99.41	37.19 \pm 17.64	31.94 \pm 18.20	68.62 \pm 46.14**	140.84 \pm 106.33**	NA	123.80 \pm 82.85
TNF-α	218.20 \pm 209.12	162.35 \pm 164.42	14.08 \pm 12.24	27.32 \pm 30.86	5.69 \pm 7.93**	22.23 \pm 24.78**	NA	101.16 \pm 156.99
VEGF	10.12 \pm 10.20	5.99 \pm 4.27	11.71 \pm 7.06***	2.22 \pm 1.73***	22.26 \pm 20.13*	11.19 \pm 12.15*	23.86 \pm 22.23	36.34 \pm 23.13
MMP2	2568.18 \pm 1778.38*	3479.08 \pm 1791.96*	NA	NA	2111.76 \pm 1083.59	2763.70 \pm 1568.04	995.95 \pm 185.50*	2246.11 \pm 1121.06*
Pro-MMP9	1304.92 \pm 209.12*	2092.44 \pm 164.42*	NA	NA	5429.75 \pm 4704.50	4496.59 \pm 4084.62	84.84 \pm 48.81	36.34 \pm 23.13

Table IV. bFGF: basic Fibroblasts Growth Factor. EGF: Epidermal Growth Factor. TNF- α : Tumor Necrosis Factor-alpha. VEGF: Vascular Endothelial Growth Factor. MMP2: metalloproteinase 2. Pro-MMP9: pro-metalloproteinase-9. Data are expressed mean \pm SD. Each measure is repeated in triplicate. Statistical analysis: * $p < 0.05$; ** $p < 0.01$; *** $p < 0.001$; unpaired T-test between corresponding treated or untreated tissues.

After 1 hour from the wound induction, a significant increase in Pro-MMP-9 levels was found in treated wounds when compared to the untreated; this effect recovered significant levels at 7 days, (Fig. 46 D) where MMP-2 levels (Fig. 46 D) highly increased only in treated wounds.

In addition, we observed a significant decrease in bFGF and VEGF levels in the treated wounds after 6 and 24 hours from the wound induction (Fig. 46 B, C). Finally, a significant increase of EGF was found only at 24 hours from the wound induction in treated tissue (Fig. 46 C).

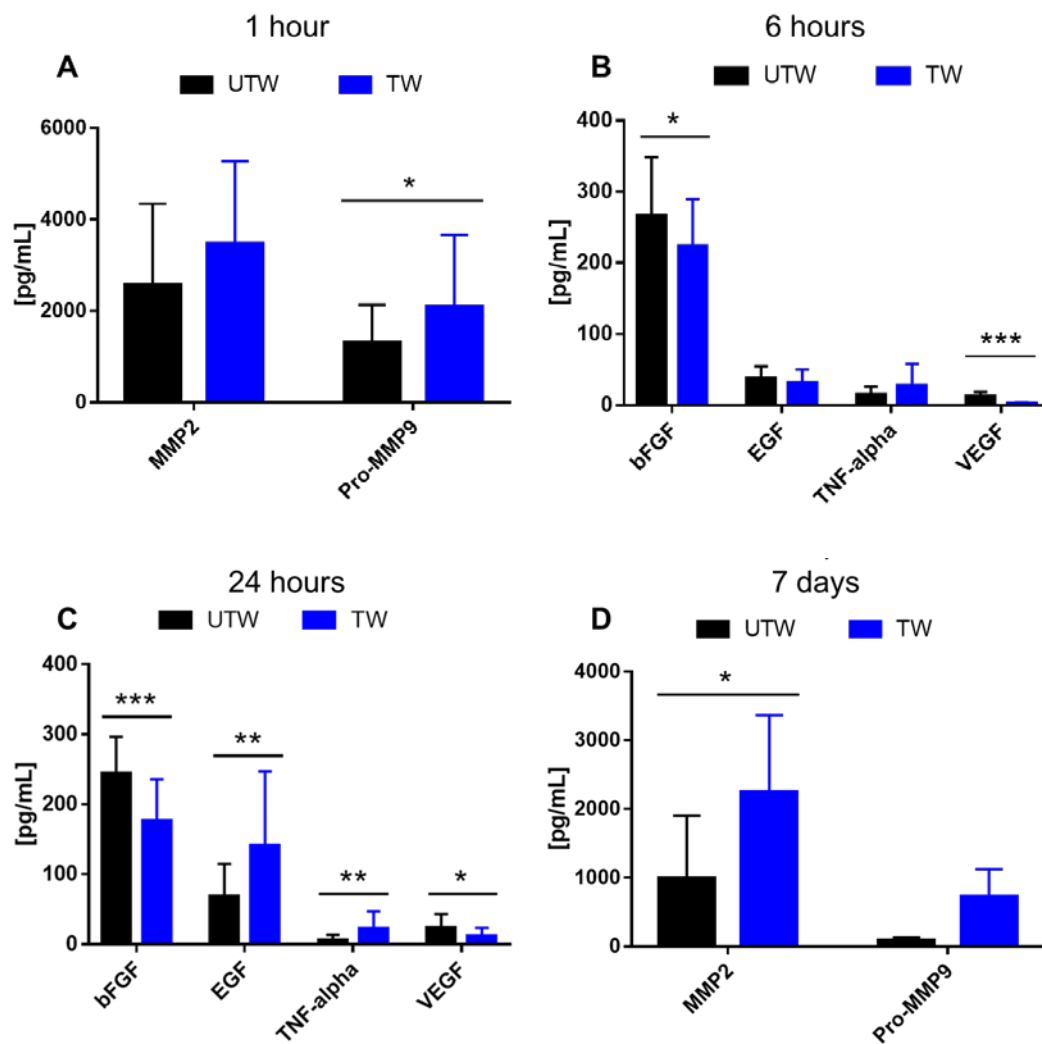


Fig. 46. Blue LED light significantly modulates MMP-2 and MMP-9, bFGF, and VEGF. bFGF: basic Fibroblasts Growth Factor. EGF: Epidermal Growth Factor. TNF- α : Tumor Necrosis Factor-alpha. VEGF: Vascular Endothelial Growth Factor. MMP2: metalloproteinase 2. Pro-MMP9: pro-metalloproteinase-9. Data are expressed mean \pm SD. Each measure is repeated in quadruplicate; N=3 animals for each experimental condition. Statistical analysis: * $p < 0.05$; ** $p < 0.01$; *** $p < 0.001$; unpaired T-test between corresponding treated or untreated tissues.

4.3 Confocal microscopy characterization of cultured fibroblasts

Cultured fibroblasts were characterized by using immunofluorescence staining revealed by the confocal microscopy before starting all the experiments.

From our investigations, we observed that until the 5th passage cell culture, the cultured fibroblasts expressed a cytosolic precursor of type I collagen (marked with anti-HSP47 antibody (Heat shock protein-47)) or type I collagen (revealed by anti-Coll I antibody) (Fig. 47 A, B). At the same time points, a small number of other cells also expressed the typical marker of myofibroblasts, alpha-SMA (Fig. 48). This demonstrated, as shown in Fig. 47 A, B and Fig. 48, that in our cultures two different cell populations, fibroblasts and myofibroblasts are present, in line with the literature¹⁶³. Conversely, starting from the 6th passage in cell cultures, fibroblasts cells became alpha-SMA⁺ and co-localized with type I collagen (Fig. 49).

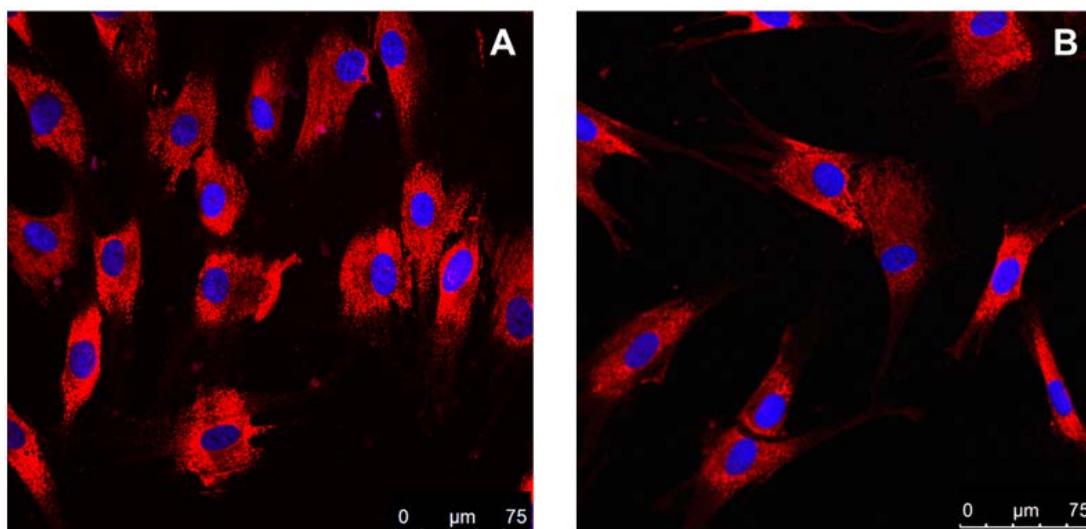


Fig. 47. **A:** Immunofluorescence staining in cultured fibroblasts isolated from keloid tissue which expresses HSP47 (red), a typical cytosolic precursor of type I collagen. Cells nuclei were colored in blue (DAPI). **B:** Immunofluorescence staining in cultured fibroblasts isolated from keloid tissue which expresses type I collagen (red). Cells nuclei were colored in blue (DAPI). Scale bar calibration: 75 μm .

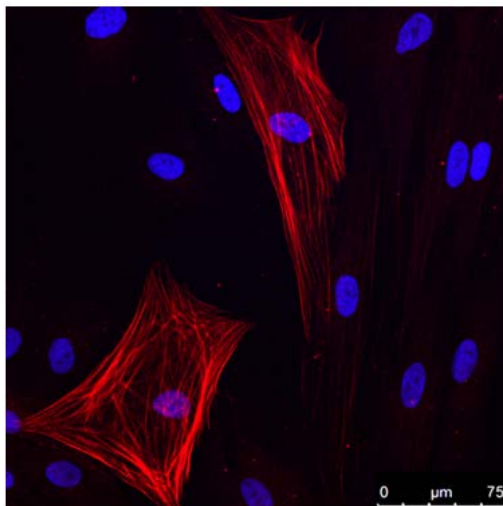


Fig. 48. Immunofluorescence staining in cultured fibroblasts isolated from keloid tissue which expresses alpha-SMA (red), a typical marker of myofibroblasts. Cells nuclei were colored in blue (DAPI). Scale bar calibration: 75 μm .

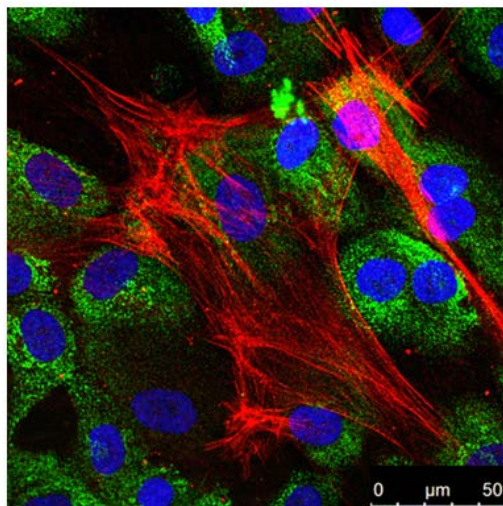


Fig. 49. Immunofluorescence staining in cultured fibroblasts isolated from keloid tissue in which alpha-SMA (red) co-localized with type I collagen (green). Cells nuclei were colored in blue (DAPI). Scale bar calibration: 50 μm .

4.4 Effects of blue LED light on cell metabolism of cultured fibroblasts

4.4.1 Healthy fibroblasts

After 24 hours from the treatment, fibroblasts isolated from healthy donors did not change significantly their metabolism at all the treatment time tested, in comparison to the untreated sample. Forty-eight hours after the treatment, the metabolism showed a significant increase strictly dependent on irradiation times (Fig. 50).

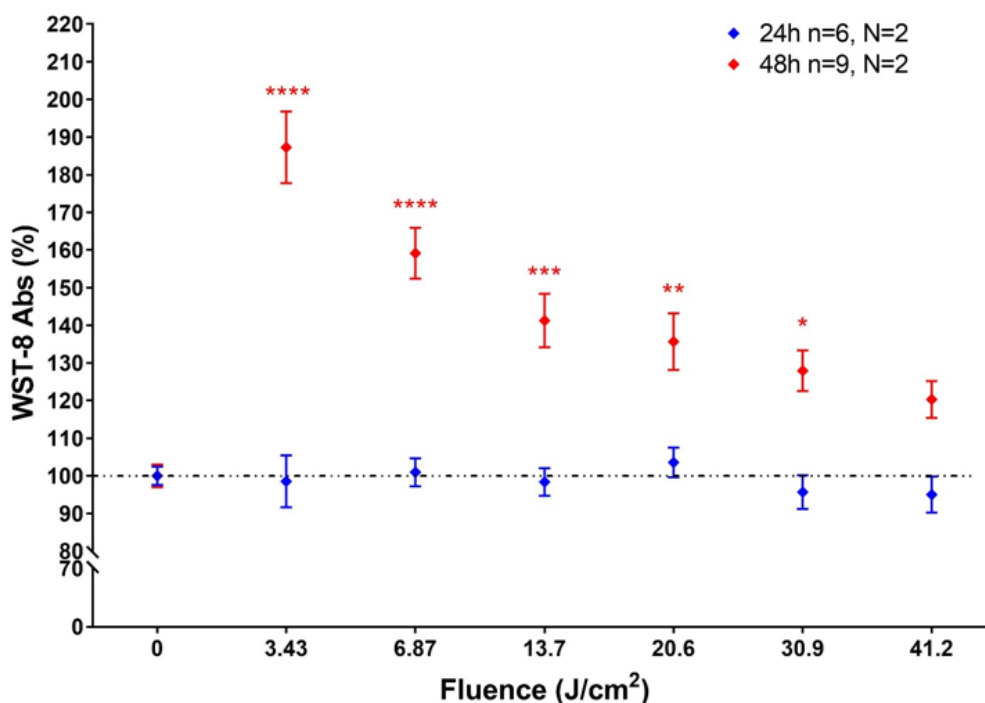


Fig. 50. Blue LED light effects on cell metabolism of healthy cultured fibroblasts. Data are expressed as mean \pm SEM. Each measure is repeated in duplicate at 24 hours and in triplicate at 48 hours after treatment. Statistical analysis: * $p < 0.05$; ** $p < 0.01$; *** $p < 0.001$; **** $p < 0.0001$ vs control (not irradiated), one-way ANOVA followed by Dunnett's multiple comparison test. Note the increase in cell metabolism induced by blue LED light 48 hours after irradiation.

4.4.2 Keloid fibroblasts

Fibroblasts from keloid tissues

Differently from what observed in healthy fibroblasts, treatment with the blue LED light induces a significant decrease in keloid fibroblasts metabolism. This effect is dose-dependent, starts at 24 hours from irradiation, and becomes more pronounced after 48 hours. In particular, at 24 hours after treatment, the decrease reached significant levels at fluence values ranging from 6.87 to 41.2 J/cm²; while at 48 hours after the treatment, a significant decrease was reached at fluences from 13.7 to 41.2 J/cm² (Fig. 51).

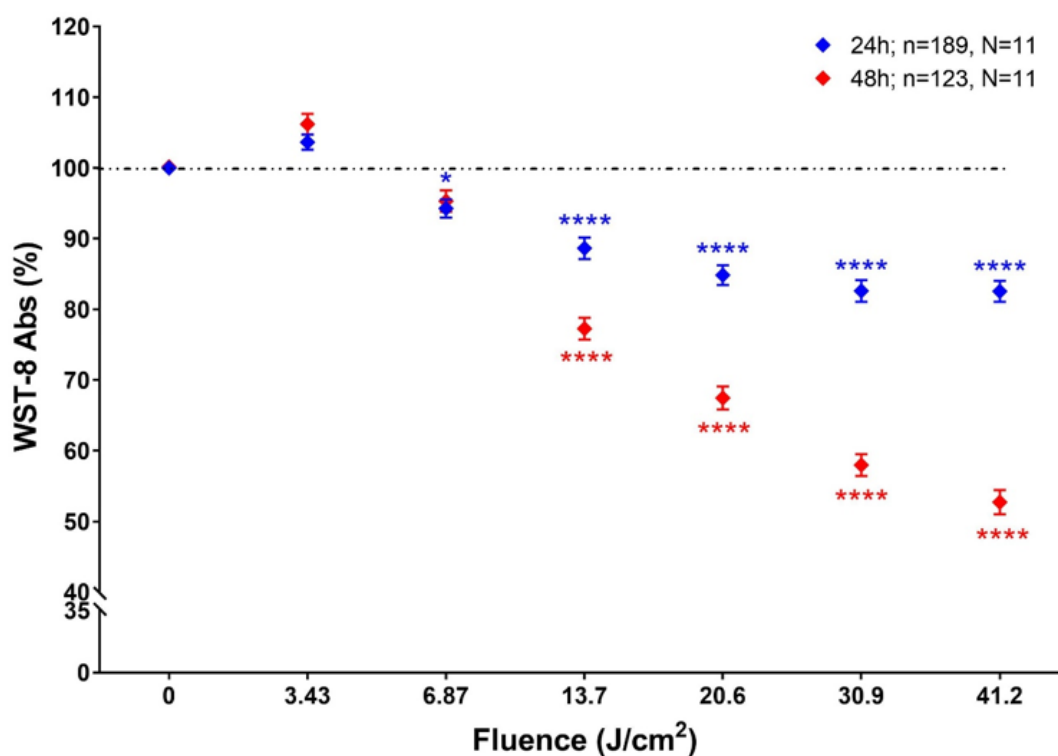


Fig. 51. Effects of blue LED light on cell metabolism in human keloid fibroblasts. Data are expressed as mean \pm SEM. Each measure is repeated in triplicate at 24 hours and in duplicate at 48 hours after treatment. Statistical analysis: * $p < 0.05$; **** $p < 0.0001$ vs control (not irradiated), one-way ANOVA followed by Dunnett's multiple comparison test. Note the decrease in keloid cell metabolism induced by blue LED light applying different doses.

Fibroblasts from keloid perilesional tissues

The results achieved in fibroblasts from keloid perilesional tissues showed that the absorbance of WST-8 decreases at increasing fluence. In this case, only the radiation doses of 30.9 and 41.2 J/cm² induced a significant reduction in WST-8 absorbance at 24 hours whereas, at 48 hours after the treatment, significant values were achieved by applying doses ranging from 20.6 to 41.2 J/cm² (Fig. 52).

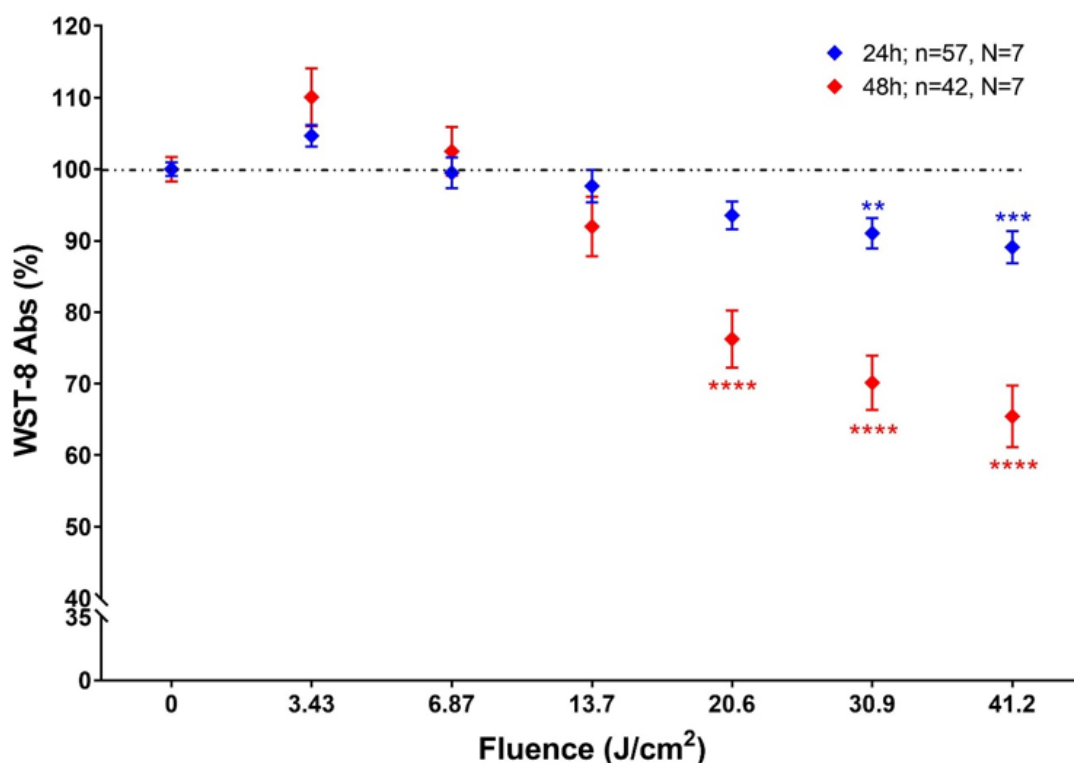


Fig. 52. Effects of blue LED light on cell metabolism in cultured perilesional fibroblasts. Data are expressed as mean±SEM. Each measure is repeated in triplicate at 24 hours and in duplicate at 48 hours after treatment. Statistical analysis: ** $p < 0.01$; *** $p < 0.001$; **** $p < 0.0001$ vs control (not irradiated), one-way ANOVA followed by Dunnett's multiple comparison test. Note that blue LED light reduces cell metabolism at 24 and 48 hours from the treatment, depending on the fluence.

4.5 Effects of blue LED light on cell proliferation of cultured fibroblasts

4.5.1 Healthy fibroblasts

Twenty-four hours after the irradiation with the blue LED light, the absorbance of SRB did not show significant changes in comparison to the untreated samples. On the contrary, 48 hours after the treatment, light doses of 30.9 and 41.2 J/cm² induce a significant decrease in comparison to the control (Fig. 53).

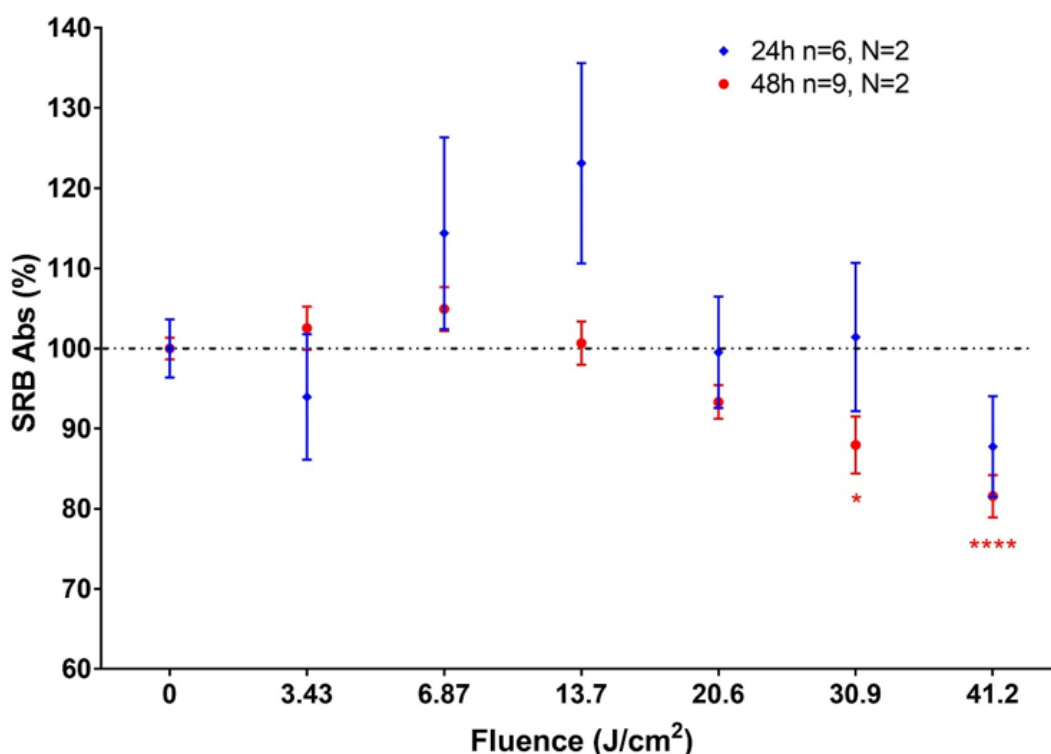


Fig. 53. Effects of blue LED light on cell proliferation in cultured healthy fibroblasts. Data are expressed as mean±SEM. Each measure is repeated in duplicate at 24 hours and in triplicate at 48 hours after treatment. Statistical analysis: * $p < 0.05$; **** $p < 0.0001$ vs control (not irradiated), one-way ANOVA followed by Dunnett's multiple comparison test. Note that blue LED light reduces cell proliferation only 48 hours after the treatment, in correspondence of the two higher doses of blue LED light.

4.5.2 Keloid fibroblasts

Fibroblasts from keloid tissues

Cultured fibroblasts isolated from keloid tissue reduced their proliferation rate starting at 24 hours, with an irradiation dose in the range 20.6÷41.2 J/cm². This effect is also evaluated and is more pronounced at 48 hours after the treatment when the SRB absorbance decreases in correspondence of fluence in the range 13.9÷41.2 J/cm² (Fig. 54).

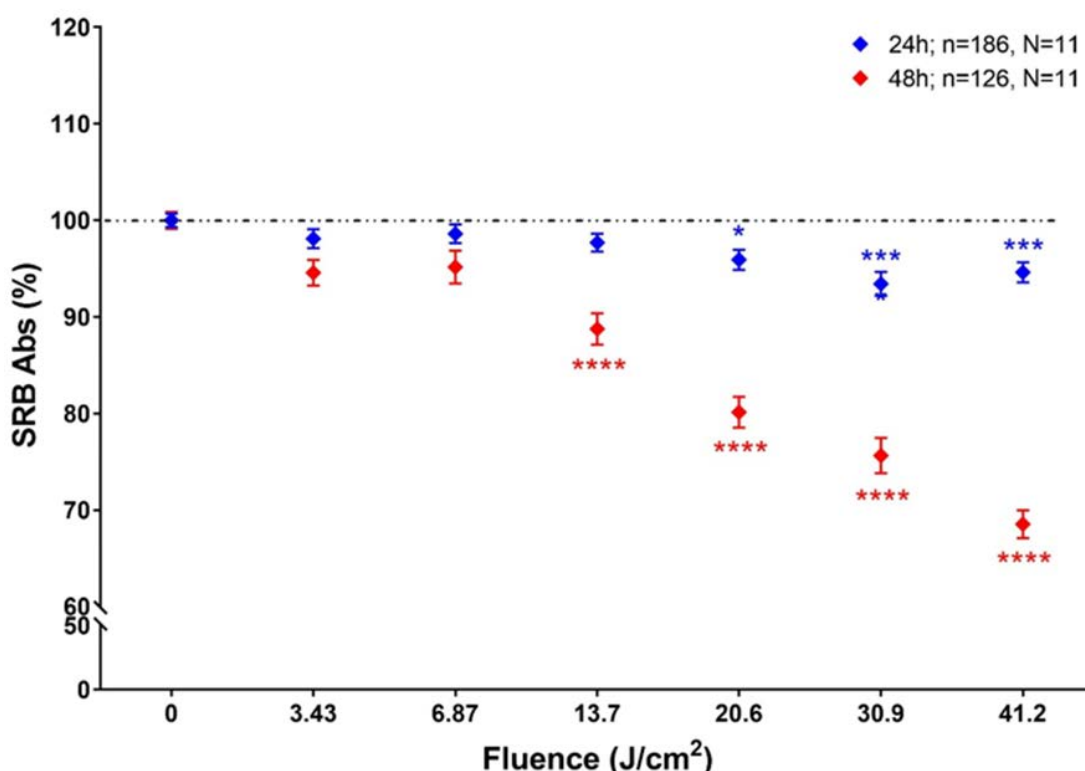


Fig. 54. Effects of blue LED light on cell proliferation in cultured fibroblasts isolated from keloid tissues. Data are expressed as mean±SEM. Each measure is repeated in triplicate at 24 hours and in duplicate at 48 hours after treatment. Statistical analysis: * $p < 0.05$; *** $p < 0.001$; **** $p < 0.0001$ vs control (not irradiated), one-way ANOVA followed by Dunnett's multiple comparison test. Note that blue LED light reduces cell proliferation at 24 and 48 hours from the treatment, depending on fluence.

Fibroblasts from keloid perilesional tissues

Results obtained in fibroblasts from keloid boundary tissues demonstrated a reduction in the absorbance of SRB at both after 24 hours and 48 hours. Concerning data collected at 24 hours, only the higher dose of irradiation with blue LED light induces a decrease in SRB absorbance, while at 48 hours, the doses of 20.6, 30.9 and 41.2 J/cm² are able to significantly reduce SRB absorbance (Fig. 55).

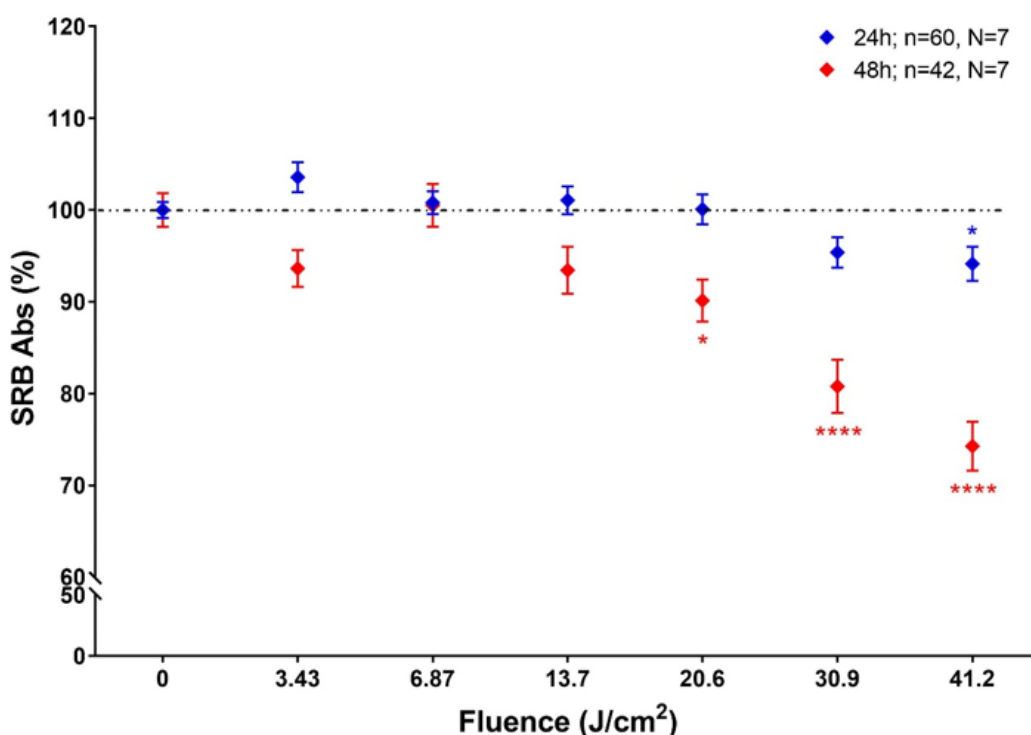


Fig. 55. Effects of blue LED light on cell proliferation in cultured fibroblasts isolated from keloid perilesional tissues. Data are expressed as mean±SEM. Each measure is repeated in triplicate at 24h and in duplicate at 48h after treatment. Statistical analysis: * $p < 0.05$; **** $p < 0.0001$ vs control (not irradiated), one-way ANOVA followed by Dunnett's multiple comparison test. Note that blue LED light reduces cell proliferation only with the higher dose of blue LED light after 24 hours and in a dose-dependent manner at 48 hours from the treatment.

4.6 Trypan Blue staining

All these results indicate that blue LED light induces a reduction in cell metabolism and proliferation, especially in keloid tissue and after 48 hours from the irradiation. This effect was in particularly evident in a range of fluences from 20.6 to 41.2 J/cm² and never observed in fibroblasts from healthy tissue, in which an opposite effect on cell metabolism was observed. However, in

order to avoid a possible cytotoxic effect induced by blue LED light on fibroblasts viability, we performed a Trypan Blue staining in keloid fibroblasts irradiated with 41.2 J/cm^2 of blue LED light, after 24 and 48 hours.

The Fig. 56 A-D shows that cultured fibroblasts did not appear blue-colored, indicating cellular membrane integrity. These results demonstrated the lack of a necrotic process. The same experimental procedures were performed in healthy fibroblasts, in fibroblasts from keloids and in fibroblasts isolated from perilesional tissue. In all these cases, the experiments demonstrated the same results.

In order to obtain a positive control, the same experiments performed in cells treated with 70% ethanol for 30 minutes. As shown in Fig. 57, cell damage was evidenced by Trypan Blue staining.

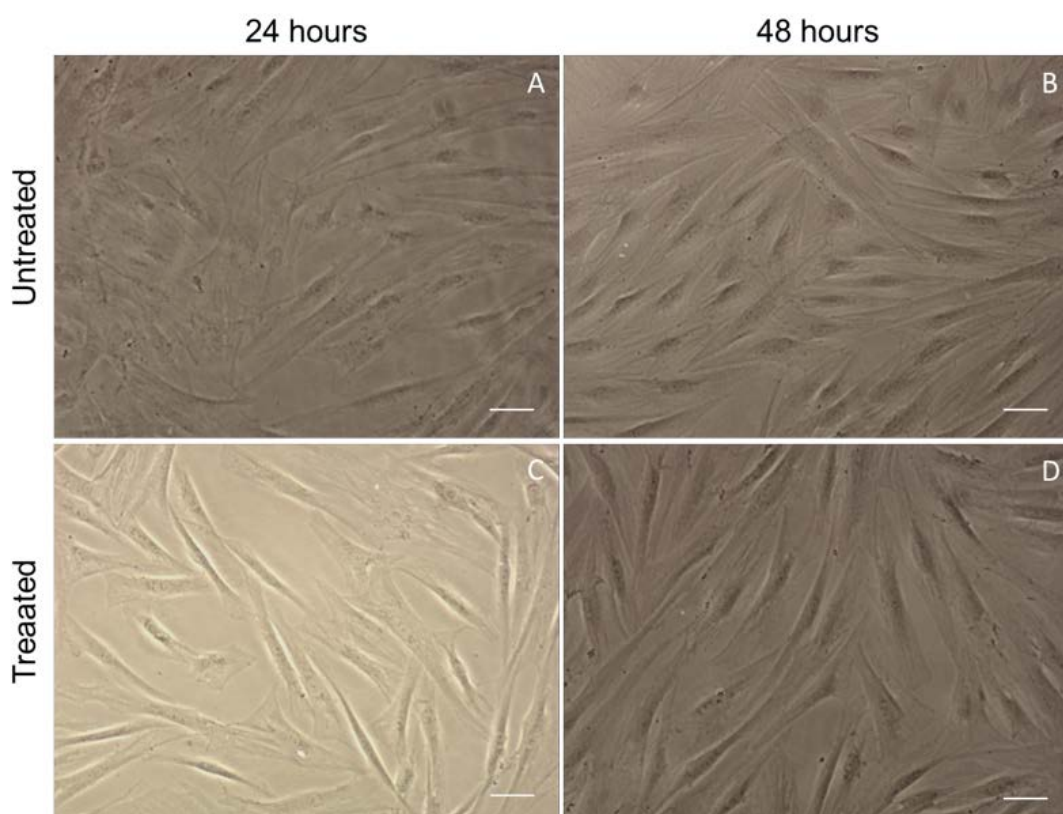


Fig. 56. Bright field representative photomicrographs of cultured human keloid fibroblasts (10X magnification) stained with Trypan blue, in different experimental groups. **A, B**: untreated cells; **C, D**: treated with a 41.2 J/cm^2 blue light dose. Note that all the cells are alive since they appear colourless. Scale bar calibration: $50 \mu\text{m}$.

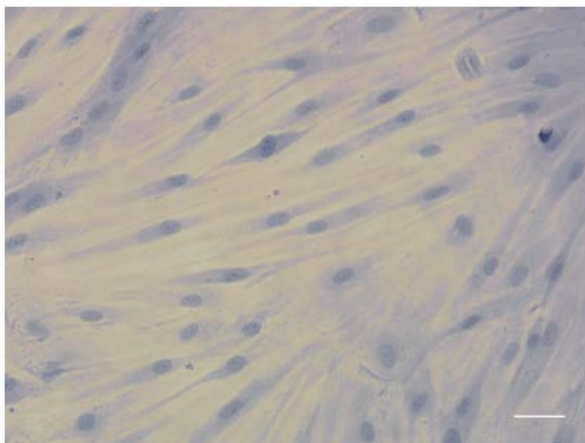


Fig. 57. Bright field representative photomicrograph of cultured human keloid fibroblasts (10X magnification) stained with Trypan blue, after ethanol treatment. Note that all cells are dead since they are stained in blue. Scale bar calibration: 50 μm .

4.7 DAPI staining

DAPI staining was performed after irradiation with 41.2 J/cm² blue LED light at 24 and 48 hours and repeated at least in triplicate. This experimental procedure was performed in healthy fibroblasts, in fibroblasts from keloids (Fig. 58) and in fibroblasts isolated from perilesional tissue. Blue LED light at 41.2 J/cm² did not affect apoptosis, estimated as the number of pycnotic nuclei in the culture until 48 hours after irradiation (Fig. 58 A-D) in all tissues examined.

No significant differences in the number of pycnotic nuclei were found in all experimental groups (Table V).

	24 hours		48 hours	
	CTRL	Blue LED light	CTRL	Blue LED light
Keloid fibroblasts	3.53±2.3	2.06±2.08	2.33±1.52	3.33±1.5
Boundary fibroblasts	4.86±3.78	3.31±2.08	3.66±2.08	4.12±3.37
Healthy fibroblasts	2.96±1.15	4.23±3.51	4.33±2.51	3.33±1.52

Table V. Each value represents the number of pycnotic nuclei in cultured fibroblasts obtained from different tissues. Data are expressed as mean±SD and are calculated at least in triplicate for each sample.

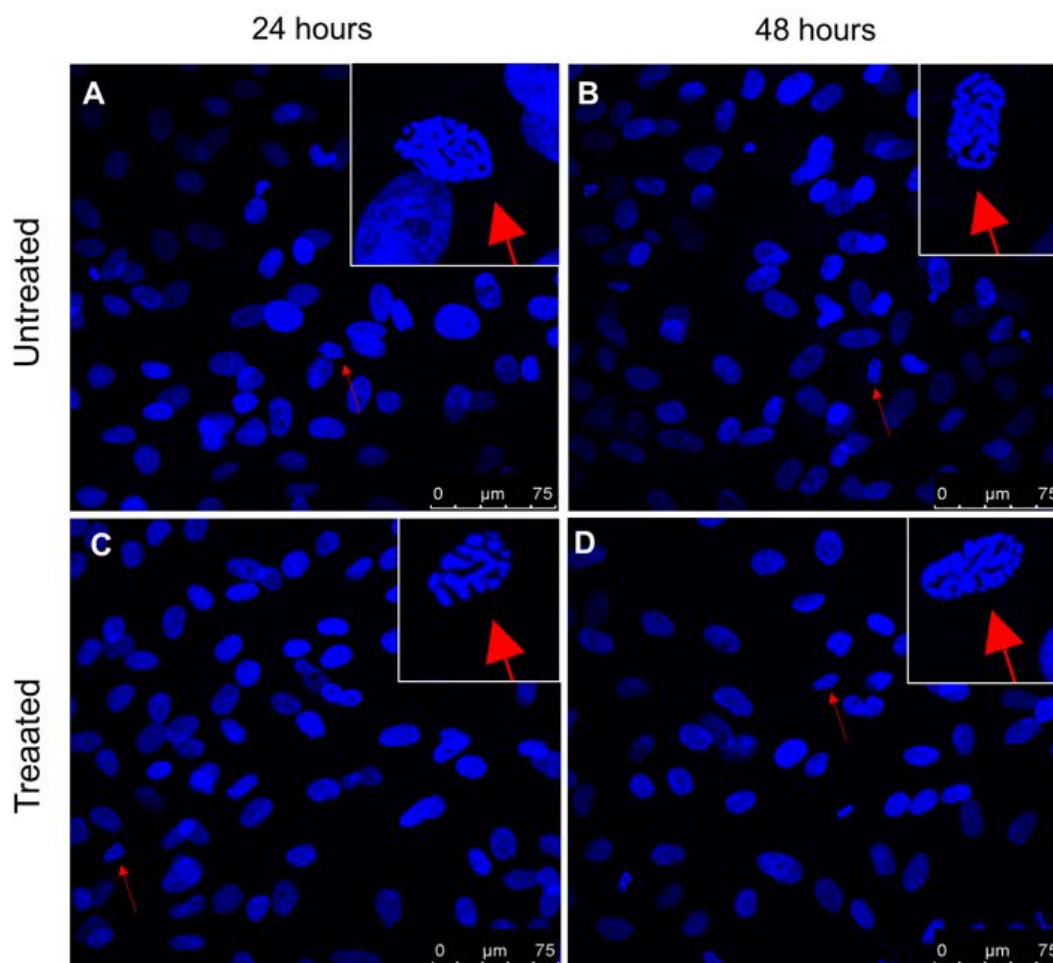


Fig. 58. **A-D**: Cultured human keloid fibroblasts at confocal microscopy (40X magnification) acquired in different experimental conditions and at different times from irradiation. Nuclei are colored with DAPI in blue. Arrows indicate the apoptotic-stained nuclei, which is also shown in the corresponding inset at higher magnification. Calibration bars: 75 μm .

4.8 Selective adenosine A_{2A} receptors antagonists and fibroblasts proliferation

The analysis performed with SRB demonstrated that the blue light induces a decrease in keloid fibroblast proliferation in a dose-dependent manner. In the next series of experiments, we evaluated the effects of light (20.6 J/cm^2) on cell proliferation in cultured fibroblasts in the presence of selective A_{2A} adenosine receptors antagonists. We have chosen this fluence on the basis of our previous results (see Fig. 54). Indeed, it appears as the minimal efficacious fluence able to significantly affect fibroblast proliferation.

In Fig. 59, a summary of the effects induced by 20.6 J/cm^2 blue LED light dose on cell proliferation is reported.

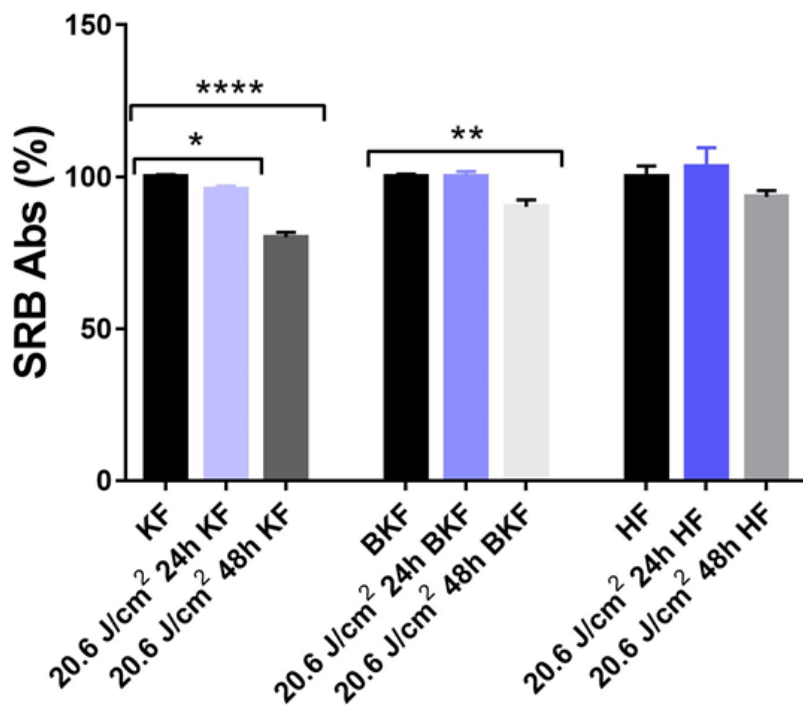


Fig. 59. Blue LED light effects on proliferation rate in human fibroblasts isolated from different tissues. Each column represents the mean \pm SEM of proliferation rate, expressed as the percentage of respective untreated tissue. KF: keloid fibroblasts; BKF: boundary keloid fibroblasts; HF: healthy fibroblasts. Statistical analysis: * $p < 0.05$; ** $p < 0.01$; **** $p < 0.0001$ vs respective untreated tissue, one-way ANOVA followed by Dunnett's multiple comparison test.

We further studied the effects of adenosine A_{2A} receptors in blue LED light effect-induced on cell proliferation. The analysis was performed 24 hours after the application of 20.6 J/cm² alone or in cells pre-incubated with A_{2A} antagonists. As shown in Fig. 60, a modest but significant reduction of cell proliferation was observed 24 hours after irradiation.

The NPD150, applied at a concentration of 100 nM, was ineffective in modifying fibroblasts proliferation when applied alone and failed to prevent the reduction in SRB absorbance induced by the blue LED light.

ZM241385, the other selective adenosine A_{2A} receptor antagonist tested, significantly reduced cell proliferation. However, the compound was unable to modify the effect induced by blue LED light on this parameter.

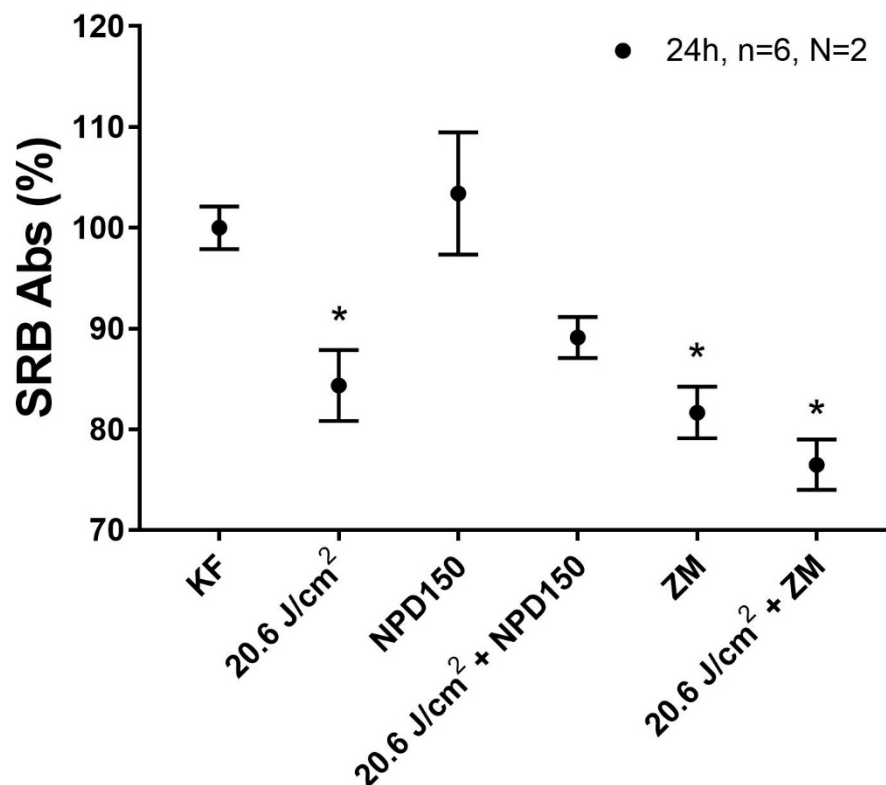


Fig. 60. Effects of blue LED light on the proliferation rate in cultured fibroblasts isolated from keloid tissue in the absence or in the presence of selective adenosine A_{2A} antagonists. SRB assay results are obtained in keloid fibroblasts after 24 hours from light irradiation at a fluence of 20.6 J/cm^2 . Data are expressed as mean \pm SEM. Each measure is repeated in triplicate. Fibroblasts were cultured in the absence of any treatments (KF). Each selective A_{2A} antagonist was applied alone or in combination with light irradiation. NPD150: 100 nM ; ZM241385: $1 \text{ }\mu\text{M}$. Statistical analysis: $*p < 0.05$, vs KF, one-way ANOVA followed by Bonferroni multiple comparison test.

4.9 Electrophysiological recordings

Electrophysiological recordings were performed on 43 fibroblasts isolated from different human tissues. Human keloid fibroblasts showing, on average, a V_m of $-54.6 \pm 3.6 \text{ mV}$, a C_m of $47.0 \pm 8.3 \text{ pF}$ and a R_m of $467.6 \pm 144.0 \text{ M}\Omega$; healthy fibroblasts presented a V_m of $-63.7 \pm 4.7 \text{ mV}$, a C_m of $47.0 \pm 13.4 \text{ pF}$ and a R_m of $460.0 \pm 113.1 \text{ M}\Omega$; boundary keloid fibroblasts presented a V_m of $-50.9 \pm 7.6 \text{ mV}$, a C_m of $66.0 \pm 27.2 \text{ pF}$ and a R_m of $159.2 \pm 68.1 \text{ M}\Omega$.

As shown in Fig. 61 A, we applied a voltage ramp protocol (from -80 to $+80 \text{ mV}$, 800 ms duration: middle inset) in cultured human keloid fibroblast before and 3 minutes after the treatment with a 21.6 J/cm^2 dose of blue LED light. This dose of irradiation was chosen on the basis of previous results

obtained on cell metabolism and proliferation. We observed that the light increased the outward currents. Light-sensitive current, obtained by subtraction of the ramp recorded in control condition from the ramp recorded after the light application was a voltage-dependent outward conductance (Fig. 61 B). Ramp-evoked outward currents were absent, as well as the effect of light, when extra- and intracellular K^+ ions were replaced by equimolar Cs^+ , demonstrating that blue LED light activation increases voltage-dependent K^+ currents in cultured keloid fibroblasts (data not shown). The maximal effect of the blue light was reached within the first 5 min application (Fig. 61 C) and was statistically significant in 18 cells investigated (Fig. 61 D, from 35.3 ± 6.6 pA/pF before to 40.6 ± 6.5 pA/pF after 3 min of blue LED light application). According to the increase in K^+ currents, blue LED light caused a modest, but not significant, change in membrane potential in keloid fibroblasts (from -54.6 ± 3.6 mV before to -56.3 ± 3.4 mV at 3 minutes after irradiation, $n=9$).

Similar experiments were conducted on fibroblasts isolated from boundary keloid tissues and from healthy skin biopsies. No significant effect was produced by blue LED light applying at 20.6 J/cm^2 on outward potassium currents elicited by ramp protocol in both boundary and healthy fibroblasts (Fig. 62 C-F). The percentage of the current amplitude measured (at +80 mV) 5 minutes after the application of blue LED light was of $98.4 \pm 5.7\%$ when compared to those recorded immediately before light, in boundary fibroblasts and of $100.7 \pm 8.2\%$ in healthy fibroblasts. At the same times, the percentage of outward potassium currents, calculated at +80 mV, was of $125.0 \pm 7.5\%$ in keloid fibroblasts. All together, these results indicate that blue LED light is able to modulate ionic potassium currents only in fibroblasts isolated from keloid.

It is well established that selective adenosine A_{2A} receptor stimulation promotes the synthesis of collagen type I and type III, mediators of fibrosis and scarring.²⁸² Conversely, blockade or deletion of this adenosinergic receptor in mice protects against bleomycin-induced dermal fibrosis, a murine model of scleroderma. Adenosine deaminase (ADA) is the principal catabolic enzyme for adenosine *in vivo*, and its deficiency leads to the spontaneous development of pulmonary fibrosis in mice.²⁸³ The A_{2A} receptor stimulation modulates collagen balance via cAMP/PKA/p38-MAPK/Akt pathways.

For this reason, we perform a further series of experiments in which the effect of light on outward potassium currents in keloid fibroblasts was evaluated in the presence of ZM241382, a selective adenosine A_{2A} antagonist. As depicted in Fig. 63 A, B, the increase in outward currents induced by the irradiation was reduced in the 3 cells pre-incubated with the A_{2A} antagonist.

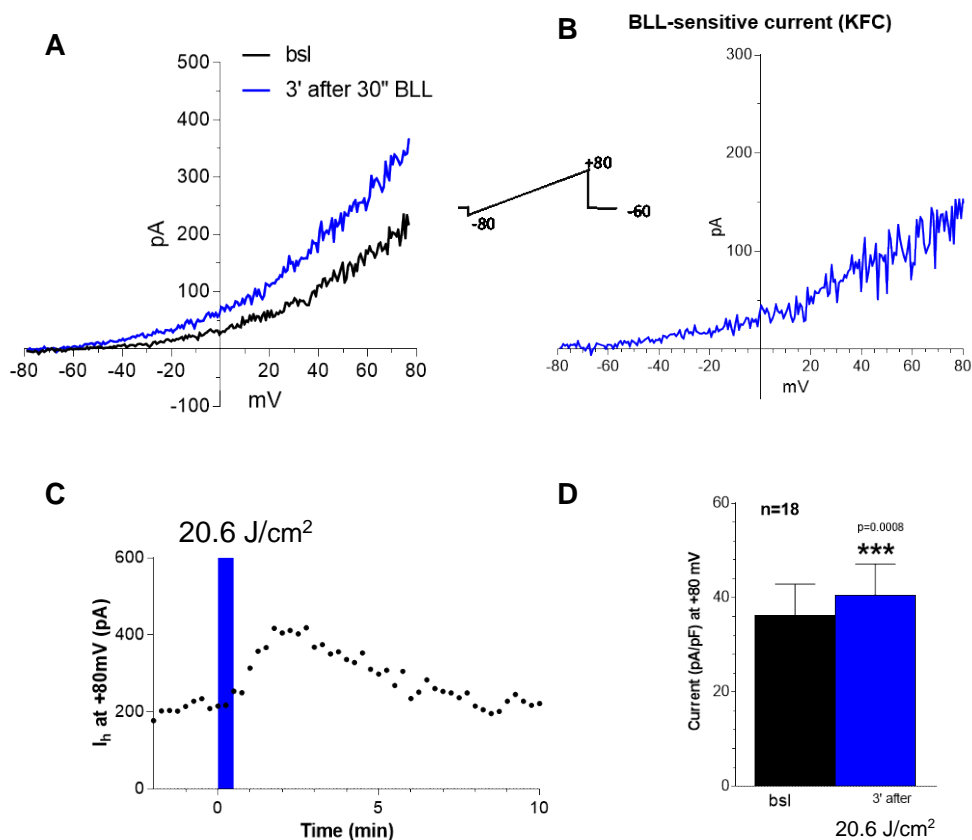


Fig. 61. Blue LED light increases outward currents in cultured human keloid fibroblasts. **A**: Original whole-cell patch-clamp current traces evoked by a voltage ramp protocol (from -80 to +80 mV, 800 ms, inset) in a keloid fibroblast (KFC), before (baseline: bsl) or after the application of 20.6 J/cm² of the blue LED light (BLL: 3 min). **B**: Net BLL-sensitive current, obtained by subtraction of the trace recorded in control from the BLL ramp in the same cell. **C**: time course of ramp-evoked currents at +80 mV in the same cell shown in **A**. **D**: Pooled data of ramp sensitive currents measured at +80 mV after blue LED light irradiation *** $p < 0.001$; Student-t test, $n=18$ are the number of observations.

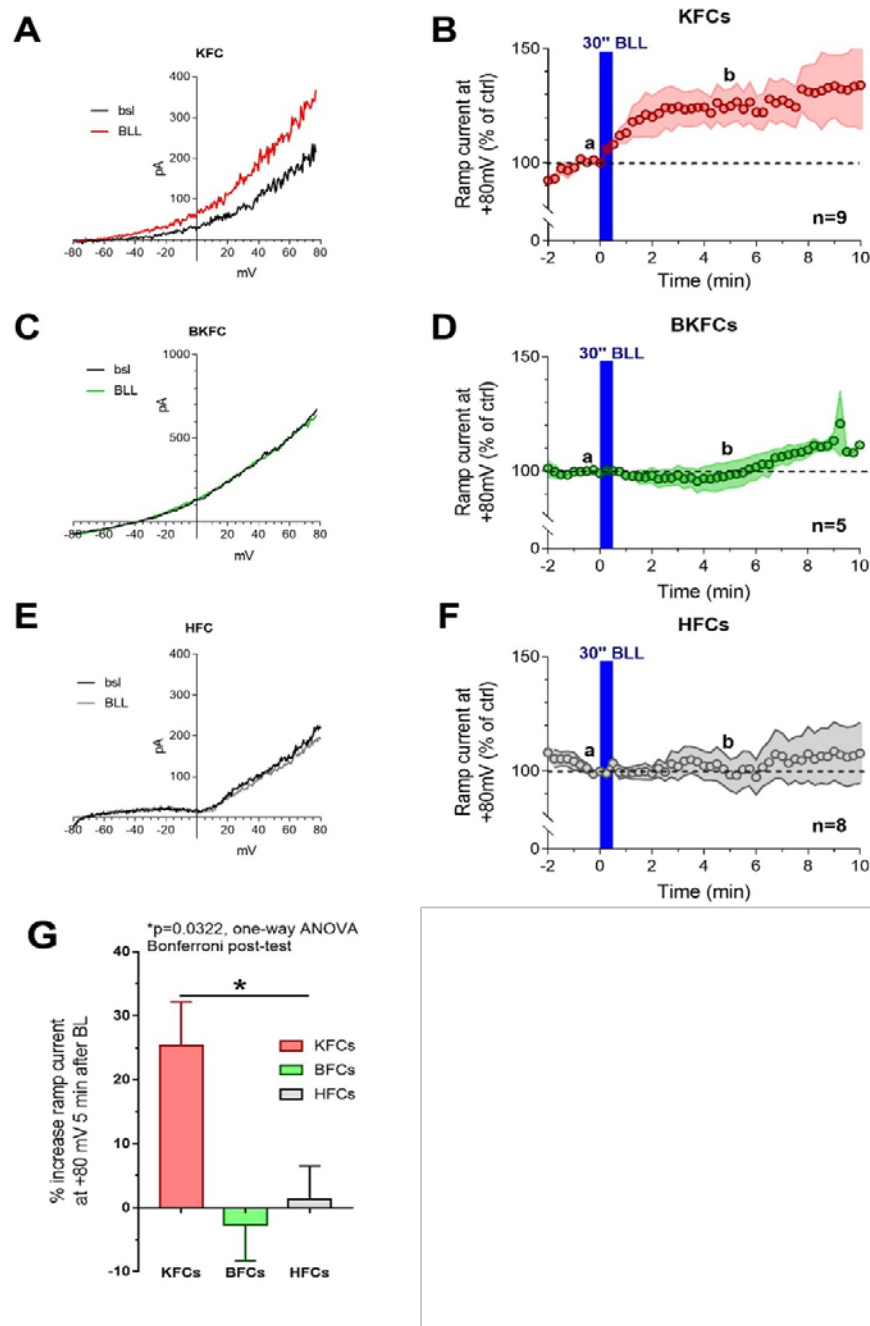


Fig. 62. Blue LED light irradiation increases outward potassium currents only in keloid fibroblasts. **A**: Original whole-cell patch-clamp current traces evoked by a voltage ramp protocol (from -80 to +80 mV, 800 ms) in a typical keloid fibroblast cell (KFC) before (baseline: bsl) or after the application of 21.6 J/cm² of Blue LED Light (BLL, 5 min). **B**: Time course of ramp-evoked currents at +80 mV in KFCs cells before, during and after irradiation, (mean±SEM, n=9). **C**: Original whole-cell patch-clamp current traces evoked by a voltage ramp protocol (from -80 to +80 mV, 800 ms) in a boundary fibroblast (BKFC) before (baseline: bsl) or after the application of 21.6 J/cm² of Blue LED Light (BLL, 5 min). **D**: Time course of ramp-evoked currents at +80 mV in boundary keloid fibroblasts (BKFCs) cells before, during and after irradiation (mean±SEM, n=5). **E**: Original whole-cell patch-clamp current traces evoked by a voltage ramp protocol (from -80 to +80 mV, 800 ms) in a typical healthy fibroblast (HFC) before (baseline: bsl) or after the application of 21.6 J/cm² of blue LED Light (BLL, 5 min). **F**: Time course of ramp-evoked currents at +80 mV in HFCs before, during and after irradiation (mean±SEM, n=8). **G**: Each column bar represents the percentage increase in ramp-evoked outward potassium currents in different experimental groups. #*p* < 0.05 vs KF, one-way ANOVA, Bonferroni post-test.

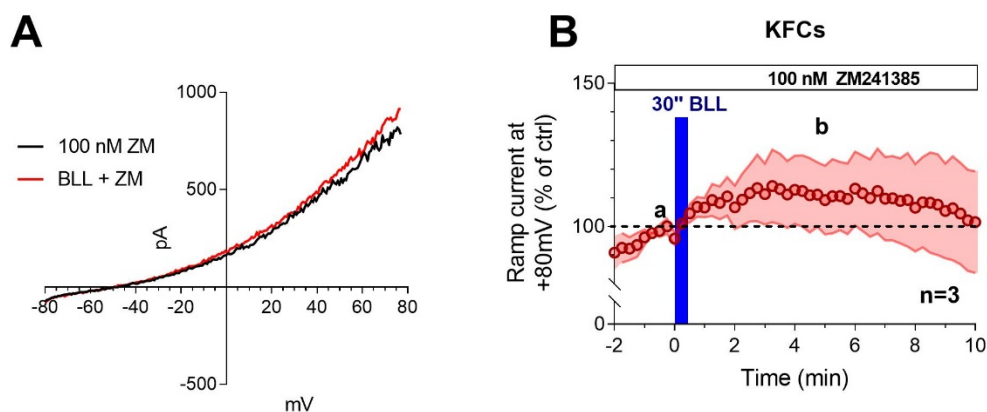


Fig. 63 The selective antagonism of adenosine A_{2A} receptors reduces the increase in outward potassium currents induced by blue LED light in keloid fibroblasts. The recording was performed in the presence of 100 nM ZM241385 (ZM), a selective adenosine A_{2A} antagonist. **A**: Original whole-cell patch-clamp current traces evoked by a voltage ramp protocol (from -80 to +80 mV, 800 ms) in a typical keloid fibroblast (KFC) before or after the application of 21.6 J/cm² of blue LED Light (BLL +ZM, 5 min) in the presence of 100 nM ZM. **B**: Time course of ramp-evoked currents recorded at +80 mV in KFCs before, during and after irradiation applied in the presence of 100 nM ZM (mean \pm SEM, n=3).

4.10 Raman spectroscopy

Since Cyt C contains a heme group that absorbs light in the 510-550 nm range, the resonant Raman scattering of Cyt C can be distinctly observed using a 532 nm wavelength for Raman excitation, allowing label-free detection of Cyt C in living cells. A free Cyt C solution at 100 μ M concentration was measured as a reference sample to elucidate the contribution of Cyt C in the Raman spectrum of the whole fibroblast cells (Fig. 64 B). Specifically, this experiment enabled the identification of Cyt C peaks and provided a picture of the spectral variation occurring on Cyt C signals by the blue LED irradiation. A coffee ring stain of the Cyt C solution (Fig. 64 A) was inspected under the micro-Raman and Raman spectra were acquired in different points of the sample using 20.6 and 41.2 J/cm² fluences of the blue LED illumination.

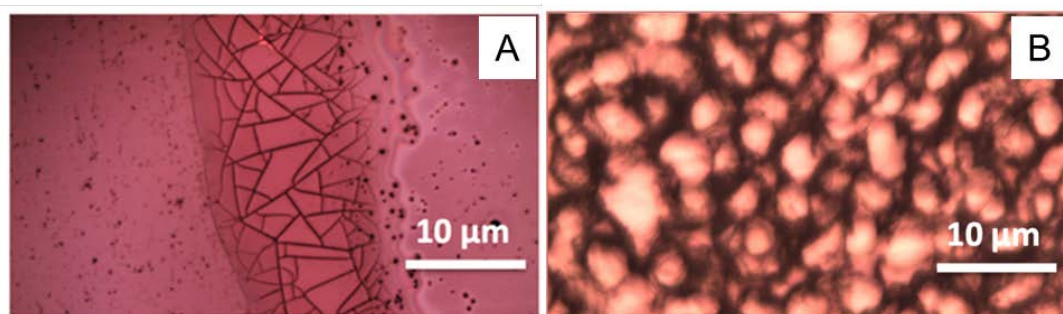


Fig. 64. **A**: Cyt C coffee ring stain sample prepared for Raman measurements. **B**: Fibroblast pellet sample prepared for Raman measurements.

The excitation laser used for Raman measurements was focused on different areas of the cell and for each point, a single spectrum was acquired. By working at low power laser intensities we did not observe any possible photoreduction or photo-oxidation of Cyt C during the Raman spectrum acquisition.

In Fig. 65 the Raman spectrum of a typical fibroblast sample is shown, that is averaged over five different measured cells on the fibroblast pellet. The main assignment of the peaks in the spectrum is reported in Table VI.

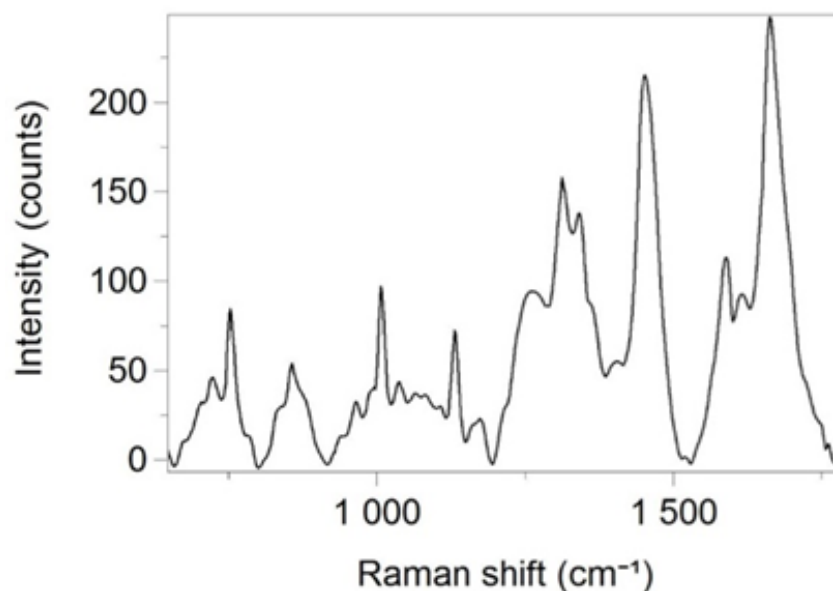


Fig. 65. Raman spectrum of the fibroblast pellet averaged over 5 different cells.

The measured spectrum contains intense peaks that are known to occur in biological samples, such as the ring breathing of phenylalanine, CH₂ deformation and Amide I vibrational mode of peptide bonds.³⁰³⁻³⁰⁴⁻³⁰⁵⁻³⁰⁶ In addition to these typical Raman shifts, strong peaks appear at 750, 1125, 1335 and 1585 cm⁻¹ that can be assigned to vibration modes of Cyt C.³⁰⁷

Peak position (cm ⁻¹)	Assignment	Peak position (cm ⁻¹)	Assignment
725	Adenine (DNA)	1305	Amide III (proteins) Adenine (DNA)
750	Cytochrome c	1335	Cytochrome c
830, 850	Tyrosine (proteins)	1375	Adenine, Guanine, Thymine (DNA)
932	C-C backbone (proteins)	1450	CH ₂ /CH ₃ bending (proteins) CH ₂ scissoring (lipids)
1003, 1030	Phenylalanine (proteins)	1566	Phenylalanine, Tryptophane (proteins)
1090	C-N stretching (proteins) C-C (lipids) O=P=O stretching (DNA)	1585	Cytochrome c
1125	Cytochrome c	1618	Tyrosine, Phenylalanine (proteins)
1230	Amide III (proteins) Cytosine (DNA)	1650-1670	Amide I (proteins) C=C stretching (lipids)
1265	Amide III (proteins)		

Table VI. Peak assignments of the Raman spectrum reported in Fig.58. Modified from Zhu, 2011.³⁰⁸

The spectral region of interest for the Cyt C redox state is reported for all the samples not irradiated and irradiated (Fig. 66). The Raman peaks at 1125 and 1335 cm⁻¹ show an enhancement of intensity upon LED irradiation. Since these peaks are reliable Cyt C redox indicator and are mostly contributed by the reduced form of Cyt C, this result proves that their intensity increase induced by LED treatment is due to reduction of Cyt C. As shown in Fig. 60, the same trend is found for the 1125 and 1335 cm⁻¹ Raman peaks in the free Cyt C sample, indicating that the blue LED light has a direct and specific effect on Cyt C molecules.

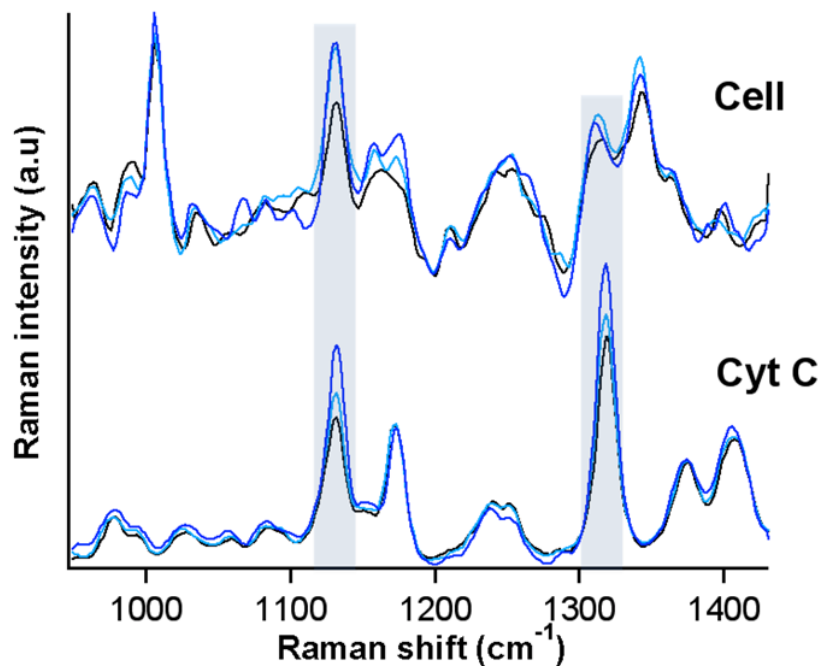


Fig. 66. Raman spectra of free Cyt C and fibroblast cell upon blue LED irradiation. The graphs show not irradiated samples (black line); 20.6 J/cm² dose-treated samples (light blue lines); 41.2 J/cm² dose-treated sample (dark blue line).

5. DISCUSSION AND CONCLUSIONS

The wound healing effects of low-dose laser treatments were first described over 50 years ago.³⁰⁹ Various doses and wavelengths ranging from 405 to 1000 nm appear to provide therapeutic benefits for a broad range of chronic wounds.³⁰⁹ Currently, the uptake of energy-based devices for medical treatment is increasing rapidly, due to the appeal of their practicality, simplicity of use and reported efficacy.³¹⁰ Within this trend, skin health attracts particular interest, underlined by the large burden of skin diseases, from the healing stimulation of chronic and hard-to-heal wounds to a new approach in the treatment of fibrotic pathologies such as keloids.³¹¹ The non-invasive nature of light, free of potential systemic side effects, makes it a very attractive treatment modality, where skin interaction with light with subsequent photochemical, photothermal and photomechanical processes drive the therapeutic effects.^{63,312}

In this work, we use a new based-blue LED light device that emits in the VIS spectrum ranging from 410 to 430 nm. The beneficial effects of this device in the wound healing process has been demonstrated, both in physiological healing and in several pathological conditions, also in humans.²⁰⁻²¹ However, the cellular mechanism/s underlying these effects are not well characterized.

Concerning the cellular and molecular mechanisms responsible of the therapeutic effects of photobiomodulation in wound healing, many information have been proposed by *in vitro* experiments in which several cell types (fibroblasts, lymphocytes, osteoblasts, stem cells, and smooth muscle cells) were used.³¹³⁻³¹⁴⁻³¹⁵⁻³¹⁶⁻³¹⁷⁻³¹⁸⁻³¹⁹⁻³²⁰⁻³²¹ In all these works, it has been indicated mitochondria as important players able to initiate beneficial processes in wound healing.³²²⁻³²³ These processes starting with the absorption of specific wavelengths of light by components of the mitochondrial respiratory chain such as Cyt C, and flavin dehydrogenases. This primary absorption stimulate a cascade of secondary reactions at cellular level involving intracellular signalling and leading to stimulation of cytokine reactions, NO production,³¹⁴⁻³¹⁵ release of growth factors,³²⁴⁻³²⁵⁻³²⁶ up-regulation of ATP,^{27,327} increased cellular metabolism and therefore cell proliferation.^{27,33,323,327} As concern the absorption of the light by specific molecules, in our work we conducted a Raman spectroscopy investigation

about Cyt C measured directly on single fibroblast cell. Accordingly with the literature,^{32-33,328} our results indicate that the blue LED light directly affects the Cyt C, inducing a change in the redox status of this molecule.

Our results, obtained using *in vivo* different rodent models of wound healing, demonstrate that the blue LED light treatment accelerates the wound healing process by modulating the number of neutrophils, the mast cells degranulation and promoting the macrophages switch from M1 to M2 phenotype.

We demonstrate that the blue LED light-treated wounds show a significant increase of inflammatory cell infiltrate starting 1 hour after abrasion and reaching the maximum significant level at 6 hours from treatment. Also neutrophils increase their levels at 24 hours from the wound induction in the untreated wound in comparison to the treated ones. These data suggest an acceleration of the inflammatory process in the treated wound in our experimental conditions. In addition, we observe a modulation by the blue LED light in mast cells degranulation.³²⁹ Differently from De Castro *et al.*,³³⁰ that identify a decrease in the number of mast cells after application of 10 J/cm² (630 ± 10 nm), we do not observe differences in the number of these cells, but an increase in their granulation activity after irradiation. Mast cells and macrophages can be stimulated by the light to release growth factors and other substances which play a role in the proliferation of fibroblasts, endothelial cells, and keratinocytes maintained in adverse conditions. Moreover, also the development of granulation tissue is mainly controlled by growth factors released by macrophages.³³¹ At the times considered, our findings demonstrate that macrophages M2 subpopulations reached high levels in the treated samples, but not in the untreated, accordingly with literature.³³² Taken together, our observations, demonstrate that the blue LED light induces an improvement of the acute wound healing process, allowing an early onset into the inflammatory phase, and overall the reduction of the healing time in superficial skin abrasions.

As concern our study *in vivo* model of chronic wound, we demonstrated that the blue LED light affects pro-MMP-9 and MMP-2 at the early stage (1 hour) and at the later stage (7 days) from the wound induction, respectively. The involvement of MMP-2 and MMP-9 in wound healing has been

demonstrated.³³³ The MMP-2 is expressed at the edge of the acute wounds, moreover it is linked with the appearance of laminin-332 and with the increase in keratinocytes migration,³³⁴ indeed MMP-9 knockout mice display a delay in the wound closure,³³⁵ demonstrate that the MMP-9 is necessary in the final phase of the wound healing process. Accordingly with literature, our findings demonstrate that both the pro-MMP-9 and MMP-2 levels are increased at the initial and in the final stage of the wound healing process. We suppose that at early times after the wound induction, the blue LED light induces an increase of matrix degradation with the purpose to prepare the wound bed to a new collagen deposition while, at later time in the healing process, this increase may become an indicator both of the angiogenetic process and the closure of the wound. The angiogenesis is an important process during wound healing, with the generation of blood vessel-rich granulation tissue, a critical step in tissue regeneration. Both MMP-2 and MMP-9 play a role in regulating angiogenesis during wound healing through the activation of proangiogenic cytokines, including TNF- α .³³⁶⁻³³⁷⁻³³⁸ In our results TNF- α is modulated by the blue LED light and it appears significantly increased at 24 hours in the treated samples if compared to the untreated. Surprisingly, we found that blue LED light reduces the levels of bFGF and VEGF in chronic wounds. We suppose that these effects may be linked to an accelerating of inflammation in treated wounds, if compared to the untreated and a different time-courses of these growth factors during the our observations.

A cellular type surely involved in the wound healing process and in the blue LED light effect, are fibroblasts.³³⁸ Our experiments conducted on cultured human fibroblasts demonstrate that the blue light can modulate both cell metabolism and proliferation in concentration-dependent manner just after 24 hours from the irradiation. In particular, in fibroblasts isolated from keloid tissue, both cell metabolism and proliferation are subjected to a decrease, while in fibroblasts obtained from healthy donors, this effect is not evident at 24 hours and, surprisingly, after 48 hours cell metabolism increases its levels. In this work we used a WST-8 reagent as an indicator of cell metabolism because cell viability was indirectly determined by measuring metabolic activity; this test is coupled with SRB assay to study cell proliferation. The results obtained from both assays are supported by Trypan Blue and DAPI

stainings, which excluded cell necrosis and apoptosis, respectively. Taken together, the results obtained by all these procedures demonstrate that the decrease in cell metabolism cannot be ascribed to cytotoxic effect; furthermore, the same doses of light produce an increase in metabolism of fibroblasts isolated from healthy skin.

We suppose that the decrease in cell metabolism mainly observed in keloid fibroblasts are related to a reduction in their cellular energetic state and ATP synthesis. Recently, it has been reported that blue light irradiation exerts a suppressive effects on human dermal fibroblasts, including reduction of mitochondrial activity, metabolism, cell motility, proliferation, TGF β ₁ levels, and type I collagen synthesis.²⁸ Our results are in line with the literature:²⁸ we found a clear reduction in cell metabolism and proliferation in keloid fibroblasts, while this decrease is less pronounced in fibroblasts obtained from boundary tissue and is never evident in fibroblasts isolated from healthy donors. All these data suggest that the irradiation with the blue LED can be a potential treatment for the prevention and reduction of tissue fibrosis, such as hypertrophic scar and keloids, as also reported in literature.^{339,58,75}

Patch clamp experiments performed in this work demonstrate that the blue LED light is able to increase outward potassium current only in keloid fibroblasts; this effect is coupled to modest and not significant membrane hyperpolarization. The increase in potassium conductance may sustain the effect on cells proliferation accordingly with Yun *et al.*³⁴⁰ Currently, we have not determined the nature of the potassium outward current involved in the light effect. It is well established that in non-excitabile cells, such as fibroblasts, the modulation of potassium currents is strictly dependent to the variation of membrane potential and to cell cycle³⁴¹ that subsequently can influence the fibroblasts proliferation rate. Actually, we do not have data about a possible modulation of the cell cycle induced by the blue LED light and further experiments will be necessary to investigate this essential question.

In response to cellular stress, ATP is released into extracellular space and subsequently dephosphorylated to adenosine by ecto-nucleotidases including ectonucleoside triphosphate diphosphohydrolase 1 (CD39) and Ecto-5'-nucleotidase (CD73).²⁴⁹ Adenosine plays a principal role in the wound healing process. Under physiologic conditions, extracellular adenosine level in

cells and tissue fluids are in the nanomolar range, while adenosine rises substantially during different forms of cellular distress.³⁴² Adenosine orchestrates the cellular response by acting on its specific receptors, named A₁, A_{2A}, A_{2B}, and A₃, of which A_{2A} has emerged as an important mediator of fibrosis and tissue remodeling.²⁸³ All of the cellular subtypes involved in wound healing (macrophages, epidermal cells, fibroblasts, and microvascular endothelial cells) express functional adenosine receptors.³⁴³

Interestingly, the selective antagonism of adenosine A_{2A} receptors reduces cell proliferation of keloid fibroblasts at 24 hours after treatment and this effect is not further modified in the presence of blue LED light application. The antagonist of A_{2A} adenosine receptors, ZM 241385, when applied in combination to blue LED light reduces the increase in outward potassium currents induced by irradiation in keloid fibroblasts. The involvement of adenosine A_{2A} receptors in cell proliferation and differentiation by the modulation of outward potassium currents is already described for other cellular types.³⁴⁴ Therefore, there is a necessity to further characterize the A_{2A} adenosine receptors interacting with blue LED light effects in skin fibrosis.

In conclusion, we hypothesized that adenosine A_{2A} receptors may be involved in aberrant fibrotic progression and that the block of adenosine A_{2A} receptors would therefore reduce chronic scarring. These findings suggest that topical administration of an adenosine A_{2A} antagonist in combination with blue LED light treatment, will diminish scar size and scar recurrence in patients with keloid.

At the end of this first part of this work, we would like to highlight the limitations of this study, related to the use of *in vitro* cultures. Such a basic model does serve as a very relevant tool, enabling us to study the impact of the blue LED light on fibroblasts in a simple way. However, at the same time it is still not clear to what extent the same experimental outcomes can be directly extrapolated to the *in vivo* case, where intercellular communication and extracellular environment interactions play a significant role. Cultured dermal fibroblasts lack the environmental conditions, such as the interaction with epidermal keratinocytes, the extracellular matrix, the blood and interstitial fluid flows. At the same time, the translation from *in vitro* to *in vivo* requires consideration of light propagation in a scattering and absorbing medium of

complex geometry such as human skin, blood- and melanin-free cellular monolayer of dermal fibroblasts. Indeed, the propagation of photons in the skin is strongly altered by the presence of pigments and diffracting structures. In the blue spectrum, already along the path from the top of the papillary dermis to the bottom of the reticular dermis, light will be strongly attenuated: while 80% of the input photons will reach the top of the papillary dermis, only 10% will interact with the bottom of the reticular dermis. Moreover, the attenuation of light will naturally depend on the skin type and individual physiology.³⁴⁵ This is an important consideration to take into account when attempting to apply optical treatment parameters, found effective *in vitro*, to *in vivo* model.

This study does open up new opportunities for developing therapies for different skin fibrosis conditions, but additional steps need to be followed while translating the findings obtained using *in vitro* cell culture of dermal fibroblasts to *in vivo* case both from the biological and from biomedical optics perspectives.

PART TWO

1. INTRODUCTION

1.1 Introduction

Oligodendrocyte progenitor cells (OPC) are a population of cycling cells which persist in the adult central nervous system (CNS) where, under opportune stimuli, they differentiate into mature myelinating oligodendrocytes (OL). During brain injury or demyelinating pathologies, OPCs are massively recruited to the site of lesion to remyelinate damaged axons. Growing evidence shows that failure of myelin formation in myelin diseases arises from the disruption of OPC differentiation. For this reason, therapeutic strategies aimed at fostering this process could be of interest in brain damage or demyelinating pathologies such as multiple sclerosis (MS).

OPC differentiation is a postnatal process characterized by the loss of proliferative activity and by the acquisition of a multidendritic morphology.³⁴⁶⁻³⁴⁷⁻³⁴⁸⁻³⁴⁹⁻³⁵⁰ On the basis of the expression of distinct stage-specific surface antigens, three phases of differentiation are distinguished: i) proliferating, bipolar OPCs, ii) post-mitotic, multi-branched O4⁺ pre-oligodendrocytes (pre-OLGs) and iii) mature, highly arborized myelinating myelin oligodendrocytes (OL) which are positive for associated glycoprotein (MAG) and/or myelin basic protein (MBP).³⁵¹⁻³⁵²

During their maturation, oligodendroglial cells display profound changes in the expression of voltage-gated ion channels including inward and outward rectifying K⁺ channels,³⁵³ Na⁺ and Ca²⁺ channels.³⁵⁴ Immature OPCs show a remarkable expression of outward delayed rectifier K⁺ currents (I_k) characterized by low voltage- and time-dependent inactivation.³⁴⁸ About 60% of OPCs also express a rapidly activating, transient outward current (I_A), showing clear time-dependent (approximately 50 ms) and voltage-dependent (above -40 mV) inactivation.³⁴⁸ During development, membrane outward K⁺ conductances (both I_k and I_A) are strongly downregulated up to almost complete disappearance while a parallel increase of inwardly rectifying Kir current amplitude develops until they become the main conductance in mature OLs.^{344,355} Among all these voltage-dependent currents, I_k are of crucial importance in oligodendroglialogenesis since their pharmacological blockade by tetra-ethyl-ammonium (TEA) in OPC cultures is sufficient to delay the expression of mature OL markers such as MBP and MAG.^{344,356} Hence,

treatments aimed at modulating these currents may affect oligodendroglialogenesis.

Adenosine is an endogenous neuromodulator that recently emerged as a most pervasive mechanism for intercellular communication in the nervous system. Its actions are mediated by the activation of four metabotropic P₁ purinergic receptors: the G_i-coupled A₁ and A₃ receptors and the G_s-coupled A_{2A} and A_{2B} subtypes.²⁴⁷ The P₁ receptors are known to be expressed at all maturational stages of oligodendroglial cells³⁵⁷ where they exert a role in cell development. Furthermore, the expression by oligodendrocytes of the equilibrative nucleoside transporters ENT1 and ENT2, as well as adenosine degrading enzymes such as adenosine deaminase and adenosine kinase suggests a major role of purinergic signalling in oligodendroglialogenesis.³⁵⁷

1.1.2 Demyelinating diseases: Multiple Sclerosis

Multiple Sclerosis (MS) is a chronic disease of the CNS that mainly presents in young adults, creating a substantial health-care burden at individual, family and community levels.³⁵⁸ MS is primarily considered to be an immune-mediated disease and is characterized by focal areas of inflammatory demyelination that spread in the brain and in the spinal cord with time, driven by infiltration of lymphocytes. According to this view, the first years of relapsing-remitting MS (RRMS), the form of MS that many individuals with the disease initially develop, are characterized by recurrent episodes of neurological dysfunction from which the individual usually recovers, and the frequency of such episodes can be even markedly reduced by treatments that modulate or suppress the immune system.³⁵⁹

The classic pathological hallmark of MS was long considered to be the presence of focal white matter demyelinating lesions. However, with time, it became clear that pathological changes are also detectable in normal-appearing white matter, as well as in the CNS grey matter, with the presence of focal grey matter lesions and grey matter atrophy.³⁶⁰ Neuronal axons are affected in the early stages of MS.³⁶¹ Over time, axonal damage and diffuse microglial activation dominate MS-related pathological changes and are accompanied by progressive, mostly untreatable, accumulation of neurological

disability affecting many functional domains from mobility to cognition. Neuropsychological dysfunction, despite its precocious identification by Charcot, was overlooked for a long time in individuals with MS.³⁶² However, in the past three decades, cognitive impairment has been increasingly investigated and it is now recognized to be a core feature of the MS clinical picture, with a negative influence on physical independence and competence in daily activities.³⁶³⁻³⁶⁴

Current available MS therapies target immune modulation with some efficacy, however, concomitantly with adverse side effects.³⁶⁵

Oligodendrocytes are the myelin-producing cells in the CNS. Damaged oligodendrocytes no longer generate myelin and remyelination requires the generation of new mature oligodendrocytes from the differentiation of OPCs.³⁶⁶ These cellular resources are especially active after demyelinating episodes in early phases of MS. Indeed, OPCs actively proliferate, migrate to and repopulate the lesioned areas. Ultimately, efficient remyelination is accomplished when new oligodendrocytes reinvest nude neuronal axons, restoring the normal properties of impulse conduction. As the disease progresses, this fundamental process fails. Multiple causes seem to contribute to such transient decline, including the failure of OPCs to differentiate and enwrap the vulnerable neuronal axons. For example, the observation that OPCs are present in MS lesions but fail to differentiate into mature oligodendrocytes³⁶⁷⁻³⁶⁸ suggests that the remyelination process is blocked at a premyelinating stage in demyelinating lesions.

Unfortunately, despite its high prevalence and considerable impact, the precise mechanisms underlying cognitive impairment in MS are still largely unknown, and efficacious treatments for this aspect of the disease are lacking. Pathological changes in CNS white matter and specific neuronal grey matter structures could play a crucial role in the pathogenesis of MS-related cognitive impairment.³⁶⁹ Alterations in the physiological crosstalk between the immune and nervous systems might also have a role, as such crosstalk modulates synaptic transmission and the induction of synaptic plasticity in the CNS.³⁷⁰

1.1.3 Oligodendrogenesis

Stroke-induced oligodendrogenesis in the ischemic brain has not been broadly studied.³⁷¹ Oligodendrocytes, myelin-forming cells in the CNS, are vulnerable to cerebral ischemia.³⁷¹⁻³⁷² Stroke acutely induces mature oligodendrocyte damage, leading to loss of myelin, which is associated with loss of axons.³⁷¹⁻³⁷²

However, during stroke recovery, there is a significant increase in the generation of oligodendrocyte progenitor cells OPCs and some of them become mature myelinating oligodendrocytes in peri-infarct gray and white matter where sprouting axons are present.³⁷³

An increase in mature myelinating oligodendrocytes observed after stroke in the adult brain likely result from new oligodendrocytes differentiated from OPCs. During development, mature OLs are generated by cells of the embryonic ventricular zone in the brain and spinal cord, giving rise to OPCs that proliferate and migrate throughout the CNS.³⁷⁴ These OPCs can then terminally differentiate into mature OLs during a step-by-step process characterized by the downregulation of precocious markers (such as the membrane chondroitin sulfate proteoglycan, neural/glial antigen 2 (NG2), the PDGF receptor-alpha and the acquisition of immature OL antigens such as O4, followed by myelin-specific structural proteins (i.e., myelin basic protein (MBP)). Furthermore, early undifferentiated bipolar OPCs acquire a more complex morphology with many branched processes, culminating in the formation of membrane sheaths that wrap around axons.³⁷⁵ It has been demonstrated that NG2⁺ OPCs (also called polydendrocytes) are still present in the adult CNS generating a lot of interest on these cells as a reservoir of OLs to repair demyelinated lesions.³⁷⁶⁻³⁷⁷ It has been indeed reported that, under specific conditions, NG2 cells can give rise to neurons and astrocytes.³⁷⁸ This indicates that polydendrocytes exhibit additional properties apart from their assumed functions as OPCs, although this concept is currently a highly debated topic. The NG2⁺ cells have been also demonstrated to make multiple contacts with the axonal membrane at nodes of Ranvier³⁷⁹ and with synaptic terminals,³⁸⁰ suggesting a role in surveillance of neuronal activity and raising the question of whether adult NG2⁺ cells may be capable of responding to or

influencing neuronal activity.³⁸¹⁻³⁸²⁻³⁸³ In this respect, several data indicate that similar to mature OLs, these cells respond to neuronal activity and to neurotransmitters.³⁸²

1.1.4 Purinergic signalling in oligodendrogenesis

Purinergic signalling (exerted by adenosine and ATP) has recently emerged as one of the main pathways that regulate myelination in both the peripheral nervous system (PNS) and CNS. In the CNS, neurons and multiple types of glia are in close proximity, so that a signal such as ATP released by a neuron could exert effects on many nearby cells (Fig. 1).

The OLs have an essential role in efficient neurotransmission in the CNS. Myelin sheaths produced by differentiated OLs wrap and insulate axon segments, and small, electrically conductive nodes of Ranvier are spaced between myelin internodes. This arrangement allows rapid saltatory conduction of action potentials along myelinated axons and is crucial for proper nervous system development and function. Impaired myelination has been implicated in neuropsychiatric disorders and cognitive disabilities.³⁴⁶ Furthermore, the extensive physical interaction between OLs and axons allows for pre-OLGs to be involved in maintaining neuronal homeostasis. OLs assist with axonal energy metabolism by exporting lactate, an energy substrate; through myelin membranes.³⁸⁴

In addition to OLs, OPCs also contact axonal segments in the CNS. Ultrastructural studies have revealed synapse-like structures between axons and OPCs, with synaptic vesicles in the axon and structures resembling postsynaptic densities in the OPC process.³⁸⁵

More recently, live, *in vivo* imaging has demonstrated synaptic vesicle accumulation along with axonal segments during contact with OPC processes.³⁸⁶ In this study, synaptic vesicle release along unmyelinated axon segments promoted myelin sheath formation. Growing evidence points to neuronal activity and neurotransmitter release affecting OPC proliferation, migration, and differentiation, as well as myelin formation.³⁸⁷⁻³⁸⁸⁻³⁸⁹ Furthermore, continuous myelin remodeling throughout adulthood points to a need for continuous communication between neurons, OPCs, and OLs.³⁹⁰

Since ATP is released from neurons in an activity-dependent manner, ATP (or its derivatives ADP and adenosine) may be involved in the ongoing communication between neurons and myelinating glia.

In the CNS, myelination is regulated by extracellular signals and intracellular factors acting on both the various steps of OL maturation and axonal activity.³⁹¹ In detail, adenosine has been reported to inhibit OPC proliferation in the presence of the mitogenic agent PDGF and to promote cell differentiation towards premyelinating oligodendrocytes, thus globally increasing myelination, as shown by the rise of MBP⁺ oligodendrocytes in DRG/OPC treated co-cultures. Of note, the percentage of myelinating MBP⁺ oligodendrocytes was lower in co-cultures treated with the adenosine receptor antagonists alone, suggesting that endogenous sources of adenosine are sufficient to promote differentiation effects.³⁹²

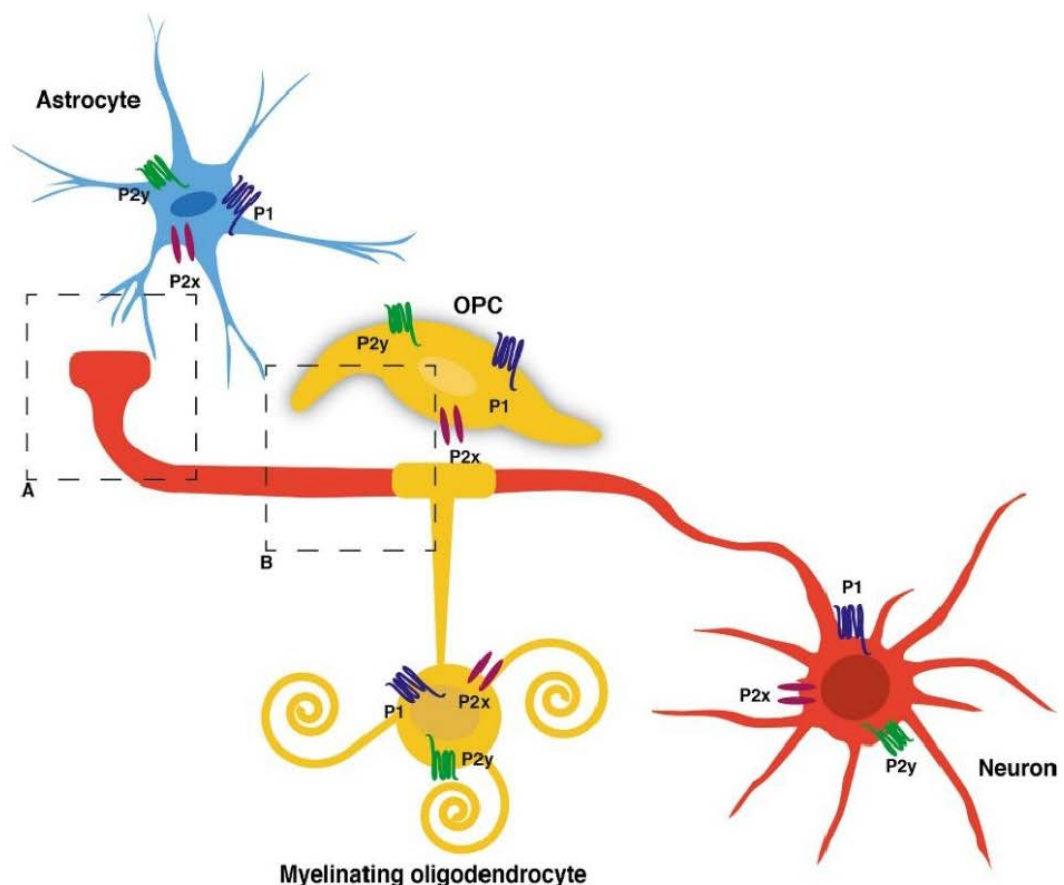


Fig. 1. Overview of purinergic signalling in CNS cells. Schematic of CNS neuron/glia interactions and purinergic receptor expression. It should be noted for neurons and glial cells: expression of receptor subtypes varies across brain regions and with development. From Welsh and Kucenas, 2018.³⁹³

Role of P₁ receptors in oligodendrogenesis

Evidence for the role of purinergic signalling in regulating OPCs, OLs, and myelination comes largely from *in vitro* studies.

Concerning oligodendrocytes, it has been demonstrated that purines exert multiple effects including increased motility, proliferation and differentiation of cultured OPCs.³⁹⁴ Among purines, adenosine is a neuromodulator of the CNS, where it acts on four subtypes of P₁ purinergic receptors (A₁, A_{2A}, A_{2B}, A₃).²⁴⁷ It is known that OPCs express all these receptors (Table I), as detected by real-time PCR in cultured OPCs, including A_{2B} adenosine receptors (Fig. 2).³⁹²

To date, a functional role has been attributed only to A₁ and A_{2A} adenosine receptors.³⁹² We elucidated the role of A_{2A} adenosine receptors on oligodendrogenesis, demonstrating that their selective activation decreases outward rectifying, sustained, I_K currents and inhibits *in vitro* OPC differentiation towards mature, myelinating oligodendrocytes, without affecting cell division.²⁹³ Conversely, adenosine, through the activation of A₁ adenosine receptor seems to be a primary activity-dependent signal inhibiting the proliferation and promoting differentiation of premyelinating progenitors into myelinating oligodendrocytes³⁹² and stimulating OPC migration.³⁹⁵ The functional role of the A_{2B} adenosine receptor in oligodendrocytes has not yet been clarified. Among adenosine receptors, the A_{2B} adenosine receptor is the least studied and still remains the most enigmatic adenosine receptor subtype because of the relatively low potency of adenosine at this receptor (EC₅₀ value of 24 µM)²⁴⁷ and the very few specific agonists that have been described so far.

However, there is a growing interest in A_{2B} adenosine receptors in recent years, as it has been shown to play a role in inflammation and cancer and is even considered a promising new pharmacotherapeutic target. Of particular note is that in the brain during different pathological conditions, such as cerebral ischemia, extracellular adenosine is elevated to levels sufficient for A_{2B} adenosine receptor activation.³⁹⁶

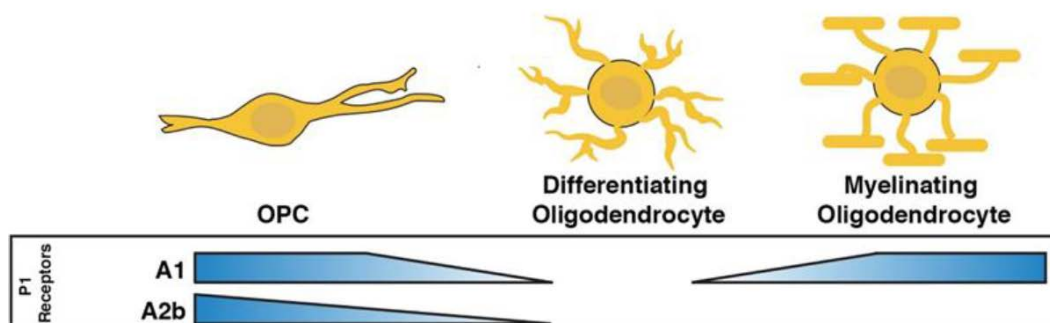


Fig. 2. Developmentally regulated expression of A₁ and A_{2B} receptors in the OLG lineage. From Welsh and Kucenas, 2018.³⁹³

Testing the hypothesis that axonally released adenosine mediated OPC proliferation and calcium signalling, Stevens³⁹⁶ demonstrated calcium responses in OPCs either via electrical stimulation of co-cultured neurons, or by directly applying the P₁ agonist NECA to OPC monocultures. Additionally, P₁ antagonists blocked the activity-dependent calcium response; supporting the conclusion, that adenosine released from firing neurons stimulates calcium signalling in OPCs. Adenosine and the P₁ agonist NECA also inhibited proliferation and promoted differentiation and myelin production. The conclusions from cell culture are supported by evidence in cerebellar slices that adenosine inhibits proliferation and increases differentiation of OPCs.³⁹⁶ More recently, *in vitro* pharmacology experiments tested the roles of specific P₁ agonists, but with some conflicting results. For example, multiple studies have reported that adenosine inhibits OPC proliferation.^{392,397} However, selective agonists for A₁ and A_{2A} adenosine receptors did not have any effect on OPC proliferation.^{293,395} In another example of conflicting results, one study found that the A₁ agonist N6-cyclopentyladenosine (CPA) promoted OPC migration in a dose-dependent manner, whereas another study reported that neither adenosine nor CPA had any effect on OPC migration.^{395,397}

Stevens *et al.*,³⁹² observed that adenosine promotes differentiation of OPCs and myelination. However, the A_{2A} agonist CGS21680 was reported to inhibit differentiation, and the A₁ agonist CPA had no effect on OPC differentiation.^{293,395}

	Expression-OPCs	Expression-mature OLs	Migration	Proliferation	Differentiation
A₁	Y (RTPCR) Y (IHC) Y (RNAseq)	Y (RTPCR) Y (IHC) Y (RNAseq)	(+) no effect	No effect	No effect
A_{2A}	Y (RTPCR) N (RNAseq)	Y (RTPCR) N (RNAseq)		No effect	(-)
A_{2B}	Y (RTPCR) Y (RNAseq)	Y (RTPCR) N (RNAseq)			
A₃	Y (RTPCR) N (RNAseq)	Y (RTPCR) N (RNAseq)			
P₁	n/a	n/a	No effect	(-)	(+)

Table I. P₁ receptor expression and function in OL lineage cells Expression-OP.

1.1.5 A_{2B} adenosine receptors

A_{2B} adenosine receptors show a low affinity for adenosine (EC₅₀ = 5-20 μM)^{233,398-399} and are associated, as the A_{2A} adenosine receptors to G_s protein; for these reasons, they were initially considered a receptor subtype with a little physiological importance.⁴⁰⁰

Recently we are beginning to understand the importance of this receptor and how much they are involved in many diseases. Moreover in physiological conditions, for their low affinity to adenosine, they are not activated; of the contrary, they are activated in pathological conditions when adenosine reaches concentrations of micromolar order, therefore it represents an interesting therapeutic target. In addition to being coupled to G_s protein, the A_{2B} adenosine receptor can be coupled to G_q protein,⁴⁰¹⁻⁴⁰²⁻⁴⁰³ to the mitogen-activated protein kinase (MAPK) and arachidonic acid pathway and to regulate the channels membrane ion probably through the βγ subunit of G protein.⁴⁰⁴⁻⁴⁰⁵

In general, A_{2B} adenosine receptors are widely expressed in numerous tissues and organs, including the vascular system, smooth muscle, gastrointestinal tract, brain tissue and bladder.⁴⁰⁶⁻⁴⁰⁷ However, the presence of these receptors is influenced by environmental stimuli, such as inflammation, cellular stress, trauma and hypoxia, which may increase their expression.^{233,408-409-410-411-412}

2. THE AIMS

In vitro studies on OPC cultures demonstrate that adenosine, by stimulating A₁ adenosine receptor, promotes OPC maturation³⁹² and migration.³⁹⁵ Our group contributed to depict the role of purinergic signalling in oligodendroglialogenesis by demonstrating that selective A_{2A} adenosine receptor activation in cultured OPCs prevents oligodendrocyte maturation by inhibiting I_K currents,²⁹³ whereas the activation of the G_i coupled purinergic P₂Y-like receptor GPR17 by its agonist UDP-glucose increases I_K currents and, hence, promotes OPC differentiation.³⁴⁴ To date, no evidence exists concerning the functional role of A_{2B} adenosine receptor in OPC cells.

Thus, the aim of the present study was to unveil the still unknown functional role of A_{2B} adenosine receptor activation in cultured OPCs. We thus investigated the effects of A_{2B} adenosine receptor ligands on: i) outward K⁺ currents and ii) myelin basic protein (MBP) and myelin-associated glycoprotein (MAG) expression at different times in cultures by using patch-clamp recordings coupled to Real-Time PCR.

3. MATERIALS AND METHODS

3.1 Cell cultures of OPCs

Purified cortical OPC cultures were prepared as described elsewhere.²⁹³ Wistar rat pups (postnatal day 1-2) were killed and cortices removed, mechanically and enzymatically dissociated, suspended in DMEM medium containing 20% fetal bovine serum (FBS), 4 mM L-glutamine, 1 mM Na-pyruvate, 100 U/ml penicillin, 100 U/ml streptomycin (all products are from EuroClone, Milan, Italy), and plated in poly-D-lysine coated T75 flasks (1 flask per animal). After 2-3 days in culture, OPCs growing on top of a confluent monolayer of astrocytes were detached by 5 hours of horizontal shaking. Contaminating microglial cells were eliminated by a 1 hour pre-shake and by further plating of detached cells on plastic culture dishes for 1 hour. OPCs, which do not attach to plastic, were collected by gently washing the dishes and replated onto poly-DL-ornithine-coated (final concentration: 50 µg/ml, Sigma-Aldrich) 13 mm-diameter glass coverslips laid in 24 multiwell chambers (10^4 cells/well: electrophysiological and immunocytochemical experiments), poly-DL-ornithine-coated 25 mm-diameter glass coverslips laid in 6 multiwell chambers (2×10^4 cells/well) or poly-DL-ornithine-coated 6 cm tissue culture dishes (3.5×10^5 cells/dish: western-blot experiments). OPC cultures were maintained in Neurobasal medium (Thermo Fisher Scientific) containing 2% B27, 4 mM L-glutamine, 1 mM Na-pyruvate, 100 U/ml penicillin, 100 U/ml streptomycin, 10 ng/ml platelet derived growth factor (PDGF-BB) and 10 ng/ml basic fibroblast growth factor (bFGF; both growth factors were purchased from PeproTech EC Ltd, London, UK) to promote cell proliferation (proliferating medium: PM).

3.2 OPC differentiation

In the whole text, the term “OPCs” (oligodendrocyte precursor cells) refers to undifferentiated bipolar or tripolar cells grown in PM. In some experiments, cells were allowed to differentiate to mature oligodendrocytes, indicated as “OLs”, by switching to a Neurobasal medium lacking growth factors (differentiating medium: DM). The day at which cells were switched from PM to DM is indicated as t_0 . In order to study the effect of A_{2B} receptor signalling on oligodendroglial maturation, OPCs were grown in DM in the

absence or presence of different pharmacological treatments for 7 days (from t_0 to t_7).

3.3 Electrophysiological experiments

Whole-cell patch-clamp recordings were performed on purified primary OPC cultures as described.³⁴⁴ Cells grown on a poly-DL-ornithine-coated 13 mm-diameter glass coverslip were transferred to a small chamber (1 ml volume) mounted on the platform of an inverted microscope (Olympus CKX41, Milan, Italy) and superfused at a flow rate of 2 ml/min with a standard extracellular solution containing (mM): HEPES 5, D-glucose 10, NaCl 140, KCl 5.4, MgCl₂ 1.2, and CaCl₂ 1.8 (pH adjusted to 7.3 with NaOH). In all electrophysiological experiments, the following adenosine receptor antagonists were added to the extracellular solution in order to prevent non-specific adenosine receptor activation upon the superfusion with various A_{2B} receptor agonist: DPCPX, SCH58261 and MRS1523, all at 100 nM concentration, in order to block A₁, A_{2A} and A₃ receptors respectively. Borosilicate glass electrodes (Harvard Apparatus, Holliston, Massachusetts USA) were pulled with a Sutter Instruments puller (model P-87) to a final tip resistance of 4–7 MΩ. Standard pipette solution contained (in mM): K-gluconate 130, NaCl 6, MgCl₂ 2, Na₂-ATP 2, Na₂-GTP 0.3, EGTA 0.6, HEPES 10 (pH adjusted to 7.4 with KOH). The calculated liquid junction potential (LJP) was 14.5 mV and this value was subtracted from all experiments. Data were acquired with an Axopatch 200B amplifier (Axon Instruments, CA, USA), low-pass filtered at 10 kHz, stored and analyzed with pClamp 9.2 software (Axon Instruments, CA, USA). All the experiments were carried out at room temperature (RT: 20–22°C).

Unless otherwise stated, cells were voltage-clamped at –70 mV. Series resistance (R_s), membrane resistance (R_m) and membrane capacitance (C_m) were routinely measured by fast hyperpolarizing voltage pulses (from –70 to –75 mV, 40 ms duration). Only cells showing a stable C_m and R_s before, during, and after drug application were included in the analysis. Immediately after breakthrough into whole-cell configuration, cell resting membrane potential (V_{rest}) was determined by switching to the current-clamp mode. A voltage ramp

protocol (800 ms depolarization from -120 to +80 mV) was recorded every 15 s to evoke a wide range of overall voltage-dependent membrane currents before, during and after drug treatments. Variations in membrane potential (V_m) induced by drug treatments were measured by calculating the reversal potential (the “zero current” potential) of ramp-evoked currents before, during and after drug application. Outward K^+ currents were evoked by a depolarizing voltage-step protocol: 10 depolarizing voltage steps (10 mV steps from -40 to +80 mV, 200 ms each) were preceded by a 60 ms pre-step potential (V_{pre}) at -80 mV. This protocol activates a mixture of outward I_K and I_A currents in cultured OPCs. Current-to-voltage relationships (I-V plots) of I_K or I_A currents were obtained by measuring current amplitude at the steady state (200-250 ms after step onset) or as a peak (1-20 ms after step onset), respectively.

Current amplitude (measured as pA) was normalized to respective cell capacitance (C_m , measured in pF) and expressed as current density (pA/pF) in averaged results. All drugs were applied by superfusion with a three-way perfusion valve controller (Harvard Apparatus, Holliston, MA USA) after a stable baseline of ramp-evoked currents was obtained. A complete exchange of bath solution in the recording chamber was achieved within 28 seconds. PCR, Western Blot and electrophysiological experiments were run in parallel in order to correlate the current profile with maturation stages of cultured cells.

3.4 Real-Time Polymerase Chain Reaction (Real-Time PCR)

Gene expression analysis was performed by Real-Time PCR, using $2^{(-\Delta\Delta C_T)}$ comparative method of quantification.⁴¹³ Briefly, total RNA (500 ng), extracted with GenElute™ Mammalian Total RNA Miniprep (Sigma-Aldrich, Milan, Italy) was reverse transcribed using iScript™ Advanced cDNA Synthesis Kit for RT-qPCR (Bio-Rad Laboratories S.r.l., Segrate (MI), Italy) according to the manufacturer's instructions. The design of MAG, MBP and A_{2B} probes was performed employing Primer Express® Software v3.0.1 (Thermo Fisher Scientific INC. Monza, Italy) that provides customized application-specific documents for absolute and relative quantitation. Rat oligonucleotide primers employed in gene expression studies are listed in Table 3. The quantification of target gene mRNA levels was performed

employing PowerUp™ SYBR™ Green Master Mix (Bio-Rad Laboratories S.r.l., Segrate (MI), Italy). Each measurement was carried out in triplicate, using the automated ABI Prism 7500 Sequence Detector System (Thermo Fisher Scientific INC) as previously described,⁴¹⁴ by simultaneous amplification of the target gene together with the housekeeping gene (β -actin and GAPDH) in order to normalize expression data. Results were analysed by ABI Prism Sequence Detection Systems software, version 1.7 (Applied Biosystems, Foster City, CA). The $2^{(-\Delta\Delta C_T)}$ method was applied as a comparative method of quantification⁴¹⁵ and data were normalized to beta-actin expression.

3.5 Drugs

2-[[6-Amino-3,5-dicyano-4-[4-(cyclopropylmethoxy)phenyl]-2-pyridinyl]thio]-acetamide (BAY 60-6582); 8-cyclopentyl-1,3-dipropylxanthine (DPCPX); 3-propyl-6-ethyl-5-[(ethylthio)carbonyl]-2 phenyl-4-propyl-3-pyridine carboxylate (MRS1523); 2-(2-furanyl)-7-(2-phenylethyl)-7*H*-pyrazolo[4,3-*e*][1,2,4]triazolo[1,5-*c*]pyrimidin-5-amine (SCH58261); 8-(4-(4-(4-chlorophenyl)piperazine-1-sulfonyl)phenyl)-1-propylxanthine, 8-[4-[[4-(4-Chlorophenyl)-1-piperazinyl]sulfonyl]phenyl]-3,9-dihydro-1-propyl-1*H*-purine-2,6-dione (PSB603); *N*-(4-cyanophenyl)-2-[4-(2,3,6,7-tetrahydro-2,6-dioxo-1,3-dipropyl-1*H*-purin-8-yl)phenoxy]-acetamide (MRS1754); tetraethyl ammonium (TEA), 4-amino-pyridine (4-AP) and forskolin were purchased from Sigma-Aldrich, Milan, Italy. *N*-(4-cyanophenyl)-2-[4-(2,3,6,7-tetrahydro-2,6-dioxo-1,3-dipropyl-1*H*-purin-8-yl)phenoxy]-acetamide (MRS1754) and *N*-(4-acetylphenyl)-2-[4-(2,3,6,7-tetrahydro-2,6-dioxo-1,3-dipropyl-1*H*-purin-8-yl)phenoxy]acetamide (MRS1706) were purchased from Tocris Bioscience, Milan, Italy. Tetrodotoxin (TTX) was purchased from Alomone labs, Jerusalem, Israel. All drugs were stored at -20°C as 10^3 to 10^4 times more concentrated stock solutions in dimethylsulfoxide (DMSO) and dissolved daily in the extracellular solution to the final concentration and applied by bath superfusion. TTX, apamin and TEA stock solutions were prepared in distilled water. All other compounds were dissolved in dimethyl sulphoxide (DMSO). Control experiments performed in the present research demonstrated that the

maximal DMSO concentration used in the present work (0.1%) was inactive in modulating membrane currents or OPC differentiation in our experimental conditions.

3.6 Statistical analysis

Data are expressed as mean \pm SEM (standard error of mean). Student's paired or unpaired *t*-tests or One-way ANOVA followed by Bonferroni's *post-hoc* test analysis were performed, as appropriate, in order to determine statistical significance (set at $p<0.05$). Data were analyzed using software package GraphPad Prism (GraphPad Software, San Diego, CA, USA).

4. RESULTS

4.1 Selective A_{2B} adenosine receptor stimulation inhibits outward K⁺ currents in cultured OPCs

Electrophysiological recordings were performed on 189 cells showing, on average, a V_m of -60.8 ± 1.6 mV, a C_m of 7.2 ± 0.3 pF and a R_m of 840.1 ± 49.7 M Ω . All experiments were done in the continuous presence of the A₁, A_{2A} and A₃ receptor antagonists DPCPX, SCH58261 and MRS1523, respectively (all 100 nM).

As shown in Fig. 3 A, we applied a voltage ramp protocol (from -120 to +80 mV, 800 ms duration: middle inset of Fig. 3 A, B) in cultured OPCs in the absence or presence of the selective A_{2B} receptor agonist BAY60-6583 (10 μ M) and we found that the compound reversibly inhibited ramp-evoked outward currents. BAY60-6583-inhibited current, obtained by subtraction of the ramp recorded in the presence of BAY 60-6583 from the control ramp, is a voltage-dependent outward conductance (Fig. 3 B). These results are in line with immunofluorescent data showing A_{2B} receptor expression on NG2⁺ cells (Fig. 3 C). The maximal effect of BAY60-6583 was reached within 5 min application (upper inset of Fig. 3 A) and was statistically significant in 51 cells investigated (Inset Fig. 4 A: $41.9 \pm 2.8\%$ current inhibition). Of note, ramp-evoked outward currents were absent, as well as the effect of BAY60-6583, when extra- and intra-cellular K⁺ ions were replaced by equimolar Cs⁺ (Fig. 4 A), demonstrating that A_{2B} receptor activation inhibits voltage-dependent K⁺ currents in cultured OPCs.

The effect of BAY60-6583 on K⁺ currents was concentration-dependent, with an EC₅₀ = 0.6 μ M (Fig.2 B: confidence limits: 0.04–9.4 μ M), and prevented by the selective A_{2B} receptor antagonist MRS1706 (10 μ M: Fig. 4 C). In accordance to K⁺ current inhibition, BAY60-6583 caused a concentration-dependent depolarization in cultured OPCs and the effect was prevented by the A_{2B} adenosine receptor antagonist MRS1706 (Fig. 4 D).

We further investigated which subtype/s of K⁺ currents are targeted by A_{2B} receptors. OPCs are known to express two distinct K⁺ currents: a sustained, delayed rectifying, I_K currents and a transient, rapidly inactivating, I_A conductance.⁴¹⁶ By applying a voltage-step protocol (from -40 to +80 mV, 200 ms step duration, V_h= -80 mV: lower inset in Fig. 5 A) we activated either

I_A and I_K in the absence or presence of 10 μM BAY60-6583. As shown in Figure 5 A, both currents were inhibited in the presence of the A_{2B} receptor agonist, with a significant decrease in peak I_A (Fig. 5 B, left panel) or steady state I_K (Fig. 5 B, right panel) starting from 0 mV.

Above data were obtained in OPCs at t_0 , which correspond to the period at which most cells are immature NG2^+ OPCs.³⁴⁴⁻²⁹³ We also tested BAY60-6583 effects on mature OLs, grown in differentiating medium up to 10-15 days (t_{10} - t_{15}). At this stage, as we previously shown,^{293,344} oligodendroglial cultures are mostly composed by highly ramified, MBP^+ and MAG^+ oligodendrocytes expressing inwardly rectifying K_r channels.^{348,355} As shown in Figure 4, BAY-60-6583 (0.1-30 μM) still inhibited outward K^+ currents in mature OLs and presented a concentration-dependence similar to what observed in immature OPCs (Fig. 6 A-E).

Similar effects to those induce by the prototypical A_{2B} receptor agonist BAY60-6583, were observed in the presence of unselective adenosine agonist NECA. The compound was applied, as in all other experimental groups, in the continuous presence of the A_1 , A_{2A} and A_3 receptor antagonists DPCPX, SCH58261 and MRS1523 (all 100 nM), respectively. As shown in Fig. 7 A, B, NECA (50 μM) mimicked BAY60-6583-mediated inhibition of ramp-evoked K^+ currents. The effect was significant in 8 cells tested (Fig. 7 B), prevented by the selective A_{2B} receptor antagonist PSB603 (10 μM : Fig. 7 C, D) and concentration-dependent, with an $\text{EC}_{50}=1.9$ μM (confidence limits: 0.4–9.0 μM : Fig. 7 E).

In order to confirm the involvement of I_A and I_K current in the A_{2B} receptor-mediated effect, we applied BAY60-6583 in the presence of a combination of the I_A blocker 4-AP (500 μM) and the I_K blocker TEA (3 mM: Fig. 8 A).⁴¹⁷ We have previously shown that, in cultured OPCs, 3 mM TEA inhibits delayed rectifier I_K currents, whereas 500 μM 4-AP is a selective blocker of transient I_A conductances.^{293,396} As shown in Fig. 8 B, only a co-application of both compounds was able to prevent BAY60-6583-mediated effect.

Concerning the intracellular mechanism by which the Gs-coupled A_{2B} receptor mediates ramp current inhibition, we tested the hypothesis of intracellular cAMP being involved, in accordance with previous data showing

that increased levels of this intracellular metabolite decreases steady-state outward K^+ conductances in ovine OPCs.⁴¹⁸ Similarly to what observed in the presence of the A_{2B} receptor agonist BAY60-6583, the adenylyl cyclase activator forskolin (FSK; 20 μ M) inhibited outward ramp-evoked K^+ currents in cultured OPCs and occluded the effect of a subsequent application of BAY60-6583 (Fig. 8 C, D).

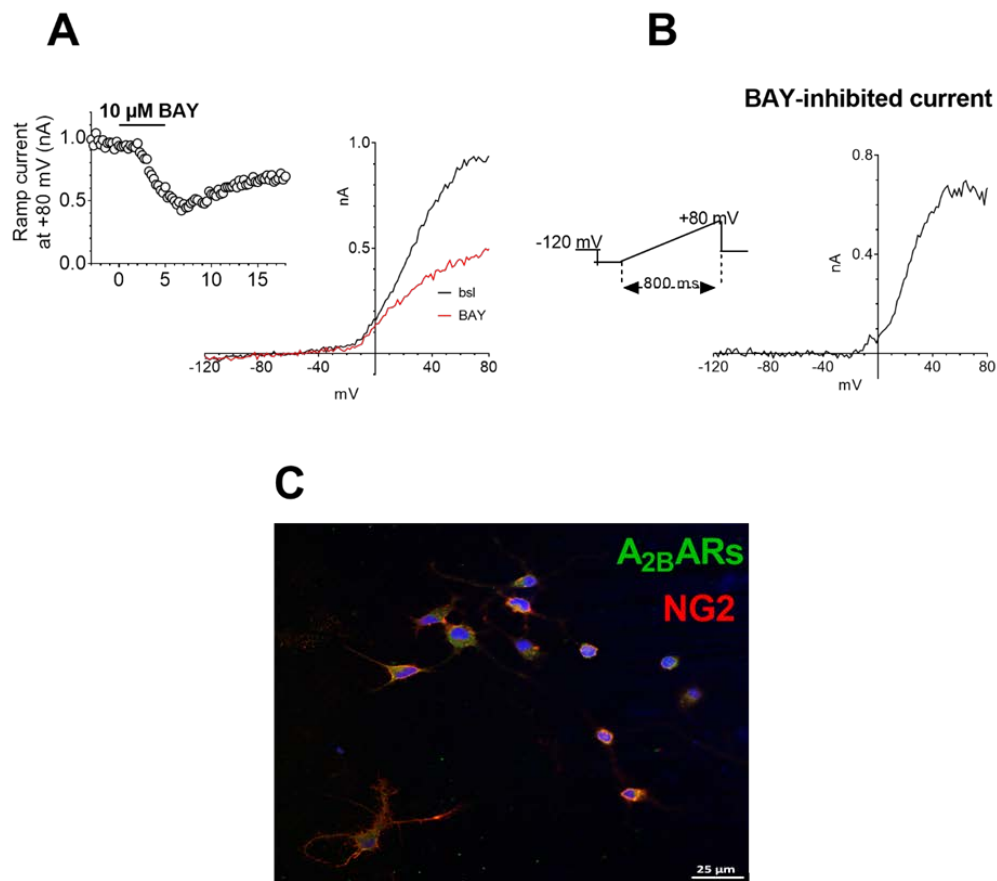


Fig. 3. The A_{2B} adenosine receptor agonist BAY60-6583 inhibits I_K and I_A outward K^+ currents in cultured OPCs. **A:** Original whole-cell patch clamp current traces evoked by a voltage ramp protocol (from -120 to +80 mV, 800 ms; upper inset) in a typical OPC before (baseline: bsl) or after the application of BAY60-6583 (BAY: 10 μ M; 5 min). *Inset:* time course of ramp-evoked currents at +80 mV in the same cell. **B:** Net BAY60-6582-inhibited current, obtained by subtraction of the trace recorded in BAY60-6583 from the control ramp, in the same cell. **C:** Confocal image of immunofluorescence staining for A_{2B} adenosine receptors (green) and NG2 (red) in OPC cultures (at t0). Cell nuclei are marked with DAPI (blue). Scale bar: 25 μ m. All experiments were performed in the presence of the A_1 , A_{2A} and A_3 receptor antagonists DPCPX, SCH58261 and MRS1523, respectively (all 100 nM).

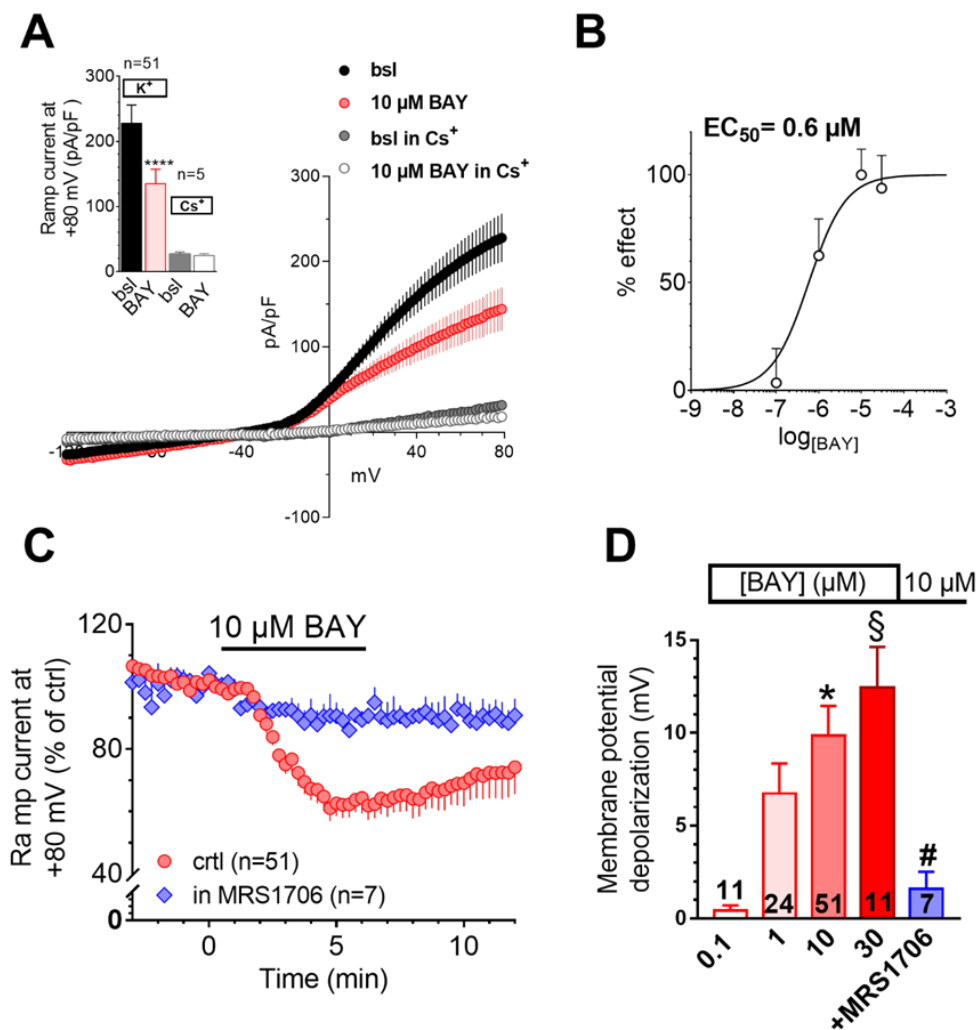


Fig. 4. The A_{2B} adenosine receptor agonist BAY60-6583 inhibits outward K⁺ currents in cultured OPCs. **A**: Averaged ramp-evoked currents, and pooled data at +80 mV (mean \pm SEM), recorded in the absence (bsl) or presence of 10 μ M BAY60-6583 (BAY) under control conditions (K⁺; n=51) or in Cs⁺-replacement experiments (n=5). ****p* < 0.001 vs respective ctrl, paired Student's t-test. **B**: Concentration-response curve of BAY60-6583 effect on ramp currents at +80 mV in cultured OPCs. EC₅₀ = 0.6 μ M, confidence limits = 0.04 - 9.4 μ M. **C**: Averaged time courses of BAY60-6583 (BAY) effect on ramp currents at +80 mV in cultured OPCs under control conditions (ctrl: red circles; n=51) or in the presence of the selective A_{2B} adenosine receptor antagonist MRS1706 (10 μ M: open diamonds: n=7). **D**: Pooled data of membrane potential depolarization induced by different concentrations of BAY60-6583 in cultured OPCs. ***p* < 0.01; §*p* < 0.01 vs 0.1 μ M BAY60-6583; #*p* < 0.01 vs 10 μ M BAY60-6583, one-way ANOVA, Bonferroni post-test. Number of observation is written in the columns. All experiments were performed in the presence of the A₁, A_{2A} and A₃ receptor antagonists DPCPX, SCH58261 and MRS1523, respectively (all 100 nM).

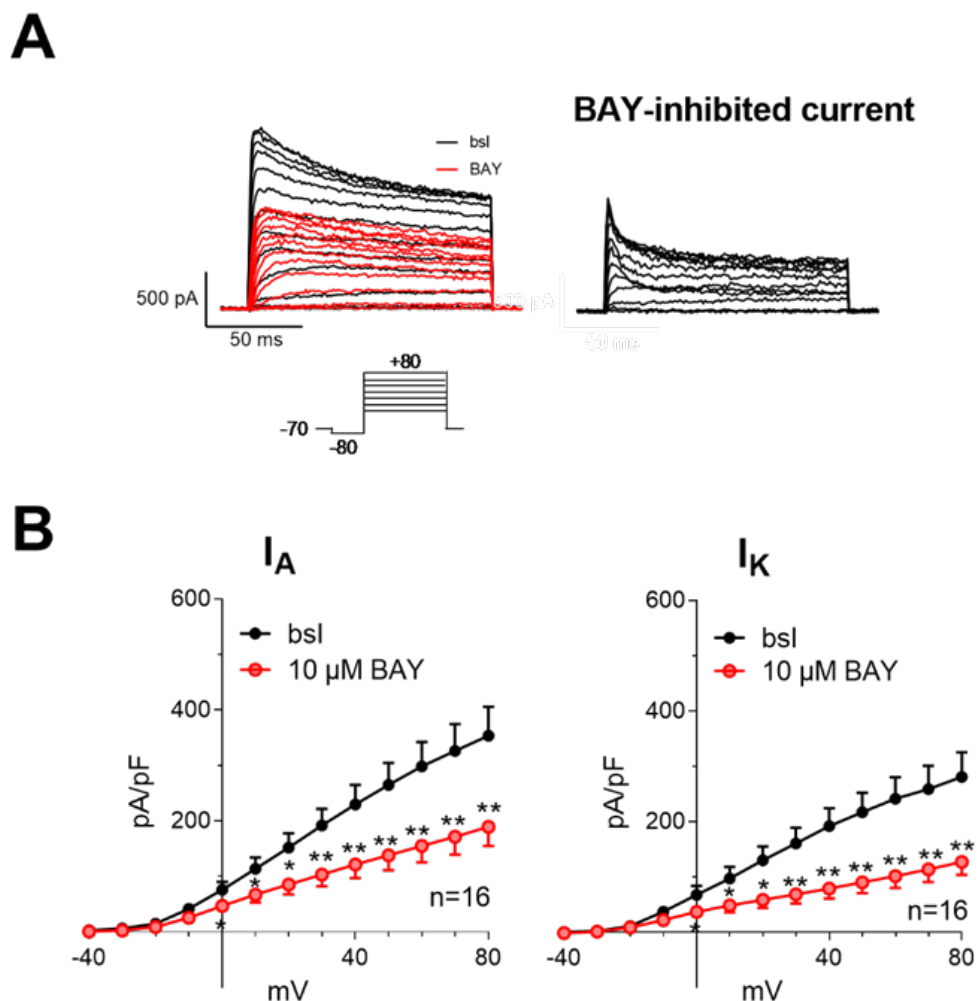


Fig. 5. The A_{2B} adenosine receptor agonist BAY60-6583 inhibits I_K and I_A outward K^+ currents in cultured OPCs. **A**: Left panel: original current traces recorded evoked by a voltage-step protocol (from -40 to +80 mV, pre-step -80 mV; 200 ms; lower panel) in a representative OPC before (bsl: black traces) or after (red traces) the application of BAY60-6583 (BAY, 10 μ M; 5 min). Right panel: net BAY60-6583-inhibited current, obtained by subtraction of the traces recorded in BAY60-6583 from respective control traces in the same cell. **B**: Averaged current-to-voltage relationship (I-V plot) of the peak, transient, I_A currents (left panel) or steady-state, sustained, I_K currents (right panel) recorded in the absence (bsl: filled circles) or in the presence (red circles) of 10 μ M BAY60-6583 in 16 cells investigated. * $p < 0.05$; ** $p < 0.01$ paired Student's t-test. All experiments were performed in the presence of the A_1 , A_{2A} and A_3 receptor antagonists DPCPX, SCH58261 and MRS1523, respectively (all 100 nM)

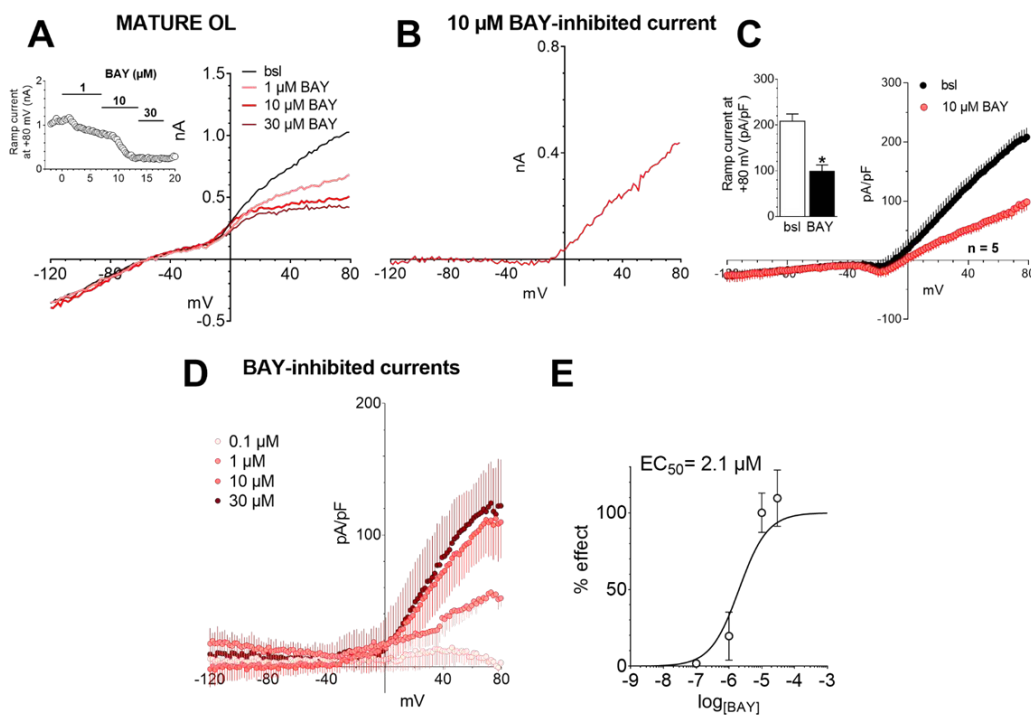


Fig. 6. The selective stimulation of A_{2B} adenosine receptors reduces outward potassium currents in mature OL. **A**: Original whole-cell patch clamp current traces evoked by a voltage ramp protocol (from -120 to +80 mV, 800 ms) in different experimental conditions: before (baseline: bsl) or after the application of various BAY60-6583 concentrations (BAY: 5 min). Inset: time course of ramp-evoked currents at +80 mV in the same cell. **B**: Net BAY60-6583-inhibited current, obtained by subtraction of the trace recorded in 10 μ M BAY60-6583 from the control ramp, in the respective cell. **C**: Averaged ramp-evoked currents, and pooled data at +80 mV (mean \pm SEM), recorded before (baseline: bsl) or after BAY60-6583 (10 μ M) application (5 min) in 5 OPCs tested. * $p < 0.05$, paired Student's t-test. **D**: Pooled data of ramp current inhibition induced by different concentrations (in μ M) of BAY 60-6583 (BAY, 0.1 μ M, $n=3$; 10 μ M, $n=4$; 30 μ M, $n=3$). **E**: Concentration-response curve of BAY60-6583 effect on ramp currents at +80 mV in cultured mature OL. $EC_{50} = 2.1 \mu$ M, confidence limits = 0.17 – 23.6 μ M.

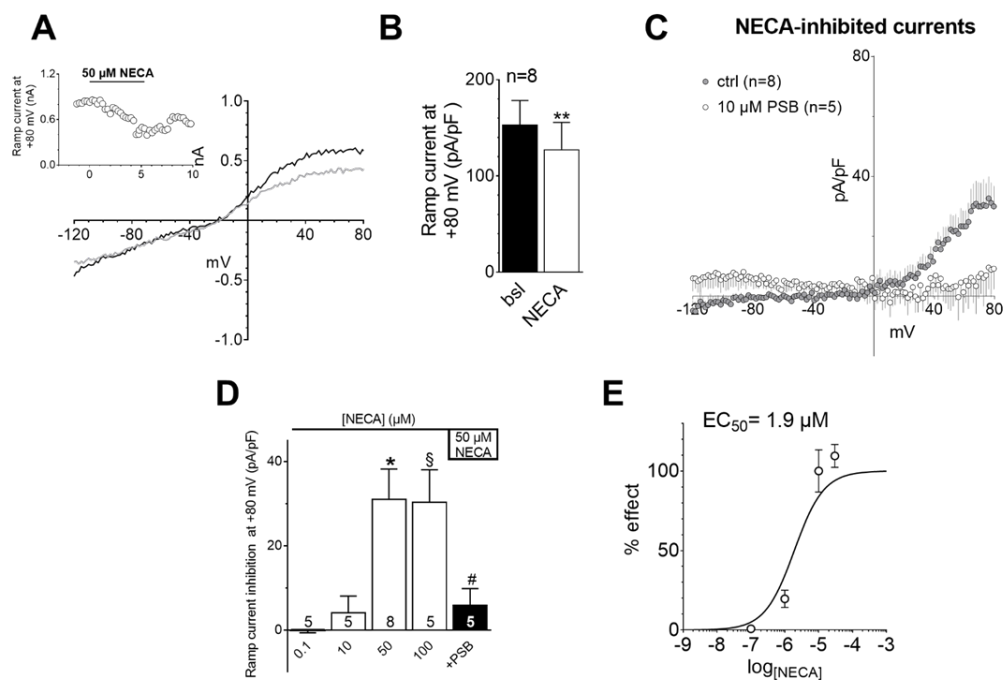


Fig. 7. The effect of BAY60-6583 on ramp-evoked K⁺ currents is mimicked by the unselective adenosine receptor agonist NECA. **A**: Original whole-cell patch clamp current traces activated by a voltage ramp protocol (from -120 to +80 mV, 800 ms) in a typical OPC before (baseline: bsl) or after the application of NECA (50 μM ; 5 min). Inset: time course of ramp-evoked currents at +80 mV in the same cell. **B**: Pooled data (mean \pm SE) of ramp current at +80 mV in the absence (bsl) or presence of 50 μM NECA in 8 cells tested. $**p < 0.01$, paired Student's t-test. **C**: Averaged NECA-inhibited currents, obtained by subtraction of the trace recorded in NECA from the control ramp in each cell, measured in the absence (control: ctrl; n=8) or in the presence of the A_{2B} adenosine receptor antagonist PSB603 (PSB, 10 μM ; n=5). **D**: Pooled data of ramp current inhibition measured at +80 mV in the presence of NECA at different concentrations (in μM) or at 50 μM in the presence of the adenosine A_{2B} receptor antagonist PSB603. $*p < 0.05$; $\$p < 0.05$ vs 0.1 μM NECA; $\#p < 0.05$ vs 50 μM NECA, one-way ANOVA, Bonferroni post-hoc test. The number of observations is written in the columns. **E**: Concentration-response curve of NECA effect on ramp current inhibition at +80 mV. EC₅₀ = 1.9 μM , confidence limits = 0.4 – 9.0 μM . All experiments were performed in the presence of the A₁, A_{2A} and A₃ receptor antagonists DPCPX, SCH58261 and MRS1523, respectively (all 100 nM).

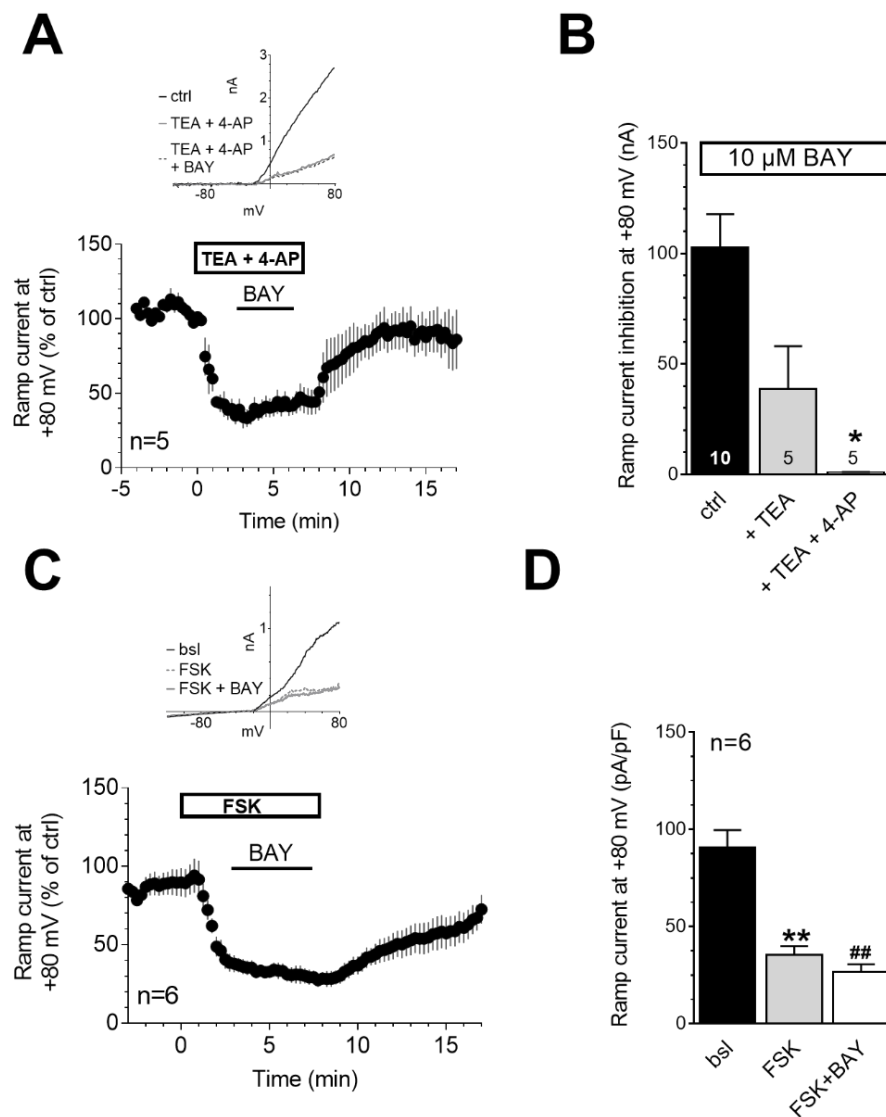


Fig. 8. The effect of BAY60-6583 on ramp-evoked K^+ currents is prevented by a combination of the K^+ channel blockers TEA and 4-AP and by the adenylyl cyclase activator forskolin. **A**: Averaged time course of ramp currents measured at +80 mV in cultured OPCs before or after the application of a combination of the I_K blocker tetraethylammonium (TEA; 3 mM) plus the I_A blocker 4-aminopyridine (4-AP; 500 μ M) or during the subsequent application of BAY60-6583 (BAY; 10 μ M). Upper panel: original ramp current traces recorded in a typical OPC at representative time points: in control conditions (bsl; black trace); after 3 min of TEA+4-AP (TEA+4-AP; dotted grey trace) or after 5 min of 10 μ M BAY60-6583 applied in the presence of TEA+4-AP (TEA+4-AP +BAY; dotted grey trace). **B**: Pooled data of ramp current inhibition measured at +80 mV in the presence of BAY60-6583 applied alone in matched controls (control: ctrl), in the presence of 3 mM TEA (+TEA) or in the combination of 3 mM TEA + 500 μ M 4-AP (+TEA+4-AP). * p < 0.05; one-way ANOVA, Bonferroni post-hoc test. Number of observations is written in the columns. **C**, **D**: Averaged time course (**C**), and pooled data (mean \pm SE: **D**), of ramp currents measured at +80 mV in cultured OPCs before or after the application of the adenylyl cyclase activator forskolin (FSK; 20 μ M) or during the subsequent application of BAY60-6583 (BAY; 10 μ M). Lower panel in **C**: original ramp current traces recorded in a typical OPC at representative time points: in control conditions (baseline: bsl; black trace); after 3 min of FSK (dotted grey trace) or after 5 min of 10 μ M BAY60-6583 applied in the presence of FSK (FSK+BAY; dotted grey trace). ** p < 0.01; ### p < 0.01, paired Student's t-test, n=6. All experiments were performed in the presence of the A_1 , A_{2A} and A_3 receptor antagonists DPCPX, SCH58261 and MRS1523, respectively (all 100 nM).

4.2 The A_{2B} receptor activation modulates oligodendrocyte maturation *in vitro*

To study oligodendroglial cell maturation *in vitro*, OPCs were lead to differentiate into mature OLs by growing for 3, 7 and 10 days in DM (mitogen-free medium). As shown in Fig. 9 A and B, a significant and time-dependent increase in MAG and MBP expression was found, compared to OPC (open bar), that was maximal at 7 days (black bar). Moreover, we dissected the time-dependent expression of A_{2B} receptor in OL compared to control OPC and found out that the expression of the receptor increases by the time of incubation with DM (Fig. 9 C).

We finally investigated the involvement of A_{2B} receptor agonists in oligodendroglial cell maturation *in vitro*, alone or in combination with A_{2B} selective antagonist. According to the results reported in Fig. 9 A, we selected 7 days of DM as the reference time to analyze OL differentiation under different conditions. At 7 day incubation in DM in the presence of the A_{2B} receptor agonist BAY60-6583 (10 μM), dramatically reverted the increase of either MAG or MBP (Fig. 10 A, B red bar compared to open bar), indicating that A_{2B} receptor stimulation counteracts OPC maturation towards OLs. These effects were reduced in the presence of 10 μM MRS1706, a selective A_{2B} receptor antagonist.

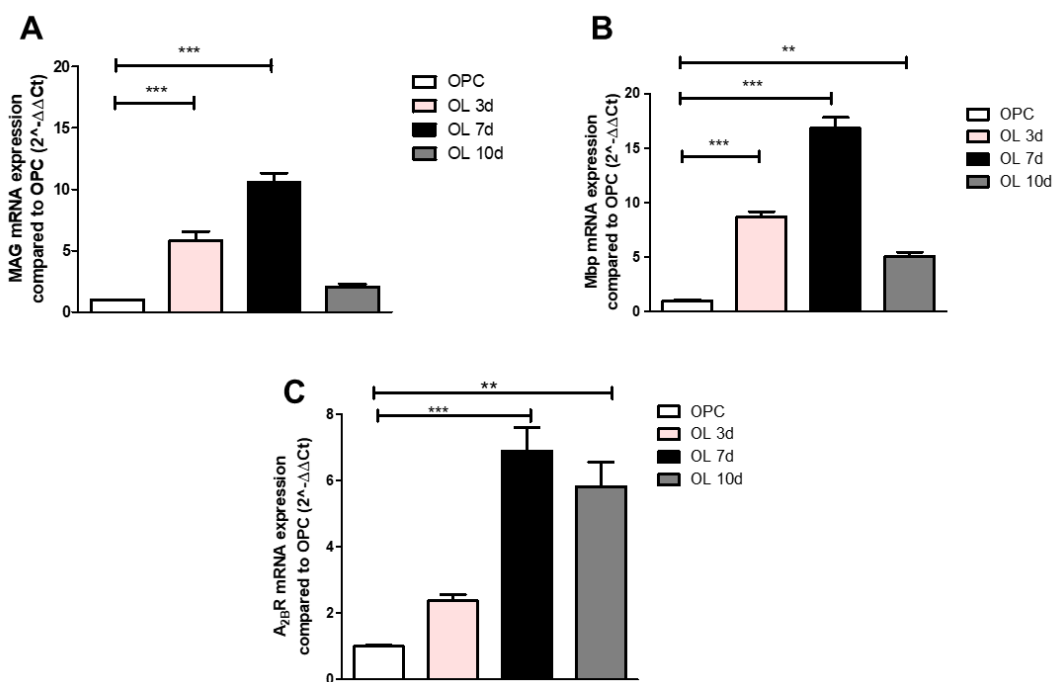


Fig. 9. Time course of oligodendrocyte marker expression, A_{2B} adenosine receptor during differentiation from OPC to OL. Gene expression analysis of oligodendrocyte differentiation markers MAG (A) and MBP (B) was performed by Real Time-PCR in OPC and 3, 7 and 10 day-differentiation (OL 3d, 7d, 10d) employing specific rat primers using SYBR green probe. Each measurement was carried out in triplicate. The 2^{-ΔΔCT} method was applied as a comparative method of quantification and data were normalized to β-actin expression. C: A_{2B} adenosine receptor expression, analyzed employing specific rat primers and SYBR Green probe, was reported in OPC and after 3, 7, 10 days (t₃, t₇, t₁₀) of DM, as 2^{-ΔΔCT} normalized to β-actin and compared to the control OPC. Data are means±SEM of three independent experiments performed in triplicate. Statistical analysis was performed using One-way ANOVA, followed by Bonferroni post-hoc test, ***p* < 0.01, ****p* < 0.001.

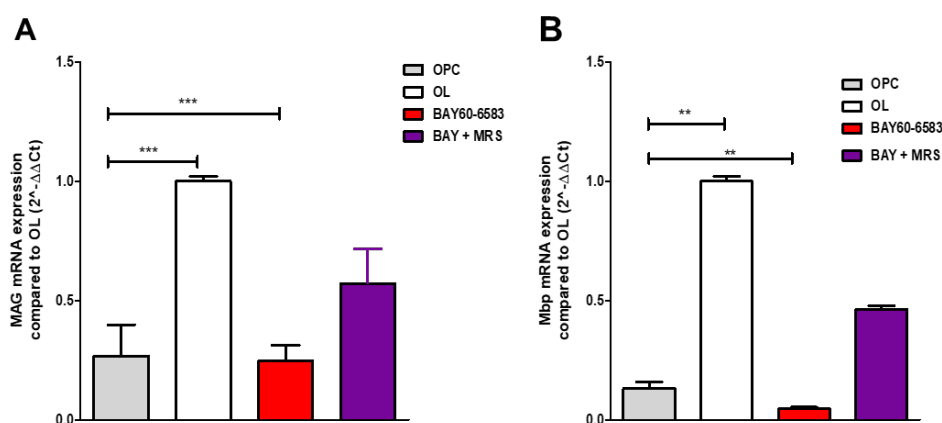


Fig. 10. A_{2B} adenosine receptor-mediated effects on oligodendrocyte differentiation *in vitro*. Gene expression analysis of oligodendrocyte differentiation markers MAG (A) and MBP (B) by Real time-PCR in OPC and after 7 days of DM (t₇ OL) in the absence or presence of: BAY60-6583 (10 μM) alone or in combination with MRS1706 (MRS, 10 μM), a selective A_{2B} adenosine receptor antagonist. The quantification of MAG and MBP mRNA was performed by Real-Time PCR employing specific primers as reported in the materials and methods section using SYBR green probe. Each measurement was carried out in triplicate. The 2^{-ΔΔCT} method was applied as a comparative method of quantification and data were normalized to β-actin expression. Data are means±SEM of three independent experiments performed in triplicate. Statistical analysis was performed by One-way ANOVA followed by Bonferroni post-hoc test ***p* < 0.01; ****p* < 0.001.

5. DISCUSSION AND CONCLUSIONS

The present work provides the first description of A_{2B} receptor-mediated effects in oligodendroglial cell cultures. We demonstrate here that the selective A_{2B} receptor activation inhibits I_K and I_A currents and delays maturation of cultured OPCs.

Adenosine participates to a number of OPC functions, from cell migration to myelin production.^{394,419} It has been recently demonstrated³⁴⁴ that A_{2A} receptor stimulation counteracts oligodendroglial cell differentiation *in vitro* by inhibiting TEA-sensitive I_K currents, whose block is known to impair OPC maturation.³⁴⁸

In the present work, we demonstrated that similar effects are achieved upon selective A_{2B} receptor stimulation. However, differently from A_{2A} receptors, A_{2B} receptor activation not only inhibits I_K conductances but also I_A transient currents. In accordance to K⁺ channel inhibition, and similarly to A_{2A} receptor activation, the A_{2B} receptor agonist BAY60-6583 also significantly depolarized cell membrane and inhibited *in vitro* OPC differentiation when added for 7 days in the culture medium of these cells.

The inhibition of TEA-sensitive I_K current in cultured OPCs is known to prevent OPC differentiation.^{394,416,420-421-422} A_{2B} receptor-mediated I_K inhibition was obtained in the present work by using two different A_{2B} receptor agonists: the prototypical, commercially available, selective A_{2B} receptor agonist BAY60-6583, and the unselective adenosine receptor agonist NECA. All compounds were applied in the continuous presence of saturating concentrations of A₁, A_{2A} and A₃ receptor antagonists to avoid nonspecific effects on other adenosine receptor subtypes. On these bases, we claim that the electrophysiological effect observed in the presence of the above-mentioned compounds is A_{2B} receptor-mediated.

We also investigated the intracellular pathway by which A_{2B} receptors modulate K⁺ currents in cultured OPCs. Our previous data showed that the G_s-coupled A_{2A} receptor decreases ramp-evoked K⁺ currents in purified OPCs,³⁹⁴ whereas the G_i-coupled GPR17 receptor increases²⁹³ the same conductances. So, we tested the hypothesis of intracellular cAMP being involved in this effect. Indeed, direct activation of adenylyl cyclase by forskolin application decreased ramp-evoked currents and occluded the effect of a further application of BAY60-6583, demonstrating that cAMP rise is involved in A_{2B} receptor-

mediated effect. Furthermore, an increase in intracellular cAMP level could be responsible also for the inhibition of oligodendroglial maturation observed in the present work upon A_{2B} receptor activation, since previous observations show that forskolin inhibits *in vitro* myelination.⁴²³

An additional proof that A_{2B} receptors are critical modulators of OPC maturation resides in the fact that this receptor subtype is clearly upregulated during cell differentiation, we hypothesize that, under demyelinating conditions where OPC migration is required, adenosine A_{2B} receptor antagonists could facilitate OPC recruitment to the injured area.

In conclusion, we demonstrated for the first time that A_{2B} receptors inhibit TEA-sensitive K^+ currents by increasing intracellular cAMP levels in cultured OPCs and inhibit OPC differentiation. Adenosine A_{2B} receptors may, therefore, represent a new molecular target for drugs useful in demyelinating pathologies, such as MS or in different demyelinating conditions induced by stroke and brain trauma.

6. REFERENCES

1. Rossi, F. *et al.* Blue LED induced thermal effects in wound healing: experimental evidence in an in vivo model of superficial abrasions. in *Energy-based Treatment of Tissue and Assessment IX* **10066**, 100660B (SPIE, 2017).
2. Jarrett, P. & Scragg, R. A short history of phototherapy, Vitamin D and skin disease. *Photochem. Photobiol. Sci.* **16**, 283–290 (2017).
3. Anders, J., Lanzafame, R. & Arany, P. Low-level light/laser therapy versus photobiomodulation therapy. *Photomed. Laser Surg.* **33**, 183–184 (2015).
4. Hourel, N. Shedding light on a new treatment for diabetic wound healing: A review on phototherapy. *Sci. World J.* (2014). doi:10.1155/2014/398412
5. Vo-Dinh, T. Biomedical Photonics handbook. (2003).
6. Light: Electromagnetic waves, the electromagnetic spectrum and photons (article) | Khan Academy. Available at: <https://www.khanacademy.org/science/physics/light-waves/introduction-to-light-waves/a/light-and-the-electromagnetic-spectrum>. (Accessed: 4th November 2019)
7. Niemz, M. *Laser-Tissue Interactions Fundamentals and Applications. Laser-Tissue Interactions* (Springer Berlin Heidelberg, 2002). doi:10.1007/978-3-662-04717-0_1
8. Home | BioOptics World. Available at: <https://www.bioopticsworld.com/>. (Accessed: 4th November 2019)
9. Schindl, A., Schindl, M., Pernestofer-Shcon, H. & Schindl, L. Low-intensity laser therapy: a review. *J. Investig. Med.* **48**, 312–326 (2000).
10. Piaggese, A; Läuchli, S; Bassetto, F; Biedermann, T; Marques, A; Najafi, B; Palla, I; Scarpa, C; Seimetz, D; Triulzi, I; Turchetti, G; Vaggelas, A. EWMA document: advanced therapies in wound management: cell and tissue based therapies, physical and bio-physical therapies smart and IT based technologies. *2018 6 (27AD)*.
11. Pini, R., Rossi, F. & Fatto, F. Laser Surgery. in *Handbook of Biophotonics* (ed. Popp, J; Tuchin, VV; Chiou, A; Heinemann, S.) (Wiley-VCH, 2011).
12. Rossi, F. *et al.* A blue-LED-based device for selective photocoagulation of superficial abrasions: theoretical modeling and in vivo validation. in *Photonic Therapeutics and Diagnostics VI* **7548**, 754807 (SPIE, 2010).
13. Alfieri, D. *et al.* Blue LED treatment of superficial abrasions. in *Photonic Therapeutics and Diagnostics IX* **8565**, 85650H (SPIE, 2013).
14. Rossi, F. *et al.* Improved wound healing in blue LED treated superficial abrasions. in *Optics InfoBase Conference Papers* (Optical Society of American (OSA), 2013). doi:10.1117/12.2032550
15. Cicchi, R. *et al.* Improvement of the healing process in superficial skin wounds after treatment with EMOLED. in *Biophotonics: Photonic Solutions for Better Health Care IV* (eds. Popp, J., Tuchin, V. V., Matthews, D. L., Pavone, F. S. & Garside, P.) 91293X (2014). doi:10.1117/12.2052188
16. Cicchi, R. *et al.* Irradiation with EMOLED improves the healing process in superficial skin wounds. in *Photonic Therapeutics and Diagnostics X* **8926**, 892604 (SPIE, 2014).

17. Rossi, F. *et al.* Healing process study in murine skin superficial wounds treated with the blue LED photocoagulator 'EMOLED'. in *Optics InfoBase Conference Papers* (OSA - The Optical Society, 2014). doi:10.1117/12.2183670
18. Rossi, F. *et al.* In vivo wound healing modulation after irradiation with a blue LED photocoagulator. in *Optics InfoBase Conference Papers Part F61-E*, (OSA - The Optical Society, 2017).
19. Magni, G. *et al.* Blue LED treatment of superficial abrasions: in vivo experimental evidence of wound healing improvement. in *Biophotonics: Photonic Solutions for Better Health Care VI 14* (SPIE-Intl Soc Optical Eng, 2018). doi:10.1117/12.2307397
20. Cicchi, R. *et al.* Observation of an improved healing process in superficial skin wounds after irradiation with a blue-LED haemostatic device. *J. Biophotonics* **9**, 645–655 (2016).
21. Mosti, G. & Gasperini, S. Observations made on three patients suffering from ulcers of the lower limbs treated with Blue Light. *Chronic Wound Care Manag. Res.* **Volume 5**, 23–28 (2018).
22. Greco, M. *et al.* Helium-Neon laser irradiation of hepatocytes can trigger increase of the mitochondrial membrane potential and can stimulate c-fos expression in a Ca²⁺-dependent manner. *Lasers Surg. Med.* **29**, 433–441 (2001).
23. Feng, R. *et al.* Photobiomodulation with red light-emitting diodes accelerates hepatocyte proliferation through reactive oxygen species/extracellular signal-regulated kinase pathway. *Hepatol. Res.* **48**, 926–936 (2018).
24. Kim, M. *et al.* Effect of 660 nm Light-Emitting Diode on the Wound Healing in Fibroblast-Like Cell Lines. *Int. J. Photoenergy* **2015**, (2015).
25. Avci, P., Gupta, G., Clark, J., Wikonkal, N. & Hamblin, M. Low-level laser (light) therapy (LLLT) for treatment of hair loss. *Lasers Surg. Med.* **46**, 144–151 (2014).
26. Freitas, L. & Hamblin, M. Proposed mechanisms of photobiomodulation or low-level light therapy. *IEEE J. Sel. Top. Quantum Electron.* **22**, (2016).
27. Gao, X. & Xing, D. Molecular mechanisms of cell proliferation induced by low power laser irradiation. *J. Biomed. Sci.* **16**, (2009).
28. Chang, L. *et al.* Proteomic Analysis Reveals Anti-Fibrotic Effects of Blue Light Photobiomodulation on Fibroblasts. *Lasers in Surgery and Medicine* (Wiley, 2019). doi:10.1002/lsm.23137
29. Chaves, M., Piancastelli, A., Araújo, A. & Pinotti, M. Effects of low-power light therapy on wound healing: LASER x LED. *An. Bras. Dermatol.* **89**, 616–623 (2014).
30. Prindeze, N., Moffatt, L. & Shupp, J. Mechanisms of action for light therapy: A review of molecular interactions. *Exp. Biol. Med.* **237**, 1241–1248 (2012).
31. Saglam, M., Kantarci, A., Dundar, N. & Hakki, S. Clinical and biochemical effects of diode laser as an adjunct to nonsurgical treatment of chronic periodontitis: A randomized, controlled clinical trial. *Lasers Med. Sci.* **29**, 37–46 (2014).
32. Karu, T. & Kolyakov, S. Exact action spectra for cellular responses relevant to

- phototherapy. *Photomed. Laser Surg.* **23**, 355–361 (2005).
33. Karu, T. Primary and secondary mechanisms of action of visible to near-IR radiation on cells. *J. Photochem. Photobiol. B Biol.* **49**, 1–17 (1999).
 34. Rodrigo, S. *et al.* Analysis of the systemic effect of red and infrared laser therapy on wound repair. *Photomed. Laser Surg.* **27**, 929–935 (2009).
 35. Powell, M., Carnegie, D. & Burke, T. Reversal of Diabetic Peripheral Neuropathy and New Wound Incidence: The Role of MIRE. *Ski. Wound Care* **17**, 298–300 (2004).
 36. Caetano, K., Frade, M., Minatel, D., Santana, L. & Enwemeka, C. Phototherapy improves healing of chronic venous ulcers. *Photomed. Laser Surg.* **27**, 111–118 (2009).
 37. Minatel, D., Frade, M., França, S. & Enwemeka, C. Phototherapy promotes healing of chronic diabetic leg ulcers that failed to respond to other therapies. *Lasers Surg. Med.* **41**, 433–441 (2009).
 38. Leite, S. *et al.* Phototherapy promotes healing of cutaneous wounds in undernourished rats. *An. Bras. Dermatol.* **89**, (2014).
 39. Reddy, G., Stehno-Bittel, L. & Enwemeka, C. Laser photostimulation of collagen production in healing rabbit Achilles tendons. *Lasers Surg. Med.* **22**, 281–287 (1998).
 40. Morrone, G. *et al.* Osteochondral lesion repair of the knee in the rabbit after low-power diode Ga-Al-As laser biostimulation: An experimental study. *Artif. Cells. Blood Substit. Immobil. Biotechnol.* **28**, 321–336 (2000).
 41. Torricelli, P. *et al.* Laser biostimulation of cartilage: in vitro evaluation. *Elsevier* **55**, 117–120 (2001).
 42. Hawkins, D. & Abrahamse, H. Effect of multiple exposures of low-level laser therapy on the cellular responses of wounded human skin fibroblasts. *Photomed. Laser Surg.* **24**, 705–714 (2006).
 43. Guffey, J. & Wilborn, J. Effects of combined 405-nm and 880-nm light on *Staphylococcus aureus* and *Pseudomonas aeruginosa* in vitro. *Photomed. Laser Surg.* **24**, 680–683 (2006).
 44. Bumah, V. *et al.* The bactericidal effect of 470-nm light and hyperbaric oxygen on methicillin-resistant *Staphylococcus aureus* (MRSA). *Lasers Med. Sci.* **30**, 1153–1159 (2015).
 45. Maclean, M., Mckenzie, K., Anderson, J., Gettinby, G. & Macgregor, S. 405 nm light technology for the inactivation of pathogens and its potential 1 role for environmental disinfection and infection control 2 3. *J. Hosp. Infect.* **88**, 1–11 (2014).
 46. Kawada, A., Aragane, Y., Kameyama, H., Sangen, Y. & Tezuka, T. Acne phototherapy with a high-intensity, enhanced, narrow-band, blue light source: an open study and in vitro investigation. *J. Dermatol. Sci.* **30**, 129–135 (2002).
 47. Dai, T. *et al.* Blue light for infectious diseases: *Propionibacterium acnes*, *Helicobacter pylori*, and beyond? *Drugs Resist. Updat.* **15**, 223–236 (2012).
 48. Bumah, V., Masson-Meyers, D. & Enwemeka, C. Blue 470 nm light suppresses the

- growth of *Salmonella enterica* and methicillin-resistant *Staphylococcus aureus* (MRSA) in vitro. *Lasers Surg. Med.* **47**, 595–601 (2015).
49. Enwemeka, C. Antimicrobial blue light: An emerging alternative to antibiotics. *Photomedicine and Laser Surgery* **31**, 509–511 (2013).
 50. Zhang, Y. *et al.* Antimicrobial Blue Light Therapy for Multidrug-Resistant *Acinetobacter baumannii* Infection in a Mouse Burn Model: Implications for Prophylaxis and Treatment of. *J. Infect. Dis.* **209**, 1963–1971 (2013).
 51. Mittermayr, R. *et al.* Blue laser light increases perfusion of a skin flap via release of nitric oxide from hemoglobin. *Mol. Med.* **13**, 22–29 (2007).
 52. Ankri, R., Lubart, R. & Taitelbaum, H. Estimation of the optimal wavelengths for laser-induced wound healing. *Lasers Surg. Med.* **42**, 760–764 (2010).
 53. Dungal, P. *et al.* Low level light therapy by LED of different wavelength induces angiogenesis and improves ischemic wound healing. *Lasers Surg. Med.* **46**, 773–780 (2014).
 54. Shnitkind, E., Yaping, E., Geen, S., Shalita, A. & Lee, W. Anti-inflammatory properties of narrow-band blue light. *J. Drugs Dermatology* **5**, 605–610 (2006).
 55. Becker, A. *et al.* Gene expression profiling reveals aryl hydrocarbon receptor as a possible target for photobiomodulation when using blue light. *Sci. Rep.* **6**, (2016).
 56. Liebmann, J., Born, M. & Bachofen, V. Blue-light irradiation regulates proliferation and differentiation in human skin cells. *J. Invest. Dermatol.* **130**, 259–269 (2010).
 57. Kim, J., Woo, Y., Sohn, K., Jeong, K. & Kang, H. Wnt/ β -catenin and ERK pathway activation: A possible mechanism of photobiomodulation therapy with light-emitting diodes that regulate the proliferation of human outer root sheath cells. *Lasers Surg. Med.* **49**, 940–947 (2017).
 58. Mamalis, A., Garcha, M. & Jagdeo, J. Light emitting diode-generated blue light modulates fibrosis characteristics: Fibroblast proliferation, migration speed, and reactive oxygen species generation. *Lasers Surg. Med.* **47**, 210–215 (2015).
 59. Barolet, D., Roberge, C., Auger, F., Boucher, A. & Germain, L. Regulation of skin collagen metabolism in vitro using a pulsed 660 nm LED light source: clinical correlation with a single-blinded study. *J. Invest. Dermatol.* **129**, 2751–2759 (2009).
 60. Sassoli, C. *et al.* Low intensity 635 nm diode laser irradiation inhibits fibroblast-myofibroblast transition reducing TRPC1 channel expression/activity: New perspectives for tissue fibrosis treatment. *Lasers Surg. Med.* **48**, 318–332 (2016).
 61. Chung, H. *et al.* The nuts and bolts of low-level laser (Light) therapy. *Ann. Biomed. Eng.* **40**, 516–533 (2012).
 62. Mignon, C., Botchkareva, N., Uzunbajakava, N. & Tobin, D. Photobiomodulation devices for hair regrowth and wound healing: a therapy full of promise but a literature full of confusion. *Experimental Dermatology* **25**, 745–749 (2016).
 63. Mignon, C., Uzunbajakava, N., Raafs, B., Botchkareva, N. & Tobin, D. Photobiomodulation of human dermal fibroblasts in vitro: decisive role of cell culture

- conditions and treatment protocols on experimental outcome. *Sci. Rep.* **7**, (20177).
64. Opländer, C. *et al.* Effects of blue light irradiation on human dermal fibroblasts. *J. Photochem. Photobiol. B Biol.* **103**, 118–125 (2011).
 65. Song, S. *et al.* cDNA microarray analysis of gene expression profiles in human fibroblast cells irradiated with red light. *J. Invest. Dermatol.* **120**, 849–857 (2003).
 66. Mignon, C., Uzunbajakava, N., Castellano-Pellicena, I., Botchkareva, N. & Tobin, D. Differential response of human dermal fibroblast subpopulations to visible and near-infrared light: Potential of photobiomodulation for addressing cutaneous conditions. *Lasers Surg. Med.* **50**, 859–882 (2018).
 67. Veroli, G. *et al.* An automated fitting procedure and software for dose-response curves with multiphasic features. *Sci. Rep.* **5**, (2015).
 68. Masson-Meyers, D. S., Bumah, V. V. & Enwemeka, C. S. Blue light does not impair wound healing in vitro. *J. Photochem. Photobiol. B Biol.* **160**, 53–60 (2016).
 69. Goldberg, M., Han, Y., Yan, C., Shaw, M. & Garner, W. TNF- α suppresses α -smooth muscle actin expression in human dermal fibroblasts: an implication for abnormal wound healing. *J. Invest. Dermatol.* **127**, 2645–2655 (2007).
 70. Modarressi, A. *et al.* Hypoxia impairs skin myofibroblast differentiation and function. *J. Invest. Dermatol.* **130**, 2818–2827 (2010).
 71. Chen, Y. *et al.* Matrix contraction by dermal fibroblasts requires transforming growth factor- β /activin-linked kinase 5, heparan sulfate-containing proteoglycans, and MEK/ERK. *Am. J. Pathol.* **167**, 1699–1711 (2005).
 72. Tafinski, L. *et al.* Blue light inhibits transforming growth factor- β 1-induced myofibroblast differentiation of human dermal fibroblasts. *Exp. Dermatol.* **23**, 240–246 (2014).
 73. Ashcroft, K., Syed, F. & Bayat, A. Site-Specific Keloid Fibroblasts Alter the Behaviour of Normal Skin and Normal Scar Fibroblasts through Paracrine Signalling. *PLoS One* **8**, (2013).
 74. Wu, C., Wu, P., Fang, A. & Lan, C. FK506 inhibits the enhancing effects of transforming growth factor (TGF)- β 1 on collagen expression and TGF- β /Smad signalling in keloid fibroblasts: Implication for new therapeutic approach. *Br. J. Dermatol.* **167**, 532–541 (2012).
 75. Lee, H. *et al.* Low-level light therapy with 410 nm light emitting diode suppresses collagen synthesis in human keloid fibroblasts: An in vitro study. *Ann. Dermatol.* **29**, 149–155 (2017).
 76. Fore, J. A review of skin and the effects of aging on skin structure and function. *Ostomy. Wound. Manage.* **9**, 24–35 (2006).
 77. Gurtner, G., Werner, S., Barrandon, Y. & Longaker, M. Wound repair and regeneration. *Nature* **453**, 314–321 (2008).
 78. Orgill, D. & Blanco, C. *Biomaterials for treating skin loss*. (Lippincott Williams & Wilkins, 2005).

79. Kanitakis Jean. Anatomy, histology and immunohistochemistry of normal human skin. *Eur. J. Dermatology* **12**, 390–401 (2002).
80. McGrath, J. A., Eady, R. A. J. & Pope, F. M. Anatomy and Organization of Human Skin. *Rook's Textb. Dermatology* (2004). doi:10.1002/9780470750520.ch3
81. Elston, W. J. T. B. D. *Andrews' diseases of the skin: clinical dermatology. Clinical Dermatology - Expert Consult - Online and Print* (2006).
82. Leyva-Mendivil, M., Page, A., Bressloff, N. & Limbert, G. A mechanistic insight into the mechanical role of the stratum corneum during stretching and compression of the skin. *J. Mech. Behav. Biomed. Mater.* **49**, 197–219 (2015).
83. Ackerman, A. Histologic diagnosis of inflammatory skin diseases: an algorithmic method based on pattern analysis. in *Histopathology* **47**, 641–647 (Williams and Wilkins, 2005).
84. Okun, M., Edelstein, L. & Fisher, B. Gross and microscopic pathology of the skin. in *Normal histology of the skin* (ed. Dermatopathology Foundation Press) (1988).
85. Woodley, D. Distinct fibroblasts in the papillary and reticular dermis: implications for wound healing. *Dematologic Clin.* **35**, 95–100 (2017).
86. Driskell, R., Lichtenberger, B., Hoste, E. & Kretzschmar, K. Distinct fibroblast lineages determine dermal architecture in skin development and repair. *Nature* **504**, 277–281 (2013).
87. Driskell, R. & Watt, F.-. Understanding fibroblast heterogeneity in the skin. *Trends Cell Biol.* **25**, 92–99 (2015).
88. Janson, D., Saintigny, G., Adrichem, A., Mahe, C. & Ghalbzouri, A. Different gene expression patterns in human papillary and reticular fibroblasts. *J. Invest. Dermatol.* **132**, 2565–2572 (2012).
89. Woodley, D. Distinct fibroblasts in the papillary and reticular dermis: implications for wound healing. *Dermatol. Clin.* **35**, 95–100 (2017).
90. Pearce, J. M. S. *Henry Gray's anatomy. Clinical Anatomy* **22**, (2009).
91. Fischer, J., Bland, K. & Callery, M. *Mastery of surgery.* (2006).
92. Singer, A. J. & Clark, R. A. F. Cutaneous Wound Healing. *N. Engl. J. Med.* **341**, 738–746 (1999).
93. Diegelmann, R. & Evans, M. Wound healing: an overview of acute, fibrotic and delayed healing. *Front. Biosci. a J. virtual Libr.* **9**, 283–289 (2004).
94. Bran, G., Goessler, U., Hormann, K., Riedel, F. & Sadick, H. Keloids: Current concepts of pathogenesis (Review). *Int. J. Mol. Med.* **24**, 283–293 (2009).
95. Percival, N. Classification of wounds and their management. *Surgey (Oxford)* **20**, 114–117 (2002).
96. Moffat, C; Vowden, P. *European Wound Management Association (EWMA). Position Document: Hard-to-heal wounds: a holistic approach.* (2008).
97. Lawrence, W. Physiology of the acute wound. *Clin. Plast.* **25**, 321–340 (1998).
98. Hart, J. Inflammation. 1: Its role in the healing of acute wounds. *J. Wound Care* **11**,

- 205–209 (2002).
99. Flanagan, M. The physiology of wound healing. *J. Wound Care* **9**, 299–300 (2000).
 100. Martin C. Robson, David L. Steed, M. G. F. Wound healing: biologic features and approaches to maximize healing trajectories. *Curr. Probl. Surg.* **38**, 72–140 (2001).
 101. Broughton, George II, Janis, Jeffrey, Attinger, C. The basic science of wound healing. *Plast. Reconstr. Surg.* **117**, 12S-34S (2006).
 102. Pool, J. Normal hemostatic mechanisms: a review. *Am. J. Med. Technol.* **43**, 776–780 (1977).
 103. Gonzalez, A., Costa, T., Araujo Andrade, Z. & Alves Peixoto Medrado, A. Wound healing-A literature review. *An. Bras. Dermatol.* **51**, (2016).
 104. Lasne, D. & Jude, B. From normal to pathological hemostasis. *Can. J. Anesth.* **53**, s2–s11 (2006).
 105. Home Page | BioNinja. Available at: <https://ib.bioninja.com.au/>. (Accessed: 4th November 2019)
 106. Cines, D. B. *et al.* *Endothelial Cells in Physiology and in the Pathophysiology of Vascular Disorders. The Journal of The American Society of Hematology* **91**, (1998).
 107. Andrews, R. & Berndt, M. Platelet physiology and thrombosis. *Elsevier* **114**, 447–453 (2004).
 108. Heemskerk, J., Bevers, E. & Lindhout, T. Platelet Activation and Blood Coagulation. *Thromb. Haemost.* **88**, 186–193 (2002).
 109. Bassé, F., Gaffet, P., Rendu, F. & Bienvenüe, A. Translocation of Spin-Labeled Phospholipids through Plasma Membrane during Thrombin- and Ionophore A23187-Induced Platelet Activation. *Biochemistry* **32**, 2337–2344 (1993).
 110. Cesarman-Maus, G. & Hajjar, K. Molecular mechanisms of fibrinolysis. *Br. J. Hematol.* **129**, 307–321 (2005).
 111. Jespersen, J. Pathophysiology and clinical aspects of fibrinolysis and inhibition of coagulation. Experimental and clinical studies with special reference to women on oral. *Dan. Med. Bull.* **35**, 1–33 (1988).
 112. Skover, G. Cellular and biochemical dynamics of wound repair, wound environment in collagen regeneration. *Clin Pod. Med Surg* **8**, 723–756 (1991).
 113. Toy, L. W. Matrix metalloproteinases: their function in tissue repair. *Journal of wound care* **14**, 20–22 (2005).
 114. Li, J., Chen, J. & Kirsner, R. Pathophysiology of acute wound healing. *Elsevier* **25**, 9–18 (2007).
 115. Koh, T. & Dipietro, L. Inflammation and wound healing: the role of the macrophage. *Expert Rev. Mol. Med.* **13**, (2011).
 116. Wang, X., Han, G., Owens, P. & Siddiqui, Y. Role of TGF β -mediated inflammation in cutaneous wound healing. *Elsevier* **11**, 112–117 (2006).
 117. Coentro, J., Pugliese, E., Hanley, G., Raghunath, M. & Zeugolis, D. Current and upcoming therapies to modulate skin scarring and fibrosis. *Adv. Drug Deliv. Rev.*

(2018). doi:10.1016/j.addr.2018.08.009

118. Robson, M., Steed, D. & Franz, M. Wound healing: biologic features and approaches to maximize healing trajectories. *Curr. Probl. Surg.* **38**, 72–140 (2001).
119. Belgique, R. Surgical biology of wound healing. in *de l'Academie royale de medecine* (2001).
120. J.Degreef, H. How to heal a wound fast. *Dermatol. Clin.* **16**, 265–375 (1998).
121. Attinger, C. & Janis, J. Clinical approach to wounds: debridement and wound bed preparation including the use of dressings and wound-healing adjuvants. *Plast. Reconstr. Surg.* **117**, 72S-109S (2006).
122. Broughton, G; Janis, JE. Attinger, C. Wound healing: an overview. *Plast. Reconstr. Surg.* **117**, 1e-S-S32e-S (2006).
123. Hunt, T., Hopf, H. & Care, Z. Physiology of wound healing. *Adv. Ski. Wound Care, suppl. Heal. Chronic Wounds Technol. Solut. Today* **13**, (2000).
124. Oskeritzian, C. Mast Cells and Wound Healing. *Adv. Wound Care* **1**, 23–28 (2012).
125. Ng, M. The role of mast cells in wound healing. *Int Wound J* **7**, 55–61 (2010).
126. Nishioka, K. & Kobayashi, Y. Mast cell numbers in diffuse scleroderma. *Jama Dermatology* **123**, 205–208 (1987).
127. Kischer, CW; Bunce, H; Shetlar, M. Mast cell analyses in hypertrophic scars, hypertrophic scars treated with pressure and mature scars. *J. Invest. Dermatol.* **70**, 355–357 (1978).
128. MY, S. Healing of physical wounds. *Nurs. Clin. North Am.* **22**, 439–447 (1987).
129. Ennis WJ, M. P. Wound healing at the local level: the stunned wound. *Ostomy. Wound. Manage.* **46**, 39S-48S (2000).
130. Witte, B. & Barbul, A. General principles of wound healing. *Surg. Clin. North Am.* **77**, 509–528 (1997).
131. Ramasastry, S. Acute wounds. *Clin. Plast. Surg.* **32**, 198–208 (2005).
132. Italiani, P; Boraschi, D. From monocytes to M1/M2 macrophages: Phenotypical vs. functional differentiation. *Front. Immunol.* **5**, (2014).
133. Forbes, S. & Rosenthal, N. Preparing the ground for tissue regeneration: from mechanism to therapy. *Nat. Med.* **20**, 87–869 (2014).
134. Wynn, T. & Chawla, A; Pollard, J. Macrophage biology in development, homeostasis and disease. *Nature* **496**, 445–455 (2013).
135. Parks, W. Matrix metalloproteinases in repair. *Wound Repair Regen.* **7**, 423–432 (1999).
136. Darby, I., Zakuan, N., Billet, F. & Desmoulière, A. The myofibroblast, a key cell in normal and pathological tissue repair. *Cell. Mol. Life Sci.* **73**, 1145–1157 (2016).
137. Tomasek, J., Gabbiani, G., Hinz, B., Chaponnier, C. & Brown, R. Myofibroblasts and mechano: Regulation of connective tissue remodelling. *Nat. Rev. Mol. Cell Biol.* **3**, 349–363 (2002).
138. Diegelmann, R. Wound healing: an overview of acute, fibrotic and delayed healing.

- Front. Bioscience* **9**, 283–289 (2004).
139. Chen, W. & Rogers, A. Recent insights into the causes of chronic leg ulceration in venous diseases and implications on other types of chronic wounds. *Wound Repair Regen.* **15**, 434–449 (2007).
 140. Greene, A. *et al.* Microdeformational wound therapy: effects on angiogenesis and matrix metalloproteinases in chronic wounds of 3 debilitated patients. *Ann. Plast. Surg.* **56**, 418–422 (2006).
 141. Desmouliere, A., Redard, M., Darby, I. & Gabbiani, G. Apoptosis Mediates the Decrease in Cellularity during the Transition between Granulation Tissue and Scar. *Am. journal Pathol.* **146**, 56–66 (1995).
 142. Ribatti, D., Vacca, R., Roncali, L. & Dammacco, F. Angiogenesis under normal and pathological conditions. *Haematologica* **76**, 311–320 (1991).
 143. Zhang, Q. *et al.* Vascular endothelial growth factor is the major angiogenic factor in omentum: mechanism of the omentum-mediated angiogenesis. *J. Surg. Res.* **67**, 147–154 (1997).
 144. Risau, W. Angiogenic growth factors. *Prog. Growth Factor Res.* **2**, 71–79 (1990).
 145. Silverstein, JJ; Rifkin, D. Endothelial cell growth factors and the vessel wall. *Semin. Thromb. Hemost.* **13**, 504–511 (1987).
 146. Oike, Y. *et al.* Angiopoietin-related growth factor (AGF) promotes angiogenesis. *Blood* **103**, 3760–3765 (2004).
 147. Clark, R. A. F. Regulation of fibroplasia in cutaneous wound repair. *Am. J. Med. Sci.* **306**, 42–48 (1993).
 148. Velnar, T., Bailey, T. & Smrkolj, V. The Wound Healing Process: an Overview of the Cellular and Molecular Mechanisms. *J. Int. Med. Res.* **37**, 1528 (2009).
 149. Pierce, G., Berg, J., Rudolph, R., Tarpley, J. & Mustoell, T. Platelet-derived Growth Factor-BB and Transforming Growth Factor Betal Selectively Modulate Glycosaminoglycans, Collagen, and Myofibroblasts in Excisional Wounds*; the Core Electron. *Am. J. Pathol.* **138**, 629–646 (1991).
 150. Baum, C. & Arpey, C. Normal Cutaneous Wound Healing: Clinical Correlation with Cellular and Molecular Events. *Dermatologic Surg.* **31**, 674–686 (2006).
 151. Falanga, V. Wound healing and chronic wounds. *J. Cutan. Med. Surg.* **3**, S1-1–5 (1998).
 152. O’Kane, S. Wound remodelling and scarring. *J. Wound Care* **11**, 296–299 (2002).
 153. Baryza, M. & Baryza, G. The Vancouver Scar Scale: An Administration Tool and Its Interrater Reliability. *J. Burn Care & amp* **16**, 535–538 (1995).
 154. Bock, O. & Mrowietz, U. Keloids. A fibroproliferative disorder of unknown etiology. *Dermatologie* **53**, 515–523 (20022).
 155. Rahban, S. R. & Garner, W. L. Fibroproliferative scars. *Clin. Plast. Surg.* **30**, 77–89 (2003).
 156. Wynn, T. Cellular and molecular mechanisms of fibrosis. *J. Pathol.* **214**, 199–210

- (2008).
157. Postlethwaite, A., Holness, M., Katai, H. & Raghov, R. Tennessee 38163; and the 1 1 Veterans Affairs Medical Center. *J. Clin. Investig.* **90**, 1479–1485 (1992).
 158. Atiyeh, B., Costagliola, M. & Hayek, S. Keloid or Hypertrophic Scar The Controversy: Review of the Literature. *Ann. Plast. Surg.* **54**, 676–680 (2005).
 159. Butler, P., Longaker, M. & Yang, G. Current Progress in Keloid Research and Treatment. *J. Am. Coll. Surg.* **206**, 731–741 (2008).
 160. Rockwell, W., Cohen, I. & Ehrlich, H. Keloids and hypertrophic scars: a comprehensive review. *Plast. Reconstr. Surg.* **84**, (1989).
 161. Ehrlich, H. *et al.* Morphological and Immunochemical Differences Between Keloid and Hypertrophic Scar. *Am. J. Pathol.* **145**, 105–113 (1994).
 162. Clore, J., Cohen, I. & Diegelmann, R. Quantitative assay of types I and III collagen synthesized by keloid biopsies and fibroblasts. *Biochim. Biophys. Acta - Gen. Subj.* **22**, 384–390 (1979).
 163. Andrews, J., Marttala, J., Macarak, E., Rosenbloom, J. & Uitto, J. Keloids: The paradigm of skin fibrosis - Pathomechanisms and treatment. *Matrix Biol.* **51**, 37–46 (2016).
 164. Tuan, T. & Nichter, L. The molecular basis of keloid and hypertrophic scar formation. *Mol. Med. Today* **4**, 19–24 (1998).
 165. Har-Shai, Y. *et al.* Keloid histopathology after intralesional cryosurgery treatment. *J. Eur. Acad. Dermatology Venereol.* **25**, 1027–1036 (2011).
 166. Alster, T. & Tanzi, E. Hypertrophic scars and keloids: Etiology and management. *Am. J. Clin. Dermatol.* **4**, 235–243 (2003).
 167. Breasted, J. The Edwin Smith Surgical Papyrus: Published in Facsimile and Hieroglyphic Transliteration with Translation and Commentary in Two Volumes. *JAMA: The Journal of the American Medical Association* **96**, 1534 (1931).
 168. Gauglitz, G. G., Korting, H. C., Pavicic, T., Ruzicka, T. & Jeschke, M. G. Hypertrophic scarring and keloids: pathomechanisms and current and emerging treatment strategies. *Mol. Med.* **17**, 113–25 (2011).
 169. Larrabee, W. F., East, C. A., Jaffe, H. S., Stephenson, C. & Peterson, K. E. Intralesional Interferon Gamma Treatment for Keloids and Hypertrophic Scars. *Arch. Otolaryngol. Neck Surg.* **116**, 1159–1162 (1990).
 170. Abrams, B., Benedetto, A. & Humeniuk, H. Exuberant keloidal formation. *J. Am. Osteopath. Assoc.* **93**, 863–865 (1993).
 171. Ramakrishnan, K., Mathangi, F., Thomas, K., Pothan, M. & Sundararajan, C. Study of 1,000 patients with keloids in South India. *Plast. Reconstr. Surg.* **53**, 276–280 (1974).
 172. Davies, D. Plastic and reconstructive surgery scars, hypertrophic scars, and keloids. *Br. Med. J. (Clin. Res. Ed).* **290**, 1056–1058 (1985).
 173. Urioste, S., Arndt, K. & Dover, J. Keloids and hypertrophic scars: review and treatment strategies. *Semin. Cutan. Med. Surg.* **18**, 158–171 (1999).

174. Muir, I. On the nature of keloid and hypertrophic scars. *Br. J. Plast. Surg.* **43**, 61–69 (1990).
175. English, R. & Shenefelt, P. Keloids and Hypertrophic Scars. *Am. Soc. Dermatologic Surg.* **25**, 631–638 (1999).
176. Ogawa, R. & Akaishi, S. Endothelial dysfunction may play a key role in keloid and hypertrophic scar pathogenesis—keloids and hypertrophic scars may be vascular disorders. *Elsevier* **96**, 51–60 (2016).
177. Fong, E., Chye, L. & Tan, W. *Keloids: time to dispel the myths? Plastic and Reconstructive Surgery* **104**, (1999).
178. Huang, C., Akaishi, S., Hyakusoku, H. & Ogawa, R. Are keloid and hypertrophic scar different forms of the same disorder? A fibroproliferative skin disorder hypothesis based on keloid findings. *Int. Wound J.* **11**, 517–522 (2014).
179. Stucker, F. & Shaw, G. An approach to management of keloids. *Arch Otolaryngol Head Neck Surg.* **118**, 63–67 (1992).
180. Moustafa, M. & Fattah, A. Presumptive evidence of the effect of pregnancy estrogens on keloid growth. *Plast. Reconstr. Surg.* **56**, 450–453 (1975).
181. Oliver, N., Babu, M. & Diegelmann, R. Fibronectin gene transcription is enhanced in abnormal wound healing. *J. Invest. Dermatol.* **99**, 579–586 (1992).
182. Babu, M., Diegelmann, R. & Oliver, N. Fibronectin Is Overproduced by Keloid Fibroblasts during Abnormal Wound Healing. *Mol. Cell. Biol.* **9**, 1642–1650 (1989).
183. Friedman, D. *et al.* Regulation of collagen gene expression in keloids and hypertrophic scars. *J. Surg. Res.* **55**, 214–222 (1993).
184. Peltonen, J. *et al.* Activation of collagen gene expression in keloids: co-localization of type I and VI collagen and transforming growth factor- β 1 mRNA. *J. Invest. Dermatol.* **97**, 240–248 (1991).
185. Mari, W. *et al.* Novel Insights on Understanding of Keloid Scar: Article Review. *J. Am. Coll. Clin. Wound Spec.* **7**, 1–7 (2015).
186. Gold, M. *et al.* Updated international clinical recommendations on scar management: Part 2 - Algorithms for scar prevention and treatment. *Dermatologic Surg.* **40**, 825–831 (2014).
187. Jalali, M. & Bayat, A. Current use of steroids in management of abnormal raised skin scars. *Surgeon* **5**, 175–180 (2007).
188. Ketchum, L., Smith, J., Robinson, D. & Masters, F. The treatment of hypertrophic scar, keloid and scar contracture by triamcinolone acetonide. *Plast. Reconstr. Surg.* **38**, 209–18 (1966).
189. Takeda, K., Arase, S. & Takahashi, S. Side Effects of Topical Corticosteroids and their Prevention. *Drugs* **36**, 15–23 (1988).
190. Slemp, A. E. & Kirschner, R. E. Keloids and scars: A review of keloids and scars, their pathogenesis, risk factors, and management. *Curr. Opin. Pediatr.* **18**, 396–402 (2006).
191. Ud-Din, S. & Bayat, A. Strategic management of keloid disease in ethnic skin: A

- structured approach supported by the emerging literature. *Br. J. Dermatol.* **169**, 71–81 (2013).
192. Al-Attar, A., Mess, S., Thomassen, J., Kauffman, C. & Davison, S. Keloid pathogenesis and treatment. *Plast. Reconstr. Surg.* **117**, 286–300 (2006).
 193. Khan, M., Bashir, M. & Khan, F. Intralesional triamcinolone alone and in combination with 5-fluorouracil for the treatment of keloid and hypertrophic scars. *J. Pak. Med. Assoc.* **64**, 1003–1007 (2014).
 194. Apikian, M. & Goodman, G. Intralesional 5-fluorouracil in the treatment of keloid scars. *Australas. J. Dermatol.* **45**, 140–143 (2004).
 195. Lebwohl, M. From the literature: intralesional 5-FU in the treatment of hypertrophic scars and keloids: clinical experience. *J. Am. Acad. Dermatol.* **42**, 677 (2000).
 196. Fitzpatrick, R. Treatment of inflamed hypertrophic scars using intralesional 5-FU. *Dermatologic Surg.* **25**, 224–232 (1999).
 197. Bijlard, E., Steltenpool, S. & Niessen, F. Intralesional 5-fluorouracil in keloid treatment: A systematic review. *Acta Derm. Venereol.* **95**, 778–782 (2015).
 198. Nanda, S. & Reddy, B. Intralesional 5-fluorouracil as a treatment modality of keloids. *Dermatologic Surg.* **30**, 54–6; discussion 56-7 (2004).
 199. Bodokh, I. & Brun, P. Treatment of keloid with intralesional bleomycin. *Ann. Dermatol. Venereol.* **123**, 791–794 (1996).
 200. Atiyeh, B. S. Nonsurgical management of hypertrophic scars: Evidence-based therapies, standard practices, and emerging methods. *Aesthetic Plast. Surg.* **31**, 468–492 (2007).
 201. España, A., Solano, T. & Quintanilla, E. Bleomycin in the Treatment of Keloids and Hypertrophic Scars by Multiple Needle Punctures. *Dermatologic Surg.* **27**, 23–27 (2001).
 202. Berman, B., Maderal, A. & Raphael, B. Keloids and hypertrophic scars: Pathophysiology, classification, and treatment. *Dermatologic Surg.* **43**, S3–S18 (2017).
 203. Bailey, J., Waite, A., Clayton, W. & Rustin, M. Application of topical mitomycin C to the base of shave-removed keloid scars to prevent their recurrence. *Br. J. Dermatol.* **156**, 682–686 (2007).
 204. Wong, T. *et al.* Silicone cream occlusive dressing – a novel noninvasive regimen in the treatment of keloid. *Dermatology* **192**, 329–333 (1996).
 205. Macintyre, L. & Baird, M. Pressure garments for use in the treatment of hypertrophic scars—a review of the problems associated with their use. *Burns* **32**, 10–15 (2006).
 206. Kelly, A. Medical and surgical therapies for keloids. *Dermatol. Ther.* **17**, 212–218 (2004).
 207. Renò, F. *et al.* In vitro mechanical compression induces apoptosis and regulates cytokines release in hypertrophic scars. *Wound Repair Regen.* **11**, 331–336 (2003).
 208. Ahn, S., Monafo, W. & Mustoe, T.-. Topical silicone gel: a new treatment for hypertrophic scars. *Surgery* **106**, 781–787 (1989).

209. Niessen, F., Spauwen, P., Schalkwijk, J. & Moshe, K. On the nature of hypertrophic scars and keloids: A review. *Plast. Reconstr. Surg.* **104**, 1435–1458 (1999).
210. Mustoe, T. *et al.* International clinical recommendations on scar management. *Plast. Reconstr. Surg.* **110**, 560–571 (2002).
211. Cheng, J., Evans, J., Leung, K., Clark, J. & Choy, T. Pressure therapy in the treatment of post-burn hypertrophic scar—a critical look into its usefulness and fallacies by pressure monitoring. *Burns* **10**, 154–163 (1984).
212. Fulton, J. Silicone Gel Sheeting for the Prevention and Management of Evolving Hypertrophic and Keloid Scars. *Dermatologic Surg.* **21**, 947–951 (1995).
213. Westra, I., Pham, H. & Niessen, F. Topical silicone sheet application in the treatment of hypertrophic scars and keloids. *J. Clin. Aesthet. Dermatol.* **9**, 28–35 (2016).
214. Gold, M., Foster, T., Adair, M., Burlison, K. & Lewis, T. Prevention of hypertrophic scars and keloids by the prophylactic use of topical silicone gel sheets following a surgical procedure in an office setting. *Dermatologic Surg.* **27**, 641–644 (2001).
215. Quinn, K., Evans, J., Courtney, J., Gaylor, J. & Reid, W. Non-pressure treatment of hypertrophic scars. *Burns* **12**, 102–108 (1985).
216. Shaffer, J., Taylor, S. & Cook-Bolden, F. Keloidal scars: A review with a critical look at therapeutic options. *J. Am. Acad. Dermatol.* **46**, S63–S97 (2002).
217. Berman, B. & Bielely, H. Adjunct therapies to surgical management of keloids. *Dermatologic Surg.* **22**, 126–130 (1996).
218. Salasche, S. & Grabski, W. Keloids of the Earlobes: A Surgical Technique. *J. Dermatol. Surg. Oncol.* **9**, 552–556 (1983).
219. Henderson, D. Discussion: the effect of carbon dioxide laser surgery on the recurrence of keloids. *Plast. Reconstr. Surg.* **87**, 50–53 (1991).
220. Har-Shai, Y., Amar, M. & Sabo, E. Intralesional cryotherapy for enhancing the involution of hypertrophic scars and keloids. *Plast. Reconstr. Surg.* **111**, 1841–1852 (2003).
221. Apfelberg, D., Maser, M., Lash, H., White, D. & Weston, J. Preliminary results of argon and carbon dioxide laser treatment of keloid scars. *Lasers Surg. Med.* **4**, 283–290 (1984).
222. Bouzari, N., Davis, S. & Nouri, K. Laser treatment of keloids and hypertrophic scars. *Int. J. Dermatol.* **46**, 80–88 (2007).
223. Norris, J. Superficial x-ray therapy in keloid management: A retrospective study of 24 cases and literature review. *Plast. Reconstr. Surg.* **95**, 1051–1055 (1995).
224. Norris, J. The effect of carbon dioxide laser surgery on the recurrence of keloids. *Plast. Reconstr. Surg.* **87**, 44–9; discussion 50-3 (1991).
225. Kuo, Y. *et al.* Activation of ERK and p38 kinase mediated keloid fibroblast apoptosis after flashlamp pulsed-dye laser treatment. *Lasers in Surgery and Medicine* **36**, (Wiley-Liss Inc., 2005).
226. Tanzi, E. L. & Alster, T. S. Laser treatment of scars. *Skin Therapy Lett.* **9**, 4–7 (2004).

227. Alster, T. & Handrick, C. Laser treatment of hypertrophic scars, keloids, and striae. *Semin. Cutan. Med. Surg.* **19**, 287–292 (2000).
228. Pedata, F. *et al.* The role of ATP and adenosine in the brain under normoxic and ischemic conditions. *Purinergic Signal.* **3**, 299–310 (2007).
229. Cristalli, G., Lambertucci, C., Marucci, G., Volpini, R. & Dal Ben, D. A2A adenosine receptor and its modulators: overview on a druggable GPCR and on structure-activity relationship analysis and binding requirements of agonists and. *Curr. Pharm. Des.* **14**, 1525–1552 (2008).
230. Burnstock, G., Cocks, T., Kasakov, L. & Wong, H. Direct evidence for ATP release from non-adrenergic, non-cholinergic ('purinergic') nerves in the guinea-pig taenia coli and bladder. *Eur. J. Pharmacol.* **49**, 145–149 (1978).
231. Zimmermann, H., Braun, N., Kegel, B. & Heine, P. New insights into molecular structure and function of ecto-nucleotidases in the nervous system. *Neurochem. Int.* **32**, 421–425 (1998).
232. Calkner, D., Müller, M. & Hamprecht, B. Adenosine regulates via two different types of receptors, the accumulation of cyclic AMP in cultured brain cells. *J. Neurochem.* **33**, 999–1005 (1979).
233. Fredholm, B., Ijzerman, A., Jacobson, K., Klotz, K. & Linden, J. International Union of Pharmacology. XXV. Nomenclature and Classification of Adenosine Receptors. *Pharmacol. Rev.* **53**, 527–552 (2001).
234. Gordon, J. Extracellular ATP: effects, sources and fate. *Biochem. J.* **233**, 309–319 (1986).
235. O'Connor, S., Dainty, I. & Leff, P. Further subclassification of ATP receptors based on agonist studies. *Trends Pharmacol. Sci.* **12**, 137–141 (1991).
236. Abbracchio, M. & Burnstock, G. Purinoceptors: are there families of P2X and P2Y purinoceptors? *Pharmacol. Ther.* **64**, 445–475 (1994).
237. North, R. Molecular physiology of P2X receptors. *Physiol. Rev.* **82**, 1013–1067 (2002).
238. Drury, A. & Szent-Györgyi, A. The physiological activity of adenine compounds with especial reference to their action upon the mammalian heart. *J. Physiol.* **68**, 213–237 (1929).
239. Berne, R. Cardiac nucleotides in hypoxia: possible role in regulation of coronary blood flow. *Am. J. Physiol.* **204**, 317–322 (1963).
240. Maenhaut, C. *et al.* RDC8 codes for an adenosine A2 receptor with physiological constitutive activity. *Biochem. Biophys. Res. Commun.* **173**, 1169–1178 (1990).
241. Jin, X., Shepherd, R., Duling, B. & Linden, J. Inosine binds to A3 adenosine receptors and stimulates mast cell degranulation. *J. Clin. Invest.* **100**, 2849–2857 (1997).
242. Kojima, S., Ohshima, Y., Nakatsukasa, H. & Tsukimoto, M. Role of ATP as a Key Signaling Molecule Mediating Radiation-Induced Biological Effects. *Dose-Response* **15**, 155932581769063 (2017).
243. Zhou, Q. *et al.* Molecular cloning and characterization of an adenosine receptor: The

- A3 adenosine receptor. *Pharmacology* **89**, 7432–7436 (1992).
244. Abbracchio, M. *et al.* G protein-dependent activation of phospholipase C by adenosine A3 receptors in rat brain. *Mol. Pharmacol.* **48**, 1038–1045 (1995).
245. Feoktistov, I. & Biaggioni, I. Adenosine A2B Receptors. *Pharmacol. Rev.* **49**, 381–402 (1997).
246. Takigawa, T. & Alzheimer, C. Phasic and tonic attenuation of EPSPs by inward rectifier K⁺ channels in rat hippocampal pyramidal cells. *J. Physiol.* **539**, 67–75 (2002).
247. Fredholm, B., Ijzerman, A., Jacobson, K., Linden, J. & Mü, C. International Union of Basic and Clinical Pharmacology. LXXXI. Nomenclature and Classification of Adenosine Receptors-An Update. *Pharmacol. Rev.* **63**, 1–34 (2011).
248. Frenguelli, B., Wigmore, G., Llaudet, E. & Dale, N. Temporal and mechanistic dissociation of ATP and adenosine release during ischaemia in the mammalian hippocampus. *J. Neurochem.* **101**, 1400–1413 (2007).
249. Latini, S. & Pedata, F. Adenosine in the central nervous system: Release mechanisms and extracellular concentrations. *J. Neurochem.* **79**, 463–484 (2001).
250. Pedata, F., Corsi, C., Melani, A., Bordoni, F. & Latini, S. Adenosine Extracellular Brain Concentrations and Role of A2A Receptors in Ischemia. *Ann. N. Y. Acad. Sci.* **939**, 74–84 (2006).
251. Latini, S., Bordoni, F., Pedata, F. & Corradetti, R. Extracellular adenosine concentrations during in vitro ischaemia in rat hippocampal slices. *Br. J. Pharmacol.* **127**, 729–739 (1999).
252. Bruns, R. & Fergus, J. Allosteric enhancement of adenosine A1 receptor binding and function by 2-amino-3-benzoylthiophenes. *Mol. Pharmacol.* **38**, 939–949 (1990).
253. Van Der Klein, P., Kourounakis, A. & Ijzerman, A. Allosteric modulation of the adenosine A1 receptor. Synthesis and biological evaluation of novel 2-amino-3-benzoylthiophenes as allosteric enhancers of agonist binding. *J. Med. Chem.* **42**, 3629–3635 (1999).
254. Hutchison, K. & Fox, I. Purification and Characterization of the Adenosine A2-like Binding Site from Human Placental Membranes. *J. Biol. Chem.* **264**, 19898–19903 (1989).
255. Kull, B. *et al.* Differences in the order of potency for agonists but not antagonists at human and rat adenosine A2A receptors. *Biochem. Pharmacol.* **7**, 65–75 (1999).
256. Rieger, J., Brown, M., Sullivan, G., Linden, J. & Macdonald, T. Design, synthesis, and evaluation of novel A2A adenosine receptor agonists. *J. Med. Chem.* **44**, 531–539 (2001).
257. Poucher, S. *et al.* The in vitro pharmacology of ZM 241385, a potent, non-xanthine, A2a selective adenosine receptor antagonist. *Br. J. Pharmacol.* **115**, 1096–1102 (1995).
258. Beukers, M. *et al.* New, non-adenosine, high-potency agonists for the human adenosine A2B receptor with an improved selectivity profile compared to the reference

- agonist N-ethylcarboxamidoadenosine. *J. Med. Chem.* **47**, 3707–3709 (2004).
259. Ji, X., Kim, Y., Ahern, D., Linden, J. & Jacobson, K. MRS 1754, a selective antagonist radioligand for A2B adenosine receptors. *Biochem. Pharmacol.* **61**, 657–663 (2001).
260. Kim, Y., Ji, X., Melman, N., Linden, J. & Jacobson, K. Anilide derivatives of an 8-phenylxanthine carboxylic congener are highly potent and selective antagonists at human A(2B) adenosine receptors. *J. Med. Chem.* **43**, 1165–1172 (2000).
261. Fredholm, B. Purinoceptors in the Nervous System. *Pharmacol. Toxicol.* **76**, 228–239 (1995).
262. Baraldi, P. & Borea, P.-. New potent and selective human adenosine A3 receptor antagonists. *Trends Pharmacol. Sci.* **21**, 456–459 (2000).
263. Van Muijlwijk-Koezen, J. *et al.* Isoquinoline and quinazoline urea analogues as antagonists for the human-adenosine A3 receptor. *J. Med. Chem.* **43**, 2227–2238 (2000).
264. Jeong, L. *et al.* N6-substituted D-4'-thioadenosine-5'-methyluronamides: Potent and selective agonists at the human A3 adenosine receptor. *J. Med. Chem.* **46**, 3775–3777 (2003).
265. Dixon, A., Gubitz, A., Sirinathsinghji, D., Richardson, P. & Freeman, T. Tissue distribution of adenosine receptor mRNAs in the rat. *Br. J. Pharmacol.* **118**, 1461–1468 (1996).
266. Schindler, C. *et al.* Role of central and peripheral adenosine receptors in the cardiovascular responses to intraperitoneal injections of adenosine A 1 and A 2A subtype receptor agonists. *Br. J. Pharmacol.* **144**, 642–650 (2005).
267. Meyerhof, W., Müller-Brechlin, R. & Richter, D. Molecular cloning of a novel putative G-protein coupled receptor expressed during rat spermiogenesis. *FEBS Lett.* **284**, 155–160 (1991).
268. Linden, J. *et al.* Molecular cloning and functional expression of a sheep A3 adenosine receptor with widespread tissue distribution. *Mol. Pharmacol.* **44**, 524–532 (1993).
269. Salvatore, C. *et al.* Disruption of the A 3 Adenosine Receptor Gene in Mice and Its Effect on Stimulated Inflammatory Cells*. *J. Biol. Chem.* **275**, 4429–4434 (2000).
270. Fraser, H., Gao, Z., Ozeck, M. & Belardinelli, L. Effects in Awake Rats. *J. Pharmacol. Exp. Ther.* **305**, (2003).
271. Erdmann, A., Gao, Z., Jung, U., Foley, J. & Borenstein, T. Activation of Th1 and Tc1 cell adenosine A2A receptors directly inhibits IL-2 secretion in vitro and IL-2-driven expansion in vivo. *Blood* **105**, 4707–4714 (2005).
272. Lappas, C., Rieger, J. & Linden, J. T Cells + Production in Murine CD4 γ IFN-Adenosine Receptor Induction Inhibits 2A A. *J. Immunol.* **174**, 1073–1080 (2005).
273. Ramkumarh, V., Stilesll, G., Beavenll, M. & Mi, H. The A3 Adenosine Receptor Is the Unique Adenosine Receptor Which Facilitates Release of Allergic Mediators in Mast Cells*. *J. Biol. Chem.* **268**, 16887–16890 (1993).
274. Holgate, S. The identification of the adenosine A 2B receptor as a novel therapeutic

- target in asthma. in *British Journal of Pharmacology* **145**, 1009–1015 (2005).
275. Press, N. *et al.* A new orally bioavailable dual adenosine A2B/A3 receptor antagonist with therapeutic potential. *Bioorg. Med. Chem. Lett.* **15**, 3081–3085 (2005).
276. Feoktistov, I. *et al.* Differential expression of adenosine receptors in human endothelial cells: Role of A2B receptors in angiogenic factor regulation. *Circ. Res.* **90**, 531–538 (2002).
277. Ramanathan, M., Pinhal-Enfield, G., Hao, I. & Leibovich, S. Synergistic up-regulation of vascular endothelial growth factor (VEGF) expression in macrophages by adenosine A2A receptor agonists and endotoxin involves transcriptional regulation via the hypoxia response element in the VEGF promoter. *Mol. Biol. Cell* **18**, 14–23 (2007).
278. Montesinos, M. *et al.* Adenosine promotes wound healing and mediates angiogenesis in response to tissue injury via occupancy of A2A receptors. *Am. J. Pathol.* **160**, 2009–208 (2002).
279. Shaikh, G. & Cronstein, B. Signaling pathways involving adenosine A2A and A2B receptors in wound healing and fibrosis. *Purinergic Signal.* **12**, 191–197 (2016).
280. Desai, A. *et al.* Adenosine A2A Receptor Stimulation Increases Angiogenesis by Down-Regulating Production of the Antiangiogenic Matrix Protein Thrombospondin 1 Recent studies in wild-type and adenosine A2A receptor knockout mice demonstrate that adenosine A2A receptor o. *Mol. Pharmacol.* **67**, 1406–1413 (1997).
281. Ernens, I., Bousquenaud, M., Lenoir, B., Devaux, Y. & Wagner, D. Adenosine stimulates angiogenesis by up-regulating production of thrombospondin-1 by macrophages. *J. Leukoc. Biol.* **97**, 9–18 (2015).
282. Chan, E. *et al.* Adenosine A2A receptors in diffuse dermal fibrosis: Pathogenic role in human dermal fibroblasts and in a murine model of scleroderma. *Arthritis Rheum.* **54**, 2632–2642 (2006).
283. Fernández, P. *et al.* Pharmacological blockade of A2A receptors prevents dermal fibrosis in a model of elevated tissue adenosine. *Am. J. Pathol.* **172**, 1672–1682 (2008).
284. Bonelli, A., Bacci, S. & Norelli, G. Affinity cytochemistry analysis of mast cells in skin lesions: A possible tool to assess the timing of lesions after death. *Int. J. Legal Med.* **117**, 331–334 (2003).
285. Michalik, M. *et al.* Asthmatic bronchial fibroblasts demonstrate enhanced potential to differentiate into myofibroblasts in culture. *Med. Sci. Monit.* **15**, 194–201 (2009).
286. Bacci, S. *et al.* Immunohistochemical analysis of dendritic cells in skin lesions: correlations with survival time. *Elsevier* **244**, 179–185 (2014).
287. Dhall, S. *et al.* Generating and reversing chronic wounds in diabetic mice by manipulating wound redox parameters. *J. Diabetes Res.* (2014). doi:10.1155/2014/562625
288. Keira, S., Ferreira, L., Gagnani, A., Silva Duarte, I. & Santos, I. Experimental model for fibroblast culture. *Acta Cir. Bras.* **19**, (2004).
289. Krassovka, J. *et al.* Blue light irradiation and its beneficial effect on Dupuytren's

- fibroblasts. *PLoS One* **14**, (2019).
290. Skehan, P. *et al.* New colorimetric cytotoxicity assay for anticancer-drug screening. *J. Natl. Cancer Inst.* **82**, 1107–1112 (1990).
291. Vichai, V. & Kirtikara, K. Sulforhodamine B colorimetric assay for cytotoxicity screening. *Nat. Protoc.* **1**, 1112–1116 (2006).
292. Orellana, E. & Kasinski, A. *Sulforhodamine B (SRB) Assay in Cell Culture to Investigate Cell Proliferation. Bio-protocol* **6**, (Bio-Protocol, LLC, 2016).
293. Coppi, E. *et al.* UDP-glucose enhances outward K⁺ currents necessary for cell differentiation and stimulates cell migration by activating the GPR17 receptor in oligodendrocyte precursors. *Glia* **61**, 1155–1171 (2013).
294. Coppi, E., Pedata, F. & Gibb, A. P2Y 1 receptor modulation of Ca²⁺-activated K⁺ currents in medium-sized neurons from neonatal rat striatal slices. *J. Neurophysiol.* **107**, 1009–1021 (2012).
295. Brazhe, N., Treiman, M., Faricelli, B., Vestergaard, J. & Sosnovtseva, O. In Situ Raman Study of Redox State Changes of Mitochondrial Cytochromes in a Perfused Rat Heart. *PLoS One* **8**, (2013).
296. Li, M. *et al.* Macrophage-derived exosomes accelerate wound healing through their anti-inflammation effects in a diabetic rat model. *Artif. Cells, Nanomedicine, Biotechnol.* **47**, 3793–3803 (2019).
297. Bacci, S. *et al.* The pro-healing effect of exendin-4 on wounds produced by abrasion in normoglycemic mice. *Eur. J. Pharmacol.* **764**, 346–352 (2015).
298. Varricchi, G. *et al.* Physiological Roles of Mast Cells: Collegium Internationale Allergologicum Update 2019. *Int. Arch. Allergy Immunol.* **179**, (2019).
299. Burnstock, G. Purinergic signalling: Its unpopular beginning, its acceptance and its exciting future. *BioEssays* **34**, 218–225 (2012).
300. Liu, N. & Zhuang, S. Tissue protective and anti-fibrotic actions of suramin: new uses of an old drug. *Curr. Clin. Pharmacol.* **6**, 137–42 (2011).
301. Qu, Y., Wang, G., Sun, X. & Wang, K. Inhibition of the Warm Temperature-Activated Ca²⁺-Permeable Transient Receptor Potential Vanilloid TRPV3 Channel Attenuates Atopic Dermatitis. *Mol. Pharmacol.* **96**, 393–400 (2019).
302. Snyder, R. *et al.* Feature using a diagnostic tool to Identify elevated Protease activity Levels in chronic and stalled wounds: a consensus Panel discussion. *Ostomy. Wound. Manage.* **57**, 36–46 (2011).
303. Brazhe, N., Treiman, M., Brazhe, A., Maksimov, G. & Sosnovtseva, O. Mapping of Redox State of Mitochondrial Cytochromes in Live Cardiomyocytes. *PLoS One* **7**, (2012).
304. Notingher, I. Raman Spectroscopy Cell-based Biosensors. *Sensors* **7**, 1343–1358 (2007).
305. Ichimura, T. *et al.* Visualizing cell state transition using raman spectroscopy. *PLoS One* **9**, (2014).

306. Swain, R., Kemp, S., Goldstraw, P., Tetley, T. & Stevens, M. Assessment of cell line models of primary human cells by Raman spectral phenotyping. *Biophotonics Photonic Solut. Better Heal. Care VI* **98**, 1703–1711 (2010).
307. Spiro, T. & Strekas, T. Resonance Raman Spectra of Hemoglobin and Cytochrome c: Inverse Polarization and Vibronic Scattering (scattering tensor/porphyrin fluorescence). *PNAS* **69**, 2622–2626 (1972).
308. Zhu, G., Zhu, X., Fan, Q. & Wan, X. Raman spectra of amino acids and their aqueous solutions. *Spectrochim. Acta Part A Mol. Biomol. Spectrosc.* **78**, 1187–1195 (2011).
309. Mosca, R., Ong, A., Albasha, O., Bass, K. & Arany, P. Photobiomodulation Therapy for Wound Care: A Potent, Noninvasive, Photoceutical Approach. *Adv. Ski. Wound Care* **32**, 157–167 (2019).
310. Metelitsa, A. & Green, J. Home-Use Laser and Light Devices for the Skin—An Update. *Semin. Cutan. Med. Surg.* **30**, 144–147 (2011).
311. Hay, R. *et al.* The global burden of skin disease in 2010: an analysis of the prevalence and impact of skin conditions. *J. Invest. Dermatol.* **134**, 1527–1534 (2014).
312. Mignon, C., Botchkareva, N., Uzunbajakava, N. & Tobin, D. Photobiomodulation devices for hair regrowth and wound healing: a therapy full of promise but a literature full of confusion. *Exp. Dermatol.* **25**, 745–749 (2016).
313. Chen, C. *et al.* Low-level laser irradiation promotes cell proliferation and mRNA expression of type I collagen and decorin in porcine achilles tendon fibroblasts in vitro. *J. Orthop. Res.* **27**, 646–650 (2009).
314. Gavish, L., Perez, L. & Gertz, S. Low-level laser irradiation modulates matrix metalloproteinase activity and gene expression in porcine aortic smooth muscle cells. *Lasers Surg. Med.* **38**, 779–786 (2006).
315. Gavish, L., Perez, L., Reissman, P. & Gertz, S. Irradiation with 780 nm diode laser attenuates inflammatory cytokines but upregulates nitric oxide in lipopolysaccharide-stimulated macrophages: Implications for the prevention of aneurysm progression. *Lasers Surg. Med.* **40**, 371–378 (2008).
316. Huang, Y., Chen, A., Sharma, S., Wu, Q. & Hamblin, M. Comparison of cellular responses induced by low level light in different cell types. *SPIE Proceeding* **7552**, (2010).
317. Kreisler, M., Christoffers, A., Willershausen, B. & D’Hoedt, B. Effect of low-level GaAlAs laser irradiation on the proliferation rate of human periodontal ligament fibroblasts: An in vitro study. *J. Clin. Periodontol.* **30**, 353–358 (2003).
318. Peplow, P., Chung, T. & Baxter, G. Laser photobiomodulation of wound healing: A review of experimental studies in mouse and rat animal models. *Photomed. Laser Surg.* **28**, 291–325 (2010).
319. Stadler, I. *et al.* In vitro effects of low-level laser irradiation at 660 nm on peripheral blood lymphocytes. *Lasers Surg. Med.* **27**, 255–261 (2000).
320. Stein, A., Benayahu, D., Maltz, L. & Oron, U. Low-level laser irradiation promotes

- proliferation and differentiation of human osteoblasts in vitro. *Photomed. Laser Surg.* **23**, 161–166 (2005).
321. Vinck, E., Cagnie, B., Cornelissen, M., Declercq, H. & Cambier, D. Increased fibroblast proliferation induced by light emitting diode and low power laser irradiation. *Lasers Med. Sci.* **18**, 95–99 (2003).
322. Quirk, B. & Whelan, H. Near-infrared irradiation photobiomodulation: The need for basic science. *Photomedicine and Laser Surgery* **29**, 143–144 (2011).
323. Baxter, G. *et al.* Low level laser therapy (Photobiomodulation therapy) for breast cancer-related lymphedema: a systematic review. *BMC Cancer* **17**, 833 (2017).
324. Hou, J. *et al.* In vitro effects of low-level laser irradiation for bone marrow mesenchymal stem cells: Proliferation, growth factors secretion and myogenic differentiation. *Lasers Surg. Med.* **40**, 726–733 (2008).
325. Júnior, A., Vieira, B., De Andrade, L. & Aarestrup, F. Low-level laser therapy increases transforming growth factor- β 2 expression and induces apoptosis of epithelial cells during the tissue repair process. *Photomed. Laser Surg.* **27**, 303–307 (2009).
326. Saygun, I. *et al.* Effects of laser irradiation on the release of basic fibroblast growth factor (bFGF), insulin like growth factor-1 (IGF-1), and receptor of IGF-1 (IGFBP3) from gingival fibroblasts. *Lasers Med. Sci.* **23**, 211–215 (2008).
327. Hawkins, D. & Abrahamse, H. The role of laser fluence in cell viability, proliferation, and membrane integrity of wounded human skin fibroblasts following Helium-Neon laser irradiation. *Lasers Surg. Med.* **38**, 74–83 (2006).
328. Karu, T. *Ten Lectures on Basic Science of Laser Phototherapy.* (2007).
329. Espinosa, E. & Valitutti, S. New roles and controls of mast cells. *Curr. Opin. Immunol.* **50**, 39–47 (2018).
330. De Castro, I. *et al.* Do laser and led phototherapies influence mast cells and myofibroblasts to produce collagen? *Lasers Med. Sci.* **29**, 1405–1410 (2014).
331. Matić, M., Lazetić, B., Poljacki, M., Duran, V. & Ivkov-Simić, M. Low level laser irradiation and its effect on repair processes in the skin. *Med. Pregl.* **56**, 137–41 (2003).
332. Krzyszczyk, P., Schloss, R., Palmer, A. & Berthiaume, F. The role of macrophages in acute and chronic wound healing and interventions to promote pro-wound healing phenotypes. *Front. Physiol.* **9**, (2018).
333. Patel, G. The role of nutrition in the management of lower extremity wounds. *Int. J. Low. Extrem. Wounds* **4**, 12–22 (2005).
334. Ladwig, G. *et al.* Ratios of activated matrix metalloproteinase-9 to tissue inhibitor of matrix metalloproteinase-1 in wound fluids are inversely correlated with healing of pressure ulcers. *Wound Repair Regen.* **10**, 26–37 (2002).
335. Butte, A., Dzau, V. & Glueck, S. Further defining housekeeping, or ‘maintenance,’ genes Focus on ‘A compendium of gene expression in normal human tissues’. *Physiol. Genomics* **7**, 95–96 (2001).
336. Mirastschijski, U. *et al.* Matrix Metalloproteinase-3 is Key Effector of TNF- α -Induced

- Collagen Degradation in Skin. *Int. J. Mol. Sci.* **20**, (2019).
337. Yen, Y. *et al.* Curcumin accelerates cutaneous wound healing via multiple biological actions: The involvement of TNF- α , MMP-9, α -SMA, and collagen. *Int. Wound J.* **15**, 605–617 (2018).
338. Frankova, J., Diamantova, D., Vrbkova, J. & Ulrichova, J. Influence of hydrogencalcium salts of oxidized cellulose on MMP-2, MMP-9 and TNF- α production and wound healing in non-healing wounds. *Acta Dermatovenerol. Croat.* **21**, 219–223 (2013).
339. Bonatti, S. *et al.* In vitro effect of 470 nm LED (Light Emitting Diode) in keloid fibroblasts. *Acta Cir. Bras.* **26**, 25–30 (2011).
340. Yun, J. *et al.* Expression of Ca²⁺-activated K⁺ channels in human dermal fibroblasts and their roles in apoptosis. *Skin Pharmacol. Physiol.* **23**, 91–104 (2010).
341. Urrego, D., Tomczak, A., Zahed, F., Stühmer, W. & Pardo, L. Potassium channels in cell cycle and cell proliferation. *Philos. Trans. R. Soc. Lond. B. Biol. Sci.* **369**, 20130094 (2014).
342. Karmouty-Quintana, H., Xia, Y. & Blackburn, M. Adenosine signaling during acute and chronic disease states. *J. Mol. Med. (Berl)*. **91**, 173–81 (2013).
343. Valls, M., Cronstein, B. & Montesinos, M. Adenosine receptor agonists for promotion of dermal wound healing. *Biochem. Pharmacol.* **77**, 1117–1124 (2009).
344. Coppi, E., Cellai, L., Maraula, G., Pugliese, A. & Pedata, F. Adenosine A_{2A} receptors inhibit delayed rectifier potassium currents and cell differentiation in primary purified oligodendrocyte cultures. *Neuropharmacology* **73**, 301–310 (2013).
345. Souza-Barros, L. *et al.* Skin color and tissue thickness effects on transmittance, reflectance, and skin temperature when using 635 and 808 nm lasers in low intensity therapeutics. *Lasers Surg. Med.* **50**, 291–301 (2018).
346. Haroutunian, V. *et al.* Myelination, oligodendrocytes, and serious mental illness. *Glia* **62**, 1856–1877 (2014).
347. Sommer, I. & Schachner, M. Monoclonal antibodies (O1 to O4) to oligodendrocyte cell surfaces: an immunocytological study in the central nervous system. *Dev. Biol.* **83**, 311–327 (1981).
348. Gallo, V. & Armstrong, R. Developmental and Growth Factor-Induced Regulation of Nestin in Oligodendrocyte Lineage Cells. *J. Neurosci.* **15**, 394–406 (1995).
349. Gard, A. & Pfeiffer, S. Two proliferative stages of the oligodendrocyte lineage (A2B5+ O4-and O4+ GalC-) under different mitogenic control. *Neuron* **5**, 615–625 (1990).
350. Warrington, A. & Pfeiffer, S. Proliferation and differentiation of O4+oligodendrocytes in postnatal rat cerebellum: Analysis in unfixed tissue slices using anti-glycolipid antibodies. *J. Neurosci. Res.* **33**, 338–353 (1992).
351. Szuchet, S. *et al.* The genetic signature of perineuronal oligodendrocytes reveals their unique phenotype. *Eur. J. Neurosci.* **34**, 1906–1922 (2011).
352. Barateiro, A. & Fernandes, A. Temporal oligodendrocyte lineage progression: in vitro models of proliferation, differentiation and myelination. *Biochim. Biophys. Acta - Mol.*

- Cell Res.* **1843**, 1917–1929 (2014).
353. Sontheimer, H. & Kettenmann, H. Heterogeneity of potassium currents in cultured oligodendrocytes. *Glia* **1**, 415–420 (1988).
354. Verkhatsky, A., Trotter, J. & Kettenman, H. Cultured glial precursor cells from mouse cortex express two types of calcium currents. *Neurosci. Lett.* **112**, 194–198 (1990).
355. Sontheimer, H. *et al.* Glial cells of the oligodendrocyte lineage express proton-activated Na⁺ channels. *J. Neurosci. Res.* **24**, 496–500 (1989).
356. Yuan, X. *et al.* Expression of the green fluorescent protein in the oligodendrocyte lineage: A transgenic mouse for developmental and physiological studies. *J. Neurosci. Res.* **70**, 529–545 (2002).
357. Fields, R. & Stevens, B. ATP: an extracellular signaling molecule between neurons and glia. *Trends Neurosci.* **23**, 625–633 (2000).
358. Ontaneda, D., Cohen, J. & Amato, M. Clinical outcome measures for progressive MS trials. *Mult. Scler.* **23**, 1627–1635 (2017).
359. Comi, G., Radaelli, M. & Soelberg Sørensen, P. Evolving concepts in the treatment of relapsing multiple sclerosis. *Lancet* **389**, 1347–1356 (2017).
360. Filippi, M. *et al.* Association between pathological and MRI findings in multiple sclerosis. *Lancet Neurol.* **11**, 349–360 (2012).
361. Calabrese, M. *et al.* Regional Distribution and Evolution of Gray Matter Damage in Different Populations of Multiple Sclerosis Patients. *PLoS One* **10**, e0135428 (2015).
362. Charcot, M. Leçons sur les maladies du système nerveux: faites a la Salpêtrière - Jean-Martin Charcot - Google Libri. *Cambridge University Press* (1877). doi:doi.org/10.1017/CBO9781139105378
363. Langdon, D. Cognition in multiple sclerosis. *Curr. Opin. Neurol.* **24**, 244–249 (2011).
364. Chiaravalloti, N. & DeLuca, J. Cognitive impairment in multiple sclerosis. *Lancet Neurol.* **7**, 1139–1151 (2008).
365. English, C. & Aloï, J. New FDA-approved disease-modifying therapies for multiple sclerosis. *Clin. Ther.* **37**, 691–715 (2015).
366. Dawson, M., Polito, A., Levine, J. & Reynolds, R. NG2-expressing glial progenitor cells: An abundant and widespread population of cycling cells in the adult rat CNS. *Mol. Cell. Neurosci.* **24**, 476–488 (2003).
367. Chang, A., Nishiyama, A., Peterson, J., Prineas, J. & Trapp, B. NG2-Positive Oligodendrocyte Progenitor Cells in Adult Human Brain and Multiple Sclerosis Lesions. *J. Neurosci.* **20**, 6404–6412 (2000).
368. Levine, J. & Reynolds, R. Activation and proliferation of endogenous oligodendrocyte precursor cells during ethidium bromide-induced demyelination. *Exp. Neurol.* **160**, 333–347 (1999).
369. DeLuca, G., Yates, R., Beale, H. & Morrow, S. Cognitive impairment in multiple sclerosis: Clinical, radiologic and pathologic insights. in *Brain Pathology* **25**, 79–98 (Blackwell Publishing Ltd, 2015).

370. Filippo, M., Sarchielli, P., Picconi, B. & Calabresi, P. Neuroinflammation and synaptic plasticity: theoretical basis for a novel, immune-centred, therapeutic approach to neurological disorders. *Trends Pharmacol. Sci.* **29**, 402–412 (2008).
371. Dewar, D., Underhill, S. & Goldberg, M. Oligodendrocytes and ischemic brain injury. *J. Cereb. Blood Flow Metab.* **23**, 263–274 (2003).
372. Pantoni, L., Garcia, J. & Gutierrez, J. Cerebral white matter is highly vulnerable to ischemia. *Stroke* **27**, 1641–1647 (1996).
373. Zhang, H., Jarjour, A., Boyd, A. & Williams, A. Central nervous system remyelination in culture - A tool for multiple sclerosis research. *Exp. Neurol.* **230**, 138–148 (2011).
374. Richardson, W., Kessaris, N. & Pringle, N. Oligodendrocyte wars. *Nat. Rev. Neurosci.* **7**, 11–18 (2006).
375. De Castro, F. & Bribián, A. The molecular orchestra of the migration of oligodendrocyte precursors during development. *Brain Res. Rev.* **49**, 227–241 (2005).
376. Nishiyama, A., Chang, A. & Trapp, B. NG2+ Glial Cells: A Novel Glial Cell Population in the Adult Brain. *J. Neuropathol. Exp. Neurol.* **58**, 1113–1124 (1999).
377. Windrem, M. *et al.* Fetal and adult human oligodendrocyte progenitor cell isolates myelinate the congenitally dysmyelinated brain. *Nat. Med.* **10**, (2004).
378. Nishiyama, A., Komitova, M., Suzuki, R. & Zhu, X. Polydendrocytes (NG2 cells): Multifunctional cells with lineage plasticity. *Nat. Rev. Neurosci.* **10**, 9–22 (2009).
379. Butt, A. *et al.* Cells expressing the NG2 antigen contact nodes of ranvier in adult CNS white matter. *Glia* **26**, 84–91 (1999).
380. Ong, W. & Levine, J. A light and electron microscopic study of NG2 chondroitin sulfate proteoglycan-positive oligodendrocyte precursor cells in the normal and kainate-lesioned rat. *Neuroscience* **92**, 83–95 (1999).
381. Butt, A., Kiff, J., Hubbard, P. & Berry, M. Synantocytes: New functions for novel NG2 expressing glia. *J. Neurocytol.* **31**, 551–565 (2002).
382. Butt, A. & Dinsdale, J. Opposing actions of fibroblast growth factor-2 on early and late oligodendrocyte lineage cells in vivo. *J. Neuroimmunol.* **166**, 75–87 (2005).
383. Nishiyama, A., Watanabe, M., Yang, Z. & Bu, J. Identity, distribution, and development of polydendrocytes: NG2-expressing glial cells. *J. Neurocytol.* **31**, 437–455 (2002).
384. Saab, A., Tzvetanova, I. & Nave, K. The role of myelin and oligodendrocytes in axonal energy metabolism. *Curr. Opin. Neurobiol.* **23**, 1065–1072 (2013).
385. Bergles, D., Roberts, J., Somogyi, P. & Jahr, C. Glutamatergic synapses on oligodendrocyte precursor cells in the hippocampus. *Nature* **405**, 187–191 (2000).
386. Hines, J., Ravanelli, A., Schwindt, R., Scott, E. & Appel, B. Neuronal activity biases axon selection for myelination in vivo. *Nat. Neurosci.* **18**, 683–689 (2015).
387. Almeida, R. & Lyons, D. On myelinated axon plasticity and neuronal circuit formation and function. *J. Neurosci.* **37**, 10023–10034 (2017).
388. Fields, R. A new mechanism of nervous system plasticity: Activity-dependent myelination. *Nat. Rev. Neurosci.* **16**, 756–767 (2015).

389. Gallo, V., Mangin, J., Kukley, M. & Dietrich, D. Synapses on NG2-expressing progenitors in the brain: Multiple functions? *J. Physiol.* **586**, 3767–3781 (2008).
390. Sampaio-Baptista, C. & Johansen-Berg, H. White Matter Plasticity in the Adult Brain. *Neuron* **96**, 1239–1251 (2017).
391. Emery, B. Regulation of oligodendrocyte differentiation and myelination. *Science (80-.)*. **330**, 779–782 (2010).
392. Stevens, B., Porta, S., Haak, L., Gallo, V. & Fields, R. Adenosine: a neuron-glia transmitter promoting myelination in the CNS in response to action potentials. *Neuron* **36**, 855–868 (2002).
393. Welsh, T. & Kucenas, S. Purinergic signaling in oligodendrocyte development and function. *J. Neurochem.* **145**, 6–18 (2018).
394. Coppi, E. *et al.* Role of adenosine in oligodendrocyte precursor maturation. *Front. Cell. Neurosci.* **9**, (2015).
395. Othman, T., Yan, H. & Rivkees, S. Oligodendrocytes Express Functional A1 Adenosine Receptors That Stimulate Cellular Migration. *Glia* **44**, 166–172 (2003).
396. Pedata, F. *et al.* Purinergic signalling in brain ischemia. *Neuropharmacology* **104**, 105–130 (2016).
397. Agresti, C. *et al.* Metabotropic P2 receptor activation regulates oligodendrocyte progenitor migration and development. *Glia* **50**, 132–144 (2005).
398. Beukers, M., Dulk, H., Tilburg, E., Brouwer, J. & Ijzerman, A. Why Are A 2B Receptors Low-Affinity Adenosine Receptors? Mutation of Asn273 to Tyr Increases Affinity of Human A 2B Receptor for 2-(1-Hexynyl)adenosine. *Mol. Pharmacol.* **58**, 1349–1356 (2000).
399. Sachdeva, S. & Gupta, M. Adenosine and its receptors as therapeutic targets: An overview. *Saudi Pharm. J.* **21**, 245–253 (2013).
400. Sun, Y. & Huang, P. Adenosine A2B Receptor: From Cell Biology to Human Diseases. *Front. Chem.* **4**, (2016).
401. Gao, Z., Chen, T., Weber, M. & Linden, J. A2B adenosine and P2Y2 receptors stimulate mitogen-activated protein kinase in human embryonic kidney-293 cells. cross-talk between cyclic AMP and protein kinase c pathways. *J. Biol. Chem.* **274**, 5972–5980 (1999).
402. Linden, J., Thai, T., Figler, H., Jin, X. & Robeva, A. Characterization of Human A 2B Adenosine Receptors: Radioligand Binding, Western Blotting, and Coupling to G q in Human Embryonic Kidney 293 Cells and HMC-1 Mast Cells. *Mol. Pharmacol.* **56**, 705–713 (1999).
403. Panjehpour, M., Castro, M. & Klotz, K. Human breast cancer cell line MDA-MB-231 expresses endogenous A 2B adenosine receptors mediating a Ca 2+ signal. *Br. J. Pharmacol.* **145**, 211–218 (2005).
404. Donoso, M., López, R., Miranda, R., Briones, R. & Huidobro-Toro, J. A2B adenosine receptor mediates human chorionic vasoconstriction and signals through arachidonic

- acid cascade. *Am. J. Physiol. - Hear. Circ. Physiol.* **288**, H2439–H2449 (2005).
405. Schulte, G. & Fredholm, B. The Gs-coupled adenosine A2b receptor recruits divergent pathways to regulate ERK1/2 and p38. *Exp. Cell Res.* **290**, 168–176 (2003).
406. Wang, J. & Huxley, V. Adenosine A2A receptor modulation of juvenile female rat skeletal muscle microvessel permeability. *Am. J. Physiol. - Hear. Circ. Physiol.* **291**, H3094–H3105 (2006).
407. Yaar, R., Jones, M., Chen, J. & Ravid, K. Animal models for the study of adenosine receptor function. *J. Cell. Physiol.* **202**, 9–20 (2005).
408. Hart, M., Jacobi, B., Schittenhelm, J., Henn, M. & Eltzschig, H. Cutting Edge: A2B Adenosine Receptor Signaling Provides Potent Protection during Intestinal Ischemia/Reperfusion Injury. *J. Immunol.* **182**, 3965–3968 (2009).
409. Haskó, G., Csóka, B., Németh, Z., Vizi, E. & Pacher, P. A2B adenosine receptors in immunity and inflammation. *Trends Immunol.* **30**, 263–270 (2009).
410. Kolachala, V. *et al.* TNF- α upregulates adenosine 2b (A2b) receptor expression and signaling in intestinal epithelial cells: A basis for A2bR overexpression in colitis. *Cell. Mol. Life Sci.* **62**, 2647–2657 (2005).
411. Kong, T., Westerman, K., Faigle, M., Eltzschig, H. & Colgan, S. HIF-dependent induction of adenosine A2B receptor in hypoxia. *FASEB J.* **20**, 2242–2250 (2006).
412. Xaus, J. *et al.* IFN-gamma up-regulates the A2B adenosine receptor expression in macrophages: a mechanism of macrophage deactivation. *J. Immunol.* **162**, 3607–14 (1999).
413. Livak, K. & Schmittgen, T. Analysis of Relative Gene Expression Data Using Real-Time Quantitative PCR and the 2 C T Method. *METHODS* **25**, 402–408 (2001).
414. Donati, C. *et al.* Sphingosine 1-Phosphate Mediates Proliferation and Survival of Mesoangioblasts. *Stem Cells* **25**, 1713–1719 (2007).
415. Schmittgen, T. & Livak, K. Analyzing real-time PCR data by the comparative C T method. *Nat. Protoc.* **3**, 1101–1108 (2008).
416. Knutson, P., Ghiani, C., Zhou, J., Gallo, V. & McBain, C. K Channel Expression and Cell Proliferation Are Regulated by Intracellular Sodium and Membrane Depolarization in Oligodendrocyte Progenitor Cells. *J. N* **17**, 2669–2682 (1997).
417. Gutman, G. *et al.* International Union of Pharmacology. LIII. Nomenclature and molecular relationships of voltage-gated potassium channels. *Pharmacol. Rev.* **57**, (2005).
418. Soliven, B., Szuchet, S., Arnason, B. & Nelson, D. Forskolin and phorbol esters decrease the same K⁺ conductance in cultured oligodendrocytes. *J. Membr. Biol.* **105**, 177–186 (1988).
419. Fields, R. & Burnstock, G. Purinergic signalling in neuron–glia interactions. *Nat. Rev. Neurosci.* **7**, 423–436 (2006).
420. Attali, B. *et al.* Characterization of Delayed Rectifier Kv Channels in Oligodendrocytes and Progenitor Cells. *Journa Neurosci.* **17**, 8234–8245 (1997).

421. Chittajallu, R., Aguirre, A. & Gallo, V. Downregulation of Platelet-Derived Growth Factor-Receptor-Mediated Tyrosine Kinase Activity as a Cellular Mechanism for K-Channel Regulation during Oligodendrocyte Development In Situ. *J. Neurosci.* **25**, 8601–8610 (2005).
422. Gallo, V. *et al.* Oligodendrocyte Progenitor Cell Proliferation and Lineage Progression Are Regulated by Glutamate Receptor-Mediated K⁺ Channel Block. *J. Neurosci.* **76**, 2659–2670 (1996).
423. Vartanian, T., Szuchet, S., Dawson, G. & Campagnon, A. Oligodendrocyte adhesion activates protein kinase C-mediated phosphorylation of myelin basic protein. *Science* **234**, 1395–1398 (1986).